UNIVERSITY OF SOUTHAMPTON

FACULTY OF SCIENCE

School of Chemistry

Flexoelectricity in Liquid Crystals

Volume 1 of 2

by

Daniel Jackson

Thesis for the degree of Doctor of Philosophy

July 2007

UNIVERSITY OF SOUTHAMPTON

ABSTRACT

FACULTY OF ENGINEERING SCIENCE AND MATHEMATICS

SCHOOL OF CHEMISTRY

Doctor of Philosophy

FLEXOELECTRICITY IN LIQUID CRYSTALS

By Daniel Jackson

A rich variety of symmetric and non-symmetric liquid crystal dimers have been synthesised and studied in order to investigate their structure property relations; in particular their flexoelectric properties.

The project is introduced in Chapters 1 and 2 where Chapter 1 gives a brief general background to liquid crystals and liquid crystal synthesis, and Chapter 2 gives a more detailed background to the flexoelectric effect.

The research can be broadly divided into two parts. Chapters 3 and 4 focus on seven conventional non-symmetric liquid crystal dimer series containing two mesogenic groups ether linked through a flexible spacer. These non-symmetric dimers all contain a cyanobiphenyl mesogenic group at one end and either a poly-fluorinated biphenyl or a phenyl-cyclohexyl-alkane mesogenic group at the other. Almost all these materials possess nematic phases (and in one series a smectic phase) and show strong flexoelectric coupling to an applied field with some experiments yielding very large values for the flexoelastic ratio.

Chapter 5 focuses on two series of bent core liquid crystal dimers, where the long chain spacer is divided by a catechol or resorcinol based disruptor group. The disruptor is located in the centre of the molecule and symmetric cyanobiphenyl mesogenic groups are at each end. These materials show a curious odd-even effect in the nematic-isotropic transition temperatures which is further investigated in Chapter 6 by reducing the symmetry of the compounds and studying the changes in the transitional properties. This was achieved in one series by changing the relative position of the catechol linking group along the spacer chain or, in a different series, by altering one of the mesogenic end groups to a di-fluorinated biphenyl (a mesogenic moiety studied in Chapter 3).

The liquid crystal properties were investigated by optical microscopy, differential scanning calorimetry and deuterium NMR spectroscopy. The flexoelastic ratios were determined from the dependence of the tilt in the optic axis on an applied electric field.

Acknowledgments

For me, this PhD has been a journey – and a long one at that! As with any long journey there have been a huge number of people supporting me along the way and here I have an opportunity to thank them.

Every journey has a beginning and mine really started at St Mary's College in Southampton, a mere forty minutes walk from the university – it was here that I fell in love with chemistry and decided that I was going to do a PhD in the subject (probably earlier then most). It was here that I met and was taught for four years by Terry Simmonds the then head of Chemistry. Even at university I do not think I have ever met anyone with such an infectious enthusiasm for chemistry. Clearly (and rightly) convinced that chemistry was the most fascinating, useful, rewarding and important academic subject on the curriculum he was an inspiration to me. In fact I did not fully appreciate how large an impact he had made on my academic career in the subject until I was forced to make the adjustment to learning from other tutors at university – a culture shock which nearly saw me quit my degree. Terry's instinctive and precise knowledge of such a wide range of chemistry was set a very high standard to aspire to and one which I am convinced I have still not suitably obtained, PhD or not! I am however convinced that the most important period of learning in this subject comes at A-level and to him I owe a deep sense of gratitude for the time, energy and patience he willingly gave me ensuring a rock solid foundation in chemistry which has and will last me my career.

Moving on to university, the two most significant figures in my nearly nine-year (!) affiliation, were Martin and Geoffrey who tirelessly supervised my somewhat extended PhD. Martin's work really started some years before when he, beyond all other members of staff in the department took care to keep an eye on me during my undergraduate years. During my attempts to survive the culture shock which was doing an undergraduate degree Martin, on more than one occasion and, I think, without always realising it, provided me with the encouragement I needed to persevere and not give up. Indeed it was only at the end of my degree that I found out how much he had kept an interest in my well-being, through the friends and housemates of mine whom he knew. Martin, in a double-act with James, wooed me into reconsidering a PhD as an option after having lost confidence in my ability

during my final year in undergraduate. So in many respects I owe him not just my PhD but also my undergraduate degree as well.

Geoffrey has taken the leading role in supervising my PhD and, as such, has worn the brunt of my disappointments and been architect of my successes. He has worked tirelessly to educate me in the science of liquid crystals, explaining to me with great patience the background I needed to know to understand the subject I was studying. He was and is always generous with his time with everyone who is in his group holding an interest in not just their academic advance but also their personal well-being. The hours which Geoffrey has poured into my work is phenomenal and unlike any other supervisor in the department. His eye for detail and determination to get the best result possible meant that he not only read the liquid crystal science in my reports but also worked his way through the organic chemistry and experimental sections. His care over my work has been both constant and complete, and I am greatly indebted to him for always going beyond what is required of him as a supervisor to get the best out of my work.

Second in the line of fire after my supervisors is my advisor George, who in spite of his extremely busy schedule, always took the time to help advise, listen, explain (in some cases decode) the science I was attempting to write about in my Thesis. With a wit which is razor sharp and sense of humour which is a dry as the Sahara, George has been both kind and sensitive at the times I have needed it, offering practical advice, suitably cruel questions in my transfer viva and suffered has my sometimes hounding attempts to get his time and attention. I, to this day, do not know anyone else from whom he runs from quite as fast as me! And as a reward, I presented him with a Thesis to read which was almost as along as his.

From there I should move to my parents who, I can imagine, never dreamt this journey would take so long, have supported me unfailingly throughout. Wherever possibly they have made every attempt to lighten my load to allow me the space to do the work that needed to be done, but also to have a chance to relax between times. During these past years they have shared not only the highs and lows of the PhD, but also the many ups and downs of my personal life during this time – and there have been many. Whilst I matured and my approach to life changed, they maintained a constant support to me regardless of how well or not I was handling the situation they provided love, support, time, money and service to me throughout, never stopping and never counting the cost. They exemplified Paul's teaching to the Corinthians on love

and even in the final hours, Dad was helping with corrections and printing whilst Mum waited on us providing much needed coffee and food. As much as I owe Geoffrey and Martin for their direct support of my PhD I owe my parents more for their support of me generally through this testing time.

During the majority of the time I spent throughout my Thesis, my now ex-finaceé Zoe spent much of her time supporting me in spite of the battles she was fighting in her own life. The effort which we put in to help each other overcome the goals we had set ourselves in some respects cost us our relationship. During this time, she spent many hours, supporting me in ways which few if any saw. Her patience with me was un-ending and she bore with me during times when it all seemed hopeless (these moments happen in all PhDs I am reliably told). Not more so then when I was ill, she, along with my parents, bore the brunt of getting me back to fighting fitness. I am blessed that she has become as good a friend to me now as she was partner to me when I was doing my PhD. It is to the support which was unseen to everyone else that I thank her most whole-heartedly for.

There are three things which a PhD student needs to get right before starting, a good supervisor, a good area of study and a good group to work in. The Grossel group has been all that and more. Having working in it for nearly 2 PhDs worth of time I have seen many changes in the group dynamic as colourful characters (which seems to be a constant trait of Grosselites) have come and gone. To mention everyone would take too long in what is already going to be a rather extended acknowledgments section. However during my stay I have been blessed with two very close friends, more like family, in the form of James and Polski. James I knew in my undergraduate years and played a vital role in helping me make the decision to undertake the PhD and then, when life turned upside-down, patently listened to me as I tried hard to figure out this thing called life often keeping him awake in the early hours when clearly he needed to go to sleep! Always loyal and always ready to help – even for an 8 hour round trip to the midlands at midnight. One of my first recollections of Polski was his attempts at helping me purify a starting material. I was unable to do this and he took a couple of hours out of his afternoon to help me. This was an event which would repeat itself as he selflessly gave his time to help me, be it in the lab, online game or refitting a printer (which he did not so much help as do single handed such was my lack of skill for the task). You cannot make it through life without good friends, and I have been blessed to have these two in my life to be mine.

A few other notable mentions in the group include Alan who has been patience personified whilst I shared his fume-cupboard in my final year of writing up. He has endured my disorganisation and maintained a sense of humour which is disturbingly similar to my own (you may want to get that seen to Alan!). Andrew must clearly be mentioned as the inspiration for my use of the PhD comics in on my cover pages and Jon's general organisation in the lab, bringing order to chaos, printers to bear, computers to heel and Martin (almost) under control has been legendary. Georgie has given the group the much needed 'feminine touch' which we wayward men would have otherwise lacked, but I must particularly thank her for reading no less than two of my long chapters whilst herself battling to finish her PhD. In the midst of her stresses she took the time to work through two particularly poorly written chapters making invaluable suggestions struggling with an area of science which is hard at the best of times. I could go on, but thanks should also go to Sophie who helped me in my early years of PhDing, Michael, Alex, Andy, Chris, Francesco, Alain the plethora of project students (and anyone else I may have missed) all of whom have contributed to five enjoyable years in the group.

Outside of the Grossel group is Azizah and Tim who ran several deuterium NMR experiments which are included in the Thesis.

Within the department there are many people who should be thanked, these include Neil and Joan in NMR; the ever patient John and Julie in mass spectrometry; Claire, dealing with all matters financial in my PhD; Sally for answering with just about every other kind of departmentally related question I have ever had; Bevy for looking after me when letters had to be written, Thesis submission problems arose... (the list goes on...); and all the other administration staff who, over the years have kept the department and me afloat when all around was sinking.

Beyond the Chemistry department I must also thank Merck in Chilworth for providing a large portion of the funding, numerous materials, microscopy cells and expertise without which my research would have been impossible. All the staff at Merck were extremely helpful and readily gave up time to help me in my many desperate times working at Chilworth. I should especially like to thank Doina Ionescu, Cecile Schott and Kevin Adlem for their help in supervising my PhD from the industrial perspective. During my postgraduate work it was they who were my first port of call at Merck, locating information and showing me the complexities of making flexoelectric measurements on my samples. When a synthetic chemist attempts to do

physical chemical measurements, patience is a must and theirs with me was seemingly endless!

Also I should thank Prof. John Seddon for his work with X-ray diffraction experiments and the time he took to introduce me to Cliff Jones in the BLCS meeting.

Finally there has been huge support from friends, Lili, Phil, Louise, Moina, Alex, Faith and Hannah to name but a few. Many have listened particularly in the last days to my endless 'it's nearly finished' and then me explaining to them what was left to be done, to them, who have left chemistry years ago. The staff at St. Mary's College, particularly Bryn, who lent me their support whilst I was both teaching and PhDing at the same time, and the classes whom I taught, particularly my Year 10 (now Year 11 class of 2007) classes both of whom gave much colour to my time there (by request Sam and Izy wanted a specific mention – well girls here is it, as promised!).

I would very much like to thank all the members of SonRise Church, particularly Pastor Mary, who have continually supported me, most importantly in prayer during my entire time at University.

This leads me to the most important thank you. I entered into this PhD without thinking to ask my Heavenly Father whether this was the path He wanted me to take. In spite of that, from the very first day when I cried out to Him because it was all going wrong, He has lovingly taken care of me. He surrounded me with the best colleagues, family and friends I could hope for and blessed me with success when I was least expecting it. He has remained completely faithful and utterly constant in my life which has undergone several quantum leaps of change during this time. It is to Him that I ultimately owe my talents in this subject and the people who have supported me in achieving what I have in this work.

It is to Him that any glory from this Thesis rightly belongs, and I pray that He blesses me in the next chapter of my life as much as He as in this one.

Volume 1

Chapter 1

An introduction to Liquid Crystals

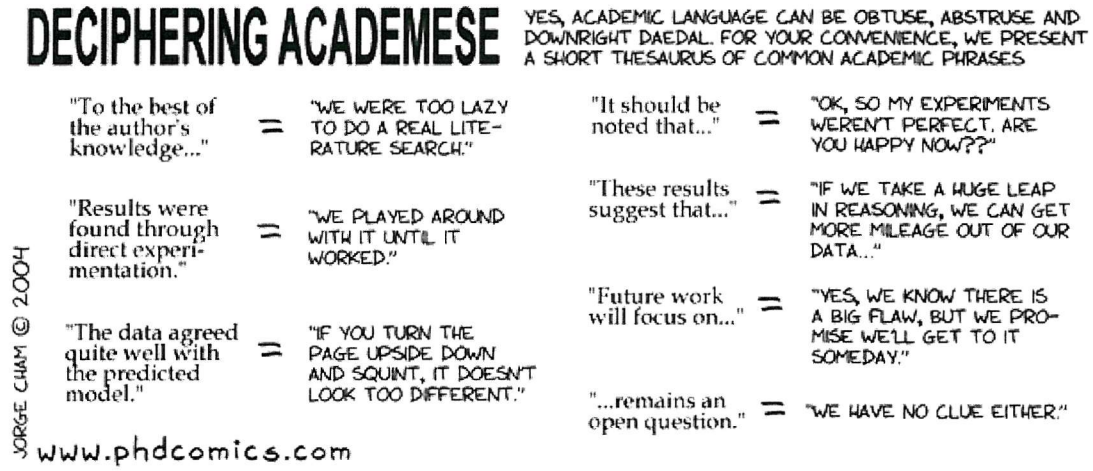

"Piled Higher and Deeper" by Jorge Cham
www.phdcomics.com

Used with permission

1. An introduction to liquid crystals

1.1. Liquids that are crystalline or crystals that flow?

We live in a world where liquid crystal based technologies have become an integral part of human life. They have spawned highly profitable markets not only in display applications but also in pigments, dyes and paints, colour changing thermometers and optical wave guiding in telecoms, the result of which can be seen in the plethora of different devices used in every day life. Yet to say that liquid crystals are a fundamental part of human life would be no exaggeration. They are present in biological cell membranes as a solution of phospholipids in water and without these liquid crystal phases, some of the complex essential biological functions would not occur thus we, and all other life on Earth, would not exist.

Liquid crystals can be broadly placed into two classes, thermotropics and lyotropics. Thermotropic liquid crystal phases respond to changes in temperature and are primarily seen in the wide variety of display devices currently on the market. Since these technologies are both popular and easily obtainable, thermotropics are often inaccurately perceived as the most commonly encountered type of liquid crystal.

Lyotropic liquid crystal phases are generated from dissolution of amphiphilic molecules in a solvent (which is normally water) and are dependent on changes both in temperature and concentration. These lyotropic phases are formed when surfactants are used, for example, they form in the residue of soap and water in soap dishes and it is these types of liquid crystal which are found in cells and so are essential to life. This Thesis will be concerned exclusively with thermotropic liquid crystals and specifically, to their potential use in novel display devices.

Liquid crystals were first observed in 1850 when myelin was mixed with water. Myelin comes from the sleeve that protects nerve cells and forms a lyotropic liquid crystal phase; however their significance was overlooked and so the discovery of liquid crystals is normally attributed to Friedrich Reinitzer in 1888.[1] When, examining cholesteryl benzoate, he noted that it had two melting points. The first was at 145.5 °C, melting from a solid to a cloudy liquid and the second at 178.5 °C where the cloudy liquid cleared. After satisfying himself that the material was pure, Reinitzer enlisted the help of Otto

Lehmann, a professor of natural philosophy in Germany. Lehmann had constructed a polarising microscope with a heating stage of reliable accuracy with which he could observe these materials under controlled conditions. He first referred to these materials as 'soft crystals' and then 'crystalline solids' but after examining many other similar samples, he became convinced that the opaque phase he was observing was a homogenous phase of matter which shared some of the properties of both liquids and crystals hence he christened them 'liquid crystals'.[1]

1.1.1. What are liquid crystals?

It is important to note that when we consider 'liquid crystals' we are actually considering a large group of materials which all exhibit a liquid crystal phase at a given temperature, pressure and/or concentration.

For centuries man has been aware, if only on a practical level, of the three common states of matter: solid, liquid and gas. Exploration of the physical behaviour of these states has shown that the physical form of any pure material can be controlled by temperature and pressure. However, liquid crystals represent a fourth and very different physical state exhibiting certain properties of both the solid and liquid phases.

At the molecular level, particles in a crystal are fixed on a lattice and have long range orientational and translational order. Orientational order can only exist if the particles are anisotropic (literally meaning 'not the same in every direction') which means we can consider such particles to be primarily a rod or disk but there are variations (sometimes quite extensive) on that basic shape. In the crystal, particles may possess a number of properties related to the orientationally ordered anisotropic constituents, but cannot flow like a fluid. In a liquid, particles have only short range translational or orientational order and are continually flowing and tumbling. In this state any bulk property relating to the anisotropy of the particles is lost and so the liquid can be described as isotropic.

If the crystalline and liquid states of matter can be thought of as two extremes of translational and orientational order, liquid crystal phases occupy a position somewhere between these two extremes (hence the term 'mesophase').

However to best understand why liquid crystalline phases form we first must look at how we describe other changes of state in relation to the moleular interaction. Regardless of

how chemists and physists choose to name and describe the nature of the forces which hold molecules together, they are all types of intermolecular force. These forces exist in a variety of forms but chiefly depend on the size (and sometimes the direction) of the attraction (or repulsion). When the distance over which the force is experienced is taken into consideration this gives an energy potential which describes the energetic stability of a molecule (or atom) as it approaches another. At long range the force is relatively small and attractive and at very short range the force is large and repulsive. There is a region where the distance is close enough for the attractive forces to be significant but far enough away for the repulsive forces to be sufficiently small to allow an energy stability well. This can be described in a Lennard-Jones (LJ) potential (see Figure 1.1 and Equation 1).[2]

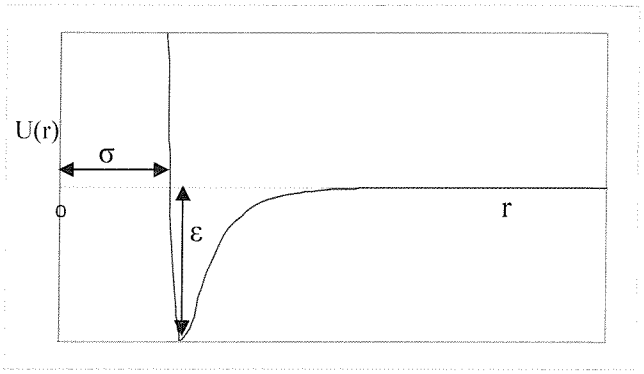

Figure 1.1 Lennard-Jones potential plot where the potential energy, U(r) is plotted against distance (r) to hard sphere radius. r is the separation distance of the two atomic or molecular centres, ε describes the depth of the energy stability well at the equilibrum bond length and σ is the hard shell limit of the two atoms corresponding to U(r) = 0 for the smallest value of r.

The potential energy is given as

$$U(r) = 4\varepsilon\left[\left(\frac{\sigma}{r}\right)^{12} - \left(\frac{\sigma}{r}\right)^{6}\right], \qquad (1)$$

where r, ε and σ are defined in Figure 1.1. The nature of the molecular interactions will depend on the size of the energy well ε. An increase in thermal energy in the system will eventually act to overcome this attractive force between molecules, breaking up a lattice in a crystal or causing the particles in a liquid to escape as a gas.

If we describe this thermal energy as k_BT, then crudely we could say that when $\varepsilon > k_BT$, the material will be a solid. When $\varepsilon \approx k_BT$ then the material would be liquid and in the case when $\varepsilon < k_BT$ the material would be gaseous.

To apply this to the case of liquid crystals we must take into consideration the anisotropy of the moleules when considering the LJ potential. Until r_0 is reached, the closer the molecules get, the larger the attractive forces between them. Therefore the orientation of one molecule to the next becomes critical to minimise the potential energy. If the situations where cylindrically symmetric molecules are (a) parallel and (b) perpendicular are considered (see Figure 1.2), the LJ potential diagrams would show that the aligned state is more energetically favourable.

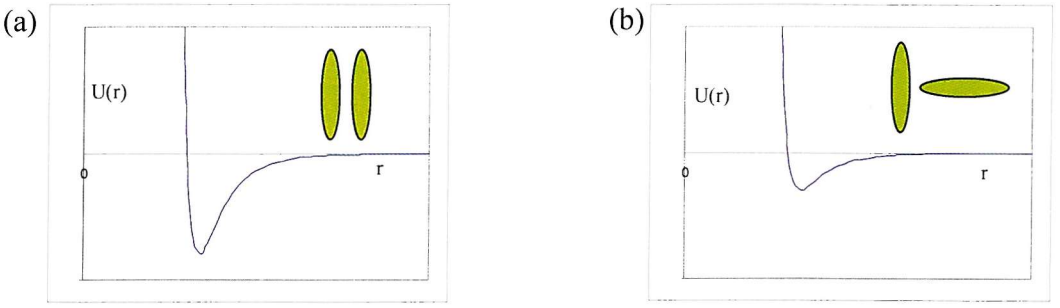

Figure 1.2 Sketch of potential curve for anisotropic molecules (a) parallel and (b) perpendicular.

Thus changes in both the orientation of the molecules and the translational position will result in different liquid crystalline phases. As noted already, when the thermal energy is large enough to overcome all energic penalties associated with destroying the orientational order, the liquid becomes isotropic.

If we take the approximation that $\varepsilon \approx k_B T$, we can see that only relatively small energies would be needed to alter the liquid crystal phase or indeed to turn the material isotropic in comparison to melting or boiling the material. It is therefore not hard to see that only subtle changes in the molecular design (and hence intermolecular forces) can radically change the properties of the liquid crystal. The temperature range where the phase is liquid crystalline can be defined as lying between two distinct points. The first is the temperature at which the thermal energy overcomes the intermolecular forces holding the crystal together and the second corresponds to the energy that causes the orientional order in the liquid crystal to break down.

Finally, it should also be noted that if the energy of fusion (to melt the sample) is also large enough to scramble any orientational order, the material will melt into an isotropic phase regardless of the molecule being anisotropic in shape (although in some cases if the material is supercooled below the melting point, a phase can be observed). In these cases

the liquid crystal phase is said to be monotropic. When the liquid crystal phase persists above the melting point the phase is described as enantiotropic.

1.1.2. Ordering in liquid crystals

If the existence of order within a liquid crystal defines the phase, it is important to be able to quantify and thus measure the degree of order within the phase. The orientational order parameter, S (see Equation 2), is commonly used as a measure of order of liquid crystals. This is related to the orientational ordering of the molecules in relation to the direction in which they are on average pointing, which is called the director, $\hat{\mathbf{n}}$.

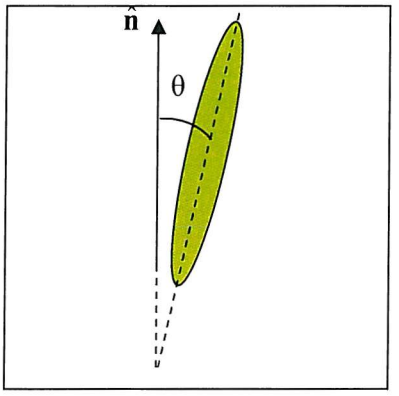

Figure 1.3 An ideal liquid crystal molecule – a rigid and cylindrically symmetric shape (shown in green) at an angle, θ, to the director $\hat{\mathbf{n}}$.

The degree of order is taken as the average of a function of the angular deviation (θ) of the mesogen molecular axis from the director (see Figure 1.3) and is normally expressed as the average of the second Legendre polynomial;

$$S = \langle P_2(\cos\theta) \rangle = \left\langle \frac{3\cos^2\theta - 1}{2} \right\rangle, \qquad (2)$$

where S is the order parameter, $P_2(\cos\theta)$* is the second Legendre function.

The limiting value for S is zero for an isotropic liquid and $S = 1$ for a perfectly aligned liquid crystal (e.g. aligned by an external field) or a crystalline solid. The order of a liquid crystal falls between these two extremes in the range $0.3 < S < 0.8$ however, at the

* Note this is the function for rods. The function for disc-like mesogens, where the director is perpendicular to the long axis, uses sin θ instead of cos θ.

transition to an isotropic phase there is a discontinuous jump to S = 0 corresponding to a first order transition. The order can be determined by measuring one of a number of macroscopic properties including the optical birefringence, nuclear magnetic resonance and Raman scattering. Additional order parameters can be defined (e.g. $\langle P_4 \cos\theta \rangle$) however, these order parameters are harder to measure than S and consequently more seldom used. Since, a rod or disc has a plane of symmetry perpendicular to the director; any property of the molecule made at an angle θ to the director will be identical to that at (π – θ). Thus it is true that for any Legendre polynomial (P_L)

$$P_L(\cos\theta) = (-)^L P_L(\cos(\pi - \theta)). \quad (3)$$

Thus for odd functions the equation is equal and opposite in sign meaning that, when an average ensemble is taken, the number of molecules at θ will cancel those at (π – θ) of which there will be the same number. As such the odd Legendre polynomials are not relevant as they average to zero.

1.1.3. Liquid crystal phases

Thermotropic liquid crystals exhibit a wide range of different phases. These phases are defined by the degree and type of orientational order (which defines the phase as liquid crystalline) as well as translational order and position (which defines the smectic phases apart from the nematic phase). As the phase changes to the next, the properties of the material also change, sometimes radically. This is often best illustrated by polarisation microscopy, observing the change in optical texture of the liquid crystal viewed through crossed-polarisers as it forms a different phase. There are at least a dozen different types of thermotropic phase and, to qualify as a thermotropic liquid crystal, it is by no means necessary that a material should exhibit all possible thermotropic liquid crystal phases, indeed no such material is currently known. However, it is common for a material to exhibit two or three phases although this does depend on the molecular building blocks used to construct the molecules as to what phases are stabilised (see Section 1.2.1). The phases encountered in this Thesis will now be briefly discussed.

1.1.3.1. Nematic (uniaxial) phase

The liquid crystal phase which is the simplest and most disordered is the nematic phase

denoted by the letter N. Nematic literally is Greek for 'thread-like' and the phase is so called because when it is viewed through a crossed polarising microscope there are often dark lines observed which resemble threads. These are defects in the orientational organisation of the director and are called disclinations. These disclinations can be regarded as rapid changes in the director over a small area in the sample and the darkness corresponds to where the director is parallel to one set of cross polarisers in the microscope. If we regard the director changing in either a circular fashion or a parabolic fashion, we obtain the patterns typically seen in the nematic (Figure 1.4).

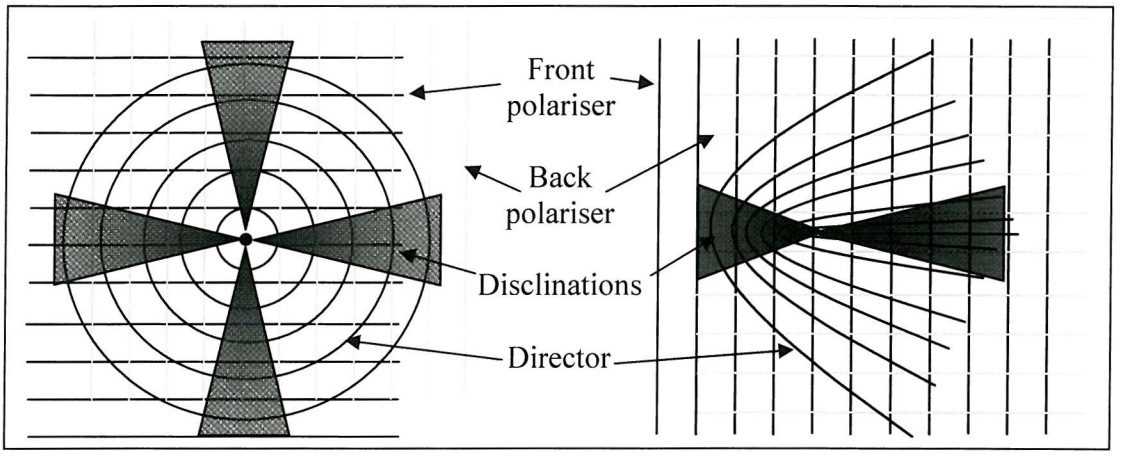

Figure 1.4 Two or four stranded crosses normally referred to as two or four brush defects forming as a result of rapid director change. This often occurs most readily close to the nematic-isotropic transition.

This characteristic pattern is referred to as a schlieren texture (see Figure 1.5).

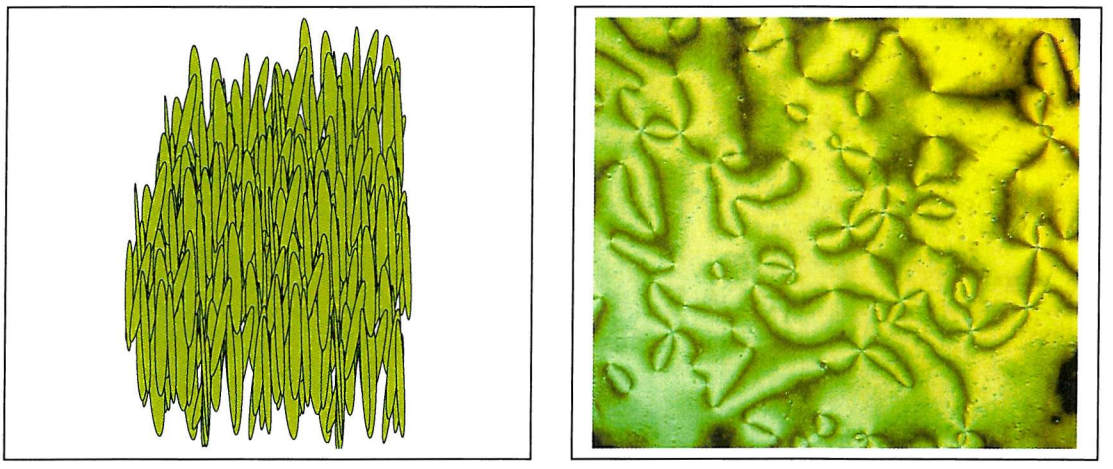

Figure 1.5 (left) Showing a highly ordered arrangement of rods which would give rise to a nematic phase. (right) an example of a nematic phase seen under a cross-polarising microscope; a characteristic schlieren texture exhibiting a variety of two and four brush defects.

For the sake of simplicity it is convenient to describe the nematic in terms of cylindrically symmetric rods which point approximately in one direction which we would call the director (see Figure 1.5). The reality is of course that real molecules are not cylindrically symmetric. Many deviate from this ideal to a considerable extent, so to define the director by the direction in which non-uniform molecules point would be ambiguous, if not impossible. Therefore it is better to describe the director based on properties related to the symmetry of the phase and so, for a uniaxial nematic, the phase has a symmetry (which in this case *is* cylindrically symmetric) about the director. So, if a tensorial property (one which operates on a vector) of the phase is considered, it will have a symmetry axis which will point in a given direction, and thus the director can be defined by this.

Although the nematic has orientational order there is no long range translational order and hence nematics characteristically have an order parameter of $S \approx 0.3$ at the N-I transition.

Being the least ordered, nematics often flow freely and normally have a lower viscosity compared with other phases. However, viscosity in liquid crystals is not just related to ease of flow but this will be covered more fully in Section 1.2.4.

1.1.3.2. Smectic phases

The next degree of order seen in liquid crystals is where the molecules, whilst still approximately orientated parallel to the director, arrange themselves into layers which are perpendicular to the director. The name smectic meaning 'soap' was given to the phase because the mechanical properties of these phases were, to early researchers, reminiscent of soaps (It is perhaps ironic that the name 'smectic' is not given to any phases in lyotropics which are the type of liquid crystal phases soap scum actually forms!).

The smectic phases represent the next level of ordering in the liquid crystal where orientational order is still essential but translational order is now also present, thus defining the difference between nematic and smectic phases. This translational order can also be quantified as

$$\tau = \left\langle \frac{\cos 2\pi z}{d} \right\rangle \tag{3}$$

where τ is the degree of translational order, (as with S, $\tau = 1$ for perfect order and $\tau = 0$ in

an isotropic liquid), z is the position along the layer normal and d is the thickness of the layer.

There are a wide range of different types of smectic phase designated by a letter A-I which relates not to their degree of order but rather the order in which they were identified as a discrete phase. This process of identification is not always trivial, especially if the optical texture seen by microscopy is ambiguous. These undetermined phases are often labelled smectic X.

The two examples described here are the smectic A, SmA, and smectic C, Sm_C, phases as they are the only examples of smectics relevant to this Thesis.

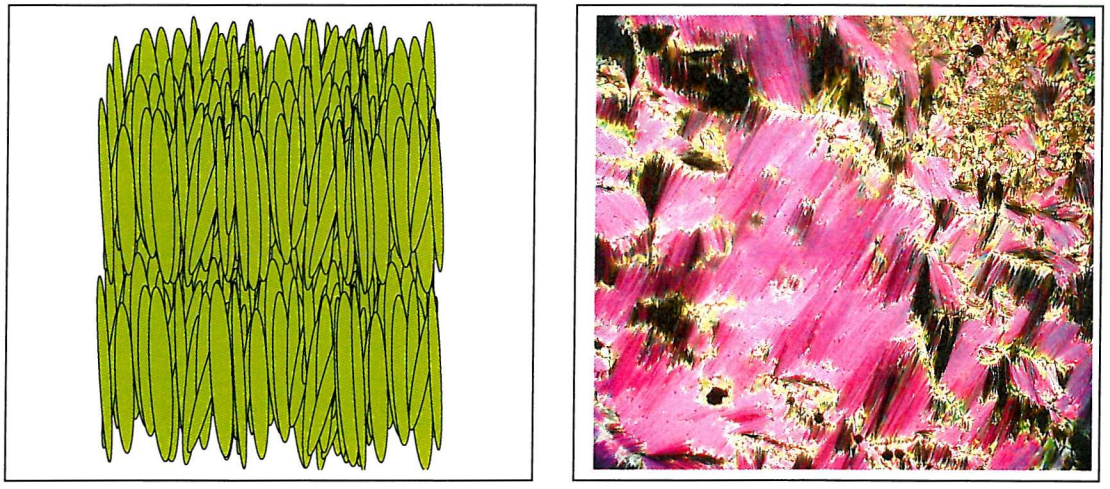

Figure 1.6 (left) Showing an arrangement of rods in layers which occurs in a smectic A phase. (right) An example of a smectic A phase seen under a cross-polarising microscope with its characteristic focal conic texture.

The smectic A phase is the most disordered of the smectic phases and is simply a layered form of the nematic. The translational position of any molecule within a layer bears no relation to the translational position of any molecule in any other layer or within the same layer. The director points along the layer normal as shown in Figure 1.6. The two and four brush disclinations of the nematic are lost and the characteristic texture given by smectic A phases is the focal conic. Smectic phases are generally much more viscous then nematics and even smectic A phases tend to take minutes to flow compared with normal nematics which take a fraction of a second. As a result in many cases after alignment of the smectic phase using, for example, an electric field, the smectic phase

will retain (remember) its aligned structure after the field has been turned off. This memory property has been used in data storage devices .[3]

Smectic C phases are very similar to their smectic A counterparts except that the director within each layer is tilted with respect to the layer normal (Figure 1.7).

The tilt is the defining characteristic of the smectic C and can be monitored up to the phase change as temperature increases. The nature of the change with temperature depends on the phase which follows. When a smectic C is followed by a nematic, the transition is first order. Therefore there is little change in the tilt angle with temperature and a discontinuous transition at the phase change. Where the smectic C moves to a smectic A, the transition is second order and the change in temperature causes a continuous change in the tilt angle up to the phase change.

Figure 1.7 (left) Showing an arrangement of rods tilted in layers characteristic of a smectic C phase. (right) an example of the optical texture from a smectic C phase seen under a cross-polarising microscope showing both a schlieren texture and a broken focal conic texture.[1]

When a smectic C forms from a smectic A phase, the optical texture tends to show a broken focal conic texture which can then give rise to a schlieren texture entirely composed of four brush defects. This is normally easily identifiable, however, in cases where the smectic C phase forms directly after the nematic, idenitification can sometimes be less trivial and the precise temperature of transition, ambiguous. In these situations homeotropically aligned cells can be used to identify the transition since these align the layer normal to the surface normal. The homeotropically aligned smectic C phase is birefringent (scatters light) allowing a texture to be observed in contrast to the nemtic,

which, under these conditions, does not. This obvious change in appearance allows straighforward assignment of the transition temperature of the phase.[4]

1.1.3.3. Chiral nematic phase

The effect of chirality on nematic phases is profound. There are two ways of introducing chirality into a liquid crystal sample. The first strategy employed was to build the chirality into the molecular structure of the rod. The first examples of this were the cholesteryl based liquid crystals first identified by Reinitzer in 1888 (cholesteryl units have many chiral centres) and, as such, these types of molecular subunits were often the chiral building block of choice (although there can be problems with chemical stability). The effect of chirality in nematics was so closely associated with cholesteryls that the phase was, in the past, commonly called a 'cholesteric phase'. This was misleading as any chiral molecule which can form a nematic phase has the potential to form a chiral phase and are thus described more generally as forming a chiral nematic phase (N*) with a characteristic finger print optical texture (see Figure 1.8).

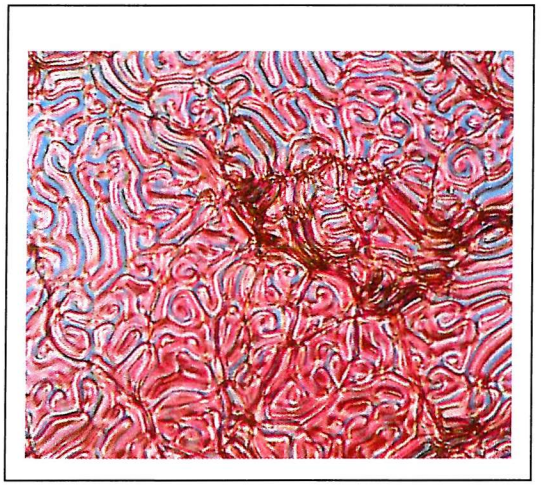

Figure 1.8 An example of the optical texture from a chiral nematic phase seen under a cross-polarising microscope.[1]

The effect of chirality on the nematic phase is very small, but over large distances (distances in nm compared with molecular dimensions in Å) the chiral environment causes the director to be rotationally offset by a small angle moving through the sample. The result is that, from a microscopic property, a macroscopic helical structure is formed by the director. The helix axis remains perpendicular to the director as it rotates through the sample. The pitch length of the helix (the distance travelled along the helix for the

director to rotate through 360°) is related closely to the temperature of the sample, the degree of chirality and the twist elastic energy of the sample (see Section 1.2.2 for explanation of elastic energy). Different microscopic enantiomeric handedness within the chiral molecules will generate a corresponding left or right handed macroscopic helix.

Making materials which are both liquid crystalline and chiral can be both synthetically difficult and expensive. However, it is possible to generate a chiral nematic phase using only 1-2 w/w% of a chiral dopant. This, the second method of forming chiral nematics, does not require the dopant to be liquid crystalline (so long as it is soluble in the nematic host) and is thought to provide an asymmetric environment which causes the non-chiral molecules to form a helical structure.

Understanding the helical structure of the chiral nematic can be difficult. A common solution is to either, trace the edge of the changing director to generate a helix, or, to take slices through the helix showing the director change (see Figure 1.9). The former can be misleading in that it begs the nonsensical question 'what is in the middle?', where as the latter can provide the idea of the helix being a layered structure. For practical purposes the helical rotation of the director is shown to be much more rapid than is actually the case. However, so long as these limitations are borne in mind, they are useful to generate a pictorial handle with which to understand various concepts relating to helical twisting in the director.

The periodic structure of the helix interacts with light, reflecting light beams of a wavelength which are determined by Bragg's law

$$\lambda = 2n(P)\cos\theta, \tag{4}$$

where λ is the wavelength, n an integer number, P is the pitch of the helix (sometimes given as Z) and θ is the angle the light makes with the helix.

If the sample is aligned so that the helix axis is parallel to the propagation of the light and if the pitch is of the same order as visible light, then colours are selectively reflected back. The pitch is temperature dependent and as such this property has given rise to colour changing thermometers, temperature sensitive inks[5] and paints (commercial car paints where the chiral nematic is polymerised causing the colour to change with viewing angle rather than on heating[6]) and is occasionally used in pigments by nature (e.g. the rose chafer beetle produces a lustrous green colour from the chiral nematic phase of the

chitin found in its outer shell[7, 8]).

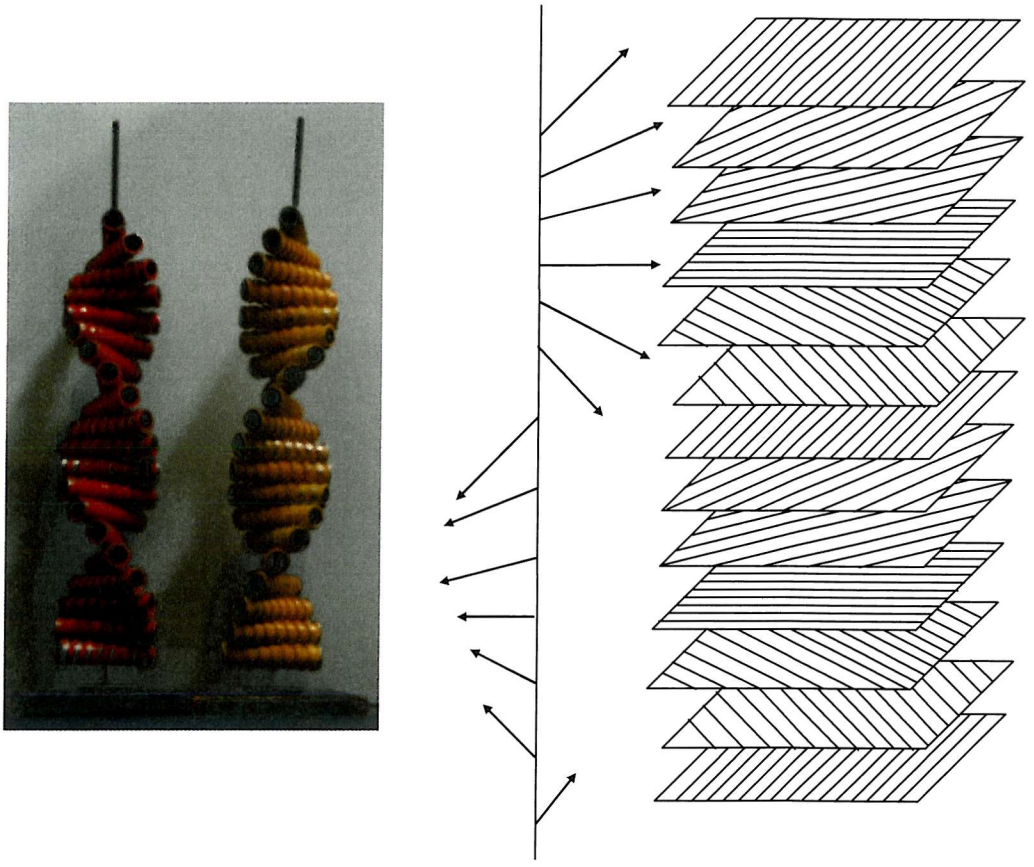

Figure 1.9 (left) Showing left (red) and right (yellow) handed helices. (right) Showing slices through the helix where the director would be pointing. It should be noted that this representation shows the director rotation occurring rapidly which is not the case in real systems where the rotation is only very slight moving along the helix axis.

Helical twisting in the nematic is essential to nearly all modern display devices since the helix is able to rotate plane polarised light as it travels down the symmetry axis for the refractive index of the helix (often the helix axis itself). This helical twisting can sometimes be generated by simply pinning the director between two plates of glass and physically twisting the plates (often used in twisted nematic displays), or employing the use of chiral nematics (e.g. super twisted nematic displayed). For a fuller description of the use of chiral nematics in display devices see Section 1.3.

1.1.3.4. Nematic (biaxial) phase

The term 'uniaxial' comes from the field of optics and describes a system where plane polarised light can only travel along one axis without the state of plane polarisation being

changed. When the sample is aligned this axis is the optic axis and corresponds to the director with all directions perpendicular being equivalent. This has a symmetry of $D_{\infty h}$. By contrast, a biaxial system has two optical axes and, when aligned, three directors, thus it can be characterised by a comparatively lower symmetry (for example, D_{2h}).

It is worth noting that there is a distinction between *molecular biaxiality*, where the symmetry of the molecule is at most D_{2h}, and *phase biaxiality* where the bulk phase itself reflects the lower molecular symmetry. For example, a typical molecule which exhibits a liquid crystal phase, 5CB, (see Figure 1.10) can be shown to be more board shaped rather than cylindrically symmetric and hence can be described as having molecular biaxiality.

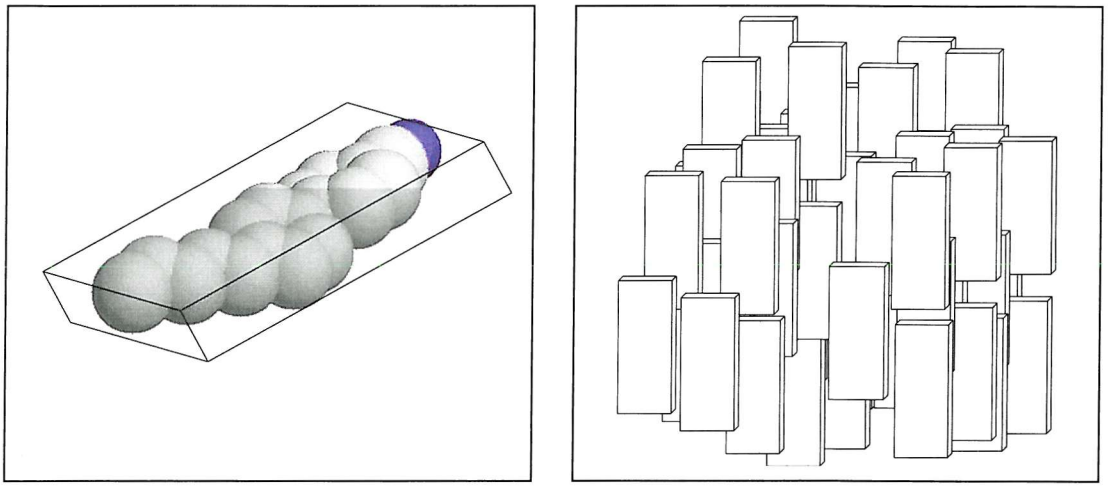

Figure 1.10 (left) Showing a typical nematogenic molecule with D_{2h} symmetry, 5CB. (right) an arrangement of lozenge shaped particles in a biaxial nematic phase.

However if these board shapes were able to be arranged in a way to reflect the molecular symmetry in the phase (see Figure 1.10 *right*) this would be described as having phase biaxiality. But in the case of 5CB, only a uniaxial nematic phase is ever observed.

From consideration of the shape of almost all molecules which give rise to nematic phases, it is clear that the molecules themselves are biaxial. Typically they are lozenge shaped cuboids with symmetry much closer to D_{2h} than $D_{\infty h}$. It was in 1970 that Marvin Freiser proposed that the reduced molecular symmetry should be reflected in the bulk by the formation of a new phase which he called a biaxial nematic (denoted by N_B compared with N_U for a uniaxial nematic)[9]. He predicted that such molecules, generally would form a uniaxial phase and then, at lower temperatures, a biaxial phase would form. It was also

suggested that the biaxiality of the molecule stabilised the biaxial phase with respect to the uniaxial phase until, at some critical maximum point (the Landau point) the isotropic phase made a transition directly into the biaxial nematic phase.

Biaxial nematic phases have been observed in lyotropic[10] and possibly polymeric systems;[11] however, the search for the biaxial nematic phase in thermotropic liquid crystals has been likened to the quest for the Holy Grail,[12] much tried but sadly unsuccessful. There is perhaps the recent exception of some V-shaped molecules made and investigated by Madsen *et al.*[13] and tetrapodes examined by Mehl *et al.*[14] The numerous 'crusades' in this field have, however, refined the process of identification of the biaxial nematic. The original methods of identification involving microscopy and conoscopy have shown themselves to be better used as indicators that a sample may be biaxial rather than a definitive test. Early claims of discovering biaxial nematics were apparently confirmed by these methods to indeed be biaxial only to be demonstrated later to be uniaxial by the more powerful technique of ^{2}H NMR spectroscopy.

The recent discoveries made by Madsen *et al* (see Figure 1.11)[13] appear to pass these definitive tests although the evidence for this is based purely on the NMR data and the results themselves are not ideal.

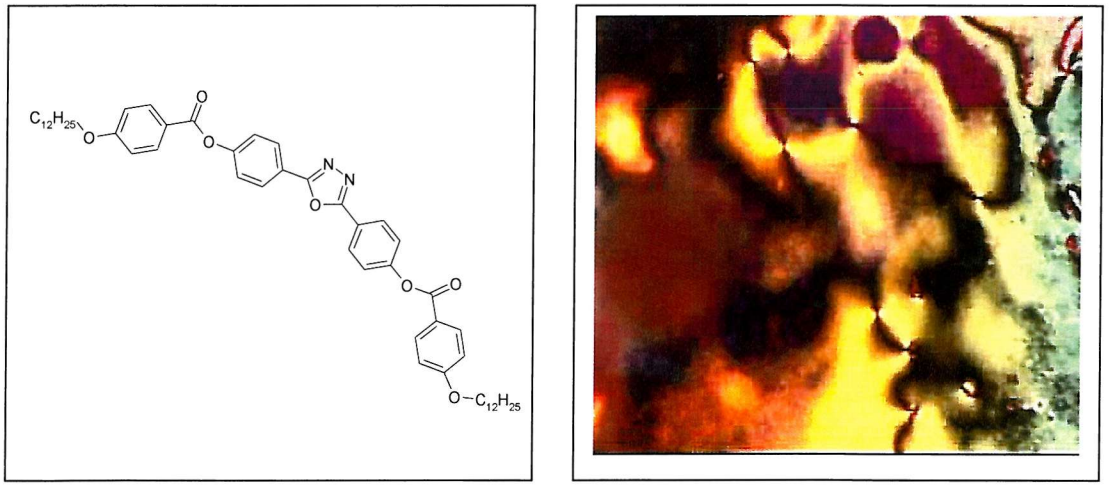

Figure 1.11 (left) Molecular structure of the compound. The recent claims to show a biaxial nematic by Madsen *et al.* (right) An example of the type of schlieren texture thought to be indicative of a biaxial nematic, dominated by two brush defects[13]

The case against this candidate is three fold. Theoretically, this shape of the material is wildly different to that predicted in theory (however this is not critical – theory can be

wrong). Experimentally, the value for the biaxiality is $\lambda = 0.1$ which, although non-zero, is small enough that it is probably within experimental error. Comparatively, a value of $\lambda = 0.6$ has been observed in lyotropic systems, six times larger than that observed for the thermotropic system. However extremely high melting points made measuring the biaxiality of the phase even more difficult. There is now interest in exploring this molecular motif with a view to lowering the melting point, allowing experiments to be performed more easily and confirm these early findings.

However there is clearly still much work to be done if this phase could, as hoped, be used in a new display device.[15] There is, however, still some doubt as to whether these new results have given birth to another red herring or whether it is the cup many hope it to be.

1.2. Properties of liquid crystals

When chemists first embarked upon the task of categorising liquid crystals, attempting to explain their wildly differing properties in terms of their molecular structure, they naturally turned to that which they were familiar with; intramolecular (e.g. conjugation) and intermolecular (e.g. dipolar) interactions generated by different chemical groups stimulated theories of molecular design which are still prevalent to this day. Compatible chemical moieties cause favourable interactions through conjugation or through supramolecular contacts which stabilise a given phase at a certain temperature. However, there is a view that molecular shape has been overlooked in the haste to explain molecular design by small group interaction. Clearly compatible groups do make a difference, but the effect of these groups (and their location) on the overall shape of the molecule must surely also play a vital role in the phase behaviour.

This section will briefly review some of these key properties; first by considering the effects of different chemical moieties on the stability of the nematic phase, followed by a brief overview of some of the bulk physical properties which can be measured.

1.2.1. Structure properties relations

The geometric motif discussed up until this point has been based mainly on a rod-like or disk-like structure. The focus of this section will be to develop this understanding with respect to molecular design, stabilising the nematic phase in particular. Increasing the stability of the nematic (increasing the temperature at which the nematic phase becomes

isotropic) and maximising the nematic range (increasing the temperature range over which the liquid crystal is a nematic) are just two key physical properties which can be favoured by proper molecular design. By looking at the wealth of materials already known to show liquid crystalline behaviour some patterns or general rules have been established.[1, 16, 17] The sheer range of molecular units makes only the briefest analysis possible and for this reason it shall be focused mainly on the types of moieties encountered in this Thesis.

At the simplest level of molecular design, liquid crystals can be thought of as consisting of four principle building blocks. These consist of one or more rigid mesogenic units, terminal units at either end, lateral groups on the side of the core and linking groups which separate the mesogenic units or link the cores to the terminal groups (see Figure 1.12). The linking group between cores will not be considered as it is not featured in any materials presented in this Thesis.

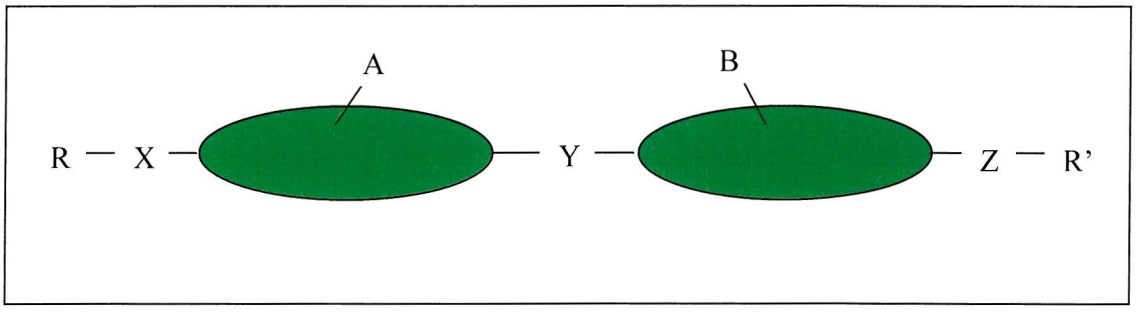

Figure 1.12 Schematic of the general structure of a mesogenic molecule. **A** and **B** are core units, **R** and **R'** are terminal groups, **M** and **N** are lateral substituents and **X**, **Y** and **Z** are linking groups.

The mesogenic units (A and B) are normally rigid structures which are almost always cyclic or bicyclic in nature. The most common example is a phenyl ring due to its stability and consequential ease of synthetic manipulation. The mesogenic unit is the most essential component of the molecule and it is possible, in a few reported cases, to use only this unit to generate a material with liquid crystal properties e.g. compound **1.**[18] As well as phenyl rings other aromatic cyclics have been used to great effect for example 1,3-pyrazole seen in **3**[19] and even non-aromatic groups such as trans-1,4-cyclohexyl seen in **4**[20] and 1,3-dioxane moieties seen in **2.**[21] These are a small cross section of a much larger range of potential moieties.[1, 17] In the given examples shown below and throughout the Thesis it will always be assume that temperatures for phase transitions are in °C, () will indicate a monotropic transition and [] a virtual transition.

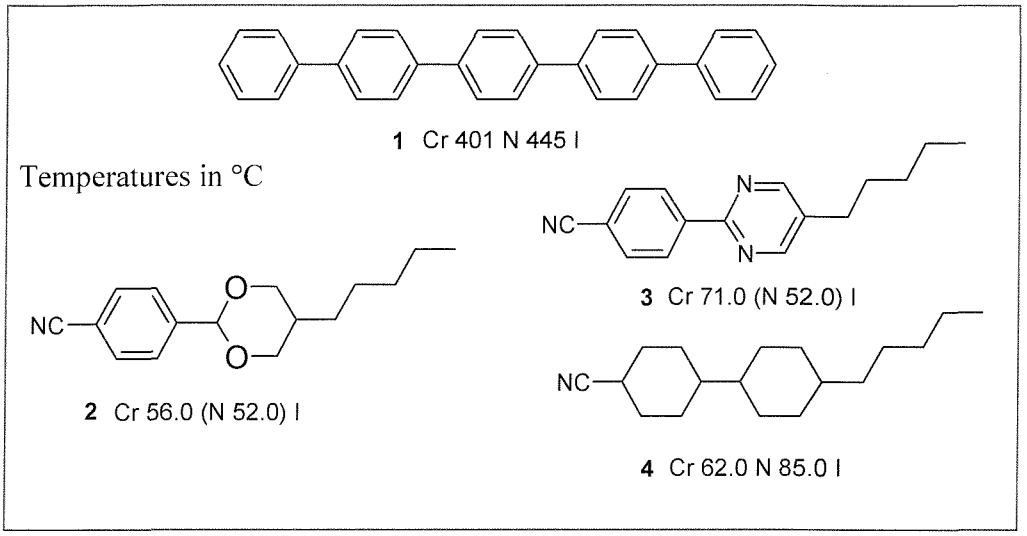

The effect on the liquid crystal phase of altering a mesogenic core can be seen by comparing analogous materials. In all cases this can only be done qualitively and with an appreciation of the molecular context. The molecular shape and chemical nature of the other parts of the molecule will alter to what extent changing a mesogenic unit will affect the phase stability. As a general rule, lateral intermolecular interactions and/or long

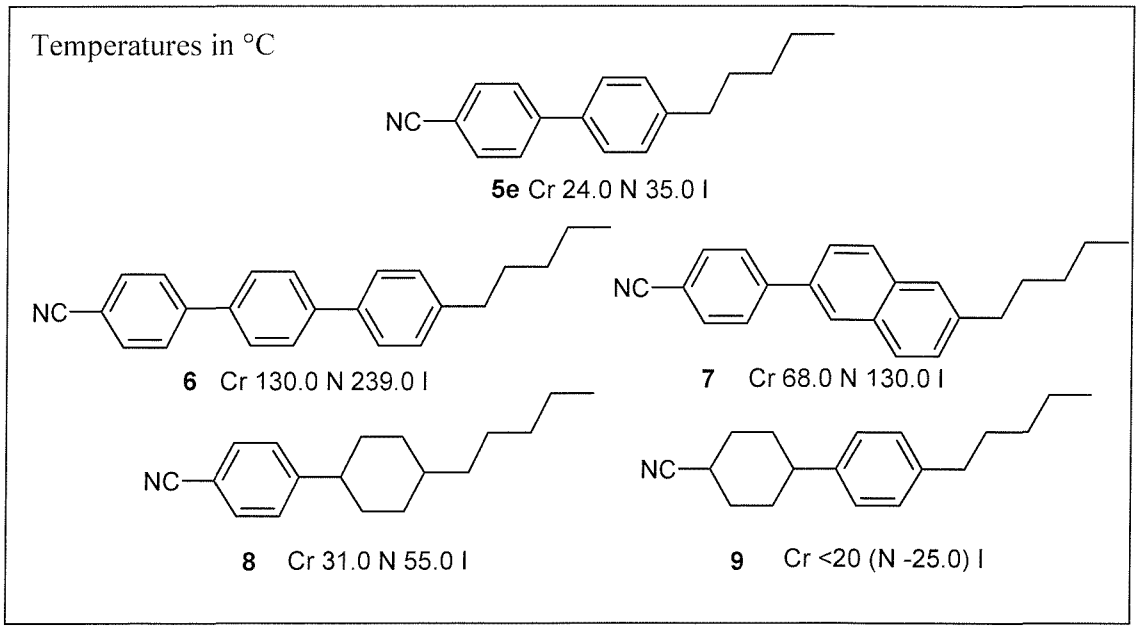

chain terminal groups will support a layered smectic phase, whereas disruption of these interactions and reinforcing a longitudinal dipole through the use of certain short terminal groups stabilises the nematic phase. Comparing the cores of compounds **5e**[22] to compounds **6-9** we see, firstly, that each of them is nematogenic. However, their nematic

range and stability vary wildly. Compound **5e**, commonly called *5CB* (*C*yano*B*iphenyl with a *5* carbon terminal group), was famously part of a series of compounds which, when used in mixtures, enabled the commercialisation of the first twisted nematic display devices which revolutionised the liquid crystal industry. One of the key features of 5CB was that it was a room temperature nematic liquid crystal. Extension of the core, as seen in compound **6**,[23] increases the melting point of the material but also vastly increases the nematic stability and hence nematic range. This is because the shape has been elongated, increasing the anisotropy of the molecule. Increasing the molecular length is an excellent way of increasing liquid crystalline stability and can even be done at the expense of broadening the molecule. As seen in compound **7**,[24] the napthyl group increases the molecular breadth but this is more than made up for by the increase in the length-to-breadth ratio. This stabilises the nematic phase and increases T_{NI} by nearly 100 °C with only a 35 °C increase in the melting point. Exchanging a phenyl for a cyclohexyl ring has a marked effect depending on which ring is exchanged. In the case of compound **8**[25] the nematic phase has been stabilised by 20 °C and the range slightly increased (although not as much as in **6** and **7**). However, if the phenyl adjacent to the cyano group is exchanged (compound **9**[26]) the melting point drops only slightly to below 20 °C whereas the T_{NI} falls over 60 °C! The role of the cyanogroup will be discussed later but its location next to the phenyl group is clearly important to the phase stability. This can be argued in terms both in terms of the conjugation to the phenyl group, and the difference in shape due to the location of the cyclohexyl ring. Using a mixture of phenyls and cyclohexyl units in the core also promotes nematic phase stability over smectic phases as the mixture of incompatible cores (aliphatic and aromatic) disfavours lamellar smectic arrangement. Although this effect could not be seen where all the materials were nematogenic, the result are marked in compounds **10**[27] and **11**.[28]

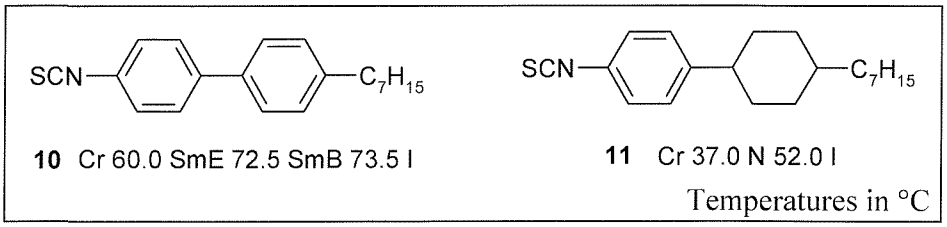

10 Cr 60.0 SmE 72.5 SmB 73.5 I

11 Cr 37.0 N 52.0 I

Temperatures in °C

There are a wide variety of terminal groups which can be used to enhance the liquid

crystalline phase. Through the wide range of materials available it has been possible to construct an order of terminal groups which decline from those which stabilise the nematic phase the most to those which do the least.

This order is: Ph>$NHCOCH_3$>CN>OCH_3>NO_2>Cl>Br>$N(CH_3)_2$>Alkyl>F>H.[16]

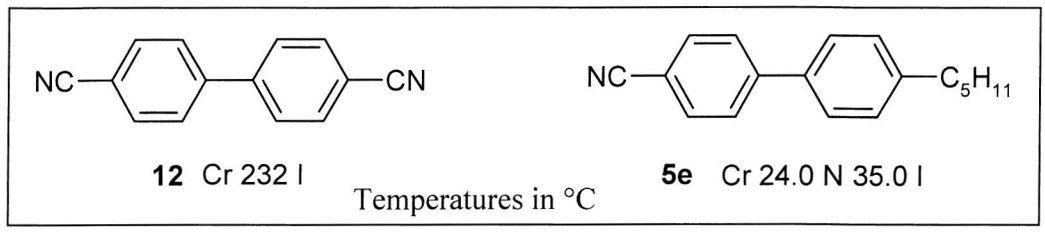

Adding a phenyl group could of course be regarded as extending the core by one more ring but in the case of the other groups, often one of these terminal groups is used in conjunction with an alkyl chain on the other end. The function of the alkyl chain is to lower the melting point (and to some extent increase the molecular length). The effect of polar groups such as CN on both sides is often to increase the melting point so much that the nematic phase is completely hidden, c.f. compound **12** with **5e**.

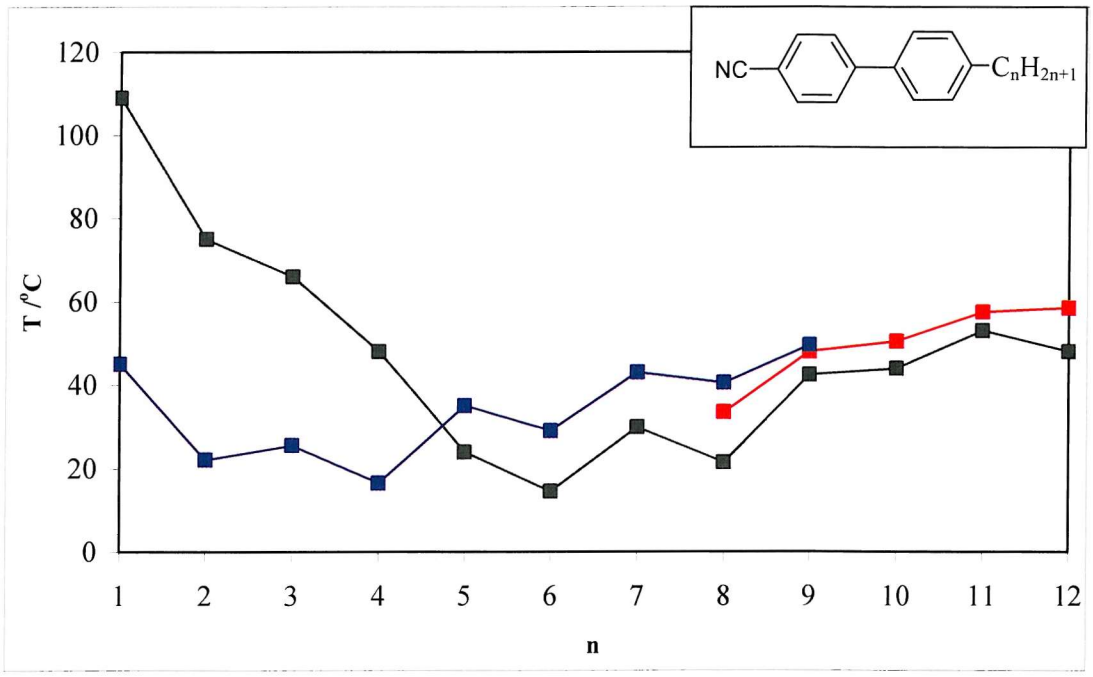

Figure 1.13 Showing graphically the odd-even effect in the nCB series. Here ■ denotes Cr-I, Cr-N, Cr-SmA; ■ denotes SmA-N and SmA-I; ■ denotes N-I.

The use of long chain alkyl groups or using them symmetrically on each end of a core

unit tends to promote smectic phases. This can be thought of as a "phase" separation of the different chemical moieties, which stabilises the lamellar smectic structure. By using an alkyl chain as a terminal group, a series of materials can themselves be generated by simply increasing the length of the chain. Looking at the nCB series (see Figure 1.13) we can see that, as expected, increasing the chain length promotes the nematic phase stability and lowers the melting point thus initially increasing the range.

Compound		chain length	Transition temperatures /°C							
No	Alkyl group		Cr		Sm_A		N		I	
5a	CH_3	1	•	109.0	-		•	[45.0]	•	
5b	C_2H_5	2	•	75.0	-		•	[22.0]	•	
5c	C_3H_7	3	•	66.0	-		•	(25.5)	•	
5d	C_4H_9	4	•	48.0	-		•	(16.5)	•	
5e	C_5H_{11}	5	•	24.0	-		•	35.0	•	
5f	C_6H_{13}	6	•	14.5	-		•	29.0	•	
5g	C_7H_{15}	7	•	30.0	-		•	43.0	•	
5h	C_8H_{17}	8	•	21.5	•	33.5	•	40.5	•	
5i	C_9H_{19}	9	•	42.5	•	48.0	•	49.5	•	
5j	$C_{10}H_{21}$	10	•	44.0	•	50.5		-	•	
5k	$C_{11}H_{23}$	11	•	53.0	•	57.5		-	•	
5l	$C_{12}H_{25}$	12	•	48.0	•	58.5		-	•	

Table 1.1 Showing the transitions for the nCB series. [ ] denotes virtual transitions below the melting point. ( ) denotes observed phases which are monotropic.[22, 23, 29]

This leads to the insurgence of a smectic phase (**5h**) which eventually dominates, becoming a more stable arrangement than the nematic thus displacing the phase altogether (**5l**). Another significant feature is the alternation of phase stability i.e. transition temperatures relating to whether there is an odd or even number of carbon atoms in the chain. This is called an odd-even effect and, if we consider the terminal chain in the all trans form, can be explained in terms of the odd number of carbons (considered in the all-trans form) increasing the molecular length thus stabilising the nematic phase or the even number of carbon atoms increasing the molecular breadth and length thus destabilising the nematic phase slightly. If we consider that the chain itself can occupy a variety of different conformations we can imagine that there are conformers which are disfavoured from a high internal energy (e.g. too many gauche links in the

chain) or are favoured by environmental stabilising effects. Exploring the latter, if we conduct a thought experiment where we take a variety of conformers supported in the isotropic phase and cool the bulk into an anisotropic phase, keeping the conformers unchanged, we would expect the more linear conformers to be supported in the phase. This would have the effect of effectively increasing T_{NI}. We find that for the even dimers, more linear conformers are energetically favourable and thus the effective increase in TNI in the thought experiment is applicable resulting in larger TNI for the even parity dimer. In the case of the odd, too many gauche links make linear conformers less favourable and so the benefit from the anisotropic environment is not significant (unless the system were sufficiently cooled such that these linear conformers were more favourable.

Linking groups are groups or atoms which can join terminal groups to a core or link cores together, the latter being beyond the scope of this discussion. Terminal linking groups can simply be a hetro atom (e.g. O or S) or a larger group (e.g. ester or ketone). The effect of the linking group depends very much on the nature of the core unit and the terminal group.

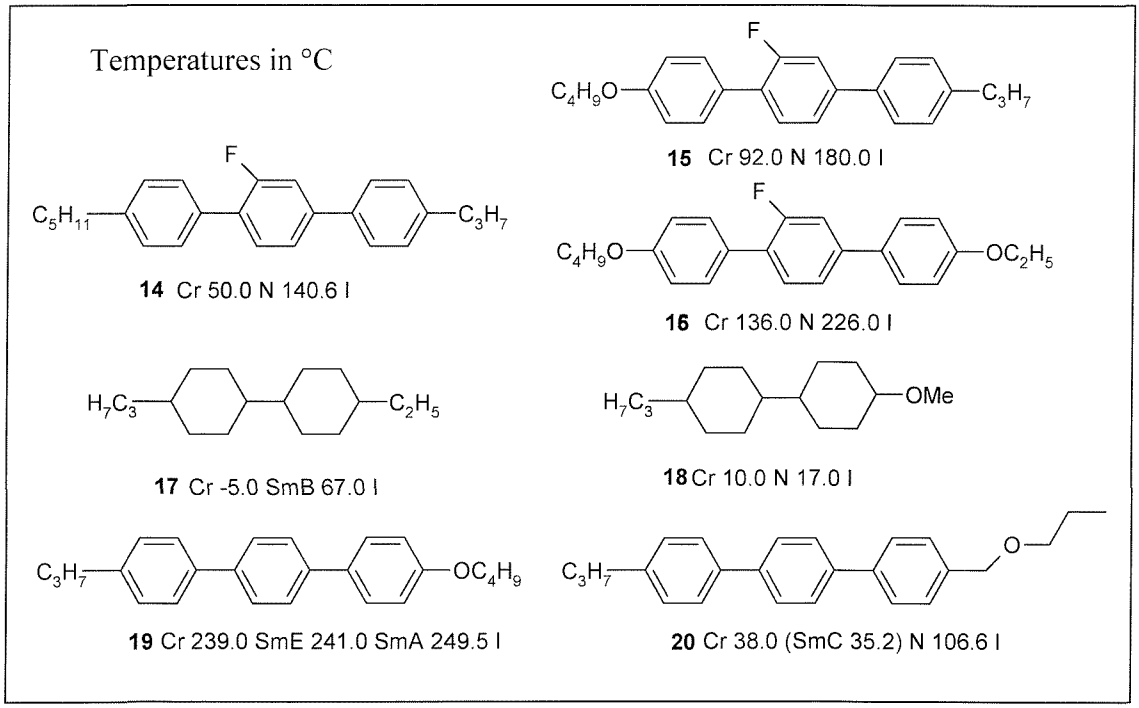

It can be shown that the effect of substituting a methylene group in the terminal chain

with an oxygen adjacent to the core stabilises the liquid crystal phase with only a moderate increase in melting point (compare compound **14** with **15** and **16**[30, 31]). Although this can be thought of as a result of conjugation to the aromatic core, the result can also be explained in terms of a subtle change in the shape anisotropy resulting in a large change in the transition temperatures. This would, therefore, explain when the core is aliphatic and conjugation cannot occur that introducing the oxygen disrupts the smectic B phase but stabilises the nematic phase slightly (compare compound **17** with **18**[31]). The effect of placing the oxygen in a position not adjacent to the core vastly lowers the liquid crystal phase stability and significantly hinders the formation of the smectic phase. The melting point is also significantly lowered thus increasing the liquid crystal range (compare compound in **20**[31] with compare compound **15** and **19**[31]).

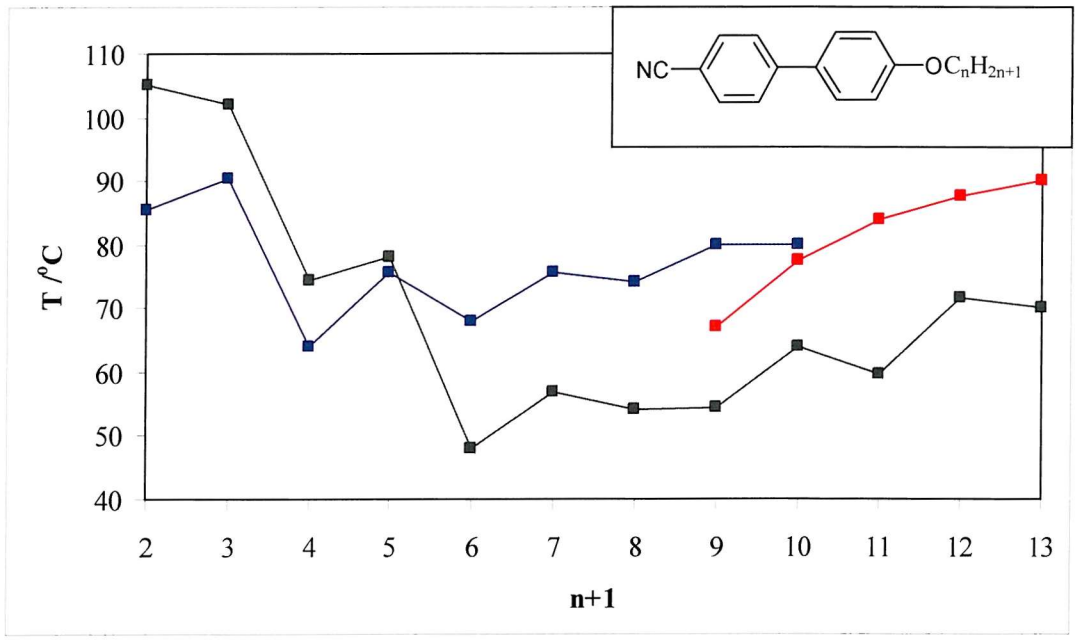

Figure 1.14 Showing graphically the odd- even effect in the nOCB series. Here ■ denotes Cr-I, Cr-N, Cr-SmA; ■ denotes SmA-N and SmA-I; ■ denotes N-I. To take into account the oxygen atom, the nOCB series is plotted on a n+1 scale to allow a fair comparison with the nCB series.

So, if we were to look at the series nOCB shown in Figure 1.14 (analogous to the nCB series in Figure 1.13), we see that the phase transitions (and melting points) are indeed higher for the nOCB series. The introduction of the smectic phase is delayed until n = 9 and the materials do not become exclusively smectogenic till n = 11. For comparison, 4-hydroxy-4'-cyanobiphenyl (constituting an n = 0 chain) has been included and shows no

liquid crystal character and a very high melting point due to hydrogen bonding.

Compound		Chain length	Transition temperatures /°C							
No	Alkyl group		Cr		Sm_A		N		I	
5a	OH	1	•	195.0		-			•	
5b	OCH_3	2	•	105.0		-	•	(85.5)	•	
5c	OC_2H_5	3	•	102.0		-	•	(90.5)	•	
5d	OC_3H_7	4	•	74.5		-	•	(64.0)	•	
5e	OC_4H_9	5	•	78.0		-	•	(75.5)	•	
5f	OC_5H_{11}	6	•	48.0		-	•	68.0	•	
5g	OC_6H_{13}	7	•	57.0		-	•	75.5	•	
5h	OC_7H_{15}	8	•	54.0		-	•	74.0	•	
5i	OC_8H_{17}	9	•	54.5	•	67.0	•	80.0	•	
5j	OC_9H_{19}	10	•	64.0	•	77.5	•	80.0	•	
5k	$OC_{10}H_{21}$	11	•	59.5	•	84.0		-	•	
5l	$OC_{11}H_{23}$	12	•	71.5	•	87.5		-	•	
5m	$OC_{12}H_{25}$	13	•	70.0	•	90.0		-	•	

Table 1.2 Showing the phases and transition temperatures. ( ) denotes temperatures observed phases which are monotropic. [22, 23, 29]

Where the core is aromatic, use of an oxygen atom conjugated to the aromatic ring has the result of increasing the molecular length (due to the COC bond angle being larger than the CCC bond angle) and can stabilise the nematic (compare series **5a-l** to series **13a-m** Figure 1.14) by as much as 60 °C. However, it should also be noted that the longer the chain, the lower the degree of stabilisation. Also, when making comparisons between the series, the linker atom should be included in the atom count of the terminal chain. Thus the transitional behaviour of 4OCB (4 + 1 atoms) should be compared to that of 5CB.

The introduction of the oxygen linker also raises the melting point but by an appreciably smaller amount. Compared to the increase in the N-I transition, linking groups to terminal chains which have wider internal bond angles with a tendency to conjugate to an aromatic core would be generally expected to stabilise the nematic phase. Therefore we would expect placing an ester group next to an aromatic system would also stabilise the nematic. However, this often increases the melting point more than a simple oxygen linker.

Finally, lateral groups by their very location will be generally destabilising to a liquid

crystalline phase. However, their purpose is often to place an off-axis dipole or some disrupting group to lower the melting point. Different liquid crystals will be affected by lateral substituents in different ways depending on the nature of the liquid crystal substrate, the type of lateral group and its location. Thus there are examples where introducing fluorine atoms can produce/enhance a smectic phase (compare **21** and **22**[32]) or completely disrupt it (compare **23** and **24**[30]) leaving a nematic phase.

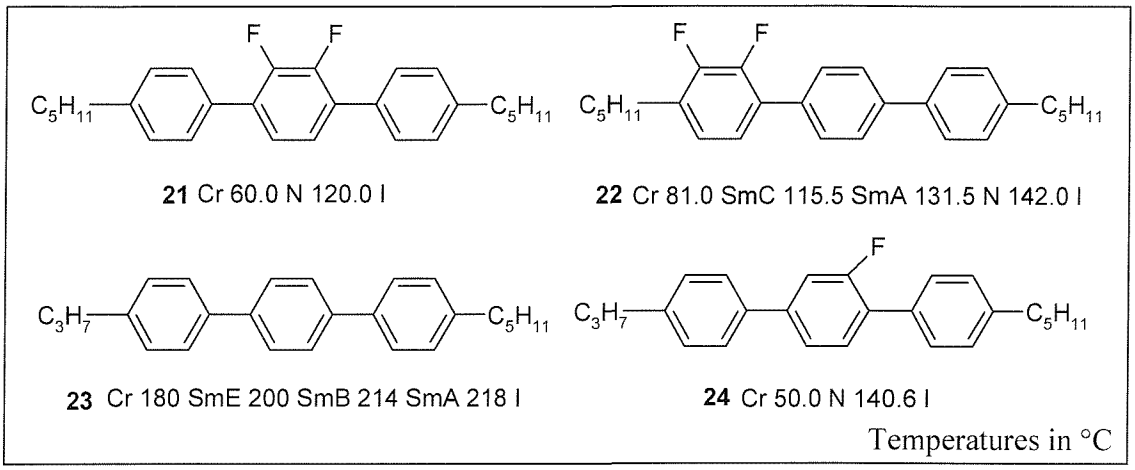

Fluorine atoms are often a favoured (although by no means the only) group as they are highly polarised but are only slightly larger than a hydrogen atom (C-F has an interatomic distance of 1.47 Å compared to C-H of 1.20 Å). Thus the melting point of a material can be reduced or the smectogenic nature of a material can be enhanced or removed with only limited impact on the length-to-breadth ratio. Such groups can also be used to alter the overall dipole moment in the material.

So far our discussion has been restricted to materials with only one mesogenic core unit. It would, of course, be possible to tether two (or more) cores with some sort of molecular spacer group. Rigid chain units (polyacetylenes or polyvinyls) have the effect of raising the melting point by such a large amount that the liquid crystal phase would be lost. Therefore the spacer is almost always a flexible polymethylene (or less commonly a polyoxymethylene) chain composed of between 3 and 12 carbon atoms long (Although shorter[33] and much longer[34] spacers have been used). Although it would be possible to construct a simple schematic for these compounds (similar to Figure 1.12 for monomers), the variety of possibilities would render it unhelpfully complicated for this level of discussion. Since a liquid crystal with one mesogenic core could be thought of as a

monomer, when two mesogenic units are connected together these are commonly called liquid crystal dimers, bis-mesogens or bimesogens. For the sake of continuity this Thesis will always refer to such compounds as liquid crystal dimers. Naturally if two mesogenic moieties can be linked together, three such units tethered together would constitute a trimer etc. There is sometimes debate as to what constitutes a 'dimer' or a 'trimer'. To avoid confusion later, a trimer will be defined here as containing 3 units which are capable of sustaining a liquid crystal phase if observed individually as a monomer with one or more terminal long chain tails. Thus **25** [**25**^{a4}, **25**^{b35}]† would be considered a trimer whereas **26**^{35} would not.

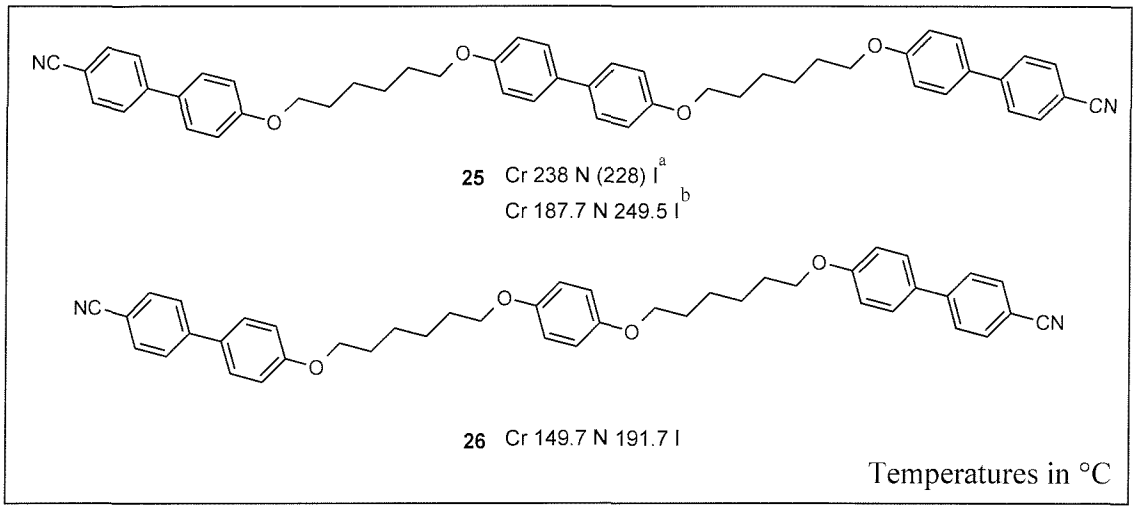

In general, the effect of chemically altering the mesogenic unit or changing the number of carbons in terminal chains tends to mirror the effects described previously for conventional monomeric liquid crystals. However, based empirically on their shape, it would be expected that these materials would behave quite differently to their monomer counterparts and this is certainly the case.

Comparing the T_{NI} of a monomer and a corresponding dimer (see Figure 1.15) shows that the nematic stability for the dimer is much larger (as expected since the molecule will be more rod-like) and the extent of the odd-even effect is much greater.

† Two materials (25^{a} and 25^{b}) made independently at different times published unknowing of the others existence. Material not available to be measured.

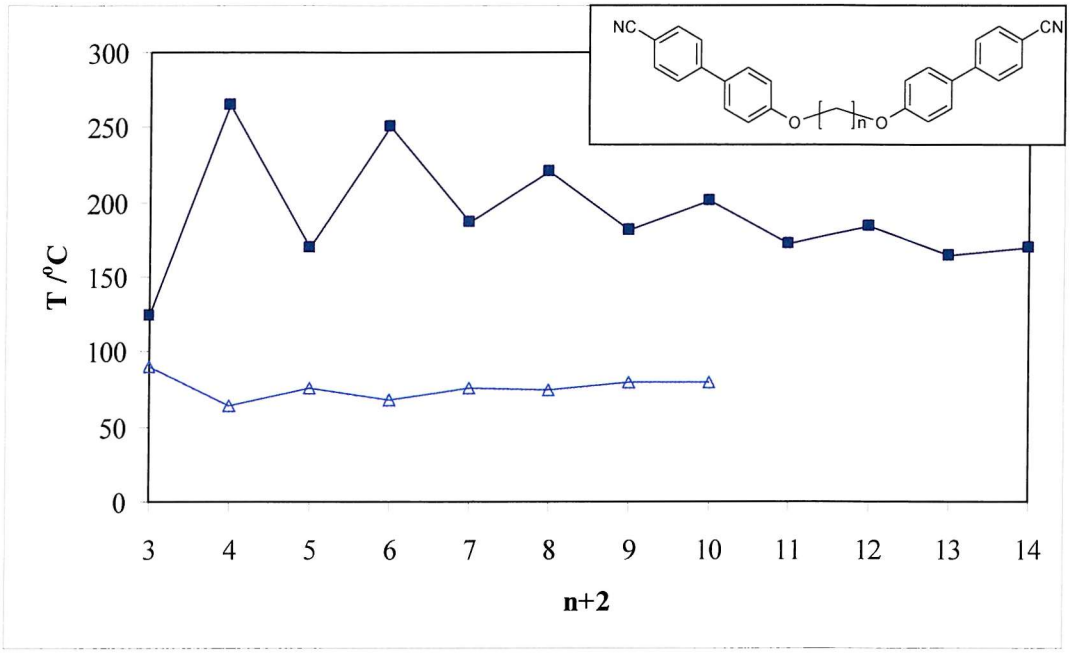

Figure 1.15 Showing graphically the pronounced odd- even effect in the CBOnOCB liquid crystal dimer series compared to the nOCB monomer series. Here ■ denotes T_{NI} for CBOnOCB and Δ denotes T_{NI} for nOCB.

Compound		Chain length	Transition temperatures /°C	
No	spacer		T_{NI} Dimer	T_{NI} Monomer nOCB
20a	OCH_2O	3	124	90.5
20b	OC_2H_4O	4	265	64
20c	OC_3H_6O	5	170	75.5
20d	OC_4H_8O	6	250	68
20e	$OC_5H_{10}O$	7	186	75.5
20f	$OC_6H_{12}O$	8	221	74
20g	$OC_7H_{14}O$	9	181	80
20h	$OC_8H_{16}O$	10	201	80
20i	$OC_9H_{18}O$	11	172	
20j	$OC_{10}H_{20}O$	12	184	
20k	$OC_{11}H_{22}O$	13	164	
20l	$OC_{12}H_{24}O$	14	169	

Table 1.3 T_{NI} transitions for symmetric oxygen linked cyanobiphenyl liquid crystal dimer series and the alkoxycyanobiphenyl monomer series. ( ) denotes observed phases which are monotropic.[33]

The nature of the odd-even effect in dimers has, in the past, been described in terms of the dimer drawn with the spacer in the all-trans configuration,[36] but the reality is that the

effect is more complicated.[37] It is true that in the case where the spacer has an even number of carbons the molecular rods at each end are antiparallel and hence the whole molecule is more rod-like whereas in the case of an odd number of carbons the rods are inclined and the overall shape is bent but this only considers the all-trans conformations (see Figure 1.16 (top)). In reality the spacer is flexible and can adopt a variety of conformations therefore a more realistic approach should appreciate that only a certain proportion of the molecules at any one time would be in the all-trans position. To a reasonable approximation the remaining conformations can be thought of as having one or more gauche links. The proportion of bent to linear dimers for both odd and even parities has been determined at T_{NI}[38] and from this we know that there are many more bent conformers in the case of odd dimers than for the even. Therefore we might expect that the odd-even effect in T_{NI} is related to the even dimers having more linear conformers and as such a higher T_{NI}. Analysing the even dimers, linear conformers are generated using only one gauche link which, energetically speaking, is cheap. Therefore coupling between shape and the ordering in the liquid crystal to support more linear conformers is more likely as there is a small enough cost in energy to support those conformations. In the case of odd dimers, two gauche links are required to obtain 'linear' conformers (in fact the molecules are more a broad U-shape with mesogenic groups parallel, see Figure 1.16).

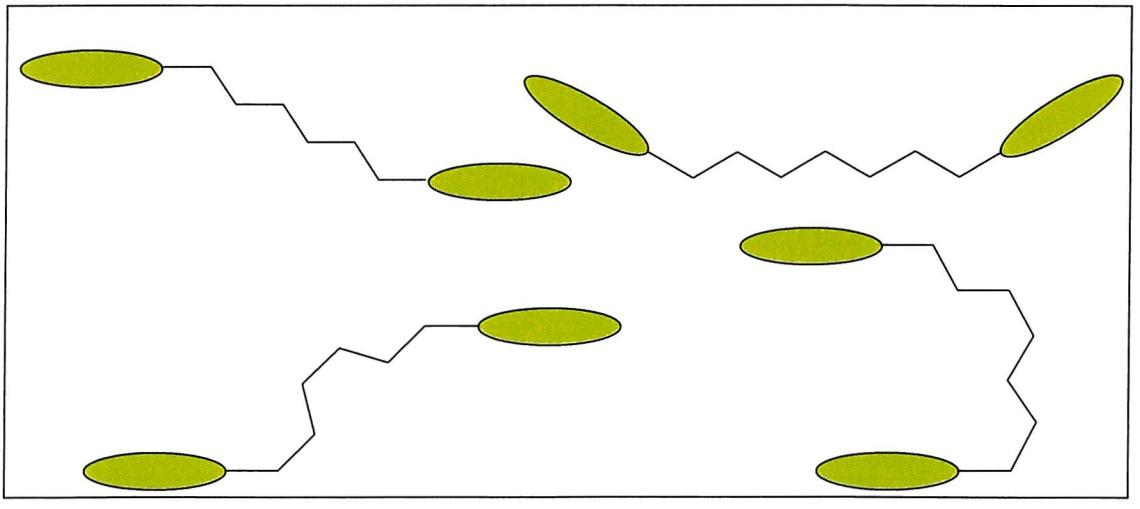

Figure 1.16 Schematic of even (left) and odd (right) dimers where the all-trans conformation is shown for both (top) along with the linear conformers are given from one or more gauche links (bottom).

The cost in terms of energy for two gauche links is relatively high and cannot be paid by

increased stability from coupling to the order in the bulk. The result is a very large difference in the odd-even effect for short spacer groups. As the spacer becomes very large there are small rotations in the chain which are of low energy which, over a large number of atoms, can help make otherwise bent conformers more linear as shown in Figure 1.17[34].

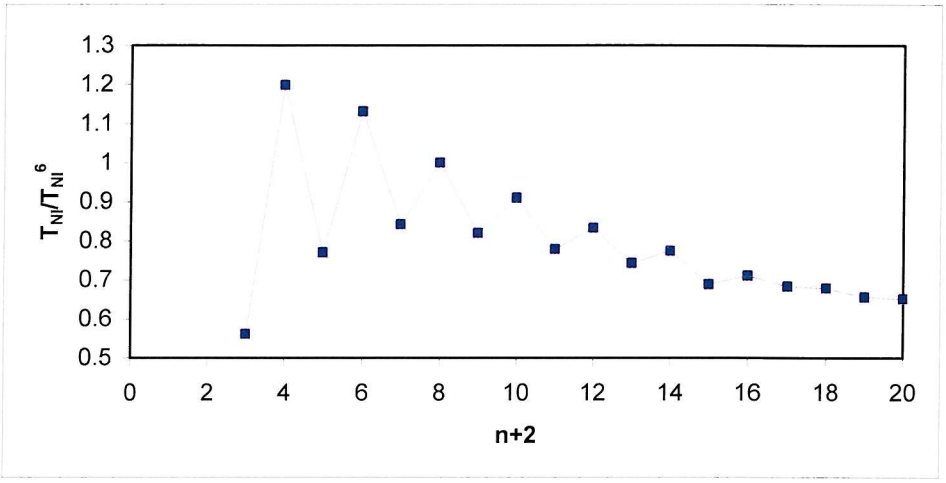

Figure 1.17 The attenuation in the T_{NI} transtion for CBOnOCB. The transitions are plotted for T_{NI}/T_{NI}^6 as a function of the spacer. Here, T_{NI}^6 is the N-I transition for the n = 6 member of the series.

The overall trend is for the T_{NI} to fall as the spacer becomes larger and dilutes the stabilising effect of the mesogenic groups but the slight rotations in the spacer chain result in the difference in the odd-even dimers being attenuated to almost nothing.

The noticeable difference between the monomer and dimer behaviour is the lack of smectic behaviour in the CBOnOCB series even at spacer lengths greater than n = 12.[34] The CBnCB series does show smectic behaviour in one case[39] but, unlike the monomer in the CBn and CBOn series, it is generally not observed in the symmetric series. Smectic phases in dimers can be readily accessed, for example, using dimers with non-cyano terminal groups. Alternatively dimers with different mesogenic groups where, for example, one has a long chain terminal group can give access to a variety smectic phases. An example would be a Schiff-base moiety on one end of a cyano biphenyl (e.g. compound **27**[40]) or even with symmetric Schiff-base mesogenic units.[37]

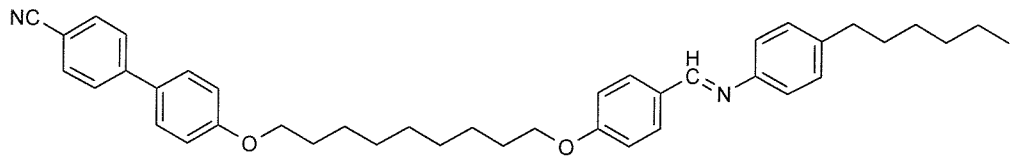

27 Cr (62) SmI 83 SmC 112 SmA 118 N 149 I

These are called non-symmetric dimers and it is common for them to also show a pronounced odd-even effect. There are two clear factors to appreciate when considering what influences the phase behaviour of dimers. As shown previously, the choice of substituents of the mesogenic units will play a crucial role in either stabilising or destabilising the nematic phase. Care must be taken in the selection of terminal groups and lateral substituents so as not to reduce the nematic range so that it is completely hidden under the crystal phase. However, the overall shape of the dimers is also very, if not most, important. The pronounced odd-even effect is related more to the shape of the whole molecule rather than the composition of chemical subunits. Thus any attempt to affect the geometry of a molecule would be expected to have a profound impact on the nature of the odd-even effect and the stability of the phase.

1.2.2. Elastic constants

In the first analysis of liquid crystal phases it is convenient to assume that, for example, the director in a nematic is uniform throughout the sample. The reality is that this is not the case although uniform director alignment can, for example, be induced by surface forces or by using an aligning electric or magnetic field. The variation of the director though a sample (where there are no disclinations) is relatively small as viewed through a microscope and as such it can be assumed that orientational and positional orders do not vary. In the perfectly aligned state there is no deformation and thus the elastic energy is zero. Any deviation of the director from this uniform aligned state will require energy to be paid in terms of elastic energy. Because the orientational and positional order is taken to not vary over small regions, when considering the free energy of the system, orientational and positional order parameters can be considered constant and the elastic energies can be considered exclusively. This consideration of the free energy under these conditions with these assumptions is described in continuum theory.[1]

The equilibrium state of a non-chiral liquid crystal is for the director to be uniform, just as, by analogy, a spring or an elastic band would wish to be at some equilibrium position. Where this is not the case in the liquid crystal this could be likened to a spring being stretched or bent, or an elastic band being twisted. However in the case of liquid crystals there are three dimensions to consider which complicates the matter as there are three director components thus opening up the possibility of many different terms in the free energy expression.

The number of these terms can be reduced by applying certain physical restrictions, considering the implications of the phase symmetry and ignoring situations where surface effects are significant. The terms can be grouped together conveniently and are quoted below as an expression for the energy per unit volume, f_v, in terms of vectors for splay twist and bend.

$$f_V = K_1 S + K_2 T + K_3 B, \tag{5}$$

where K_1, K_2 and K_3 are elastic constants which represent how stiff the director is in relation to its perturbation they have units joules/metres or newtons.[41-44] S, T and B are scalar combinations of the deformation vectors for the splay, twist and bend deformation respectively shown in Figure 1.18.

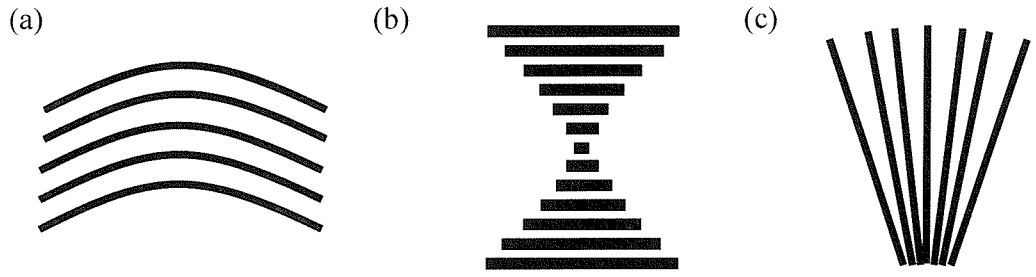

Figure 1.18 Fundamental deformations in the director (a) bend, (b) twist, (c) splay.

In this case, the elastic constants are analogous to the spring constant which governs elasticity in springs. The more ordered the system the more the system will resist the deviation of the director from its uniform/equilibrium state and therefore, the larger the orientational order parameter, the bigger these constants will be. One effect of increasing the twist elastic constant is the effect on the pitch of the helix in chiral nematics. Forming the helix costs twist elastic energy and the larger K_2 is, the larger the cost in energy and

hence the larger the pitch of the helix.

1.2.3. Dielectric anisotropy and magnetic susceptibility

A key behaviour that has enabled liquid crystals to be used in display devices is the way in which they respond to the application of an electric field. As described in the section on display devices, using an electrical field to cause an optic effect is crucial for their success. This section describes very briefly how this works in the bulk and how we can relate that to the molecule commenting on the factors required to increase or minimise this effect.

If a nematic is placed in an electric field the sample will become polarised. The field induces a small charge separation on the molecules which generates a small dipole moment. Since the field will cause all these dipoles to point, on average, in the same direction, the sum of the dipoles in a given volume of the bulk material generates a net dipole moment per unit volume in the material. This net dipole moment is equivalent to a polarisation in the material and for small electric fields the polarisation is proportional to the field thus:

$$\mathbf{P} = \varepsilon_0 \chi_e \mathbf{E} \tag{6}$$

where **P** is the polarisation, **E** is the electric field, ε_0 is the permittivity of free space and χ_e is the electric susceptibility of the material. Given the anisotropy of the material it is not surprising that the value of the polarisation also depends on the direction of the field with respect to the director. Thus, if we assume a fixed director, there would be two values for χ_e corresponding to the parallel and perpendicular situations. To describe this fully, **P** and **E** can be written as column matrices representing P_x, P_y, P_z and E_x, E_y, and E_z respectively. Therefore, $\boldsymbol{\chi}_e$ must be defined as a tensor, a mathematical entity which operates on a vector to give another vector. Hence

$$\begin{pmatrix} P_x \\ P_y \\ P_z \end{pmatrix} = \varepsilon_0 \begin{pmatrix} \chi_\perp & 0 & 0 \\ 0 & \chi_\perp & 0 \\ 0 & 0 & \chi_\parallel \end{pmatrix} \begin{pmatrix} E_x \\ E_y \\ E_z \end{pmatrix}, \tag{7}$$

which can be written as:

$$\mathbf{P} = \varepsilon_0 \boldsymbol{\chi}_e \mathbf{E} \tag{8}$$

where χ_e is the electric susceptibility tensor.

The electric field and the polarisation can together be used to define the electric displacement so

$$\mathbf{D} = \varepsilon_0 \mathbf{E} + \mathbf{P}, \tag{9}$$

and since **E** and **P** have a linear relationship, **D** is often expressed as

$$\mathbf{D} = \varepsilon_0 \boldsymbol{\varepsilon} \mathbf{E}, \tag{10}$$

where $\varepsilon = (1 + \chi_e)$ and is the relative permittivity or dielectric constant and is a tensorial property.

Just as with the electric susceptibility the dielectric constant has components parallel to the director, $\varepsilon_{\parallel}$, and perpendicular, $\varepsilon_{\perp}$. The difference between these values is the dielectric anisotropy

$$\Delta\varepsilon = \varepsilon_{\parallel} - \varepsilon_{\perp}, \tag{11}$$

where $\Delta\varepsilon$ can be positive or negative depending on the dipole moment, polarisability and geometry of the molecule.

It can be shown that

$$\Delta\varepsilon = (\alpha_l - \alpha_t) + \left(\frac{\mu^2}{3k_B T}\right)\left(\frac{3\cos^2\theta - 1}{2}\right), \tag{12}$$

where μ^2 becomes the net dipole, θ is the angle made by the net dipole to the director and α_l is the polarisability of the molecule along the long axis and α_t is the polarisability across the molecule. The difference between the two is normally small and positive (in comparison to the magnitude of the net dipole) for materials like those of the nCB or nOCB series.

Therefore we can see that a large net dipole along the long molecular axis will cause the molecules to orient themselves on average in the same direction as the field, thus aligning the director parallel to the field. This corresponds to $\varepsilon_{\parallel} > \varepsilon_{\perp}$ and hence $\Delta\tilde{\varepsilon}$ is positive. Conversely if the net dipole is across the molecule then the director will tend to align perpendicular to the field and corresponds to $\varepsilon_{\parallel} < \varepsilon_{\perp}$ and results in negative $\Delta\tilde{\varepsilon}$. It also follows that the more ordered the system, the larger the effect of the field. Thus, when the perminent dipole is large and the dielectric constant is dominated by the orientational contribution, the anisotropy follows the order parameter and decreases with increasing

temperature.

The effect of a magnetic field on a liquid crystal is analogous to that of an electric field. Thus an applied magnetic field **H** will create a magnetic dipole moment on the molecule resulting in a net magnetic dipole moment **M**. **H** and **M** are related linearly for weak magnetic fields and the size of **M** depends on the molecular orientation thus there are two magnetic susceptibility coefficients relating **M** and **H**.

$$M_{\parallel} = \chi_{m\parallel} H_{\parallel} \tag{13}$$

and

$$M_{\perp} = \chi_{m\perp} H_{\perp} \tag{14}$$

where χ_m is the magnetic susceptibility tensor and is analogous to electric case. As expected for organic molecules which are generally closed shell systems, almost all liquid crystals are diamagnetic. The magnetic susceptibility anisotropy can be defined as

$$\Delta\chi_m = \chi_{m\parallel} - \chi_{m\perp}, \tag{15}$$

where $\chi_{m\parallel}$ and $\chi_{m\perp}$ are small and negative (a result of the materials being diamagnetic) and $\Delta\chi_m$ can be either negative or positive. The relation of the molecular alignment in a magnetic field to molecular constitution is somewhat less intuitive than for the electric case, however as a general rule, we can divide calamitic (i.e. rod shaped) liquid crystals into two groups; those with aromatic rings and those without. In the case of materials with aromatic rings (which will include all of the materials covered in this Thesis) the energetic minimum is reached when the director is parallel to the magnetic field. This corresponds to $\Delta\chi_m$ being positive and $|\chi_{m\parallel}| < |\chi_{m\perp}|$ which is due to the aromatic ring currents reducing the magnetic flux perpendicular to it resulting in a large negative component of diagmagnetic susceptibility, $\chi_{m\perp}$. For aliphatic compounds the opposite is true and hence $\Delta\chi_m$ is negative $|\chi_{m\parallel}| > |\chi_{m\perp}|$.

1.2.4. Viscosity

Viscosity is a phenomenon which is encountered regularly in everyday life. Be it in water where the viscosity is relatively low to detergents, paints and syrups where the viscosity is larger. All liquids flow and therefore the particles in the liquid have to move when this happens. Thus, if the particles have kinetic energy, we can think of viscosity as the dispersion of that energy through the liquid as the particles overcome internal and

external stresses as the bulk moves. In the case of anisotropic particles, it is the phase symmetry which has a more significant effect on the viscosity than the particles themselves. Given the anisotropic nature of liquid crystal phases, it is not surprising that they would have differing properties to an isotropic liquid depending on the direction of the director in relation to the flow of the material and the velocity gradient.

Perhaps the simplest way to think of this is to look at three situations where the flow, **v**, and hence the velocity gradient, $\nabla \mathbf{v}$ (for definition of ∇ see Appendix A), are constant (and perpendicular) and the director, **n**, points in one of three different directions (x, y and z) (Figure 1.19).

In the case were the director points in the x direction (Figure 1.19a) it is parallel to the flow and perpendicular to the flow gradient and has a viscosity coefficient η_1. Where the director points in the z direction (Figure 1.19b) it is perpendicular to the flow but parallel to the velocity gradient is η_2 and η_3 is the viscosity coefficient for the situation where the director is perpendicular to both the flow and the velocity gradient (Figure 1.19c).

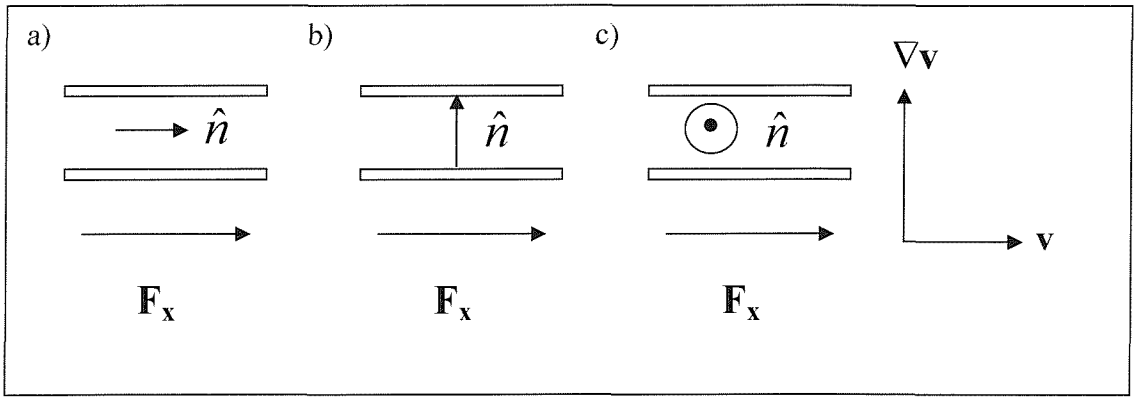

Figure 1.19 Shows the director in relation to the flow of a material (in the x direction) where the director points in a) the x direction, b) the z direction and c) the y direction

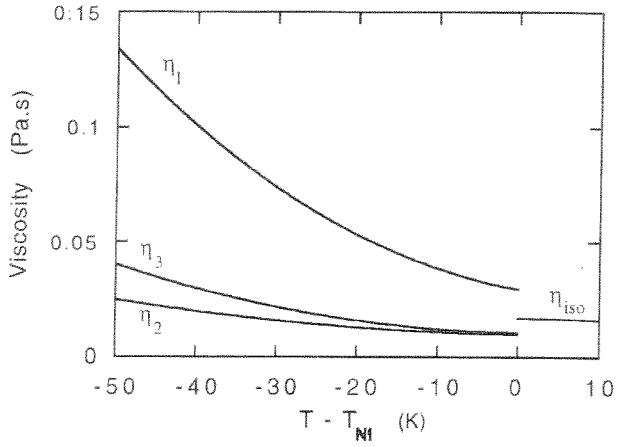

Figure 1.20 Typical variation of the three viscosity coefficients with the shifted temperature.[1]

The three coefficients typically decrease with increasing temperature, a feature typical of fluids, with η_2 being much larger than η_1 and η_3. If the viscosities are plotted against the shifted temperature (see Figure 1.20) they fall and converge discontinuously until the nematic goes isotropic in which case all the coefficients become equivalent. The shifted temperature, $T_{NI} - T$, is a way of measuring distance from the nematic-isotropic transition point.

η_1, η_2 and η_3 are known as the Miesowicz coefficients and relate to where the positions of the molecules change but the orientation does not, provided that the flow does not perturb the liquid crystal. There is a viscocity coefficient which describes the opposite situation where the orientation is changed but the molecular position remains the same.

This viscosity could be observed in a sample which had the director aligned to an electric field which spontaneously changes direction. The director would take time to align to the new electric field direction (see Figure 1.21).

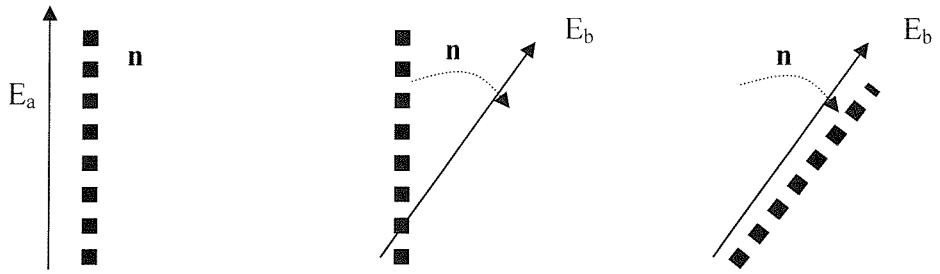

Figure 1.21 A sample with positive $\Delta\varepsilon$ and director **n**, aligned to a field E_a (left) is subject to a new field E_b whilst simultaneously field E_a is turned off (centre) causing the director to move to occupy a new position parallel to the field E_b.

This relaxation time would be related to the size of the new field E_b, the dielectric anisotropy of the liquid crystal and the rotational viscosity γ_1.

$$\tau = \frac{\gamma_1}{\Delta\varepsilon\varepsilon_0 E^2}, \qquad (16)$$

relates the relaxation time, τ, to the twist rotational viscosity, γ_1. There are other several other types of viscosity, but it is γ_1 which is important for many display devices since switching between states often depends on a rotational reorientation of the director.

1.2.5. The Flexoelectric effect

The discussion of liquid crystalline materials coupling to an electric field has thus far only been concerned with dielectric coupling, where the director aligns either parallel or perpendicular to an applied electric field. There is another electric effect, which is related to director deformation rather than alignment. This is called the flexoelectric effect.

The origins of the effect were originally explained based on symmetry arguments for the phase. It was proposed that if the director was deformed in a way that destroyed the centre of symmetry then a polarisation would be spontaneously induced. Of course if this is true, then applying an electric field to induce a polarisation would cause a spontaneous deformation in the director. This effect depends on the loss of the centre of symmetry in the director and as such there are only splay and bend deformations due to flexoelectric coupling. Thus we can write the spontaneous polarisation in terms of these deformations,

$$\mathbf{P} = e_s\mathbf{S} + e_b\mathbf{B}, \qquad (17)$$

where **P** is the polarization, **S** and **B** are vectors for splay and bend, similar to those seen in the elastic free energy equation although, in this case, S and B are both vectorial. This defines e_1 and e_3 as the flexoelectric coefficients for splay and bend respectively.

To help scientists, particularly chemists, better understand the effect, the deformation of the director is often described in terms of molecular rearrangement of molecules (which contain a non-centrosymmetric shape and polarity). Such shapes include banana, pear and tear motifs. In such materials if the director is deformed (either bent or splayed or a combination) then the molecules will change their orientational distribution to reflect the symmetry of the deformation causing an induced polarisation in the sample. Conversely the opposite is also true, if an electric field is applied to the sample the director will

deform according to the shape and dipole of the constituent molecules shown in Figure1.22.

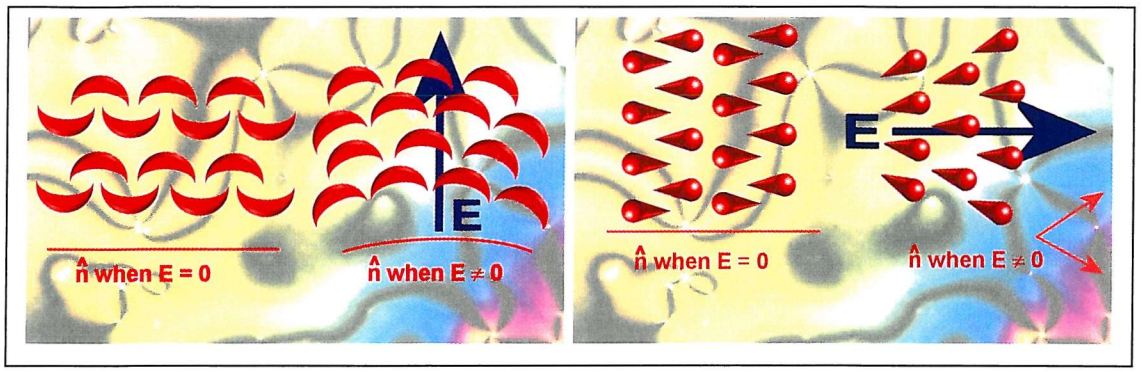

Figure 1.22 A molecular picture showing the effect of applying a field E where the director deforms due to flexoelectric coupling, which is traditionally pictured as molecules with C_{2v} symmetry re-orientating themselves resulting in the director being deformed in a way to reflect the symmetry of this re-orientation.

In sufficiently small electric fields or where materials have a smaller dielectric anisotropy the flexoelectric coupling is the dominant mechanism observed. The effect has been proposed use in novel display devices to gain sub-millisecond switching times[45] and in these cases the flexoelectric coefficients are maximized in concert with favourable conditions to obtain large switching angles corresponding to very large deformations in the director field.

The principle aim of this Thesis is to design and investigate new materials to help better understand the molecular design principles which would maximize this effect. A more in-depth explanation of the effect and a display device which depend on it is discussed in Chapter 2.

1.3. Measuring the properties of liquid crystals

For the vast numbers of properties which can be measured in liquid crystals, there are a plethora of different techniques which have been developed over the years to measure them. Only a limited number of these are applicable to this Thesis, and this section deals simply with differential scanning calorimetry (DSC) and nuclear magnetic resonance (NMR). Both techniques are concerned with obtaining information on the orientational ordering of the liquid crystal.

1.3.1. Differential scanning calorimetry (DSC)

Melting and crystallisation are both accompanied by a change in enthalpy also known as

the latent heat of fusion which is the energy required to destroy the solid lattice and form the liquid (the enthalpy change is an extensive property and is normally given per mole). The basic function of a DSC is to measure this heat change. This is achieved, in principle, by heating a sample (in a pan) of known mass and comparing the energy required (per °C), to heat this sample compared to an empty reference pan (also of known mass). Whilst there is no change in the physical state of the sample, the energy required to raise the temperature of both pans is the same. When there is a transition, the difference in the energy is plotted as a function of temperature. Normally the change in phase is melting, but in the case materials with liquid crystal properties this also applies to changes in the mesophases (e.g. from crystal to nematic or from nematic to isotropic).

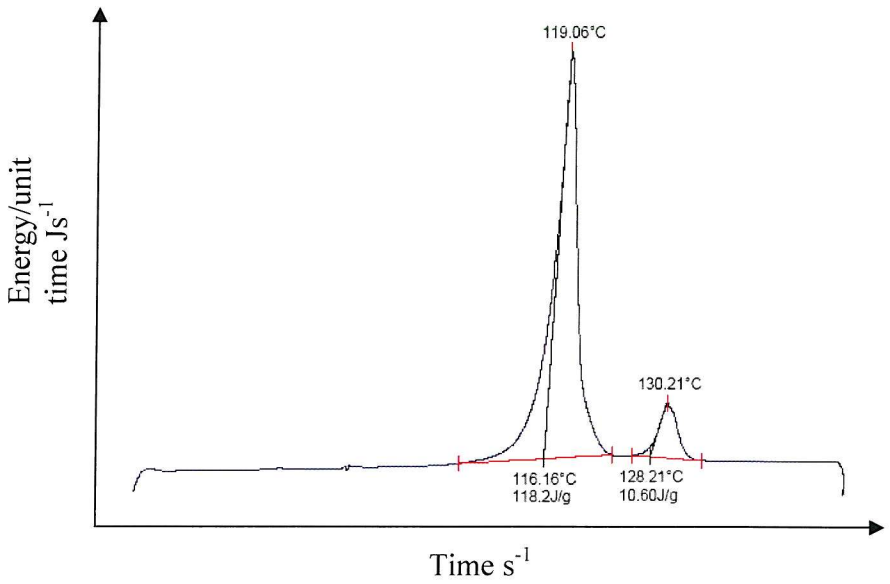

Figure 1.23 DSC plot for a typical dimeric nematogenic liquid crystal ($CBO10OBF_2$ – systematic name given in Chapter 3) showing a large change in enthalpy for melting and a comparatively small change for the N-I transition.

An example of a DSC plot is given in Figure 1.23. Since overcoming the attractive forces in the crystal requires more energy than to simply destroy the order in the liquid crystal phase, the enthalpies of melting are about 10 times larger than nematic-isotropic transitions (although this difference can vary wildly, the melting enthalpy is always significantly larger than the enthalpy change at the liquid crystal transition).

However, the liquid crystal chemist is normally less concerned about the change in enthalpy than the change in order in the liquid crystal which is the change in entropy at

the phase transition. The transitional entropy includes both the change in orientational and conformational ordering, but the orientational change generally contributes mostly to ΔS. The entropy of transition can be easily calculated from the enthalpy by using the relationship

$$\Delta G = \Delta H - T\Delta S, \tag{18}$$

where ΔG is the change in Gibbs free energy, ΔH is the change in enthalpy and ΔS is the change in entropy at a given temperature T. At the transition

$$\Delta G = 0, \tag{19}$$

and so

$$\Delta H_{trans} = T_{trans}\Delta S_{trans}, \tag{20}$$

from which we can determine ΔS. Normally ΔS is expressed as a dimensionless quantity by dividing by the gas constant $\Delta S/R$. Transitional entropies can vary by a considerable amount but for a N-I transition $\Delta S/R \sim 0.1$ would be considered small and $\Delta S/R \sim 3$, large.

1.3.2. Measuring the orientational order parameter using Nuclear Magnetic Resonance (NMR)

The use of NMR for characterising materials, typically (although by no means exclusively) organic molecules, is well known and employed extensively in the characterisation of compounds in this Thesis. This technique can also been used to investigate the ordering of materials in the liquid crystal phase.

The theoretical background to NMR and its use to determine the order parameters in liquid crystals is beyond the scope of this section which aims to introduce the concept for the context of this Thesis. A more in-depth theoretical background can be found in the literature.[4, 46, 47]

The information from an NMR spectra varies according to the abundance of the atom in question. For a typical proton spectra (100% abundant) of a pure material there are several pieces of information which can be determined:

1. From measuring the chemical shift on the spectra, we can then determine the type of chemical environment based on how de-shielded a given proton would be.
2. The relative quantity of the protons found in that environment, relative to some known deduced value for a given environment based on some prior knowledge of the molecule in question.
3. Where protons which are in close proximity to each other, their spins couple (J-coupling) from orbital overlap resulting in the signal being split into patterns based on the number of protons in the local environments.

Many other useful pieces of information can be obtained from an NMR experiment but those listed are the main tools by which a chemist may attempt to determine the structure of a compound.

Liquid crystal phases are orientationally ordered phases compared to the isotropic liquid which is completely disordered. In NMR the magnetic interactions (e.g. σ, J and q) are made up of anisotropic and scalar interactions. In the isotropic where the molecule is tumbling and rotating randomly the anisotropic parts are zero resulting in the spectra only consisting of the scalar components (e.g. σ and J but not q). For liquid crystals the nucleus of choice tends to be deuterium where the NMR is determined by the chemical shift and to less extent the spin-spin coupling.

In the nematic phase there are now contributions from both the scalar and the anisotropic parts which, for deuterium, means that the single line in the isotropic is split into a quadrupolar doublet (dependent of the number of inequivalent deuterons). The magnitude of quadrupolar splitting is determined by the order parameter and by the orientational order of the molecular axes.

One of the key developments of this technique was to measure the ordering of a sample which was not deuterated by doping the sample with a deuterated probe molecule. This was very important as deuteration of samples is expensive both in terms of materials and time and the spectra from the probes are often much simpler to interpret. Various probes have been investigated and used, but the probe of choice for compounds studied in this Thesis is anthracene-d_{10}. This is because the spectra are straightforward to interpret, the probe is rigid and symmetric, soluble in the host and does not boil before T_{NI} of the sample under investigation.

For anthracene the α, γ-deuterons are parallel to the x axis (see Figure 1.24) and so the splitting is determined by the ordering of this hence

$$\Delta\nu_{\alpha,\gamma} = \frac{3}{2} qS_{xx}, \tag{21}$$

where q is the frequency of the spectrometer 186 kHz for the spectrometer and Δυ is the splitting. For the β deuterons it is more difficult because C-D is not parallel to the molecular axes and so both are in S_{xx} and S_{zz} are involved.

For the deuterons in anthracene, the α and γ deuterons are not equivalent to β because their C-D bonds point in different directions.

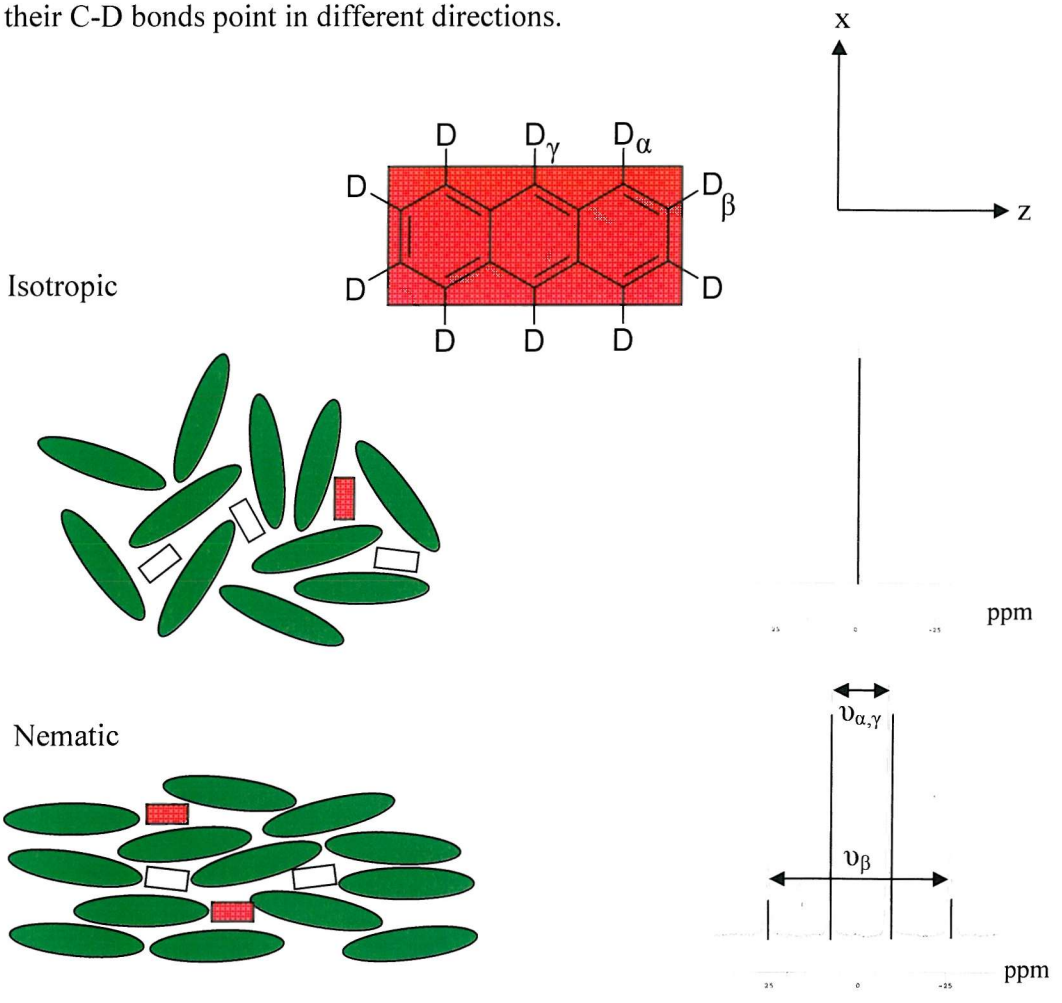

Figure 1.24 On the left shows the ordering of the probe (in red) by the host (in green) for the isotropic (top) and the nematic (bottom). The relative quantity of the probe is exaggerated for clarity. On the right is an example of the type of spectra seen for the respective phase. The wider splitting with the less intense peaks comes from the β deuterons and the smaller splitting with the more intense peaks comes from the α and γ deuterons.

The phase is uniaxial however the probe molecule is biaxial, and as such the uniaxial nature of the phase can couple to the biaxial structure of the guest (probe). Therefore we define the xyz axes (as in Figure 1.24) in the molecule and the quadrupolar splittings are determined by S_{zz} and $(S_{xx} - S_{yy})$ in the probe.

The relationship between the splitting and the ordering S_{zz} and $(S_{xx}-S_{yy})$ is given in Equation 23;

$$\Delta\tilde{\nu}_i = \frac{3}{4}q^i\left[S_{zz}\left\{3\cos^2_{za}\theta - 1 + \eta\cos^2_{zb}\theta'\right\} + \left(S_{xx} - S_{yy}\right)\left(\cos^2_{xa}\theta'' + \frac{1}{3}\eta\left(\cos^2_{xb}\theta''' + 1\right)\right)\right] \quad (23)$$

where x, y and z relate to the axes defined in Figure 1.24, q = 184 kHz and $\eta = 0.064$ (for deuterons in anthracene), a is taken to be parallel to the C-D_i bond and b, perpendicular and θ, θ', θ'' and θ''' are angles between the line a or b and the axes as noted in the subscript. The β deuterons are known to make an angle 29.5°[46] to the z axis as defined in Figure 1.24.

There are some disadvantages to using a probe. The most significant is that ideally the probe should reflect the structure of the host as closely as possibly so that the order parameter determined for the guest will be close to that of the host. The situation which is applicable to this Thesis is where the anthracene molecules sample the environment of one mesogenic group in the liquid crystal dimer giving the local ordering of this group rather than the global ordering of the dimer in the bulk depending on which region the probe is sampling. The only way to overcome this potential difficulty would be to fashion a probe which more closely fitted the dimer motif (perhaps two deuterated phenyl group linked by a flexible spacer). This however was not attempted and so this possibility must be considered when analysing the data.

1.4. Using liquid crystals in display devices (LCDs)

One of the most important achievements in the history of liquid crystals was the recognition of their potential for use as display devices. Since the first device was developed, the industry has moved, in less than four decades, from two colour displays with poor contrast and a short usable life[48, 49] to LCD high definition television screens which, in a fiercely competitive market have proved to be especially successful. There are just a few different display technologies which are employed for a range of

applications. To illustrate the fundamental design of a liquid crystal display device we shall examine the twisted nematic, one of the first and simplest marketable display devices.

1.4.1. A brief historical overview

Several years after the discovery of the curious double melting phenomenon in 1888, Lehmann was led, eventually, to conclude that liquid crystals were a uniform phase of matter distinct from both solids and liquids.[1] However, it was 80 years after their discovery that the technological potential of liquid crystals really started to be realised. Lehmann was influential in getting German and French scientists interested in making and studying these materials. He published his work 'Liquid Crystals' in 1904 but it would be nearly 20 years before a formal classification scheme would be introduced by Georges Freidel in 1922. This early classification consisted of nematic, smectic (which were recognised as layered structures) and cholesteric (now known as chiral nematic) phases. Some work on liquid crystals was done during the 1930s and 1940s although this centred more on examining the properties of liquid crystals including their elastic properties and the effect of electric fields; studies which would eventually prove invaluable for future work on displays. The first patent for a practical technology based on the liquid crystals was 'The Liquid Crystal Light valve'[50] made in 1936 by the Marconi Wireless Telegraph company. Post war work on liquid crystals, however, slowed considerably. This was possibly due to the lack of textbook information and the fact that no one saw a viable application for them.[1]

This changed just before the start of the 1960s. A new optimism for applications using liquid crystals sparked interest in Britain, the United States and the Soviet Union. An American scientist, Glenn Brown, published a lengthy review on liquid crystals[51] and founded the Liquid Crystal Institute at Kent State University, sparking a resurgence of interest in this state of matter. Shortly after this, George Gray, a British scientist, published his text 'Molecular Structure and Properties of Liquid Crystals',[52] the first English book on the subject. During the 1960s this new optimism led to resurgence in the search for liquid crystal applications. The twisted nematic (TN) display was proved by concept although the materials used were high melting.[53] A break through came however

in 1968, when the dynamic scattering mode (DSM) display device[48] was commercially released. There were many drawbacks to this technology, not least was that the chemicals used in the device degraded quite readily and the contrast was poor. However marketable display technologies in liquid crystal science took a new twist and made a significant leap forward when Gray and his colleagues developed the room temperature, stable nematic 5CB.[22] This material along with several others also investigated by Gray *et al* paved the way for mixtures which were suitable for use in TN display devices and thus enabled their commercial release. During the early 1970s the TN display quickly superseded the poor quality DSM devices as the display device of choice.

1.4.2. Twisted nematic display

To make a simple display device work the mechanism must have the functionality necessary to accomplish a small number of tasks. To make this display device commercially successful, however, there are many more properties to consider and problems to overcome. This section will address the fundamentals of the display device. The optimisation of this will be discussed in Section 1.5.

Fundamentally a display device must have at least two different states which are readily distinguishable and the ability to easily and quickly switch from one state to the other. When in either state it must be stable for long periods of time without gaining a memory (i.e. a reluctance to switch back to the other state). To accomplish this several different properties of liquid crystals are used. Their response to an electric field makes an excellent 'switch' and the optical characteristics of the chiral nematic enable the rotation of plane polarised light passing through the nematic. This is important to generate two contrasting states, a 'light' state and a 'dark' state. Polarisers filter light to allow only light polarised in one plane to pass through. When two sets of polarisers are crossed at 90° with an isotropic medium between them no light can get through. If an unaligned liquid crystal, which by its nature scatters light (birefringent), is placed between the polarisers the plane of polarisation is rotated and some of it will escape through the perpendicular polariser.

Previously generating a helical director distribution has been considered by employing a chiral dopant. However in the case where only a half turn is required, the use of an

expensive dopant can be avoided if the director is pinned (by treatment of the surface) and the plates physically twisted. Therefore, with the director twisted through 90°, the properties of optical rotation of the liquid crystal causes all of the light which propagates through the cell to pass through both crossed polarisers.

It is this principle which is used to generate the 'light' state in the display device. The cell is made with a glass front and back with crossed polarisers placed on the top and bottom plates. Behind the polariser on the bottom plate is some reflective surface like a mirror.

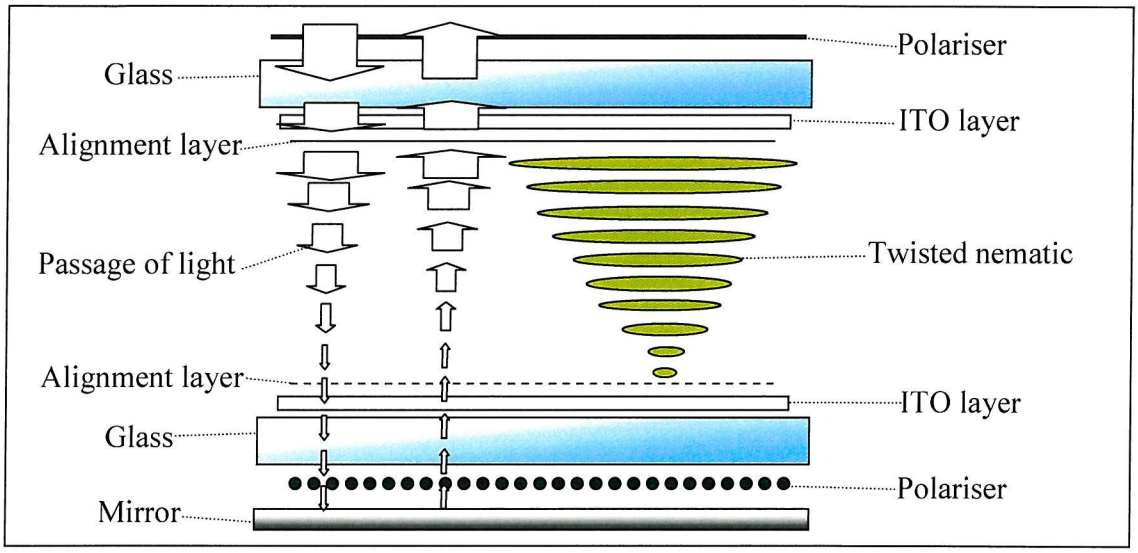

Figure 1.25 The cross section of a twist nematic cell showing the path of light through the cell in the 'light' state.

On the inside of the glass slabs are two layers, one of Indium-Tin-Oxide (the purpose of which will be described later) and the other an alignment layer. The alignment layer pins the nematic director such that it is aligned parallel to the polarisers at each end of the cell to allow all the light to travel through the cell, the liquid crystal sits in the middle of the cell like a filling in a rather elaborate sandwich (see Figure 1.25).

Light can thus travel through the polariser, is plane polarised, is then rotated through 90° by the twisted nematic and can pass through the polariser on the other side unhindered. It is then reflected back and travels the reverse journey to escape from the cell.

To generate a 'dark' state however, this chiral system needs to be destroyed in such a way that the liquid crystal no longer rotates the plane of polarisation. This may seem difficult but is in fact very straightforward.

The Indium-Tin-Oxide (ITO) layer is a transparent electrical conductor and, in this case, can act as an electrode generating an electric field. One of the key properties of the liquid crystal, is that it is has a positive $\Delta\tilde{\varepsilon}$. A crucial property of the cyanobiphenyl series developed by Gray *et al.* is the longitudinal large dipole from the cyano group which makes $\Delta\tilde{\varepsilon}$ large and positive. Once the field is turned on the director tries to align parallel to the field and thus the electrical force acting to align the liquid crystal must overcome the elastic and surface forces keeping the nematic director twisted. Once these are overcome the director first unwinds and then aligns parallel to the electric field.

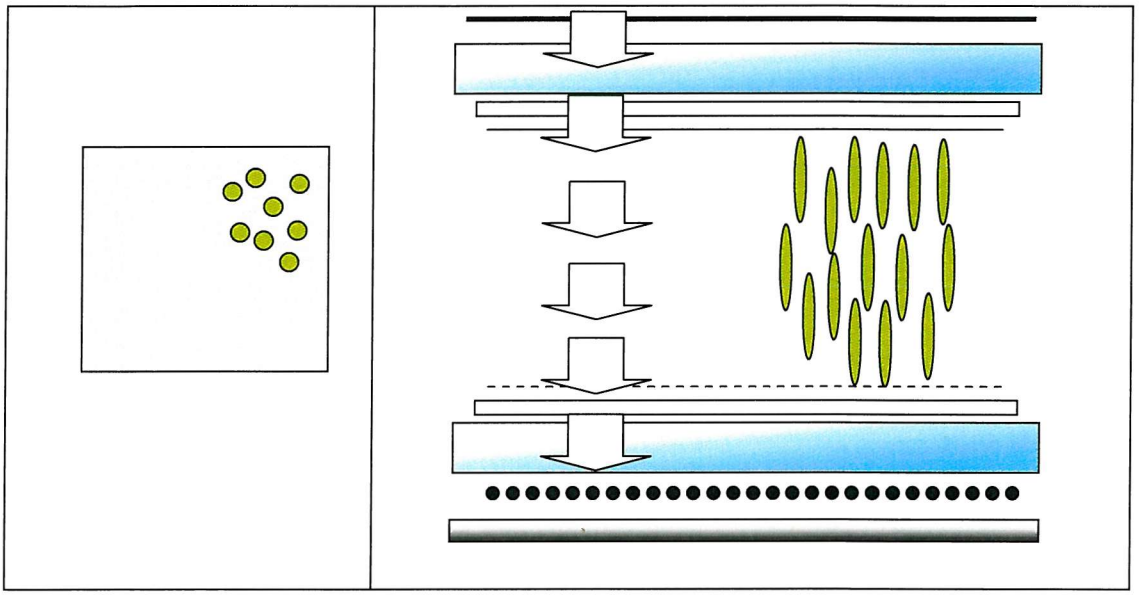

Figure 1.26 (a) Viewed from overhead the aligned nematic appears (in the plane) like an isotropic liquid. **(b)** The cross section showing the 'dark' state with the passage of light through the cell.

Looking down on the glass cell the directors, which are all now end on, appear as an optically isotropic liquid (Figure 1.26a). The light now passes through the polariser and will not be rotated as it reaches the other polariser. No light can escape through the other end to reach the reflective surface and thus no light can escape out of the cell. The image appears dark whilst the field is applied (see Figure 1.26b).

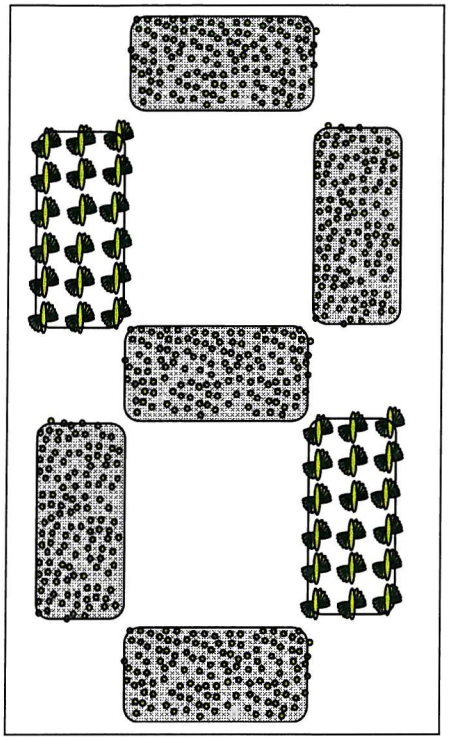

Figure 1.27 Example of 'light' and 'dark' areas of display can generate numerical figures. For example, this display shows the number 2.

When the field is turned off the liquid crystal relaxes back into the helical form. The elastic forces move the director back into their original twisted state, aligned by the layers on the top and bottom of the cell.

By coating specific areas of the film with the transparent conductor and independently turning them on and off, characters can be displayed as seen in calculators and digital wrist watches (Figure 1.27).

When the field is switched on the forces from the electric field coupling to the director have to overcome the elastic forces holding it in a helical structure. This competition of forces would be evident to the viewer purely in terms of how long it took for the display to switch from one state to the other. This can be calculated based on the rotational viscosity of the nematic, the thickness of the cell, the magnitude of the field applied and the size of the elastic forces.

$$\tau_{ON} \propto \gamma_1 d^2 \Big/ (\varepsilon_0 \Delta\tilde{\varepsilon} V^2 - K\pi^2). \tag{22}$$

Here τ_{ON} is the time to switch the cell to the 'dark' state, γ_1 is the rotational viscosity coefficient, d is the thickness of the cell, $\Delta\tilde{\varepsilon}$ is the dielectric anisotropy of the material (which, for the cyanobiphenyl mixtures, is positive and large), V is the voltage applied across the cell and K is a combination of elastic constants. The equation can clearly be

regarded as having an electric part and an elastic part. As the denominator becomes larger so the switching times get smaller, this is most easily controlled by increasing the voltage. However, the device is only as fast as its slowest switch and this is seen in the off state. Here field is turned off, V is therefore 0 and the electrical part of the equation vanishes. The elastic forces are, therefore, left to relax the director back to its original state

$$\tau_{OFF} \propto \gamma_1 d^2 / K\pi^2 . \qquad (23)$$

The factors which govern this relaxation time are harder to control. The dominant factor is the cell thickness which is normally only a few micrometers thick and unlikely to able to made much thinner. Much work has been done to lower the viscosity and materials which have higher elastic constants are sometimes introduced to mixtures to increase the value of K. However there are physical limitations of these systems and even the most optimised cells are unlikely to achieve switching times much below 1 ms.

Novel devices which can achieve sub-millisecond switching times would be useful for applications such as liquid crystal televisions where fast switching times are essential to avoid blurring of a fast moving image. It is therefore unsurprising that one of the most attractive features of flexoelectric devices are their reported fast switching times which can be as low as 10-100 μs[45].

1.5. What makes a good liquid crystal for a liquid crystal display?

In the previous section the mechanics of a simple liquid crystal display were discussed in terms of the principles with little comment on the practicalities of designing liquid crystals for this purpose. From TN displays came STN displays which are still used in some niche markets. However technology has moved on from the STN device, driven by the need for ever faster switching times to support the growing demand for liquid crystal televisions.

There are many key properties a material in a liquid crystal display needs to have to function in a marketable device. Some of these properties are ubiquitous to all display devices, others depend on the specific display device which they are designed for. One of the fundamental problems with the DSM displays was the lack of chemical stability of

the material used. Hydrolysis of the liquid crystal vastly changed its properties and rendered the display useless. The material has to be chemically, photochemically and electrochemically stable for many millions of switching cycles to be viable for display devices. Clearly any display device requires materials which are liquid crystal at room temperature (this can be achieved through use of eutectic mixtures and/or synthesising a room temperature nematic), but also they have to operate at extremes of temperature so, when the central heating breaks down in winter, the LCD television does not crystallise, nor the image disappear in the middle of a heatwave. Power consumption is also a key issue. LCDs tend to draw less power than competing flat panel devices (such as plasma screens) but it is of interest to keep the applied field as small as possible. A device which has sub-millisecond switching times is useless if it needed a 100 V field to drive it. It is normally necessary for the rotational viscosity of the material to be as low as possible. As seen with the TN cell viscosity affects the switching speed of the device and reducing it favours a faster device. To achieve this molecules with shorter chain lengths can be used (and/or with double bonds in the chains) although it is sometimes necessary to use additives which are also known to reduce the viscosity. The behaviour of the material in the presence of an electric field is crucial. In the TN cell, it was necessary to use materials with a large positive dielectric anisotropy to align the director parallel to the field at low fields, however, as we shall see in other devices, this is not always useful. Cells which exploit the flexoelectric effect require materials with small dielectric anisotropies to avoid director alignment and maximise the flexoelectric coefficients to enhance coupling to deform the director. This radically alters the molecular design which, in itself, will have an effect on the transitional properties of the material and viscosity. Increasing the elastic constants of the material generally has either a neutral or slightly positive effect in terms of switching times and is useful for the supporting macroscopic texture in cells used in flexoelectric switching devices at larger fields. Generally the birefringence of the material needs to be large to give the best transmittance of light through the cell.

Property	Optimisation	Comment
Type of phase	Nematic	For the vast majority of displays
Phase stability	Relatively high	To allow a good operational range.
Chemical stability	Essential	Necessary for the operational temperature range to be photonically stable and chemically stable for many millions of switching cycles.
Melting point	Small	So device can operate and room temperature and below.
Dielectric anisotropy	Large to favour director alignment	Needs to be large in cells where director alignment is important. For good coupling parrallel to the director, $\Delta\varepsilon$ needs to be large and positive. For perpendicular alignment, it should be large and negative.
Flexoelectric coefficients	Large to favour director deformation	Needs to be large in cells where director deformation is important. In these cases the dielectric anisotropy needs to be small as it will dominate in larger fields.
Elastic constants	Large	Depending on the cell type as to the effect, however large elastic constants (especially K_2) supports faster switching times.
Viscosity	Low	Specifically the twist rotational viscosity should be low to lower the switching time.
Birefingence	Large	To give maximum light transmittence.

Table 1.4 The physical properties to be optimised for materials to be used in liquid crystal displays

This Thesis shall explore a variety of synthetic strategies in an attempt to obtain materials with suitable properties for use in flexoelectric display devices. A brief historical and theoretical summary along with a description of relevant techniques and technologies related to flexoelectricity will set out a framework with which a synthetic strategy can be outlined. The remainder of the Thesis will look at these different strategies including extending the work by Coles *et al.* in conventional non-symmetric fluorinated dimers, investigating the effects of introducing disruptor groups in the centre of long chain dimers and discussing the contribution of the quadrupole to the flexoelectric effect.

1.6. References

1. P. J. Collings, M. Hird, *Introduction to Liquid Crystals*. Taylor and Francis: Ed. G.W. Gray, J. W. Goodby, A. Fukuda 2001.
2. J. E. Lennard-Jones, *Cohesion. Proceedings of the Physical Society* **1931**, 43, 461.
3. D. Coates, W. A. Crossland, J. H. Morrissy, B. Needham, *J. Phys. D Appl. Phys.*, **1978**, 11, 2025.

4. P. J. Barnes. Ph.D. Thesis. University of Southampton, 1994.
5. H.W.SANDS CORP., MSA5000 Temperature sensitive liquid crystal screen inks. 2007.
6. W. K. Smith, C. R. Brodersen, T. E. Hancock, D. M. Johnson, *Func. Ecol.*, **2004**, 18, 148.
7. M. Mitov, N. Dessaud, *Nat. Mater.*, **2006**.
8. P. Palffy-Muhoray, *Nature*, **1998**, 391, 745.
9. M.J. Freiser, *Phys. Rev. Lett.* , **1970**, 24, 1041.
10. L. J. Yu, A. Saupe, *Phys. Rev. Lett.*, **1980**, 45, 1000.
11. K. Severing, K. Saalwächter, *Phys. Rev. Lett.*, **2004**, 92, 125501.
12. G. R. Luckhurst, *Nature*, **2004**, 430, 413.
13. L. A. Madsen, T. J. Dingemans, M. Nakata, E. T. Samulski, *Phys. Rev. Lett.* , **2004**, 92, 145505
14. K. Merkel, A. Kocot, J. K. Vij, R. Korlacki, G. H. Mehl, T. Meyer, *Phys. Rev. Lett.*, **2004**, 93, 237801
15. G. R. Luckhurst, *Thin Solid Films*, **2001**, 393, 40.
16. G.W. Gray, *The Molecular Physics of Liquid Crystals*. Ed. G. W. Gray, G. R. Luckhurst 1979.
17. M. Hird, *Physical Properties of Liquid Crystals: Nematics*. INSPEC: Ed. D. A. Dunmer, A. Fukuda, G. R. Luckhurst 2001.
18. P. A. Irvine, D. C. Wu, P. J. Flory, *J. Chem. Soc. Faraday Trans. 1*, **1984**, 80, 1795.
19. A. Boller, M. Cereghetti, M. Schadt, H. Scherrer, *Mol. Cryst. Liq. Cryst.*, **1977**, 42, 215.
20. R. Eidenschink, D. Erdmann, J. Krause, L. Pohl, *Angrew. Chem., Int. Ed. Engl. (Germany)*, **1978**, 16, 100.
21. D. Demus, H. Zaschke, *Mol. Cryst. Liq. Cryst.*, **1981**, 63, 129.
22. G. W. Gray, K. J Harrison, J. A. Nash, *Electron. Lett.*, **1973**, 9, 130.
23. G. W. Gray, K. J Harrison, J. A. Nash, *J. Chem. Soc., Chem. Comm.*, **1974**, 431.
24. M. Hird, K. J. Toyne, G. W. Gray, S. E. Day, D. G. McDonnell, *Liq. Cryst.*, **1993**, 15, 123.

25. R. Eidenschink, D. E., J. Krause, L. Pohl, *Angrew. Chem., Int. Ed. Engl. (Germany)*, **1977**, 16, 1977.
26. A. Villiger, A Boller, M. Schadt, *Z. Naturforsch.*, **1979**, 34, 1535.
27. R. Dabrowski, E. Zytynski, *Mol. Cryst. Liq. Cryst.*, **1982**, 87, 109.
28. M. Petrzilka, K. Schleich, *Helv. Chim. Acta (Switzerland)*, **1982**, 65, 1242.
29. G.W. Gray, A. Mosely, *Mol. Cryst. Liq. Cryst.*, **1976**, 37, 213.
30. L. K. M. Chan, G. W. Gray, D. Lacey, *Mol. Cryst. Liq. Cryst.*, **1985**, 123, 185.
31. R. Eidenschink, *Mol. Cryst. Liq. Cryst.*, **1985**, 123, (57).
32. G.W. Gray, M. Hird, D. Lacey, K. J. Toyne, *J. Chem. Soc. Perkin. Trans. 2*, **1989**, 2041.
33. J. W. Emsley, G. R. Luckhurst, G. N. Shilstone, I. Sage, *Mol. Cryst. Liq. Cryst.*, **1984**, 102, 223.
34. G. R. Luckhurst, *Liq. Cryst.*, **2005**, 32, 1335.
35. H. Furuya, K. Asahi, A. Abe, *Polymer Journal*, **1986**, 18, 779.
36. J. 1. Jin, J. H. Park,, *Mol. Cryst. Liq. Cryst.*, **1984**, 110, 293.
37. R. W. Date, C. T. Imrie, G. R. Luckhurst, J. M. Seddon, *Liq. Cryst.*, **1992**, 12, 203.
38. A. Ferrarini, G. R. Luckhurst, P. L. Nordio, *Chem. Phys Lett.*, **1993**, 214, 409.
39. A. Ferrarini, P. L. Nordio, *J. Chem. Phys.*, **1994**, 100, 1460.
40. G.S. Attard, R.W. Date, C.T. Imrie, G.R. Luckhurst, S.J. Roskilly, J.M.; Seddon, L. T., *Liq. Cryst.*, **1994**, 16, 529.
41. C. W. Oseen, *Ark. Mat. Astron. Fys. (Sweden)*, **1925**, 19a, 1.
42. C. W. Oseen, *Trans. Faraday Soc.*, **1933**, 29, 883.
43. F. C. Frank, *Discuss. Faraday Soc*, **1958**, 25, 19.
44. Zocher, H., *Trans. Faraday Soc.*, **1933**, 29, 945.
45. H. J. Coles, B. Musgrave, M. J. Coles, J. Willmott,, *J. Chem. Mater.*, **2001**, 11, 2709.
46. J. W. Emsley, G. R. L., G. N. Shilstone, R. Hashim, *Liq. Cryst.*, **1986**, 1, 437.
47. P. J. Barnes, A. G. Douglass, S. K. Heeks, G. R. Luckhurst, *Liq. Cryst.*, **1993**, 13, 603.
48. G. H. Heilmeier, L. A. Zanoni, L. A. Barton, *Proc. IEEE*, **1968**, 56, 1162.

49. G. H. Heilmeier, L. A. Zanoni, L. A. Barton, *IEEE Trans. Electron. Dev.*, **1970**, 17, 22.

50. MarconiWireless Telegraph Company, Liquid Crystal Light Valve. 441274, 1936.

51. G. H. Brown, W. G. Shaw, *Chem. Rev.*, **1957**, 57, 1049.

52. G. W. Gray, *Molecular Structure and the Properties of Liquid Crystals*. Academic Press.: Ed. London, 1962.

53. M. Schadt, W. Helfrich, *Appl. Phys. Lett*, **1971**, 18, 127.

Chapter 2

An introduction to Flexoelectricity

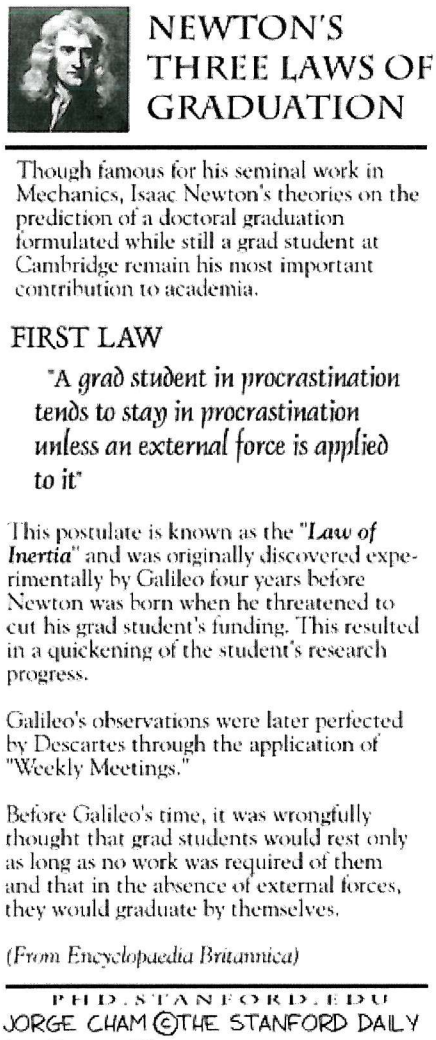

"Piled Higher and Deeper" by Jorge Cham
www.phdcomics.com Used with permission

2. An introduction to Flexoelectricity

2.1. A brief historical overview

One of the advantages of working in the field of liquid crystals is that it has existed for only a little over a century allowing the science and understanding to be well established; yet many of the people who first established and understood it are either still alive or alive in the memory of those who still work in the field. Flexoelectricity represents an area of liquid crystal science which is very much beyond its infancy in terms of understanding, yet still enjoys the benefits of research from Robert Meyer, the physicist who first predicted this property in liquid crystals likening it to piezoelectricity in crystals.[1] This property was later christened flexoelectricity by de Gennes and despite the relatively short space of time from its first conception in 1969, the history of research into flexoelectricity is too broad to fully summarize here. For the sake of brevity, the overview will focus on the initial prediction and measurements made, the insight gained from these early findings and how it influenced the design of materials to exploit the effect today.

2.1.1. Piezelectricity in liquid crystals

Piezoelectricity has been known in solids since the late 19th century when, in 1880, it was discovered by the brothers Pierre and Jacque Curie. *Piezo* comes from the greek which means 'to push' and describes the action of electricity being pushed out of the crystal as a result of the application of mechanical stress to the solid. On a microscopic scale piezoelectricity is found in materials with a non-uniform distribution of charges within the unit cell of the crystal (e.g. quartz). Overall this non-uniform distribution gives a net dipole of zero, however when then material is subject to stress, the positive and negative centres in the unit cells are displaced by an unequal amount thus generating a net electric polarization in the solid. One of the more interesting features of this effect is that it has an inverse; mechanical stress will generate a voltage and, conversely, a small voltage will induce a small change in volume (up to 4%)[2, 3].

Piezoelectric devices are in common use today and are found, for example, in air bag sensors; here the shock of impact generates an electric impulse which triggers the airbag to inflate.

In the middle of the 20th century, with the re-kindling of interest in liquid crystals, fuelled by the desire to find new applications for them, there was a great deal of interest in taking behaviour that were well-known in crystals and looking for analogous properties in liquid crystals. Piezoelectricity was one such property and it was in 1969 that Robert Meyer published his paper which, based on symmetry arguments, related the polarization in crystals induced by stress to a spontaneous polarization in liquid crystals based on deforming the director.

As with any such analogy there are some key differences. The principle difference between piezoelectricity in solids and flexoelectricity in liquid crystals is that the piezoelectricity is tensorial, having components in three dimensions dependent on the location of the charges in the solid, and the latter is only vectorial as it simply relates to a vectorial deformation in the director and the direction and magnitude of the net polarization which is induced. The more specific differences relate to the centre of inversion is preserved in a piezoelectric solid, where the external action is stress. In the flexoelectric effect, the deformations lead to the destruction of the centre of inversion. A more detailed description of this is given by Rudquist and Lagerwall.[4]

There are three fundamental deformations which are used to describe distortions in the director in liquid crystals. These are splay, twist and bend and have been described in Chapter 1 in relation to the elastic constants. In the case of flexoelectric polarization there are only two relevant deformations, splay and bend, and their relationship to the polarization is described in Equation 1

$$\mathbf{P} = e_1\mathbf{S} + e_3\mathbf{B}, \tag{1}$$

where e_1 and e_3 are the flexoelectric coefficients for splay and bend respectively and **S** and **B** are the vector combinations for the director for the splay and bend deformations. (these are sometimes referred to as e_s and e_b as seen in Equation 17 on p38 of Chapter 1). The actual representations for **S** and **B** and the sign conventions for e_1 and e_3 are discussed in Section 2.3.

The twist deformation is not included and if we consider the distribution of the director in the helix we can see why. In the helix, the director points in all directions along the deformation axis. If we compare that with the splay and bend deformations the director has a non-homogeneous distribution along the line of deformation. Therefore if we consider the polarization we see that for the twist deformation the net polarization would be zero, whereas for splay and bend the result is non-zero and possesses a C_{2V} symmetry perpendicular to the polarization direction. In terms of symmetry we can say that the centre of inversion is destroyed for the splay and bend deformations but is maintained in the twist deformation. Therefore the flexoelectric polarisation induced by director deformation can only come from splay and bend and so there is no twist component in the equation for flexoelectric polarisation.

2.1.2. The flexoelectric behaviour

One of the important similarities between piezoelectricity and flexoelectricity is that both effects have an inverse. Just as with a piezoelectric solid, if an electric field is applied then the solid will change volume; for a liquid crystal, application of an electric field will cause the director to be deformed. This is sometimes referred to as the converse flexoelectric effect.[5] Generally, to utilize the flexoelectric effect it is preferable to deform the director with a field rather than generate a polarization from a mechanical deformation, so the focus of this Thesis (and the majority of reported literature on this effect) is on this so-called converse flexoelectric effect.

Meyer's prediction was based on symmetry arguments as are the analogous effects in piezoelectric solids. To help understand how the director becomes deformed at the molecular level, Meyer also included details of the molecular shape that such materials should possess to best support such deformations. Clearly the material must, have some electric component to generate a polarization once the director has been deformed or, if a field is applied, there needs to be an electric component to couple to the field (this was originally assumed to be dipolar although it was shown later that it could also be quadrupolar).[6] Although Meyer's work was based on symmetry arguments applicable to the director, the diagrams he included in his paper suggest a relationship between the symmetry of the molecules in the liquid crystal and the director deformation. It could be

postulated that in order for the symmetry of the molecular orientational distribution to be changed by a deformation in the director field, you require the symmetry of the deformation to be analogous to that of the molecule. In his paper, Meyer uses the pictures shown in Figure 2.1[1] to illustrate this microscopic rearrangement analogous to the director deformation.

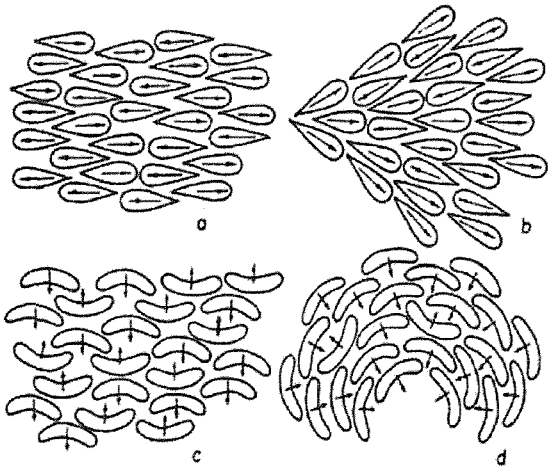

Figure 2.1 diagram of non-symmetric molecules where the director is deformed as (b) and (d) and undeformed as in (a) and (c). In the case of the undeformed director the arrangement of the polar molecules results in a zero net polarisation. In the case where the director is deformed, a net polarisation is induced[1].

To illustrate the implications of shape on this effect further we could consider a more primitive shape to show the different deformation in the director (see Figure 2.2). What is crucial in these diagrams, however, is the similarity in the shapes (representing molecules) that generate a bend or splay deformation. By making the point that the shapes that support a splay or bend deformation can be very similar then a molecule which has the ability to change its shape (e.g. a liquid crystal dimer with a flexible spacer) could be expected, depending on its structure, to potentially support both deformations.

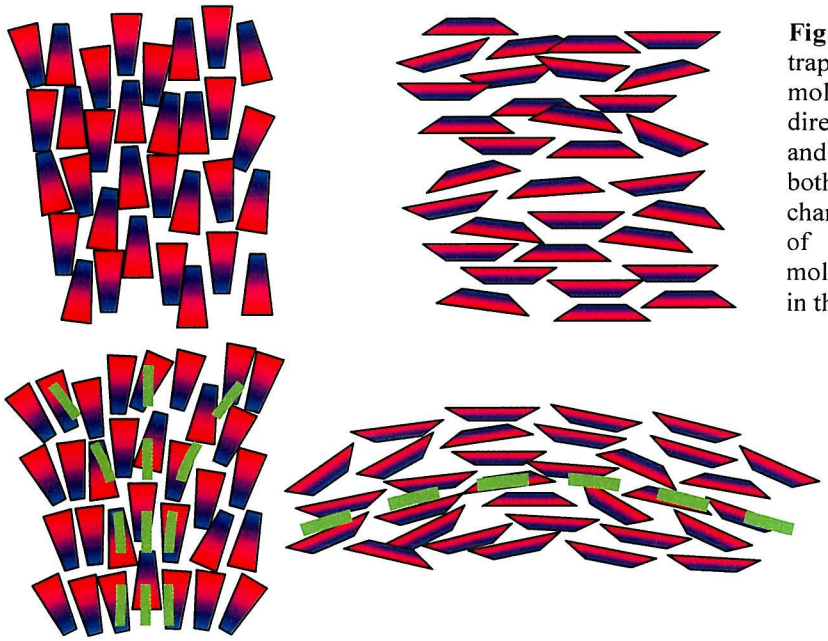

Figure 2.2 Diagram of trapezium shaped molecules representing the director in the undeformed and deformed states for both splay and bend. By changing in the dimensions of the component molecules we see a change in the type of deformation.

In the initial haste to investigate this effect, measurements were made on liquid crystals based on ease of availability rather than suitability in terms of their molecular shape.

2.1.3. The first measurements made

The history of flexoelectric measurements is a capricious one. Many different research groups made measurements on different types of common liquid crystals and came up with very different answers, often using very different techniques on, sometimes, identical compounds. Therefore, trying to give a full chronology of the early measurements of the flexoelectric coefficients would detract from the scientific context in which the information in this Thesis lies. As such a brief commentary of some of the notable measurements and predictions made over the first thirty years of research in the field (prior to the use of liquid crystal dimers as flexo-materials) is made. Focusing on both the materials and the results rather than the intricacies of the experimental detail, however, a more comprehensive account of this can be found elsewhere.[5] All values given in this Section are reported using Meyer's original definition for splay and bend deformations (explained in Section 2.1.2).

The first flexoelectric coefficient to be reported was e_3 for MBBA (n-4'-methoxybenzylidene-n-butylanilin) (see Figure 2.3) in 1970.[7] However, this and other

measurements on the same compound over the next three years gave a mixture of results which varied by an order of magnitude (from 1.2×10^{-12} Cm^{-1} to 1.0×10^{-11} Cm^{-1}) with no clarification of the sign of e_3. It became apparent that surface effects were also contributing to the measurements and that the actual value of e_3 for MBBA lay between these two values.

In 1971 Helfrich introduced the first model[8] which quantitatively assessed the molecular properties which were needed to produce a large flexoelectric effect based on Meyer's model. This model has been used up until quite recently and is described in slightly more detail in Chapter 4. Other attempts at relating the molecular shape and electrostatic properties to the flexoelectric effect include work by Osipov[9] and by Singh[10] during the 1980s and then more recently by Ponti[11] and by Ferrarini.[12]

More measurements on e_3 were later carried out again on MBBA, BMAOB (p-methoxyazoxybenzene) and BBBA (n-4'-butoxybenzylidene-n-butylaniline) (see Figure 2.3) during the early 1980s.[13] All the measurements gave e_3 of the order $1x10^{-12}$ Cm^{-1}, taken over a variety of measurements temperatures and again uncertainties about contributions from the surface forces hampered the consistency of results. The relationship between flexoelectric coefficient and the order was also probed and found to be weaker than $e \propto S$. Still there was much uncertainty about the sign of the value with both positive and negative results being published.

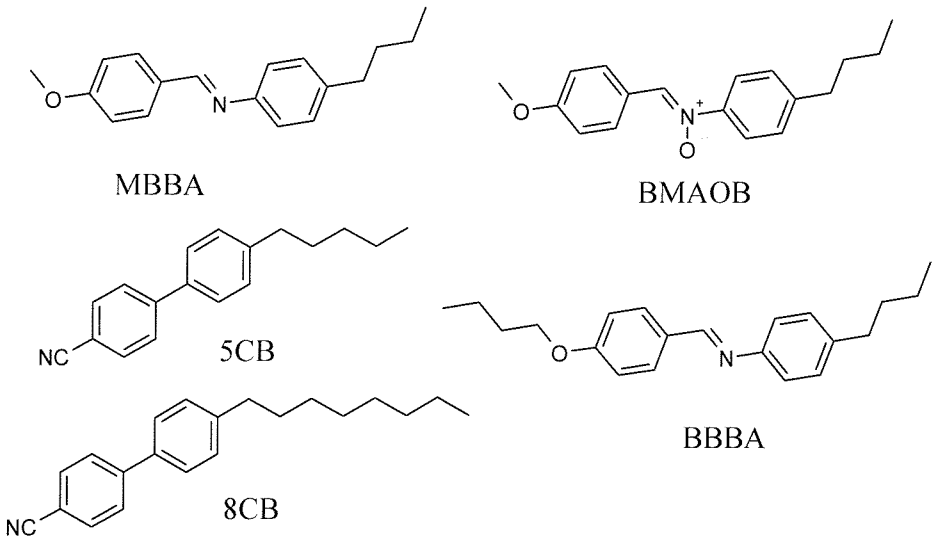

Figure 2.3 The molecular structures of materials mentioned in this section with abbreviations.

Around this time the first pure splay flexo-measurements were made on MBBA.[14] The result was found to be $+(3.0 \pm 0.7)\times10^{-12}$ Cm^{-1} at room temperature with the sign determined from the control experiment.

The measurements described so far have been on the converse flexoelectric effect, however during the late 1970s and early 1980s measurements on the direct flexoelectric effect (i.e. the polarisation generated from a deformation) were made using acoustic pulses to deform the director generating a spontaneous polarization. These measurements were originally made on 8CB and an azoxy compound and then later on MBBA and results for e_3 were ($|e_3| \approx 3\times10^{-13}$ Cm^{-1})[15, 16] and combinations of e_1 and e_3 were also reported. Other experiments involving laser pulses of samples doped in anthracene (for absorption purposes) were made[17, 18] giving results for 5CB ($e_1 + e_3 = 4.7\times10^{-12}$ Cm^{-1} at 30 °C)[17] and MBBA ($e_1 + e_3 = -2.3\times10^{-12}$ Cm^{-1} at 36 °C).[17] Once again there were published results which gave conflicting evidence for the sign for 5CB, although, for a given convention (described later) the cumulative combination of e_1 and e_3 is generally considered to be positive.

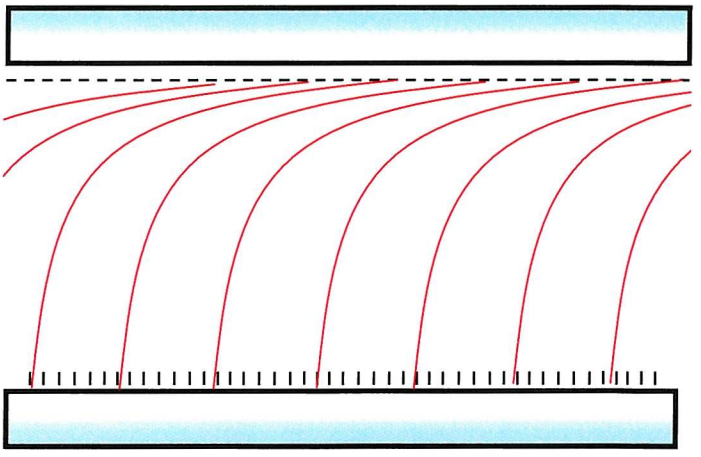

Figure 2.4 A hybrid aligned nematic (HAN) cell where the inside surface of the top plate is treated to stabilise planar alignment whereas the inside surface of the bottom plate is treated for homeotropic alignment. If the surface anchoring forces are strong, the director (in red) goes through a splay/bend deformation as the it moves from planar to homeotropic alignment.

Measurements of combinations of the (converse) flexoelectric effect were made using a hybrid aligned nematic (HAN) cell where one surface is treated for homeotropic alignment and the other uniform planar alignment. This forces a splay/bend geometry

(see Figure 2.4) and a variety of measurements of the combination of e_1 and e_3 have been reported (summarized in Table 2.1 below based on a table of information by Petrov[19]).

In 1987 Meyer and Patel introduced the idea of using a uniform lying helix (ULH) geometry to exploit what they termed the flexoelectro-optic effect (described in more detail in Section 2.5). Although presented as being a reliable method of measuring the flexoelectric effect, it also could be used as the basis for a display device. It is this methodology which is used to measure the flexoelastic ratios reported in this Thesis and has been enhanced since its inception. Improvements that have been made, for example, include using a HAN cell to support the ULH geometry, as well as a polymer support method which stabilizes the ULH texture.[20]

Substance	$(e_1 + e_3)$ /10^{-12} Cm^{-1}	T /°C	Ref	$(e_1 - e_3)$ /10^{-12} Cm^{-1}	T /°C	Ref
5CB	-4.7	30	[17]			
MBBA	-2.3	36	[17]			
MBBA	25	Room	[21]			
MBBA	-15 ± 2	Room	[22]			
MBBA	-29.2 ± 20%	20	[23, 24]	+3.3 ± 0.7	20	[25]
MBBA	-54 ± 10	30	[26]	+14 ± 1	30	[26]
8OCB	+21 ± 5	73	[24, 27]			
BMAOB				-5.7	25	[28, 29]
ZLI-4792	≤|10|	30	[26]	-15 ± 1	30	[26]

Table 2.1 Table of early results for a variety of liquid crystals.[5]

Looking at the materials in Table 2.1 and Figure 2.3 we can see that the molecular shape of the compounds were ill-suited for large flexoelectric coefficients and many of the obstacles faced by early experimentalists were made more difficult because the effect they were measuring was so small. It was first noted by Durand[30] that liquid crystal dimers with odd spacers would have a suitable shape to have large flexoelastic properties although it was Coles *et al.* who first published results on such materials.[31]

A more detailed look at the flexoelectic effect in liquid crystal dimers, the literature values for liquid crystal dimers and the results which are in the literature are given later.

To conclude, we can see that measuring the flexoelectric effect is experimentally hard to achieve reliable and accurate results. Particularly measuring individual coefficients where surface forces were also an issue. Work done recently by Ewings *et al.* [32, 33] has produced

a methodology which gives individual values for e_1 and e_3 by producing results for $e_1 + e_3$ and $e_1 - e_3$. However, this technique has not been currently designed to make higher temperature measurements. The majority of the results reported in the last ten years are a combination of e_1 and e_3 and it is during this time, with the increased number of compounds measured with good agreement, that confidence in the results and the techniques used to determine them has grown.

2.2. Considering the quadrupolar contribution to the flexoelectric effect

It was in 1977 that Prost and Marcerou considered the possibility that there was also a contribution to the flexoelectric effect from the electric quadrupole as well as from the electric dipole.[6] The origin of the mechanism is somewhat harder to see and is shown in Figure 2.5. In principle, instead of a polarization being induced as a result of molecules with an asymmetric shape flipping resulting in a director deformation, they proposed that more rod-like molecules would reorientate themselves where the polarization in one plane could be altered by the inclusion of charges from a different plane.

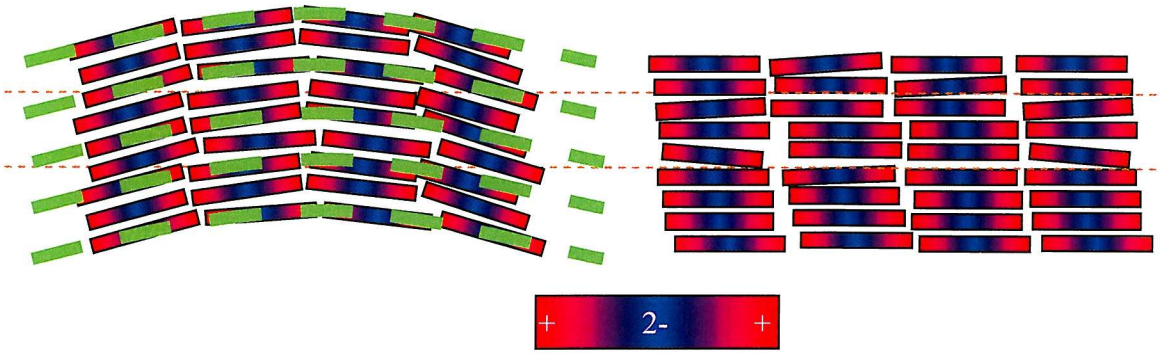

Figure 2.5 The molecules, represented by symmetric units with a charge distribution denoted by the red/blue colour, are distributed showing a deformed (left) and undeformed (right) director. The blue region has twice the charge of the edges and is opposite in sign. We can see in a layer, there is a difference in the spatial distribution of charge (i.e. there is more blue in the deformed layer than in the undeformed layer where there is approximately the same amount of red and blue).

The diagrams from Meyer's shape-dipole model are somewhat more intuitively seductive in their appearance. In principle where the Meyer model gave an imbalance in the net dipole due to a re-orientation of the molecules based on their shape, the quadrupolar mechanism gives a redistribution of the charge in space which supports the deformation. By taking the layer through a deformed and undeformed examples (orange horizontal lines) we can count the number of positive and negative charges and we find (in the

example above) that there are a balanced number of charges in the undeformed section whereas there is a net negative charge in the deformed region about -1.

The pictorial evidence is not very compelling, the mathematical proof is involved and quadrupolar interactions are harder to visualise than dipoles, so it is not surprising that not much attention is generally given to the quadrupolar contribution to the flexoelectric coefficient. One of the notable exceptions to this however is work done by Ferrarini on modeling the flexoelectric coefficient.[12] Her approach has included the quadrupolar contribution in her flexoelectric calculations and a more detailed description at some of her work in this area is given in Chapter 4.

The mathematical analysis of the quadrupolar contribution is beyond the scope of this Thesis, but in terms of liquid crystal design it is useful to appreciate, in the light of a possible quadrupolar contribution, what characteristics affects the electric quadrupole as well as the electric dipole.

The dipole moment describes two charges of opposite sign (±q) separated by a distance (r). The quadrupole moment differs as it describes two sets of two charges, each set being equal and opposite in sign (±q). The distance to each charge is in relation to an origin as shown in Figure 2.7.

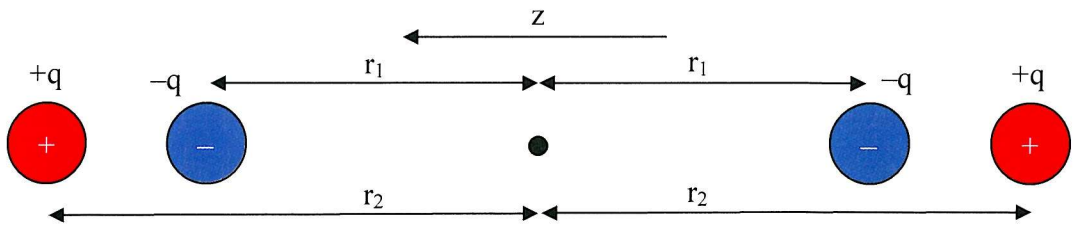

Figure 2.6 Layout of charges from the origin (•) to the charges that would give a quadrupole moment.

Formally the component(s) of the quadrupole tensor are defined as

$$Q_{\alpha\beta} = \frac{1}{2}\sum_i 3q_i\left(r_\alpha^{(i)} r_\beta^{(i)} - r_i^2 \delta_{\alpha\beta}\right), \qquad (2)$$

where α and β are either the x, y or z direction, Q is the quadrupole tensor, q is the charges summed over all i, r_α and r_β are lengths in the direction of α and β, r_i is the total length and $\delta_{\alpha\beta} = 1$ when $\alpha = \beta$ and zero at all other times. For the situation described in Figure 2.6 it can be shown that the z component of quadrupole tensor is

$$Q_{zz} = 2q\left(r_2^2 - r_1^2\right), \qquad (3)$$

where Q_{zz} is the quadrupole. To maximize the quadrupole moment therefore the charges should be large, the distance between the sets of charges to be large, and the distance between the individual charges, small.

Taking the liquid crystal dimer motif we can see in a simplified example (see Figure 2.5), that the charges on the mesogenic units are separated by the flexible chain and as such the structure of the dimer lends itself well to increasing the quadrupole moment. Furthermore, if we ignore the contribution from the aromatic rings we can pictorially see that using a small highly charged group, for example a cyano group, at the end of each mesogenic arm will increase the quadrupole for this geometry.

However, considering the dimer in Figure 2.7, this is not the only conformer (or spacer parity) which can be adopted by a liquid crystal dimer and so we must consider how the quadrupole moment might vary with conformation.

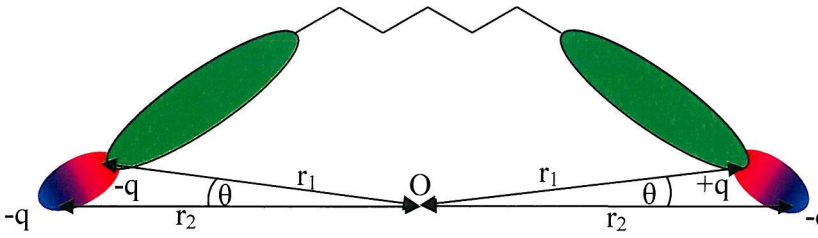

Figure 2.7 Diagram of more realistic example. Shown is a schematic of an odd dimer in the all trans state with cyano groups on the end is labelled in terms of the charges and the distances to an origin O.

Treatment of this problem is more complicated as now there are two charges are in a plane rather than a straight line. Although the relationship would be more complicated, fundamentally the size of the quadrupole depends the same distances r_1 and r_2. However, changes in conformation are critical because, as we can see from Figure 2.7, if the dimer were to become more linear, the ratio of r_1 to r_2 would increase and as such the quadrupole moment would increase. The more bent the conformer the more this would lead to a reduction in the ratio, making the quadrupole moment small.

Conversely when the molecule is most linear the net dipole, μ, is small because the local dipoles are anti-parallel and thus cancel. The net dipole becomes larger as the molecules become more bent as the resolved component of μ perpendicular to the long molecular axis becomes larger.

This leads to an interesting conclusion. Making the molecule more linear should increase the quadrupolar contribution to the flexoelectric effect in whereas making the shape more asymmetric will increase the dipolar contribution to the effect.

Further examination of this observation is given in Chapter 4 where, using the Ferrarini model, we examine the individual contributions to the flexoelectric effect first in a model example and then in liquid crystal dimers.

2.3. Notation and conventions for flexoelectricity

As more people contributed to the understanding of the flexoelectric effect, there have inevitably been some variation in notation and most importantly two distinct conventions have arisen, which in principle concern the description of the bend deformation. As an aid for understanding the literature, we now give a brief description of the notation for each of the deformations.

2.3.1. Splay and Bend

Meyer's original equation for describing the spontaneous polarization resulting from the deformation of the director which we can recall (see Equation (1)) as

$$\mathbf{P} = e_1\mathbf{S} + e_3\mathbf{B}, \tag{1}$$

where, in his original paper, Meyer defined the splay deformation as

$$\mathbf{S} = \mathbf{n}(\nabla \cdot \mathbf{n}), \tag{4}$$

and the bend as

$$\mathbf{B} = (\nabla \times \mathbf{n}) \times \mathbf{n}; \tag{5}$$

e_1 and e_3 are the flexoelectric coefficients associated with the splay and bend deformations respectively. We shall see later how this relates to the direction of the polarization with respect to the direction of the splay and bend deformation vectors.

With regards to the notation, **n** is the vector describing the director and, in Cartesian co-ordinates, has components n_x n_y and n_z such that

$$\mathbf{n} = \begin{pmatrix} n_x \\ n_y \\ n_z \end{pmatrix}, \tag{6}$$

∇ (the del operator) is a vector consisting of three partial derivative operators and is used in the description of the change in a vector gradient (given as $\nabla\mathbf{n}$) and thus

$$\nabla = \begin{pmatrix} \frac{\partial}{\partial x} \\ \frac{\partial}{\partial y} \\ \frac{\partial}{\partial z} \end{pmatrix}, \tag{7}$$

which makes

$$\nabla\mathbf{n} = \begin{pmatrix} \frac{\partial n_x}{\partial x} \\ \frac{\partial n_y}{\partial y} \\ \frac{\partial n_z}{\partial z} \end{pmatrix}. \tag{8}$$

The full dot and cross products for the splay and bend are given in Appendix A however we can see that the deformations for both splay bend can be described in terms of changes in the director and director gradient as we would expect.

Mathematically there are some other notations used to denote dot and cross products for vector components and the del operator. These are not very common in the literature surrounding flexoelectricity but they do exist. Therefore it is helpful to be aware that the divergence (given the notation div) is written as

$$\mathrm{div}(\mathbf{n}) = (\nabla \cdot \mathbf{n}), \tag{9}$$

and therefore we can re-write Equation (4) as

$$\mathbf{S} = \mathbf{n}\mathrm{div}(\mathbf{n}). \tag{10}$$

Similarly the analogous cross product needed in the bend deformation can be expressed as the curl of the vector and thus is written as

$$\mathrm{curl}(\mathbf{n}) = (\nabla \times \mathbf{n}), \tag{11}$$

which can also be written as the rotation rot(**n**) where

$$\mathrm{rot}(\mathbf{n}) = \mathrm{curl}(\mathbf{n}) = (\nabla \times \mathbf{n}). \tag{12}$$

Thus we can write Equation (4) for **B** as either

$$\mathbf{B} = \mathrm{curl}(\mathbf{n}) \times \mathbf{n} \text{ or } \mathbf{B} = \mathrm{rot}(\mathbf{n}) \times \mathbf{n}. \tag{13}$$

This original definition of the director bend deformation used by Meyer is not the only definition which exists. Indeed mathematical descriptions for splay, twist and bend have existed for the elastic constants before Meyer published his paper on flexoelectricity. It is unfortunate that Meyer chose to express the definition for the bend deformation in a slightly different way to the more widely used Oseen-Zocher-Frank expression.[34-37] The physical significance of these differences is given in Section 2.1.2. Considering the mathematical differences in the vector notation; here the bend coefficient is expressed as

$$\mathbf{B}_1 = \mathbf{n} \times (\nabla \times \mathbf{n}), \tag{14}$$

which can identically be expressed as

$$\mathbf{B}_1 = \mathbf{n} \times \nabla \times \mathbf{n}, \tag{15}$$

which is related to Meyer's original definition

$$(\nabla \times \mathbf{n}) \times \mathbf{n} = -(\mathbf{n} \times \nabla \times \mathbf{n}), \tag{16}$$

with a fuller explanation of this is given in Appendix A.

This leads to a potential confusion in the definition of the flexoelectric coefficients since the sign difference is incorporated in the flexoelectric coefficient and in the literature there is no specifically stated relationship using two unique symbols representing the difference for these coefficients. Rudquist and Lagerwall[4] make the point that there should be some convention and then present the case for using Equation 14 with e_s and e_b for the flexoelectric coefficients for splay and bend respectively. There is some consensus[38] that for the Meyer definition e_1 and e_3 should be used and for the Rudquist and Lagerwall proposed definition it should be e_s and e_b where

$$e_1 = e_s \text{ and } e_3 = -e_b, \tag{17}$$

and

$$\mathbf{P} = e_s\mathbf{S} + e_b\mathbf{B}, \tag{18}$$

Although this does communicate the difference between the two expressions for the bend coefficient, using s and b subscripts means there is no correlation between deformations for splay and bend for the flexoelectric coefficients and the elastic constants where rotation is K_1 and K_3, never K_s and K_b. To make matters worse the convention which uses the Oseen-Zocher-Frank deformations does not use the 1 or 3 subscript.

The following section describes the notation which will be used throughout this Thesis which uses some of the justifications found in the Rudquist and Lagerwall paper.[4]

2.3.2. The convention for the coefficients

If we consider the splay and bend deformations in terms of their mathematical definition, each deformation can have the positive direction either being defined as towards or away from some arbitrary origin shown in Figure 2.8.

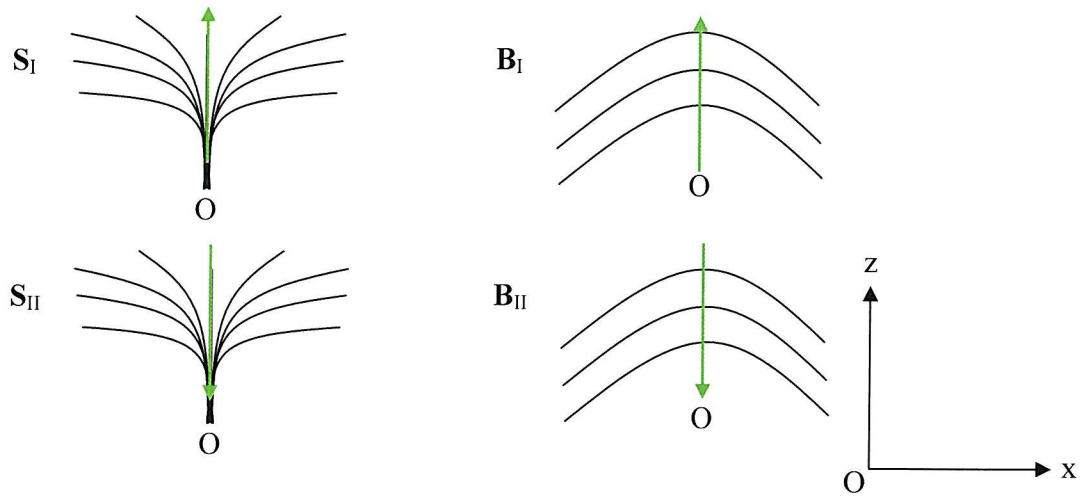

Figure 2.8 Taking the origin O as labelled in each diagram, the positive direction for each deformation is defined here either away or towards that origin with the z axis running up the centre of symmetry bisecting the deformation

These four possibilities have been labelled **S** or **B** for the deformation and I (for the positive direction as away from the origin) and II (for the positive direction being towards the origin) consistent with the notation used by Rudqust and Lagerwall.[4] Although mathematically there is a difference in the deformation vector, physically, without using a probe with a defined positive and negative sense (for example, the application of an

electric field where the polarity is defined), there is no difference between S_I and S_{II} or B_I and B_{II}.

However, if we now consider the polarisation the sense of the director deformation becomes significant. In Section 2.3.1 we noted that there were two definitions for the bend deformation which differed by sign which mathematically corresponds to the positive direction of the deformation being either towards or away from the origin. The definition originally given by Meyer given in Equation 3 using the notation in Figure 2.8 is

$$\mathbf{B}_{II} = (\nabla \times \mathbf{n}) \times \mathbf{n}, \tag{19}$$

and that taken from the elastic deformations is

$$\mathbf{B}_{I} = \mathbf{n} \times \nabla \times \mathbf{n}. \tag{14}$$

In the flexoelectric effect there is a spontaneous polarization induced as a result of the director deformation. This polarization can also be defined as either up or down. This therefore creates two possibilities for each of $\mathbf{S}_I$, $\mathbf{S}_{II}$, $\mathbf{B}_I$ and $\mathbf{B}_{II}$ shown in Figure 2.9.

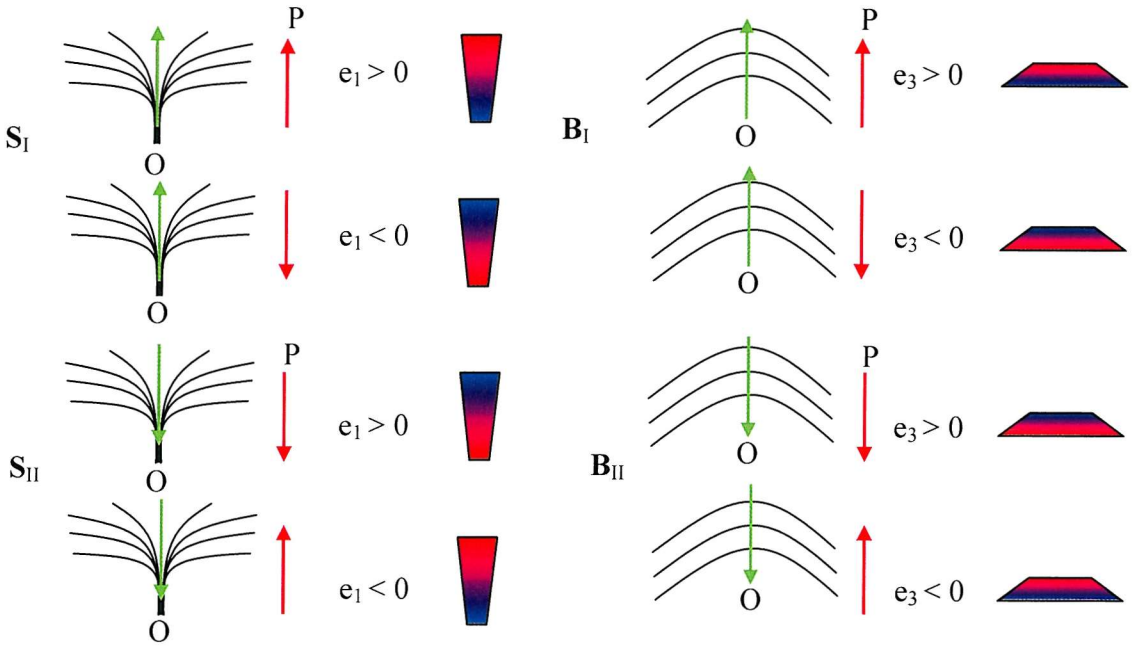

Figure 2.9 The different deformations, showing the different possible deformation directions with relation to an origin O and the polarisation of the sample which correlates to the polarity of the molecule shown in red and blue, where red denotes positive charge and blue negative.[4]

Here we can see as with Equation (16)

$$e_3\mathbf{B}_{II} = -e_3\mathbf{B}_I, \tag{20}$$

however, since we make reference to the flexoelectric coefficient without always defining which vector notation for the deformation we are using, a standard notation needs to be established to relate unambiguously the flexoelectric coefficients for bend for each convention. Thus

$$e_3 = -e_3^m, \tag{21}$$

where e_3^m is defined as flexoelectric coefficient for the bend deformation as originally proposed by Meyer and e_3 is the alternative based on the vector deformation used to define the elastic constants. In this Thesis we shall use e_3 rather than e_3^m (unless specifically stated). There is a fundamental advantage to using the notation which is consistent with that employed by the elastic energy, which is essentially used universally. However, there are other advantages of using the convention as adopted by Rudquist and Lagerwall which is made clear in their paper[4] when they consider the polarization in both a HAN cell and in a ULH geometry.

In the case of the HAN cell we can see that the contributions from the splay and bend can either be in the constructive or destructive sense. So for a given field the direction of the polarization can be defined to either point in the same direction for both deformations or different directions (see Figure 2.10).

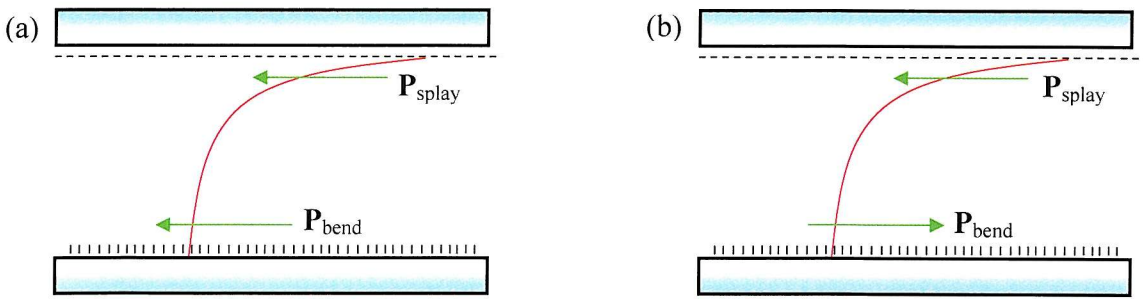

Figure 2.10 Diagram of a HAN cell showing the deformed director in red and the polarisation direction for splay and bend in green. In the case of (a) the positive direction of polarisation for both deformations are in the same direction, in (b) they are opposing each other.[4]

Experiments performed by Dozov *et al.* show that, using the Meyer convention (which corresponds to Figure 2.10b) the deformation in the field is larger (i.e. the splay and bend contributions are adding constructively) for $e_1 - e_3^m$ and smaller (i.e. adding destructively) for $e_1 + e_3^m$. Rudquist and Lagerwall argue in their paper that it would be more intuitive to have the constructive addition correspond to the sum of the coefficients which is the case for $e_1 + e_3$.

Similarly in the case of the uniform lying helix geometry (described in detail in Section 2.4) the tilt in the optic axis on application of the electric field depends on the stability of the splay/bend periodic structure given in Figure 2.11. Again it makes more sense to use $e_1 + e_3$ to denote constructive addition of the polarization for splay and bend (a) rather than the $e_1 - e_3^m$ (b).

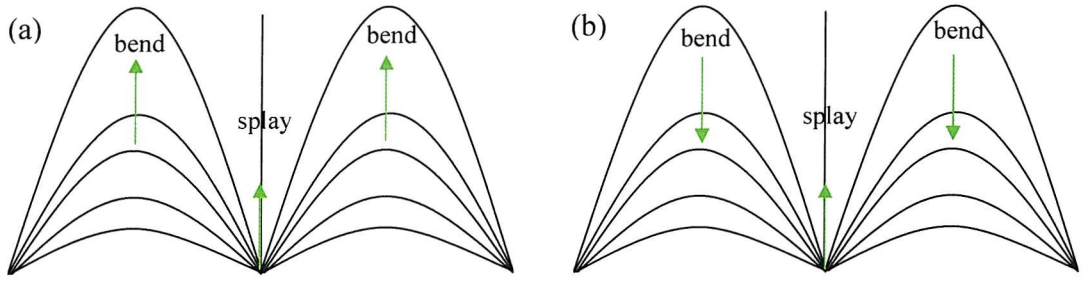

Figure 2.11 The splay/bend periodic deformation thought to be responsible for driving the director tilt in the ULH geometry.[4, 39] In the case of (a) the positive direction of polarisation for both deformations are in the same direction, in (b) they are opposing each other

With the ULH cell, the positive direction of the tilt of the optic axis with respect to the helix axis is defined is not only affected by the sign convention used, but also on the handedness of the helix and the direction of the field. The standard diagram for the change in optic axis is given in Figure 2.12 and angle and direction of the optic axis tilt is generally considered to be the positive direction.

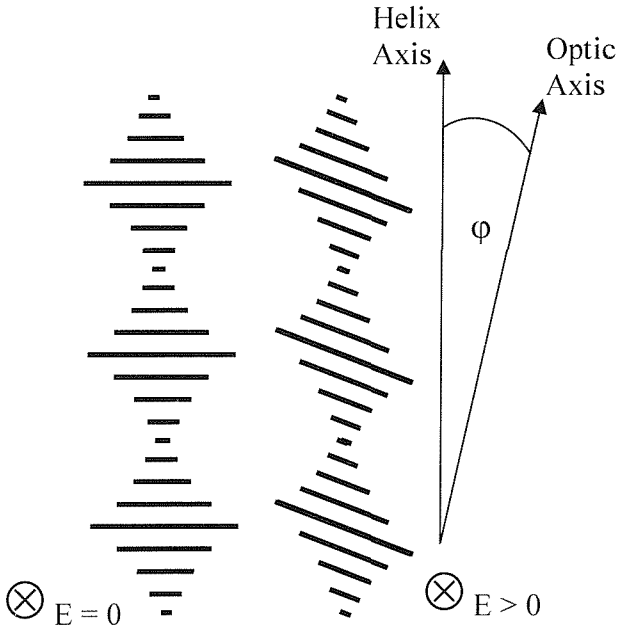

Figure 2.12 The ULH with the applied field E applied perpendicular to the projected plane of the helix.[40]

Thus for a right handed helix and a positive field perpendicular to the helix axis $e_1 + e_3$ would give a positive (clockwise) tilt in the optic axis.

So to conclude, the notation for Meyer's original definition of the flexoelectric polarization is written

$$\mathbf{P} = e_1(\nabla \cdot \mathbf{n}) + e_3^m(\nabla \times \mathbf{n}) \times \mathbf{n}, \tag{22}$$

and the alternative definition which is used throughout the rest of the Thesis is written

$$\mathbf{P} = e_1(\nabla \cdot \mathbf{n}) + e_3(\mathbf{n} \times \nabla \times \mathbf{n}). \tag{23}$$

2.4. Exploiting the flexoelectro-optic effect

To measure the flexoelectric coefficients the properties which are directly related to the effect need to be considered. These are the director deformation and the polarization and could be measured in two ways:

1) Deform the director in the sample and measure the polarization.
2) Apply an electric field to a sample which deforms the director and measure the magnitude of this deformation.

The method of choice is generally the second and the director deformation is measured indirectly. For the ULH experiment this is done by monitoring the intensity of light passing through the cell and crossed polarisers.

Using a ULH geometry as a way to observe the flexoelectric effect on the optical properties of a liquid crystal (the flexoelectro-optic effect) was first proposed by Meyer and Patel in 1987.[39] The method they described involved using a chiral nematic with a positive dielectric anisotropy. By heating the sample into the isotropic phase and allowing it to cool to the chiral nematic in the presence of an electric field set perpendicular to the plane of the cell, the helix orientates itself with its axis parallel to the cell surface. Uniform alignment of the helix axis can be achieved by gentle shearing of the cell described in a later procedure by Rudquist *et al.*[41] A field was created by applying a square wave potential across the cell which causes the director to tilt back and forth allowing the full range of optical rotation to be measured. Measurements were taken by varying the potential applied to the cell and monitoring the transmitted light intensity passing through the crossed polarisers and the cell using a photodiode connected to an oscilloscope. The modern practical set up is almost identical to this and is described in more detail later.

Meyer and Patel go on to explain how this method relates to the flexoelectric effect of the nematic. What follows is a qualitative description of how the effect leads to a resultant change in light intensity caused by a tilt in the optic axis. For diagrammatic purposes the molecules shown are a pictorial representation of dimers with a bent spacer chain. As we have seen, dimers were not the original materials used and tested, however this Thesis is concerned with this molecular motif so it is appropriate to represent the liquid crystal in this way.

The ULH in the undeformed state is hard to describe in a totally accurate fashion. A way of representing the phase could be as a series of layers where the director in adjacent layers are rotated slightly with respect to the previous layer in either a left or right handed fashion (see Chapter 1). The chirality can be either built into the nematogenic molecule (as was the case for Meyer and Patel) or the system can be doped (as is the case for all the compounds considered in this Thesis) with a chiral additive.

We can see in Figure 2.13 that we can look at the projection of the director layers where the length of the lines represents the director rotation (the short lines are where the director points out of the plane) or if we rotate the z axis through 90° we can see the change in the director by taking different slices through the helix. How the layers line up next to each other as the helix rotates is important and so different points in the twist are highlighted in green in both diagrams.

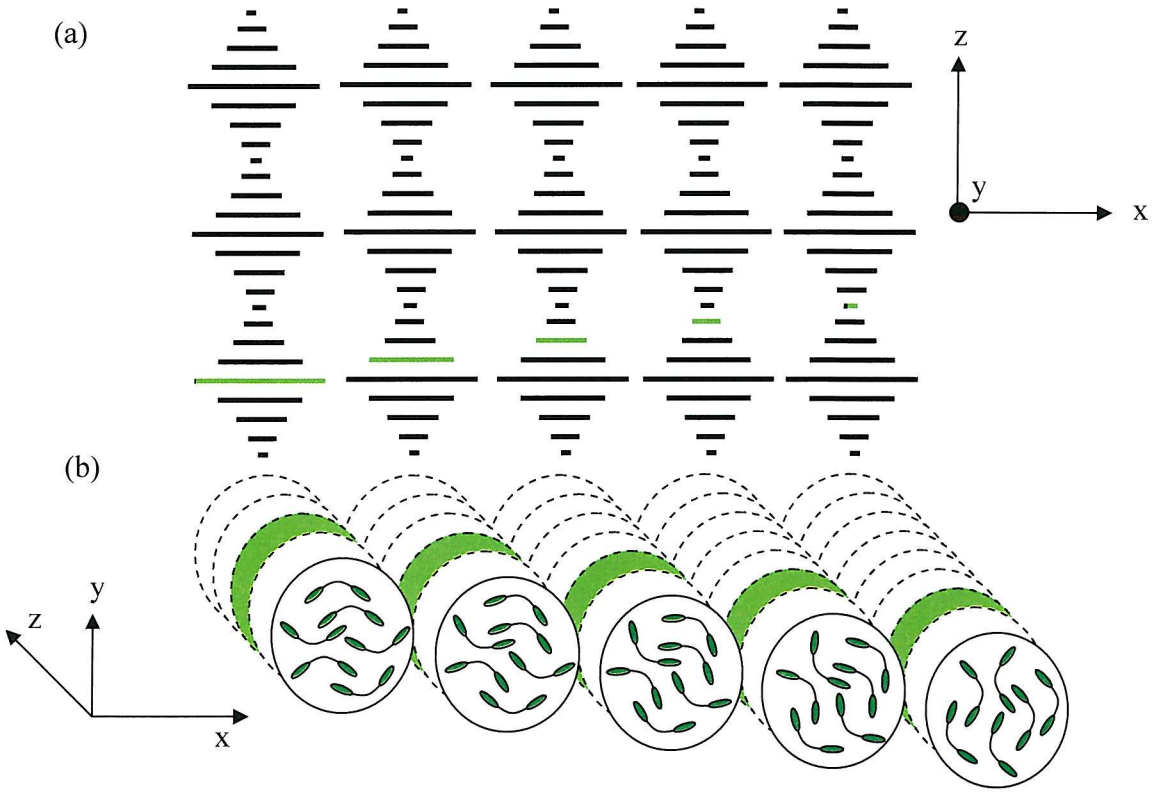

Figure 2.13 (a) A ULH geometry with a left-handed helix whose axis is parallel to the plane of the page. The lines represent the projection of the director onto the page and the lines in green represent the slices taken through the helix seen in (b). In (b) the helix axis is rotated through 90° and the director is represented in a molecular sense using an idealised bent dimers. Sections are taken at different points in the helix showing the director rotation in terms of the molecules. The sample is unpolarised and so there is no splay or bend deformation in the director

Before considering what happens when the field is applied, we must consider the type of geometric structure which would be supported by the flexoelectric effect. The work by Bouligand on biological systems helps us in this task. This showed a periodic splay-bend geometry which arose from chiral systems he was studying, such as crab and insect cuticle. By making cuts across helices he describes the periodic structure which is shown in Figure 2.14.

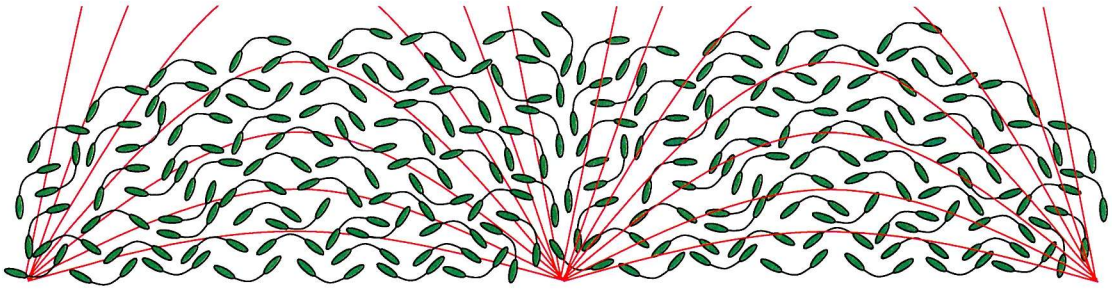

Figure 2.14 Splay/bent periodic structure proposed by Meyer and Patel[39] as being responsible for the tilt in the optic axis due to flexoelectric coupling. Shown here is the director in red and shapes representing idealised bent dimers which have been arranged in this periodic fashion but with the polarisation of the molecular distribution function.

A basic outline of the type of periodic structure is given in Figure 2.14 showing that throughout the structure there are regions where the director is bent and regions where it is splayed. If an electric field is applied and the material has a suitable shape anisotropy and net dipole then this structure can be supported through flexoelectric coupling. The direction of this structure depends on the polarity of the field and the sum of the molecular dipoles.

However, we can see from Figure 2.13 that even if we were to deform the layers over several helices then there would still be a discontinuation as we moved across the structure (shown by the step like fashion in green). However, if the director rotated in the plane of the projected helix, it would tilt to allow the deformed directors on different layers to meet, the splay/bend periodic structure is reinforced as shown in Figure 2.15. Looking down the helix axis at the director at different sections along the helix we see that there is half a splay/bend periodic structure (the director direction is depicted in red). Thus the driving force for the tilt in the optic axis is the stabilization of this periodic structure across the helices. Also shown in Figure 2.15 is the optic axis, the dashed red line, and how that axis moves in relation to the tilt in the director normal.

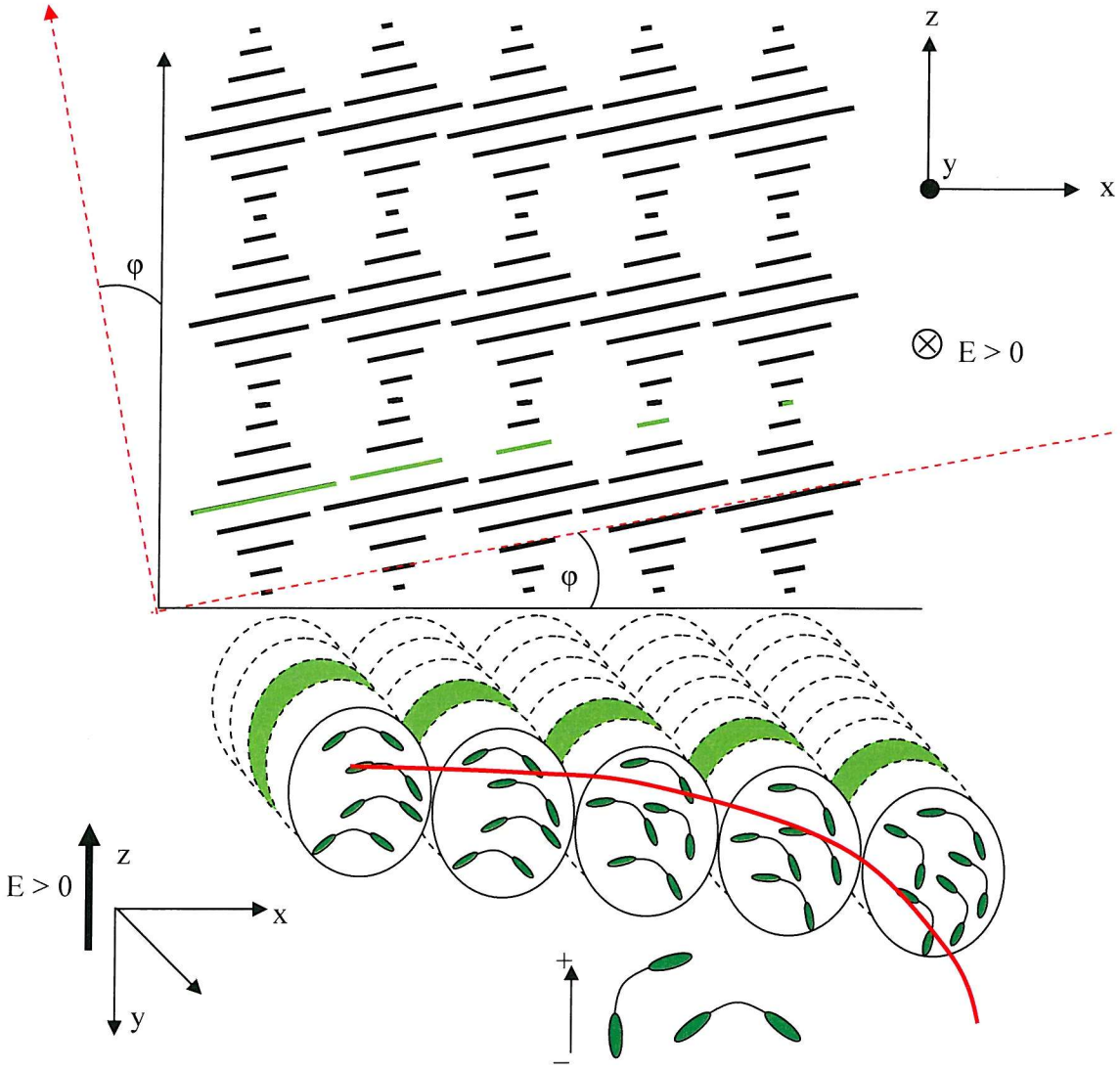

Figure 2.15 (a) A ULH geometry with a left-handed helix whose axis is parallel to the z axis. The lines represent the projection of the director onto the page and the lines in green represent the slices taken through the helix seen in (b). In (b) the helix axis is rotated through 90° and the director is represented in a molecular sense using idealised bent dimers. Sections are taken at different points in the helix showing the director rotation in terms of the molecules. A field (E) runs perpendicular to the helix axis parallel to (z) and anti-parallel to the y axis. The director is deformed and the optic axis is tilted to stabilise the periodic splay/bend structure (half a period shown). Because the helix has been drawn in the left handed form, φ is positive moving to the left.

The sign and size of the flexoelectric coefficients affects this structure significantly. If the sign of $e_1 + e_3$ is negative this would correspond to the direction of polarization in the sample being reversed which has the effect of switching the optic axis to the other side of the helix axis. This should be expected, since, by definition both deformations reduce the

symmetry of the phase to $C_{\infty V}$ parallel to the direction of polarisation and C_{2V} about the line perpendicular to the line of polarisation. Therefore it is not surprising that the change in sign consitutes a rotation through 180° about the line perpendicular to the polarisation. The larger the size of the flexoelectric distortion of the director (i.e. the larger the value of $e_1 + e_3$) the smaller the distance between periods in the structure, and therefore, the larger the tilt to accommodate across a smaller number of helices. This is shown in Figure 2.16 where different tilts in the helices are stabilized for each sized Bouligand constructs are given below.

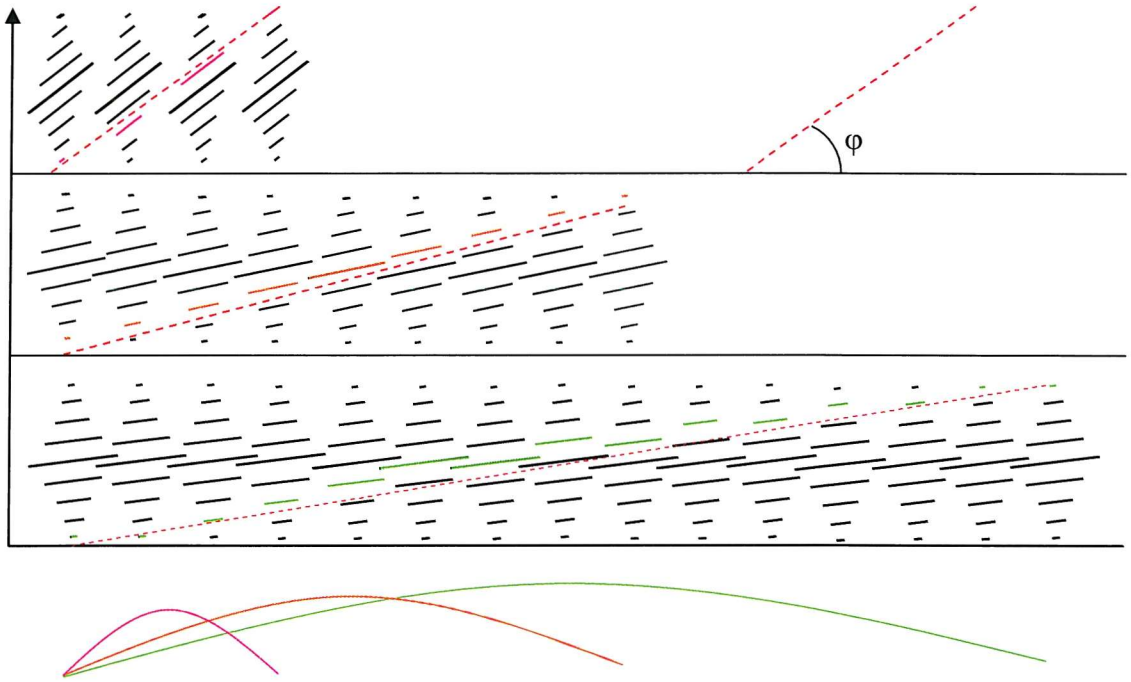

Figure 2.16 Diagram relating the size of the Bouligand construct to the size of φ. For shorter periodic structures the maximum gradient is steeper meaning that a period in the structure spans fewer helices. This drives the director in the helices to tilt more. The smallest period (in magenta) gives the largest tilt angle (a), less steep for the orange larger period (b) and the largest period (c) spans the most helices.

Having considered the principles behind this effect we can now consider the relationship between the tilt in the optic axis, φ, and the mean flexoelectric coefficient, $\bar{e}$, which is given by

$$\tan\phi = \left(\frac{\bar{e}E}{\bar{K}}\right)\left(\frac{P_0}{2\pi}\right), \qquad (24)$$

where E is the field (Vm^{-1}), $\overline{K}$ is the elastic constant (N) and P_0 is the pitch at zero field (m). As described in Chapter 1, the elastic constant can be thought of as how stiff the director is and consequently how resistant the director is to being deformed from its uniform state. Therefore, the larger the elastic constant the smaller tan(φ) will be. The description of the trigonometric dependence on the tilt angle to the physical properties is given by Meyer and Patel in their seminal paper.[39] The relationship of the pitch (the distance that must be travelled along the helix axis for the director to have rotated through 360°) and the angle of tilt is illustrated in Figure 2.17. As the pitch gets smaller (the helix gets tighter), tan(φ) gets smaller.

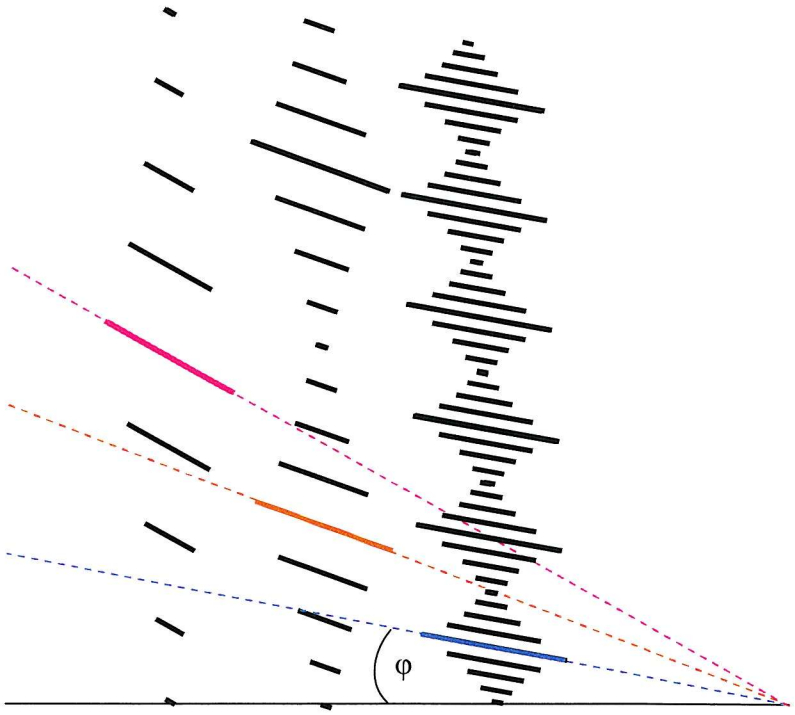

Figure 2.17 A visual representation of the relationship between the change in pitch to an increase in φ.

Devices which exploit the flexoelectro-optic effect are dependent on having a large and fast switching angle. The speed of switching will be considered later, however the size of the angle can be more conveniently related to the flexoelectric coefficients divided by the elastic constants called the flexoelastic ratio $\left(\overline{e}/\overline{K}\right)$. From the description given it appears that to increase the angle of switching we need to increase the pitch and the field (as well

as $\bar{e}/\bar{K}$). This is a complicated requirement because increasing the pitch effectively unwinds the helix and thus it is more easily unwound by an applied field. The threshold electric field for unwinding a helix in a chiral nematic, E_{th}, is related to the inverse of the dielectric anisotropy and the pitch is given by

$$E_{th} = \frac{\pi^2}{P_0}\left(\frac{4\pi K_2}{\Delta\varepsilon}\right)^{1/2}. \tag{25}$$

Thus a large pitch will give a small threshold field and so where $\Delta\varepsilon$ is the dielectric anisotropy and K_2 is the elastic constant for the twist deformation. Therefore to maximize the pitch in Equation (25)[41] the ideal liquid crystal for maximizing tan(φ) would need to minimize $\Delta\varepsilon$. Physically this is made harder since the relationship between the threshold field and the dielectric anisotropy is quadratic in E compared to the switching angle which is linear in E. This has two implications, the first being that any reduction in $\Delta\varepsilon$ will have diminishing returns in increasing E_{th}; secondly an increase in the field will cause both a flexoelectric and dielectric response, with the dielectric coupling quickly dominating due to the quadratic relationship. This expressed most clearly in the free energy density expression for a chiral nematic given by

$$F = \frac{1}{2}\left\{K_1\mathbf{S}'^2 + K_2\left(\mathbf{T}'+q_0\right)^2 + K_3\mathbf{B}'^2\right\} - \left\{e_1\mathbf{E}\cdot\mathbf{S} + e_3\mathbf{E}\cdot\mathbf{B}\right\} + \left\{\frac{\varepsilon_0\Delta\varepsilon}{2}\left(\mathbf{E}\cdot\mathbf{n}\right)^2\right\}, \tag{26}$$

where **S**, **B** and **T** are the vectors for bend, twist and splay, q_0 is the $2\pi/P_0$, ε_0 is the electric constant and $\Delta\varepsilon$ is the dielectric anisotropy. In this complicated expression we can see that it can be broken down into three more familiar components shown in Equation (27) and given in Equations (28)-(30).

$$F_{total} = F_{elastic} + F_{flexoelectric} + F_{electric}, \tag{27}$$

$$F_{elastic} = \frac{1}{2}K_1\left(\nabla\cdot\mathbf{n}\right)^2 + \frac{1}{2}K_2\left(\mathbf{n}\cdot\nabla\times\mathbf{n} + q_0\right)^2 + \frac{1}{2}K_3\left(\mathbf{n}\cdot\left(\nabla\cdot\mathbf{n}\right)\right)^2, \tag{28}$$

$$F_{flexoelectric} = e_1\mathbf{E}\cdot\mathbf{n}\left(\nabla\cdot\mathbf{n}\right) + e_3\mathbf{E}\cdot\left(\mathbf{n}\times\nabla\times\mathbf{n}\right), \tag{29}$$

$$F_{electric} = \frac{\varepsilon_0 \Delta\varepsilon}{2}(\mathbf{E}\cdot\mathbf{n})^2. \quad (30)$$

We can see from this, the dependence of the dielectric component of the free energy is quadratic in E compared to the linear dependence on E for the flexoelectric contribution. Historically there have been two methods for minimizing the dielectric coupling which would rotate the director rather than deform it. The original method introduced by Rudquist *et al.*[41] involved a chiral nematic with a dielectric anisotropy which was temperature sensitive. At a certain temperature the sign changed and thus if measurements were made at this temperature, the dielectric anisotropy is zero. This has been shown to work very well, but is very hard to achieve and makes measurements at different temperatures very difficult.

The alternative method is to use materials which have a small dielectric anisotropy. This is generally hard to achieve with standard monomeric liquid crystals, however it was demonstrated by Coles *et al.* that small dielectric anisotropies could be achieved using liquid crystal dimers. This indeed allowed larger fields to be applied resulting in greater flexoelectric coupling and consequently larger switching angles.

The switching speed in the ULH cell is surprisingly not dependent on the flexoelectric coefficient and is given by

$$\tau = \frac{\gamma_1}{\bar{K}}\left(\frac{P_0}{2\pi}\right)^2, \quad (31)$$

where τ is the switching time (s) and γ_1 is the twist viscosity (Nm^{-2}). If we assume that the driving force for the tilt of the director is the stabilization of the splay/bend periodic structure, then we could imagine that the larger the flexoelectric coefficients, the bigger the driving force for the tilt in the director (and so the faster the director tilts), and also the bigger the angle that the director moves through. Hence, just like a pendulum, the time is constant and therefore independent of the flexoelectric coefficients. By maintaining a large pitch we increase τ which results in slow switching times. Therefore to achieve a faster switching time we must reduce the pitch which unfortunately also reduces the switching angle.

2.5. Using liquid crystal dimers as a design motifs

As we have seen, many of the initial measurements were made on room temperature nematic liquid crystals which, considering their molecular structure, do not possess much of the non-symmetric shape anisotropy which is suggested as necessary in Meyer's seminal paper. By examining the materials in Figure 2.3, the azo and azoxy compounds are almost linear whereas there is only a slight bend in 5CB and 8CB as drawn. However, given the aliphatic chain is mobile, it could be thought of as sweeping out a cone shaped region as it moves reducing the molecular non-symmetry.

As originally suggested by Durand[30] liquid crystal dimers have, by comparison, an ideal geometry (see Figure 2.18) where, due to the flexible spacer a multitude of different asymmetric conformers can be adopted and whilst also being relatively straightforward to synthesise[42] and tend to give well stabilized liquid crystal phases (increasing the likelihood that the phase will be enantiotropic). However their major drawback is that they have typically high melting points.

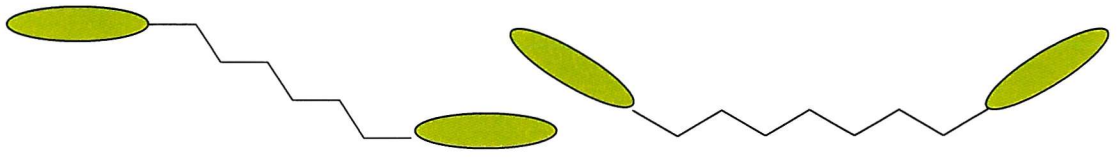

Figure 2.18 The basic shape of odd and even dimers drawn in their all-trans form

Reported syntheses by Vorlander of what would be recognized now as a liquid crystal dimer date back as far as 1927.[43] Synthesis of liquid crystal polymers and individual dimeric systems where known by the early 1980s, however, it was not until 1983 that investigations into the properties of whole series of liquid crystal dimers were made. This started with the synthesis of symmetric cyanobiphenyl dimers[42] leading to a plethora of different symmetric and non-symmetric dimer, trimers and oligimers being synthesized.[44-49]

As mentioned in Chapter 1 and revisited later in Chapter 3, it is easy to make the mistake of only considering the all-trans conformers and ignoring the vast number of other conformers that are likely in the liquid crystal phase. Consideration of all the conformers in the distribution can only be done by calculation, however, it is important to appreciate

that even dimers possess bent conformers (up to 50% in the conformational distribution) and, as might be expected, the odd dimers show many more bent conformers (around 90% in the conformational distrubution) but also some linear conformers.[50]

Flexoelectric measurements over the last 10 years have been focused quite heavily (although not exclusively) around probing the flexoelectro-optic effect.[51] One of the driving forces for the research has been to try and make materials which could be used in a display device by creating a ULH geometry in a cell which can be used to exploit the flexoelectro-optic effect. The principles surrounding such a cell are described in detail in Section 2.4 and the practical setup is outlined in Section 2.6. One of the key problems in these devices is that the size of the field applied to the device can cause the helix to unwind due to dielectric coupling to the liquid crystal. This is explained in Section 2.4 and the problem has been overcome using liquid crystal dimers. This is because for most dimers, due to symmetry, $\varepsilon_{\parallel}$ is reduced by anti parallel dipoles in the more liner dimers cancelling each other partially or totally (with the exception of broad U-shaped conformers sometimes achieved in odd dimers). The effect of this was first demonstrated by Coles *et al.* who compared 7CB and 7OCB to CBO8OCB.[40] Despite the dimer having an even parity spacer (which was due to poor solubility of the chiral dopant in the other homologues[52]) the flexoelastic ratio was notably higher than for the monomers. This was largely due to the higher threshold field for unwinding the helix allowing a much larger field to be applied. However it was also evident that for similar fields, the dimer still showed a larger flexoelectric coupling than monomers.

Much of the work surrounding flexoelectric measurements on liquid crystal dimers originated from Coles' group with a variety of different materials examined, including dimers which incorporated a cholesterol unit to build chirality into the system;[31] and symmetric and non-symmetric dimers with fluorinated mesogenic groups, which showed extremely large flexoelastic ratios, some as large as 1.74 $CN^{-1}m^{-1}$ (compared to ~0.4 $CN^{-1}m^{-1}$ for 5CB[19]).

2.6. Making practical measurements

To make measurements on a sample, the liquid crystal has to be in a chiral nematic phase with the helix axis lying in the plane of the cell. The direct property we are measuring is

the change in light intensity which requires the sample to be mounted on a heating stage on a microscope with a photodiode attachment (specific details as to the model and make of the instruments used are given in Chapter 7 under the general experimental section). The reading from the photodiode is taken from an oscilloscope as a potential is applied across the cell. The potential is generated as an alternating square-wave signal with a 1 kHz frequency. This field is amplified 50x and connected to a HAN cell via wires which are soldered to a conductive surface on the cell. It should be noted that the switching times typically found for the flexoelectro-optic effect are of the order 10-100 μs which is between 10 and 100 times faster than the alternating potential and so the change in optic axis follows the change in field closely without much noticeable lag in the signal. A diagram of the microscope setup is given in Figure 2.19 and a diagram of the cell used is given in Figure 2.20.

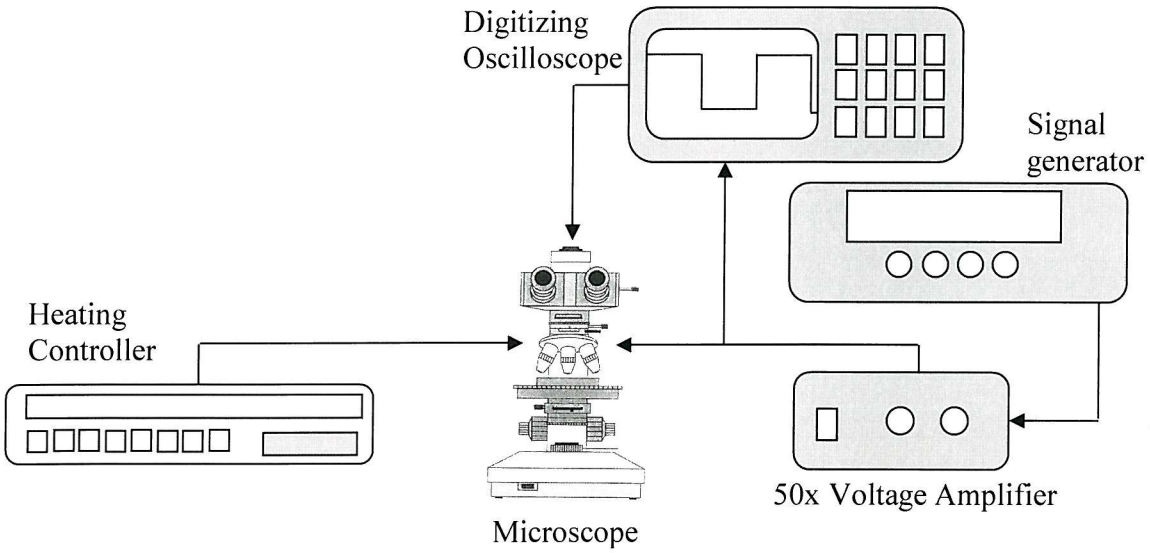

Figure 2.19 The experimental setup used to measure the switching angle showing the general setup of the apparatus.

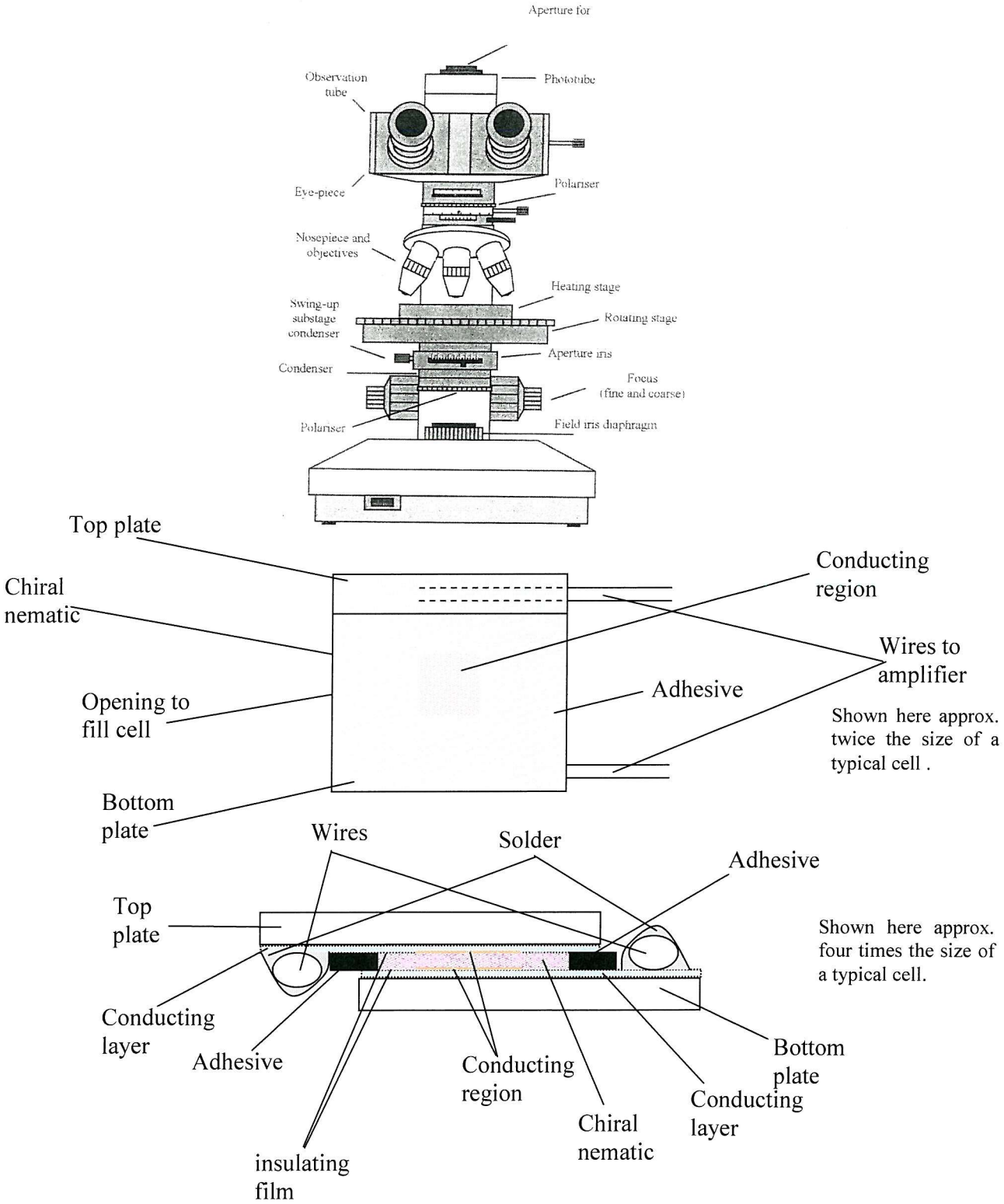

Figure 2.20 (Top) An annotated example of the type of microscope used.[53] (Middle) A Diagram of a HAN cell supplied by Merck showing a plan view. (Bottom) A cross section of this HAN cell. The cells used were all ~5 μm thick, with the exact value recorded on each cell.

The nematic used is doped (if not already chiral) with a chiral dopant which is dissolved into the host. The cell is then filled by sitting the open end in a puddle of molten liquid crystal normally heated well into the isotropic phase to reduce the viscosity. Typically the cells reported in this Thesis were 5 μm thick, although other thicknesses could be used. The sample then fills the cell by capillary-action. Once the cell is filled, wires are hot soldered on to the conductive overhanging edges of the cell. Once soldered, these joints are then typically taped over (not shown in the diagram) to increase their strength. HAN cells are used here as the hybrid surfaces tend to support the lying helix geometry well. The cell is then placed on the hot-stage of the microscope and attached to the stage by means of heat-proof tape. The sample was then heated into the isotropic and then cooled into the chiral nematic causing a standing helix (where the helix axis is perpendicular to the plane of the cell) to form in the cell which is typically seen as a dark region (as the light is not scattered and cannot pass through the crossed polarisers). A moderately low potential is applied (typically 7.5 V, corresponding to 1.5 MVm^{-1} or 1.5 $V\mu m^{-1}$) which reorientates the helix axes parallel to the plane of the cell. The field is then increased to the threshold value and the helical structure unwinds giving a dark state. The cell is manipulated mechanically by pressing down on the top layer with a spatula to cause the nematic to flow and the field is reduced allowing the helix to reform but in a uniform direction. Mechanical motions in the same direction are normally used to encourage a completely uniform state to form. Rotating the sample using the turntable, on which the hot-stage is mounted, gives a change of light intensity corresponding to the helix axis being aligned parallel to one of the crossed polarisers (dark state) or being at 45° to the crossed polarizer (light state). The turntable has a 0 - 360° range with a Vernier scale which allows the rotation angle of the sample to be accurately measured. The error on reading the Vernier scale can be estimated to ±0.1° and the accuracy by which the dark state can be determined is also around ±0.1° assuming a good signal to noise ratio. Measurements can be undertaken of the intensity of the light through the sample (as seen by the photodiode) as a function of angle at a given field. The ULH structure is maintained by the field, if the field is too low then the structure will collapse and if the field is too high then the helix will unwind again destroying the structure. Thus an evenly spread range of increasing potentials were used. The range of potentials tends to be

employed was arbitrarily decided based on how the material appeared to behave under the microscope (using the naked eye) at high and low fields although normally a range of at least 10 V, often more than a 20 V range was used.

The procedure for making a measurement for a given potential is described here and the explanation of what is happening and why this procedure is used then follows.

The sample was rotated to the dark state which is normally determined by using the flat line signal on the oscilloscope (see Figure 2.21A) rather than looking down the microscope directly as this was more accurate. The sample was then rotated by +22.5° and the difference of intensity for the + and – rotations were easily seen on the square-wave signal given (see Figure 2.21B). The difference between the + and – intensities was determined using guidelines (see Figure 2.21C). Half the difference between these two intensities was measured (see Figure 2.21D) and the sample was then rotated about this mid point so that the upper intensity lay on the mid line (this angle was taken as $+\varphi$ shown in Figure 2.21E) and then the sample was rotated in the other direction so the lower intensity lay on the mid line (this angle was taken as $-\varphi$ shown as Figure 2.21F). $\Delta\varphi$ was determined as the difference between these two angles. This process was then repeated for all the potentials in the range being measured.

The results for $\tan(\varphi)$ were then plotted against the change in field; according to theory this should be a linear relationship passing through the origin. The field is taken as the potential divided by the thickness of the cell (thickness is found recorded on each cell).

Taking Equation 24,

$$\tan\phi = \left(\frac{\bar{e}E}{\bar{K}}\right)\left(\frac{P_0}{2\pi}\right), \tag{24}$$

we can see that using the gradient of the plotted line and the pitch of the system, we can determine the flexoelastic ratio. This is explained using an example in Chapter 3.

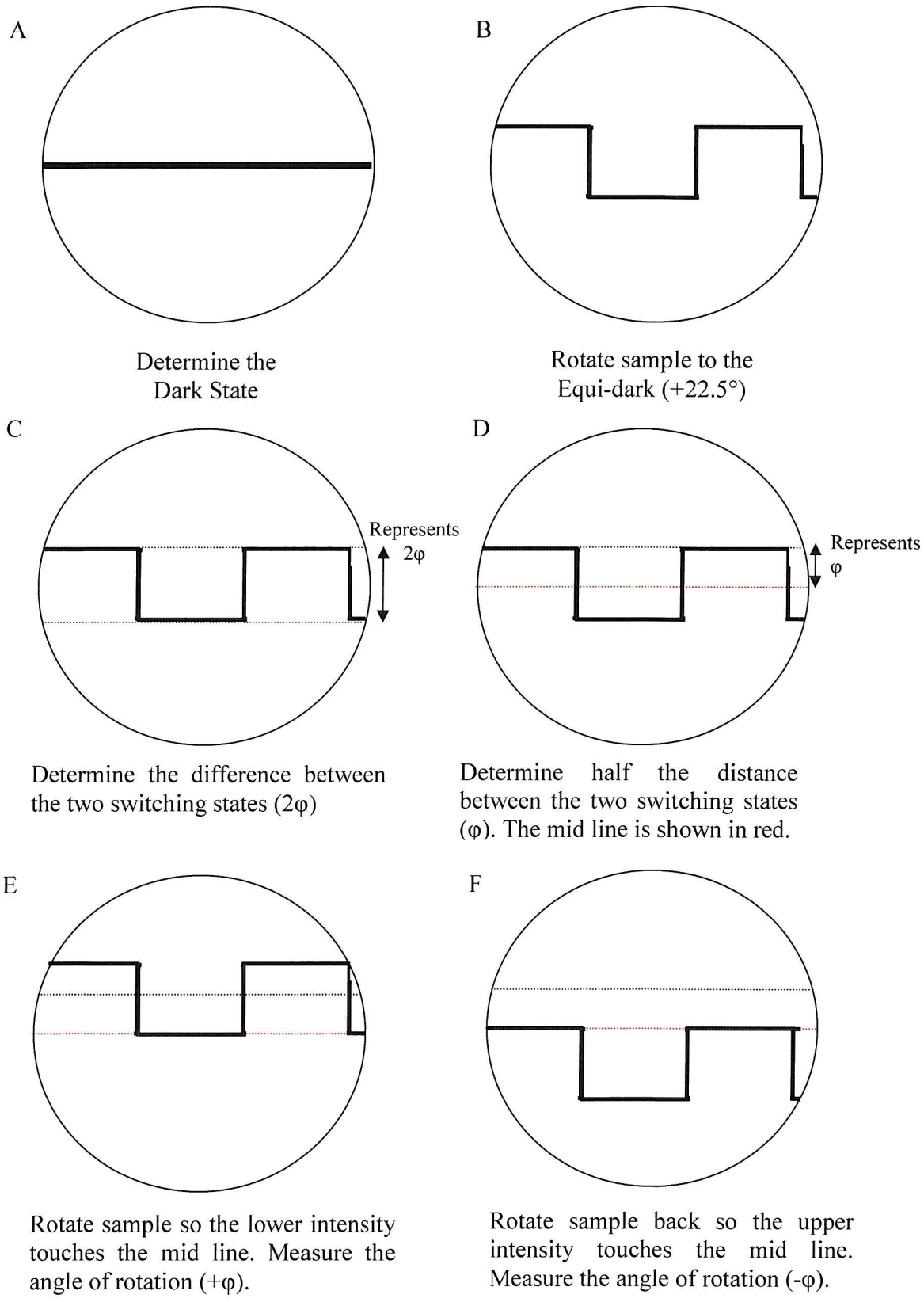

Figure 2.21 Shown are some typical sketched examples of idealised signals from the photo-diode as seen on the digital oscilloscope for different stages through the process of measuring $\Delta\varphi$ for an applied field.

The methodology for making these measurements can, at first, appear confusing as it is not intuitively obvious why an angle of 22.5° is used for the first rotation rather than 45°. This results from the relationship between the intensity of the light transmitted through the sample and the rotation angle of the optic axis (which is itself related to the size of the field and the flexoelastic ratio). This is given as

$$I(E) = I_0 \sin^2\{2[\Psi_0 + \varphi(E)]\}\sin^2\left(\frac{\pi d}{\lambda}\Delta n\right), \tag{32}$$

where I(E) is the intensity of light seen through the sample at field E, I_0 is the intensity of maximum light that can pass through the cell at E = 0, $\varphi(E)$ is the rotation angle of the optic axis at field E, Ψ_0 is the angle of the helix axis away from the polarizer (normally set to 22.5° at E = 0), d is the thickness of the cell, λ is the wavelength of light and Δn is the refractive index of the cell.

We can see from Equation 32 that for a given cell, $\left(\frac{\pi d}{\lambda}\Delta n\right)$ will be a constant and I_0 will be a constant and therefore we can simplify the equation to

$$\frac{I(E)}{I_0 C} = \sin^2\{2\Psi\}, \tag{33}$$

where

$$C = \sin^2\left(\frac{\pi d}{\lambda}\Delta n\right), \tag{34}$$

and

$$\Psi = \Psi_0 + \varphi(E). \tag{35}$$

The relationship between the scaled light intensity and the angle of rotation away from the polarizer is now simply a quadratic sin relationship. Before we consider (2Ψ), we should look at how $\sin^2(2\Psi)$ varies with increasing angle, and this is shown in Figure 2.23. We can see that gradient of the line is at its steepest when $2\Psi = 45°$ and thus $\Psi = 22.5°$. Given the rotation in the optic axis deviates $\pm\varphi$ from the helix axis and this, in an AC field, would give an alternating change in the light intensity which is related to the

change in polarity of the field. The amplitude of the intensity will, however, vary depending where on the $\sin^2(2\Psi)$ curve the helix axis is located and how large φ is.

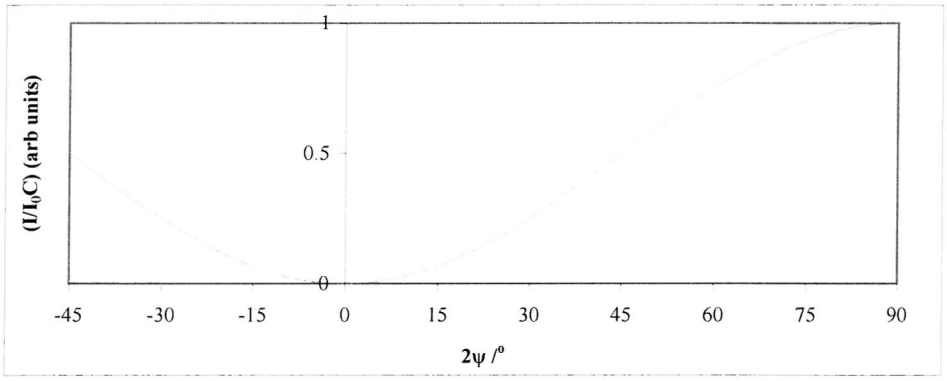

Figure 2.22 Plot of $\sin^2(2\Psi)$ where $\Psi = (\Psi_0 + \varphi)$, Ψ_0 is the angle between the helix axis and the polariser at E = 0 and φ is the rotation angle in the optic axis.

Thus to achieve the maximum difference in the light intensity for the switching angle φ, we need ideally to set the helix axis to be at the point where the gradient of the curve is steepest (at E = 0) which corresponds to the $2\Psi = 2\Psi_0 = 45°$ thus $\Psi = 22.5°$.

This is illustrated in Figure 2.23 and 2.24 where the helix axis (HA) in red and the tilted optic axis (blue) are shown with respect to the crossed polarisers (the axes) and the corresponding points are shown on a $\sin^2(2\Psi)$ plot.

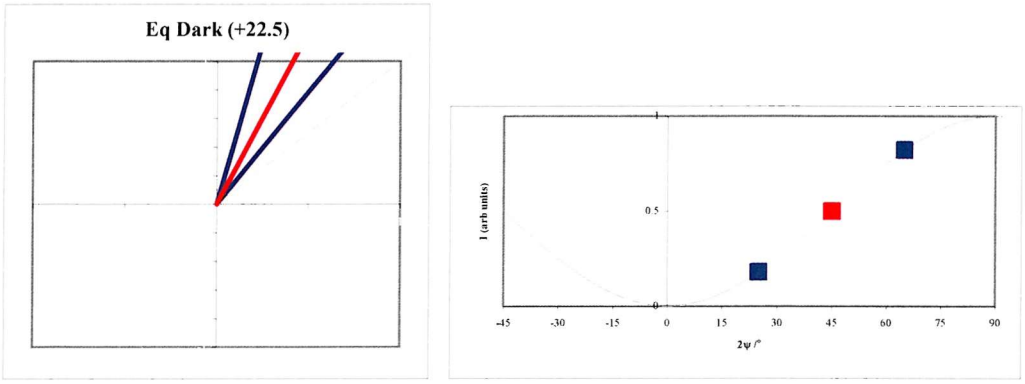

Figure 2.23 The HA is at 22.5° and there is maximum difference in intensity for $\pm\varphi$. The example shown plotted on a $\sin^2(2\Psi)$ graph and as a projection on crossed polarisers.

In Figure 2.23 the helix axis is position is set ($\Psi_0 = 22.5°$) to give the optimum difference in intensity for $\pm\varphi$ (which for this example $\varphi = 10°$). If we compare this situation with Figure 2.24 we see that the helix axis is set to a different value (($\Psi_0 = 12.5°$) and that the

intensity for $-\varphi$ is somewhat smaller compared to that at $+\varphi$. It should also be noted that although the apparent difference appears quite small, this is a ratio and so the real values may reflect quite a significant difference, especially if $\bar{e}/\overline{K}$ is small.

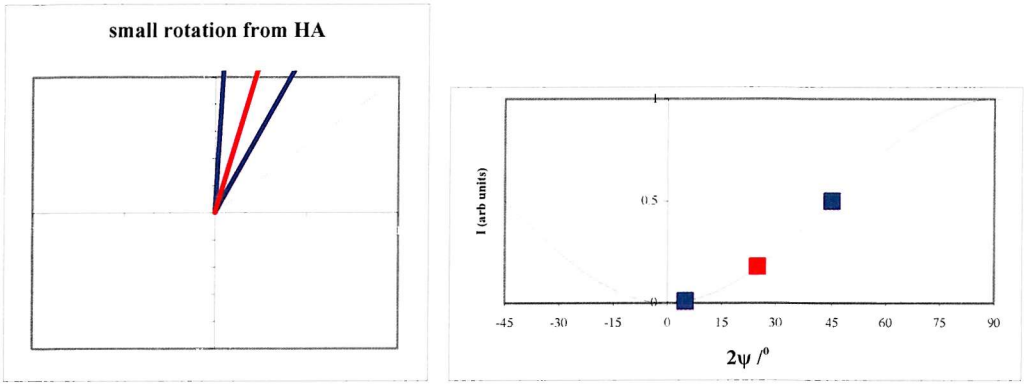

Figure 2.24 HA is 12.5° from the polarizer resulting in only a small difference for $-\varphi$. The example is shown plotted on a $\sin^2(2\Psi)$ graph and as a projection on crossed polarisers.

For the sake of completeness Figure 2.25A-D shows for a complete measurement at a given field E, the position of the different axes with respect to the polariser axes, how this relates to the $\sin^2(2\Psi)$ curve and how this may appear on an idealised oscilloscope reading.

A

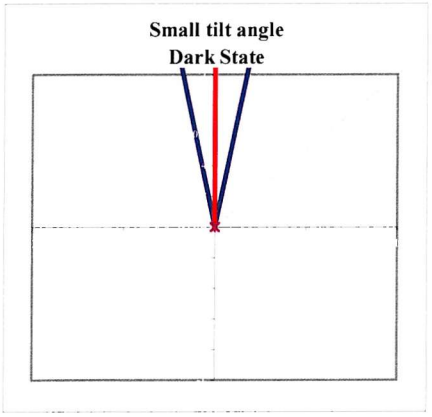

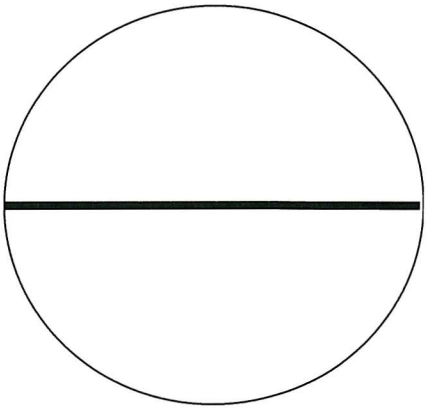

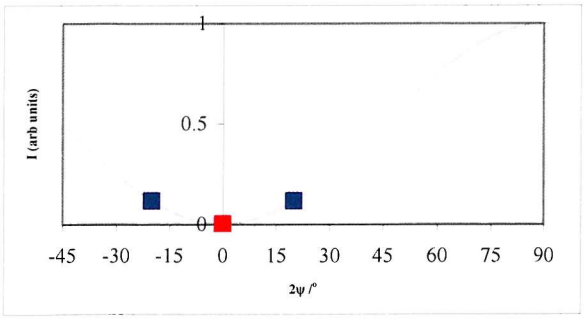

The sample is rotated to the dark state which is normally determined by using the flat line signal on the oscilloscope rather than looking direct optical observation as this is more accurate.

B

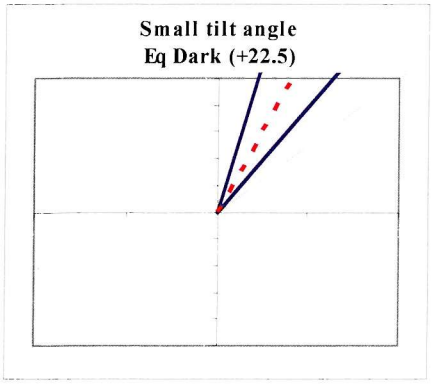

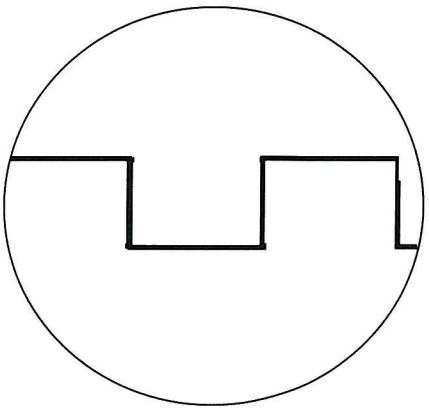

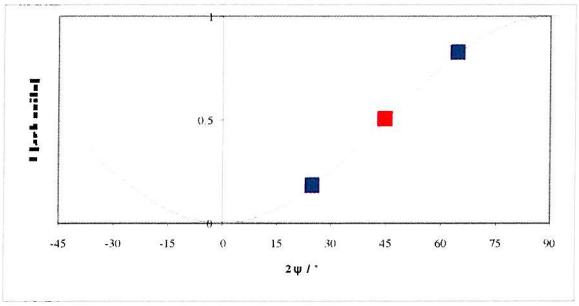

The sample is then rotated by +22.5° the difference of intensity for the + and – rotations are easily seen on the square-wave signal given.

C

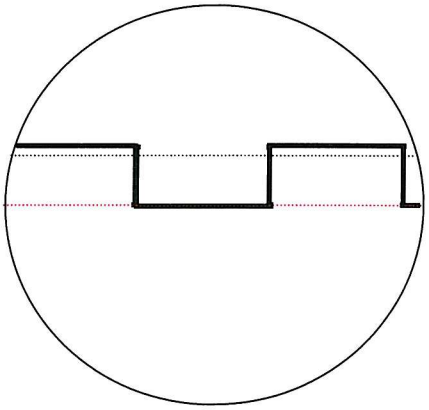

The difference between the + and – intensities is determined using guidelines. Half the difference between these two intensities is measured and the sample is then rotated about this mid point so that the upper intensity lies on the mid line (the angle is taken as +φ)

D

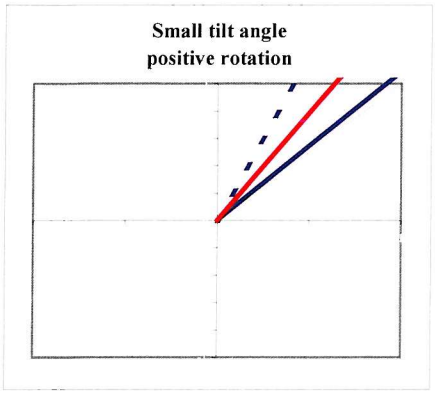

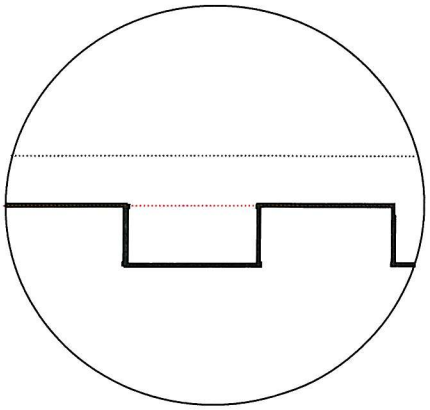

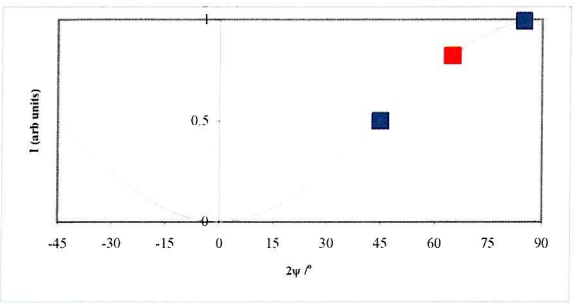

The sample is rotated in the other direction so the lower intensity lies on the middle line (this is angle is taken as $-\varphi$. $\Delta\varphi$ is given as the difference between these two angles.

Figure 2.25 Plots and diagrams showing where the helix axis and optic axes lie in respect to the crossed polarisers; where each axis fall on the scaled light intensity plot; and how this may correspond to the oscilloscope reading for a typical measurement to determine φ for a given field E. Note in this example φ = 10°.

This technique therefore is well suited to materials with small switching angles (less than $2\varphi < 45°$) and a moderate field. Those materials with a large flexoelastic ratio or a moderate flexoelastic ratio and a large threshold field can result in switching angles which are greater than 45°. This presents several problems as the intensity starts becoming smaller which, experimentally results in the intensity reading to dip down coming back on itself making readings more awkward to take and consequently more difficult to measure with a high degree of accuracy. Normally sufficient readings can be made at smaller fields to be able to generate the linear relationship from which we can determine the flexoelastic constants.

As a final note the size of the switching angle is determined by a combination of the pitch, the size of E and the flexoelastic ratio. To support the ULH there is a minimum field which has to be applied which varies depending on the material and the quantity of chiral dopant added. The pitch varies according to the temperature, the quantity of chiral

dopant and the properties of the host liquid crystal. The pitch cannot be too large else again the ULH cannot be supported at low fields and is too easily unwound at high fields. Therefore for a material, doped with a similar quantity of chiral dopant there are practical constraints placed on the experiment which means a compromise must be reached. Generally a 2-4 mmol% quantity of chiral dopant (comparable to that found in the literature[52, 53]) will make the helix small enough to have a reasonable E_{th} and support the ULH at low fields (as low as 0.5 $V\mu m^{-1}$). The field is varied over a range of values, however if $\bar{e}/\bar{K}$ is sufficiently large under these conditions then as the field is increased the switching angle can quickly become larger than 45°. As mentioned previously, in these cases, a range of smaller fields are used to determine the linear relationship between tan(φ) and the field.

2.7. References

1. R. B. Meyer, *Phys. Rev. Lett.*, **1969**, 22, 918-921.
2. Piezelectric materials; Introduction: The Piezoelectric effect. http://www.piezomaterials.com/ (2007),
3. PiezosystemsInc, Introduction to Piezoelectricity. *Catelogue*, 2006; Vol. 7, p 57.
4. P. Rudquist, S.T. Lagerwall, *Liq. Cryst.*, **1997**, 23, (4), 503-510.
5. D. A. Dunmur, A. Fukuda, G. R. Luckhurst, *Liquid Crystals: Nematics*. 2001.
6. J. Prost, J. P. Marcerou, *J. Phys. (Paris)*, **1977**, 38, 315.
7. W. Haas, J. Adams, J. B. Flannery, *Phys. Rev. Lett. (USA)*, **1970**, 25, 1326.
8. W. Helfrich, *Z. Naturforsch.*, **1971**, 26a, 833.
9. M. A. Osipov, *Sov. Phys. JETP (English Trans.)*, **1983**, 58, 1167.
10. Y. Singh, U. P. Singh, *Phys. Rev. A* **1989**, 39, 4254.
11. S. Ponti, C. Ferrero, S. Zumer, P. Ziherl, *Liq. Cryst.* , **1999**, 26, 1171.
12. A. Ferrarini, *Phys. Rev. E*, **2000**, 64, 021710.
13. B. A. Umanski, L. M. Blinov, M. I. Barnik, *Kristallografiya (USSR)*, **1982**, 729.
14. H. P. Hinov, A. I. Derzhanski, *Liquid Crystals and Ordered Fluids*. Plenum Press: Ed. A. C. Griffin, J. E. J. New York - London, 1984; Vol. 4, p 1103.
15. S. V. Yablonski, L. M. Blinov, S. A. Pikin, *Pis'ma Zh. Eksp. Teor. Fiz (USSR)*, **1984**, 40, 226.

16. S. V. Yablonski, L. M. Blinov, S. A. Pikin, *Mol. Cryst. Liq. Cryst.*, **1985**, 127, 381.
17. L. M. Blinkov, L. A. Beresnev, S. A. Davydyan, S. G. Kononov, S. V. Yablonski, *Ferroelectrics (UK)*, **1988**, 84, 365.
18. L. M. Blinkov, D. B. Subachyus, S. V. Yablonski, *J. Phys. II (France)*, **1991**, 1, 459.
19. A. G. Petrov, *Physical properties of Liquid Crystals: Nematics*. INSPEC: Ed. D. A. Dunmur, A. Fukuda, G. R. Luckhurst 2001.
20. P. Rudquist, L. Komitov, S.T. Lagerwall, *Liq. Cryst.*, **1998**, 24, 329.
21. N. V. Madhusudana, G. E. Durand, *J. Phys. Lett. (France)*, **1985**, 46, 195.
22. B. Valenti, C. Bertoni, G. Barbero, P. Taverna-Valabrega, R. Bartolino, *Mol. Cryst. Liq. Cryst.*, **1987**, 146, 307.
23. I. Dozov, I. P., Ph. Martinot-Lagarde, G. E. Durand, *Ferroelectr. Lett. Sect.*, **1984**, 2, 135.
24. J. P. Marceroux, J. Prost, *Mol. Cryst. Liq. Cryst.*, **1980**, 58, 259.
25. I. Dozov, Ph. Martinot-Lagarde, G. E. Durand, *J. Phys. Lett. (France)*, **1982**, 43, 365.
26. T. Takahashi, S. Hashidate, H. Nishijou, M. Usui, M. Kimura, T. Akahane, *Jpn. J. Appl. Phys. (Japan)*, **1998**, 37, 1982.
27. P. R. M. Murthy, V. A. Raghunathan, N. V. Madhusudana, *Liq. Cryst.*, **1993**, 14, 483.
28. B. A. Umanski, V. G. Chigrinov, L. M. Blinov, Yu. B. Pod'yachev, *Zh. Eksp. Teor. Fiz. (USSR)*, **1981**, 81, 1307.
29. M. I. BarnikI, L. M. Blinov, A. N. Trufanov, B. A. Umanski, , *J. Phys (France)*, **1978**, 39, 417.
30. G. E. Durand, Personal Communication, 10th ILLC, to G. R. Luckhurst, 1984.
31. B. Musgrave, P. Lehmann, H. J. Coles, *Liq. Cryst.*, **1999**, 26, 1235.
32. R. A. Ewings, C. Kischka, L. A. Parry-Jones, S. J. Elston, *Phys. Rev. E*, **2006**, 73, 011713
33. C. Kischka, L. A. Parry-Jones, S. J. Elston, P. Raynes Poster Presentation. Oxford Flexoelectricity Meeting, 2006.

34. F. C. Frank, *Discuss. Faraday Soc*, **1958**, 25, 19.
35. C. W. Oseen, *Ark. Mat. Astron. Fys. (Sweden)*, **1925**, 19a, 1.
36. C. W. Oseen, *Trans. Faraday Soc.*, **1933**, 29, 883.
37. Zocher, H., *Trans. Faraday Soc.*, **1933**, 29, 945.
38. Conference meeting, Flexoelectricity in Liquid Crystals. Oxford University: 2006.
39. J. S. Patel, R. B. Meyer, *Phys. Rev. Lett.*, **1987**, 58, 1538.
40. H. J. Coles, B. Musgrave, M. J. Coles, J. Willmott,, *J. Chem. Mater.*, **2001**, 11, 2709.
41. P. Rudquist, M. Buivydas, L. Komitov, S.T. Lagerwall, *J. Appl. Phys.*, **1994**, 76, 7778.
42. J. W. Emsley, G. R. Luckhurst, G. N. Shilstone, I. Sage, *Mol. Cryst. Liq. Cryst.*, **1984**, 102, 223.
43. D. Vorlander, *Z. Phys. Chem.*, **1927**, 126, 449.
44. V. Percec, A. D. Asandei, G. Ungar,, *Chem. Mater.* , **1996** 8, 1550.
45. G. Ungar, J. Zhou, V. Percec, P. Chu, *Makromol. Chem., Makromol. Symp.*, **1995** 98 951.
46. A. G. Douglass. Ph.D. Thesis. University of Southampton, 1998.
47. C. T. Imrie. Ph.D. Thesis. University of Southampton, 1988.
48. P. J. Barnes. Ph.D. Thesis. University of Southampton, 1994.
49. R. W. Date. Ph.D. Thesis. University of Southampton, 1991.
50. A. Ferrarini, G. R. Luckhurst, P. L. Nordio, *Chem. Phys Lett.*, **1993**, 214, 409.
51. S. M. Morris, M. J. Clarke, A. E. Blatch, H. J. Coles, *Phys. Rev. E*, **2007**, 75, 041701.
52. B. Musgrave. Ph.D. Thesis. University of Southampton, 1999.
53. M. J. Clarke. Ph.D. Thesis. University of Southampton, 2004.

Chapter 3

Investigating the flexoelectric effect in non-symmetric conventional liquid crystal dimers

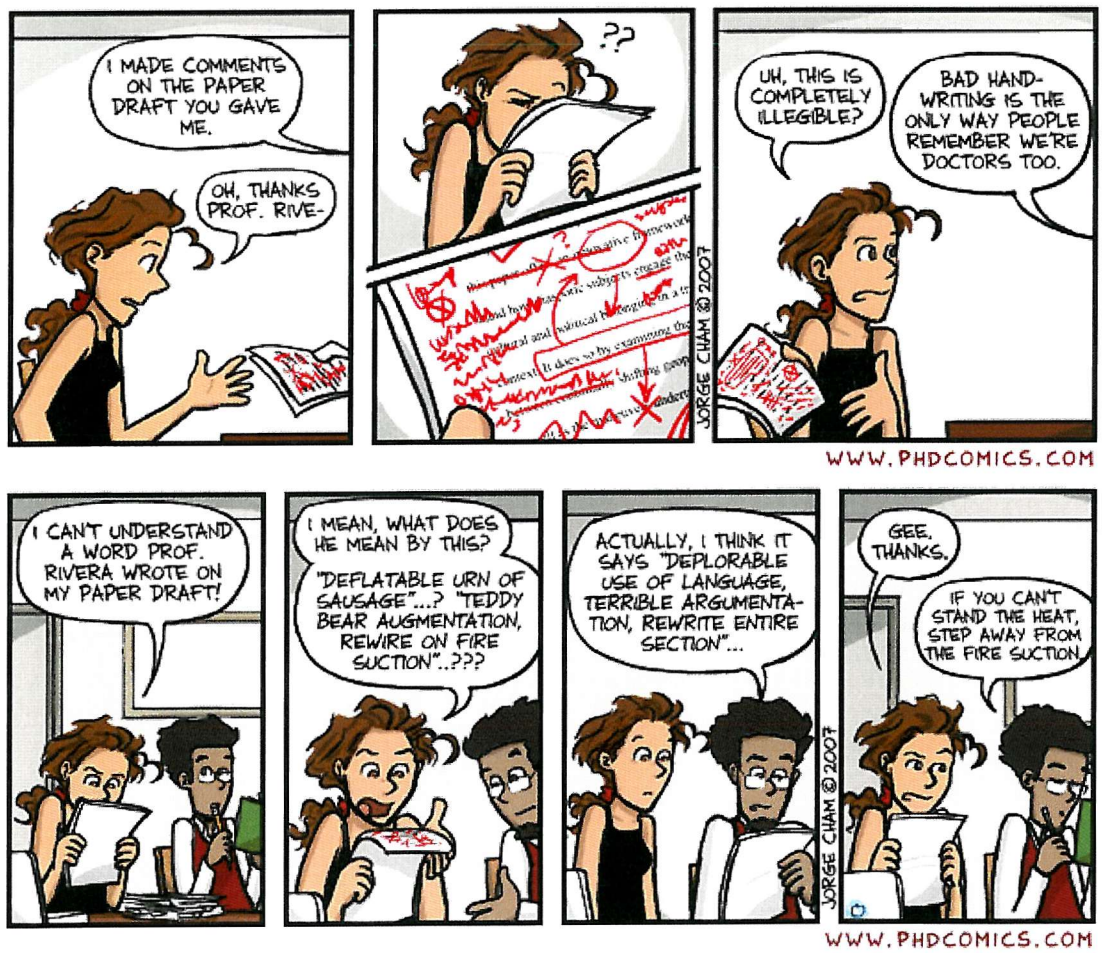

"Piled Higher and Deeper" by Jorge Cham
www.phdcomics.com

Used with permission

3. Investigating the flexoelectric effect in non-symmetric conventional liquid crystal dimers

3.1. Introduction: Setting the benchmark

Many years have now passed since the suggestion first made by Durand that liquid crystal dimers should have large flexoelectric coefficients[1] and yet the number of known examples in the literature is still relatively small.[2-6] Although Durand's comment was almost lost in obscurity, his concept was later realized and now widely accepted by those investigating the flexoelectric effect. Dimers are generally considered by researchers looking to make materials suitable for use in, for example, flexoelectric based display devices. In the field, one of the most successful of those researchers is Coles who has studied a variety of different dimers and has published a range of results, the most recent of which are still, after five years, the materials with the largest reported flexo-elastic ratios, a feature crucial for certain flexoelectro-optic devices.[2] More recently he has investigated other materials attempting to manipulate the shape and structure of the molecules to further enhance these properties, however, with only limited reported success.[2, 6, 7] In spite of having made several successful materials for flexoelectric devices, Coles has yet to translate this into a successful blueprint for designing materials with alternative structural moieties.

So in order to make materials with properties suitable for flexoelectric devices, it is the types of materials shown in Figure 3.1 which clearly set the benchmark with which other contenders should be compared.

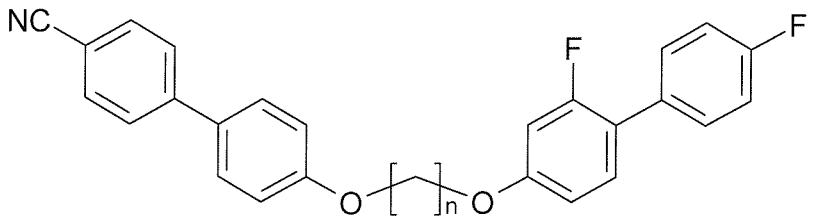

Figure 3.1 A series of dimers (n = 3-12) presented by Coles *et al*, reported as having very large switching angles and fast switching times in a ULH cell (see Chapter 2), therefore being very suitable for exploiting the flexoelectric effect in optical devices.[2, 8]

The materials shown in Figure 3.1 were designed for use in a ULH cell first described by Meyer and Patel[9] and give very large switching angles and fast switching times. So why

are these materials so well-suited to this flexoelectro-optic device? The answer to this lies in the structure of the dimers which results in a small dielectric anisotropy compared to the corresponding monomers and relatively favourable elastic constants, the significance of which are both described in Chapter 2. The other significant property is clearly the flexoelectric coefficients, which in the case of dimers can be understood to result from the large number of bent conformers and the corresponding net transverse dipole originating from the hetro-atom substituents and spacer linkers. However, other than an appreciation for the need of a dipole and the ability for the molecule to adopt a non-centrosymmetric shape, there is very little, if any, information regarding the molecular detail of what contributes to the appearance of large flexoelectric coefficients. As mentioned previously, Coles has reported materials with very large flexoelastic constants, he has not described why be believes this particular structure to be so good.

As commented in Chapter 2, new non-dimer liquid crystal materials have very recently been reported as having very large (by several orders of magnitude) flexoelectric coefficients.[10] These measurements have been made with a completely different methodology to a ULH[9] or in-plane switching HAN cell,[3] however, the same methodology is reported to give results comparable to the literature values for 5CB.[11, 12]

In the event of sparse scientific evidence, the scientist has one of two recourses: either they make measurements or devise a theoretical model. In the case of the chemist, or chemical physicist, this can be achieved by either synthesizing the materials and making physical measurements on the products or by adopting a molecular modelling approach. Clearly the results from theory can direct the practical approach and real physical measurements are invaluable in forming a basis for refining our understanding of theory. Thus the optimum approach should be a two pronged attack using both theory and practical results to achieve our aims.

In this Chapter we discuss a practical approach guided by the results from Coles *et al.* to help gain some insight into how the flexoelectric effect can be influenced by changing the molecular structure and, using this data, try to develop some rudimentary principles by which materials could be designed to yield larger flexoelectric coefficients.

3.2. Synthesis of novel non-symmetric dimers.

To explore how the flexoelectric coefficients vary through changing a biphenyl moiety on one end of a non-symmetric dimer a number of moieties were considered. The 2,4-difluorobiphenyl dimers were successful because they delivered relatively large flexoelastic ratios ($\bar{e}/\bar{K} > 1$), low melting points (below 100°C) and a small $\Delta\varepsilon$ (to avoid dielectric coupling at low fields). Guided by this success, it was important to make at least one material with two fluorines included in these positions. Thus the *2*, 3',4',5'-tetrafluorobiphenyl moiety was considered and for comparison 3',4',5'-trifluorobiphenyl group was also selected. The 4'-difluorobiphenyl is already known[13] and these dimers tended to show little or no liquid-crystalline behaviour. Also included was a biphenyl with an $-OCF_3$ group in the 4' position and an off-axis fluorine in the 3' position. The $-OCF_3$ group should enhance N-I transitions since it possesses a similar shape to OCH_3[14] only possessing a larger dipole at the end of the group. Thus in total three novel fluorinated/cyanobiphenyl non-symmetric dimer series were synthesized along with the synthesis of the ether linked cyanobiphenyl/2,4'-diflurobiphenyl dimer originally synthesized by Coles *et al.*[2] for comparison. The fluorinated mesogenic group took the general form shown in Figure 3.2.

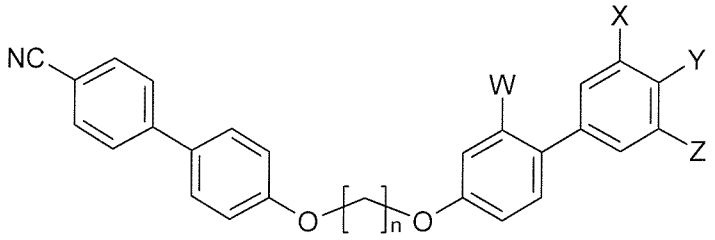

Figure 3.2 General diagram of fluorinated the dimers synthesized, where n = 4 – 11, W, X and Z = -F or -H and Y = -F, -H or $-OCF_3$ (see scheme 3.2).

As both the name and structure of each material is rather large and spacious, a set of mnemonics are given in Figure 3.3 with the full systematic name for each series.

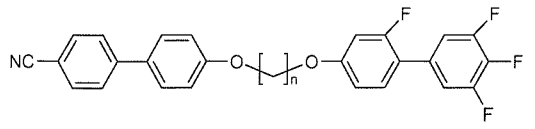

α -(4'-cyanobiphen-4-yloxy)-
ω-(3,3',4',5'-tetrafluorobiphen-4-yloxy)alkane;

$CBOnOBF_4$

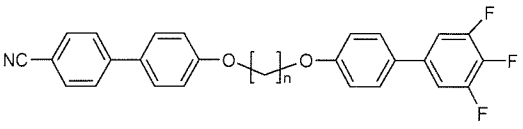

α -(4'-cyanobiphen-4-yloxy)-
ω-(3',4',5'-trifluorobiphen-4-yloxy)alkane;

$CBOnOBF_3$

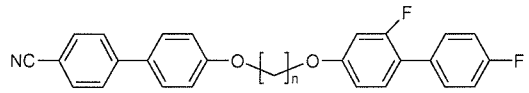

α -(4'-cyanobiphen-4-yloxy)-
ω-(3,4'-difluorobiphen-4-yloxy)alkane

$CBOnOBF_2$

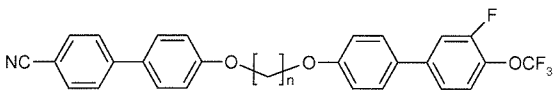

α -(4'-cyanobiphen-4-yloxy)-
ω-(3'-fluoro-4'-oxytrifluoromethylbiphen-4-yloxy)alkane;

$CBOnOBFOCF_3$

Figure 3.3 Structures, systematic names and mnemonics for the non-symmetric liquid crystal dimers reported in this Chapter.

3.2.1. Details of the synthesis

In all cases the fluoro-substituted biphenyl mesogenic groups were supplied by Merck as 4'-hydroxyl derivatives which were powdered solids of purity greater than 90±5% by NMR. Some attempt was made to purify these precursors further however this tended to consume large amounts of the valuable biphenyl. Although not identified, the impurities were found to be polar and appeared not to give significant side reactions, therefore the precursor was used unpurified as supplied. The impurities were then easily removed by column chromatography, since the product was much less polar than the precursor. In all cases synthesis of the dimers was a two stage process each with a common first step (see Scheme 3.1).

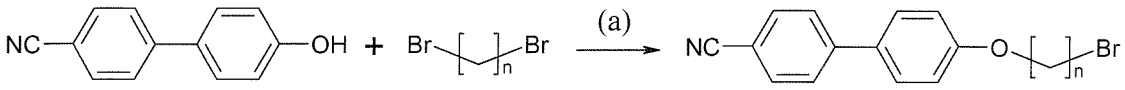

(a) Acetone (reflux), K_2CO_3, NaI

n = 4 – 11

Scheme 3.1 Williamson synthesis of the cyanobiphenyloxy-α-alkyl-ω-bromide series.[15]

Alkylation of the 4-hydroxy-4'-cyanobiphenyl using an α,ω-dibromoalkane was achieved via a Williamson synthesis. In these syntheses however, a ten fold excess of dibromoalkane was used to favour high yields (typically around 90%) and to control the selectivity of the reaction resulting in almost entirely mono-substitution. The reaction was

originally conducted in distilled acetone under nitrogen with ground potassium carbonate as the base and a sodium iodide catalyst.

Number of methylene carbons in the spacer chain (n)	Yield of pure product
4	90%
5	87%
6	77%
7	82%
8	97%
9	85%
10	95%
11	92%
12	91%

Table 3.1 Product yields of the cyanobiphenyloxy-α-alkyl-ω-bromide series synthesised and purified.

Later, in reactions with less stringent conditions, it was shown that undistilled N-grade acetone under an atmosphere of air (undried) gave comparable yields of cyanobiphenyloxy-α-alkyl-ω-bromide (n = 4 – 12) with no complications in purification techniques or compromise in the purity of the product. Yields were found to be comparable to literature values (See Table 3.1).[15]

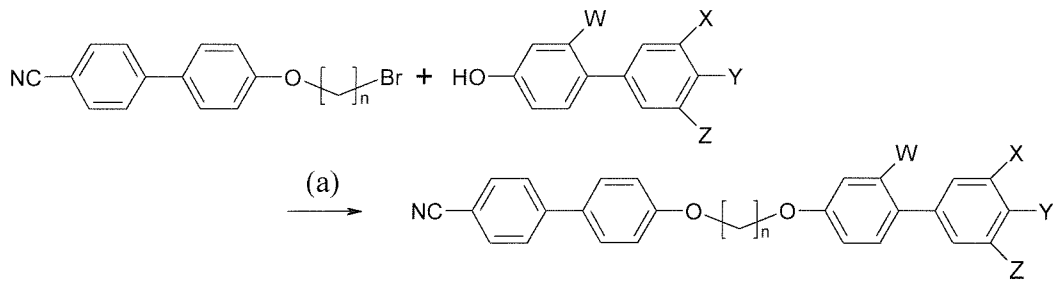

(a) Butanone (reflux), K_2CO_3, NaI

n = 4 – 11

Scheme 3.2 Williamson synthesis of various non-symmetric cyanobiphenyl dimer series.

The second step in the synthesis involved substitution of the ω-bromide with the fluorinated biphenyl of choice (Scheme 3.2).

Preliminary reactions were conducted under similar conditions to that shown in Scheme 3.1 using acetone as the solvent, potassium carbonate as the base and a sodium iodide catalyst. The reaction generally showed only a 50-60% conversion when refluxed in acetone compared with a 60-80% conversion when butan-2-one (methyl ethyl ketone) was employed as a solvent giving access to higher temperature reflux conditions. No significant improvement was made over butan-2-one using DMF or cyclohexanone.

n	CBOnOBFOCF$_3$	CBOnOBF$_4$	CBOnOBF$_3$	CBOnOBF$_2$
4	76%	67%	81%	45%
5	77%	68%	46%	74%
6	64%	53%	69%	67%
7	35%	41%	88%	40%
8	80%	46%	21%	74%
9	88%	88%	58%	85%
10	63%	37%	76%	96%
11	76%	41%	59%	68%

Table 3.2 Product yields of the pure material for each of the four series. Literature values for CBOnOBF$_2$ dimers are unavailable.

Again dry, distilled butan-2-one and a nitrogen atmosphere were originally used, however, later experiments showed that undistilled (and unpolymerised) butan-2-one in air (undried) gave similar yields (Table 3.2).

Purification of the products by column chromatography was generally unachievable eluting with DCM/40-60 petrol (DCM being the solvent of choice for all these compounds). However, separation was achieved using a low polarity mix of diethyl ether/40-60 petrol (1-5%) which was complicated only by the fact that the products were sparingly soluble in the eluent and the crude product was absorbed onto silica prior to cooling (N.B. the CBOnOBF$_2$ series was separable using a DCM/ 40-60 petrol eluent). Generally, for materials with a longer methylene spacer chain, separation by column chromatography became smaller and purification became more difficult. It was later noted that purification could be greatly aided by successive recrystalisation from hot acetonitrile/water which, when cold, solubilises the cyanobiphenyloxy-α-alkyl-ω-bromide.

Higher yields (e.g. CBO9OBF$_4$, CBO9OBFOCF$_3$, CBO9OBF$_2$) were obtained for reactions done on a larger scale and overall tend to average between 50 – 70% with some notable exceptions. Generalising, the more polar the fluorinated mesogenic groups (e.g. CBOnOBFOCF$_3$ and CBOnOBF$_2$) tended to give better column separation compared to dimers with different mesogenic groups, especially where the alkyl chain is shorter and hence purification was easier and higher yields were obtained.

More specifically, the CBOnOBF$_4$ series gave smaller yields. This was because this series was one of the first synthesized and thus acetone was used as a solvent originally. Also the purification processes were still being refined. In the case of the -OBFOCF$_3$ series, this was the first material from that series made. The material was passed through a column four times using various different DCM/petrol based solvent systems before an ether/petrol eluent was discovered to give better separation.

The yield for the n = 8 spacer for the CBOnOBF$_3$ series was low due to a coloured impurity which only appeared during the reaction had to be removed using decolourising charcoal which vastly lowered the yield. The CBOnOBF$_2$ series could all be purified using a DCM/petrol eluent which, due to the better solubility, made handling the material more straightforward. The n = 7 bromo-alkane precursor was later found to have significant amounts of crystallisation solvent trapped in the crystal. This was later removed under heated vacuum, however the reduced amount of material in the reaction mixture resulted in a lower overall yield.

3.2.2. Analysing the molecular characterization

As well as optical microscopy, each material was characterized by NMR (^{1}H, ^{13}C), IR, DSC, and mass spectroscopy. In the case of novel series, a combustion analysis of one member of the series was obtained. The data for these materials can be found in Chapter 7.2.2-5.

All the materials gave good clean (spectra with no impurities and no solvent peaks except $CHCl_3$ and a small quantity of DOH) NMR spectra with all the peaks assigned either by comparison with literature assignment or, in the case of novel compounds, comparison with assignments from starting materials. The spectra showed the materials to be pure.

The IR spectra gave characteristic stretches for aromatic and aliphatic protons and cyano groups consistent with these types of materials.

Because there were no sufficiently acidic or basic protons on the molecules, mass spectroscopy had to be done by electron ionization (EI), a hard ionization technique, rather than electrospray (ES). The advantage of ES is that it shows only the molecular ion and so gives a clear indication of any impurities. Although the fragmentation patterns produced by EI are more chaotic, the isotope pattern of bromine is still clearly apparent making this the analytical technique of choice for detecting the presence of any 4'-cyanobiphenyl-4-oxy-α-alkyl-ω-bromide. The reported materials show no evidence of bromine atoms being present and exhibit fragmentation patterns consistent with the expected products.

Optical microscopy, phase behaviour and DSC data is analysed separately in Section 3.3.

3.3. Properties of dimers

Analysing the properties of similar liquid crystal dimers tends to lead to familiar reoccurring patterns in their properties. This behaviour may be an odd-even effect in, for example, the T_{NI} which varies with the parity of the flexible spacer linking the two mesogenic groups. In the following section we look at the general properties of liquid crystal dimers and why we expect them to behave in the manner they do. This includes the observations in the melting points as well as liquid-crystalline properties such as the T_{NI} and the transitional entropy.

3.3.1. Melting points of dimers

The melting point is related to a number of properties. In essence these involve the size of the attractive intermolecular force fields exerted between the constituent atoms of one molecule and their nearest atomic neighbours. The size of these forces depend principally on three properties:

1. The type of attractive force between atoms (e.g. dipolar or quadrupolar electrostatic interactions, or quantum mechanical dispersion forces).
2. The distance over which the field exists.
3. The distance between the atoms affected by a given field.

The location of the atoms in the most stable crystal form represents the lowest energy arrangement of the constituent molecules (as defined by intramolecular forces). This is governed by steric bulk (defined by the repulsion of the atomic shells and the position, strength and direction of the intramolecular bonds) and the energetic minimisation of the electrostatic interactions and dispersion forces.

The size of the intermolecular interactions defines the melting point of the solid and although we can determine the location of the atoms in a crystal by X-ray crystallography, it would be impossible to unravel the complex interactions to determine the size of these forces.

Applying this to liquid crystals we can see that it is much more difficult to understand the nature of the melting points across a series compared to the change in, for example, the nematic phase. The existence of the phase is very sensitive to the ordering of the constituents in the system. Therefore developing an understanding of an odd-even effect in T_{NI} (odd-even effects are relatively common in liquid crystal dimers) across a series can, and has, been achieved.[16-18] In contrast, odd-even effects in the melting points are known[19] but are far less common and decidedly harder to understand and predict. Often variations in the melting points are erratic and can differ by very small amounts in comparison with the N-I transition.[20] Attempting to understand the change in T_{NI} by considering the molecular shape and conformation in the nematic is reasonable as this will have a profound impact on the ordering in the mesophases which in turn affects T_{NI}. Trying to do the same for the melting transitions by, for example, analysis of crystal structures will not yield any useful information. Any conclusions that could be drawn from a study would be broad and as such not say anything informative about the minutia of 5-10 K changes in more than 3-400 K which are common in dimer series.[20]

This said, knowledge of the crystal structure coupled with an appreciation of the enthalpy change associated with its melting can offer clues to how the nematic may or may not behave. For example, a large change in the enthalpy from melting into the nematic may suggest a potentially significant conformational difference between the crystal and the liquid crystal. This idea is used to a limited extent in Chapter 5.

3.3.2. Liquid crystal properties of dimers

To understand better how liquid crystal properties (e.g. T_{NI}) are related to molecular shape we need to build up a picture which connects the shape and anisotropy of the molecule to the order in the liquid crystal phase. For rod-like molecules this was done in a theory proposed by Maier and Saupe[21-23] (see Figure 3.4). The anisotropic property of the rod is related to a single parameter, ε, to which the T_{NI} is predicted to be proportional ($T_{NI} = 0.2203\varepsilon/k_B$). From Maier-Saupe theory the orientational energy of the rod as its orientation with respect to the director changes, is given in Equation 1.

$$U(\beta) = -\varepsilon \overline{P}_2 P_2(\cos\beta). \qquad (1)$$

In contrast to T_{NI} the second rank orientational order parameter, $\overline{P}_2$, is predicted to be a universal function of the reduced temperature for materials in the nematic phase independent of ε. Thus for any material the order parameter would be the same for any given value of T/T_{NI}. From the theory, at the N-I transition, $\overline{P}_2$ is predicted to be 0.429 – slightly higher than the values usually found experimentally.[21-23] The entropy of transition is also predicted to be independent of ε with $\Delta S_{NI}/R$ given as 0.417, is again somewhat higher than values found experimentally.

Real mesogenic groups tend not to be perfect cylinders and are more likely to be slightly flattened into more lozenge shaped molecules which are more biaxial (see Figure 3.4).

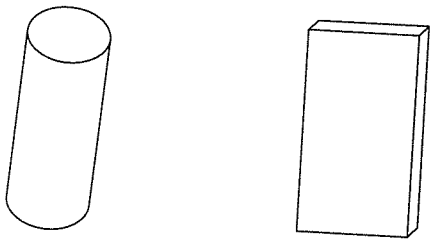

Figure 3.4 (Left) A uniaxial motif which is cylindrically symmetric about the long axis. (Right) A biaxial motif which is more board shaped lowering the symmetry from $D_{\infty h}$ to D_{2h}.

To accommodate this reduction in symmetry, the Maier-Saupe theory required an extension which dealt with the biaxiality in the molecule. The theory developed by Luckhurst, Zannoni, Nordio and Segre (LZNS)[24] uses an additional parameter, λ, which is a measure of the molecular biaxiality. In the theory all of the transitional properties depend on λ so there is no universality as found when the biaxiality parameter is zero.

According to this theory $\overline{P}_2^{NI}$ and $\Delta S_{NI}/R$ become smaller as λ increases, going to zero when λ reaches the predicted maximum biaxiality with λ of $1/\sqrt{6}$. At the point the phase type has changed to a biaxial nematic, the symmetry reflects the biaxial symmetry of the molecular constituents compared to the common nematic, which is uniaxial. The transition to this phase is predicted to be second order which is why the transitional entropy and the order parameter are expected to vanish at the transition.

Introducing a flexible spacer as seen in dimeric liquid crystal molecules complicates the theory and the calculations quite considerably. This is because the calculations now need to incorporate not only the geometry of the spacer, but also its conformational energy, its length and the parity as well as the anisotropy of the mesogenic groups. In spite of the complications this has been achieved.[16-18]

For monomers we see a dependence of the transitional properties on the conformation and indeed given the relationship of ε to T_{NI}, the more linear the conformation, the larger ε and hence the higher the prediction for T_{NI}. This dependence is even more important in liquid crystal dimers where the chain now links two mesogenic units, for example, in the symmetric cyanobiphenyl dimers CBOnOCB where CBO is the mesogenic unit and n is the number of methylene in the flexible spacer. There is a strong odd-even effect shown by the N-I transition temperatures which are higher for the even than for the odd with the difference attenuating as n increases (see Figure 3.5).

The entropy of transition also alternates, again with the odd transitions having a smaller transitional entropy than the even, however this time the alternation does not attenuate and the values of $\Delta S_{NI}/R$ for both parities increase by roughly the same amount as n increases (see Figure 3.5[19]). From this result, given the relationship between the transitional entropy and the order parameter, $\overline{P}_2^{NI}$, also alternates with spacer parity as the p-axis of the mesogenic group alternates.

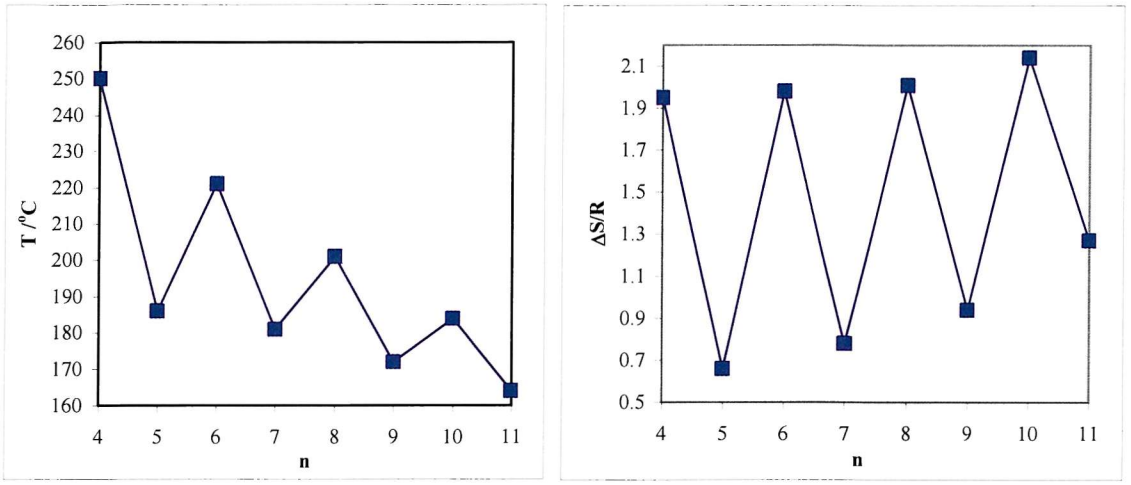

Figure 3.5 (Left) The variation in T_{NI} with spacer length and parity in a typical liquid crystal dimer (CBOnOCB) series giving rise to an odd-even effect which attenuates as n increases. (Right) The transitional entropy for the same series which alternates and on average increases with n.

The Maier-Sauper theory has been extended to include the molecular flexibility by Marceljia[18], refined by Councell *et al.*[16] and a derivation of their theory is given by Luckhurst *et al.*[17] This extension appears to work well when applied to dimers.

The properties of dimers, however, have also been predicted in a much simpler way. This is where the spacer chain is taken to be in the all-trans conformation and thus, in the even dimer, the mesogenic groups are parallel compared to the odd dimers where they are inclined (see Figure 3.6).

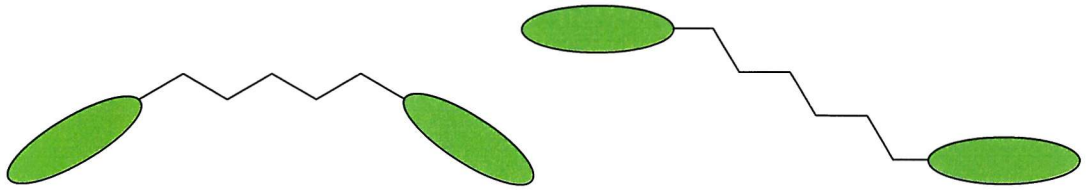

Figure 3.6 (left) An odd dimer and (right) and even dimer drawn in the all-trans form with the mesogenic groups depicted in green (not drawn to scale). The odd dimer appears more biaxial than its even counterpart.

If these were the only conformations then the even dimer would have a higher T_{NI} than the odd, and this fits the qualitative observations. However, this analysis does not hold up under further scrutiny as the even dimers should behave like monomers and the odd

dimers, with mesogenic units more off-axis than monomers should behave as worse mesogens than monomers. However, the ordering and the entropy are found to be higher for the even dimers compared with results found for monomers; whereas for the odd dimers, the ordering and entropy are found to be about the same as for monomers. This difference can be accounted for by the molecular field theory for flexible molecules[17] in which all the conformations are included together with the coupling between the orientational and conformational order (using a discrete conformational variable). It is found that the anisotropic environment favours the more elongated conformers over the bent conformers subject to the constraints of the conformational energy needed to adopt such a conformer. Therefore, since this theory applies to any flexible system, calculations using it should, in principle, be able to explain the behaviour of any variants in liquid crystal dimers.

3.4. Analyzing the physical data for CBOnOBF$_2$

Each of the series will now be considered in turn with regard to their liquid-crystalline properties. For each series we shall look at the optical textures for a few examples; the phase behaviour across the series; the ordering in the nematic for n = 9 and the N-I entropy of transition. The first series for consideration is actually not new in that it has already been characterised by Coles *et al.*[25] however when the series was originally synthesised there was no reported data for these compounds. With the recently published data on these materials they serve as a useful check on the experimental technique. The entropy of transition and the orientational ordering in the nematic were measured; these are not found in the literature, also the flexoelastic measurements made were made with a different chiral dopant so this will offer a useful comparison since these materials are the only full series of dimers which have been synthesised and their flexoelectric properties measured.

3.4.1. Optical microscopy

The samples were prepared by melting a small amount of the solid onto an untreated glass cover slip on the heating stage. After the material had melted another untreated glass cover slip was placed on top creating a sandwich of the sample between the glass surfaces (i.e. a thin film of sample). Where there was a clear discrepancy in melting point

between the solvent crystallised solid and the crystal formed from the melt, the solid was crushed between two untreated glass cover slips and the melting transition determined.

Figure 3.7 All optical texture pictures were taken on cooling, showing nematic phases. $CBO6OBF_2$ taken at 154°C, $0.99T_{NI}$ (top left); $CBO7OBF_2$ taken at 89°C, $0.94T_{NI}$ (top right); $CBO8OBF_2$ taken at 140°C, $0.99T_{NI}$ (middle left); $CBO9OBF_2$ taken at 105°C, $0.98T_{NI}$ (middle right); $CBO10OBF_2$ taken at 127°C, $0.99T_{NI}$ (bottom left); $CBO11OBF_2$ taken at 105°C, $0.98T_{NI}$ (bottom right).

All the materials showed the classic characteristics of a nematic phase, the thread-like pattern over the surface and flashing when the cover-slip was depressed. However, the results also show a variation in detail of the optical texture (see Figure 3.7). In some cases the schlieren texture was very clear (especially when cooled from the isotropic phase close to the transition as seen in n = 8). In other cases the textures were not seen so unambiguously (as seen in n = 7). There was no smectic phase seen in n = 11 as has been reported[8] although this was due to the phase not being supercooled far enough even with droplets to make such an observation.

3.4.2. Phase behaviour

To better understand the phase behaviour of the non-symmetric dimers it would be sensible ideally to compare them to both of their symmetric counterparts. The symmetric dimers with fluorinated end groups generally showed no mesogenic behaviour due to being unable to supercool far enough. Because of this not many examples were synthesised and they are not used for comparison, although a brief analysis is undertaken later to determine the virtual transitions for some of the dimers.

Literature values

n	Cr		N		I
4	•	Not Reported			•
5	•	100	•	111	•
6	•	137	•	166	•
7	•	97	•	116	•
8	•	123	•	147	•
9	•	75	•	115	•
10	•	112	•	134	•
11	•	80	•	113	•
12	•	121	•	123	•

Measured Values

n	Cr		N		I
4	•	137	•	177	•
5	•	92	•	95	•
6	•	129	•	160	•
7	•	93	•	111	•
8	•	123	•	146	•
9	•	71	•	111	•
10	•	111	•	132	•
11	•	72	•	111	•
12	•	Not Synthesised			•

Table 3.3 The transition temperatures in °C for the $CBOnOBF_2$ series showing the T_{NI} as reported in the literature[2, 8] (left) and the T_{NI} measured on the materials synthesised in-house (right). Result for n = 4 is not reported in the literature and n = 12 was not synthesised.

We see here that there are some significant disparities between the results in the literature and the measured results. The results from the materials synthesised in-house are repeatable and consistent with results obtained from DSC measurements. As mentioned

previously the NMR spectra and other characterisation data suggest a high level of purity in these compounds.

A better indication of how these results differ is shown in Figure 3.8.

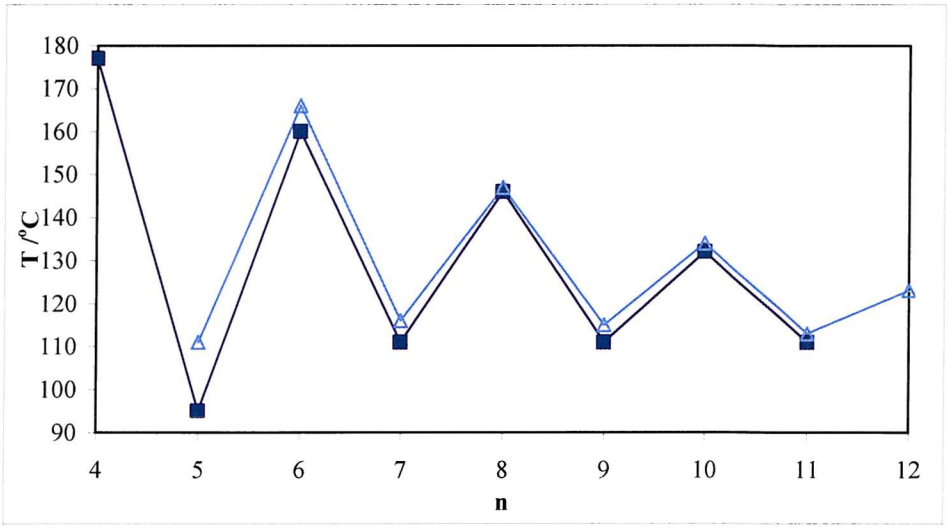

Figure 3.8 The variation in T_{NI} for literature and measured values. Here ■ is T_{NI} for $CBOnOBF_2$ (measured) and Δ is T_{NI} for $CBOnOBF_2$ (lit).

It is clear that the difference in results is not consistent across the series and agreement is better for the members with longer spacers. This difference in agreement is broadly the same for the melting points. Unless otherwise stated all results concerning the $CBOnOBF_2$ series are from results obtained from measurements made on the in-house materials.

A brief analysis of the phase behaviour is found elsewhere[8] and so not repeated here. Later, when considering materials with different fluorinated mesogenic groups, we shall see that T_{NI} results for the symmetric analogues are not available and as such are estimated by extrapolation of the T_{NI} for the a given symmetric CBOnOCB and non-symmetric homologue. In the case of the $-OBF_2$ mesogenic group the symmetric materials are known[8] and so the T_{NI} and T_{CrN} for both symmetric and the non-symmetric for n = 9 and 10 are considered and, in the case of T_{NI}, the extrapolated result is compared to the real result for the symmetric $F_2BOnOBF_2$.

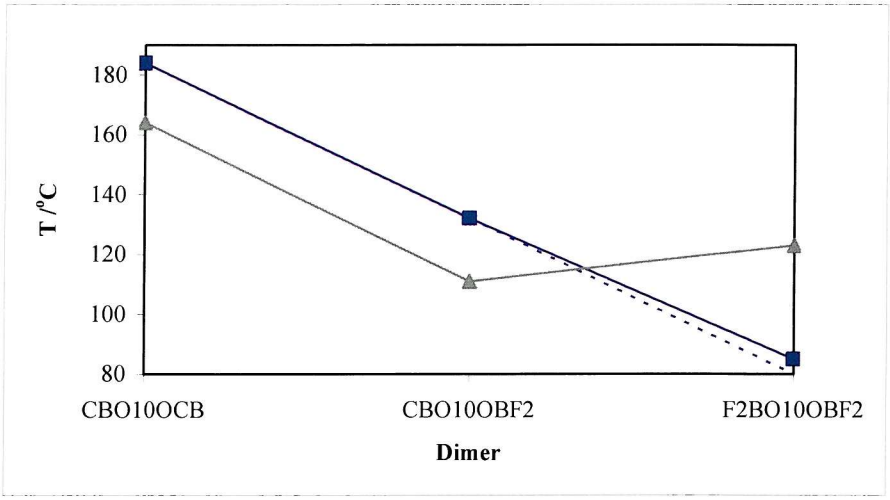

Figure 3.9 The transition temperatures for the symmetric and non-symmetric n = 10 dimers where ■ denotes T_{NI} and ▲ denotes T_{CrN}.

For n = 10 (see Figure 3.9), we can see that the extrapolated value is very close to the T_{NI} for the symmetric $F_2BO10OBF_2$ compound (only 5°C difference). It should be noted that if the literature value for T_{NI} for $CBO10OBF_2$ is used an even better fit is obtained. Interestingly we also see that the melting point for the non-symmetric material is actually lower and more favourable than the symmetric $F_2BOnOBF_2$ series. This is surprising given that the symmetric cyanobiphenyls melt at a much higher temperature.

Considering n = 9 (see Figure 3.10) we can see that the agreement between extrapolated value and the literature value for the symmetric $F_2BOnOBF_2$ is somewhat disparate (by nearly 20°C).

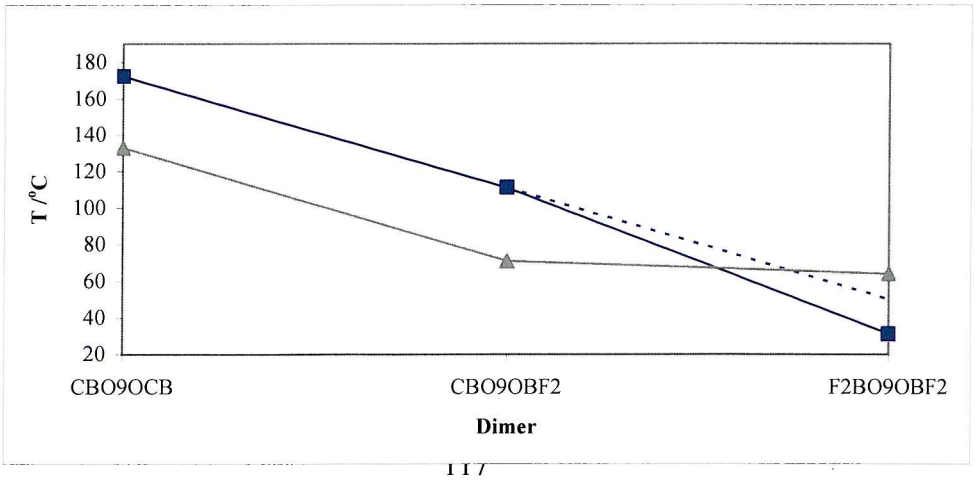

Figure 3.10 The transition temperatures for symmetric and non-symmetric n = 9 dimers where ■ denotes T_{NI} and ▲ denotes T_{CrN}.

Here the fluorinated symmetric dimer has a lower T_{NI} than predicted, which comes from the value for CBO9OBF$_2$ being higher than the mean of the two symmetric T_{NI}s. It should also be noted that contrary to the case where n = 10, the extrapolation is worse if the literature value of CBOnOBF$_2$ is used (as opposed to the in-house measurement). The melting point for F$_2$BO9OBF$_2$ is slightly lower compared to the CBO9OBF$_2$, as might be expected. However the difference in melting points is less than 10 °C which is unfortunate because there is a considerable reduction in T_{NI} across the series resulting in all but n = 11 of the F$_2$BOnOBF$_2$ series showing only monotropic nematic transitions.

3.4.3. Orientational ordering of anthracene in the nematic

All the ^{2}D NMR experiments used to determine the orientational ordering in materials reported in this Thesis were conducted by Bakir Timmi. The orientational ordering for the CBOnOBF$_2$ nematic was obtained indirectly by using a small amount of per-deuterated-anthracene to probe the order of the liquid crystal environment. The background to the technique is explained more fully in Chapter 1. There was limited time available on the spectrometer so the ordering was studied for just n = 9 for each series reported in this Chapter and compared with CBOnOCB also synthesised for this experiment (as ordering data for this material was not available in the literature).

CBO9OBF$_2$ was studied through a shifted temperature (T_s = T_{NI}-T) range from 0 to 43 °C. By contrast CBOnOCB, which has a larger nematic range but is less easily supercooled, was studied over a T_s range from 0 to 32 °C.

It should be noted that the results for CBO9OCB are very similar to those of CBO5OCB (the only odd member of the CBOnOCB series where literature data on its orientational ordering is available[26]) which is encouraging as this fits in well with the theory described in Section 3.3. Comparing the results for the non-symmetric dimer and the symmetric cyanobiphenyl dimer (see Figure 3.11), the results for S_{zz} (the ordering of anthracene along the major axis), are very similar, differing more close to T_s = 0 (~T_{NI}). Given the similarity in the shape and parity of the different hosts, this is to be expected and fits

established theory. There is some difference in the biaxiality (S_{xx}-S_{yy}) in the solute ordering, although this is very small it does show that the symmetric cyanobiphenyl dimer is slightly larger than the CBO9OBF$_2$ particularly at $T_s = 0$.

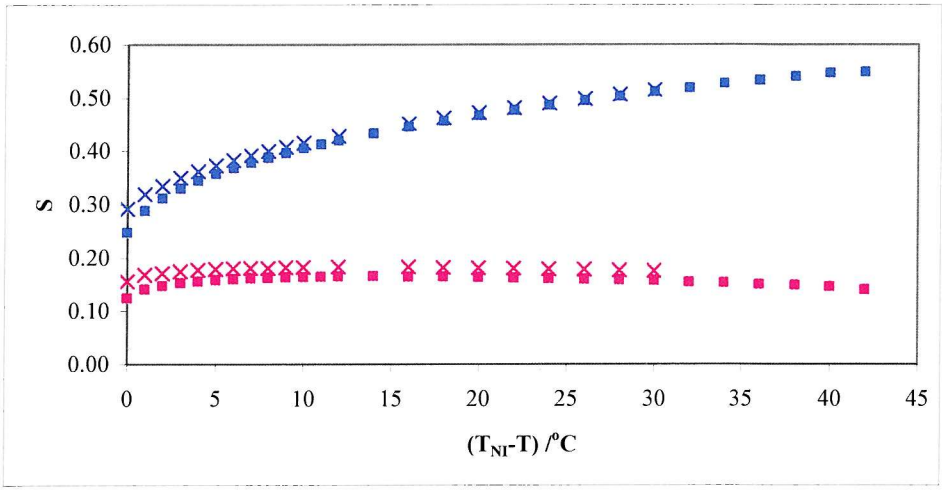

Figure 3.11 The order parameters of anthracene dissolved in CBO9OCB and CBO9OBF$_2$ as a function the shifted temperature. Here ■ denotes S_{zz} for CBO9OBF$_2$; ■ denotes S_{xx}-S_{yy} for CBO9OBF$_2$; × denotes S_{zz} for CBO9OCB and × denotes S_{xx}-S_{yy} for CBO9OCB.

More interesting is the plot of S_{zz} against S_{xx}-S_{yy} which is often used to give an indication of the biaxiality (see Figure 3.12). The difference between CBOnOCB and CBOnOBF$_2$ appears quite large but this is because the scale is small; if it were taken from zero the data would appear almost identical. Using the extended Maier-Saupe theory for biaxial molecules (e.g. the anthracene) in uniaxial nematics,[16-18] we can relate the biaxial order parameter (taken at the maximum) to the molecular biaxiality parameter λ.

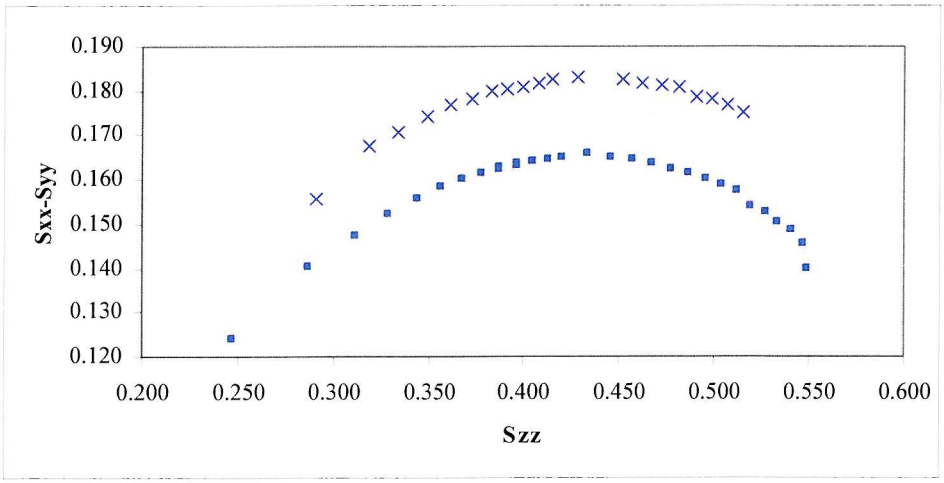

Figure 3.12 Plot of S_{zz} against S_{xx}-S_{yy} showing the difference biaxiality where ■ denotes $CBO9OBF_2$ and × denotes CBOnOCB.

Using the calculated dependence of the biaxial order parameter on the major order parameter for predicted values of the of the molecular biaxiality parameter,[27] we can estimate and compare λ for each dimer. Therefore, for CBOnOCB, λ is estimated to be about 0.43 and for $CBO9OBF_2$ it is 0.38. This demonstrates that the difference in the molecular biaxiality between the molecules is quite small.

3.4.4. Entropy of transition

The entropy data was obtained from DSC experiments conducted on the four series as described in Chapter 1. In all cases the materials were cycled through at least four heating and three cooling runs. An example of a typical DSC plot is shown in Figure 3.13.

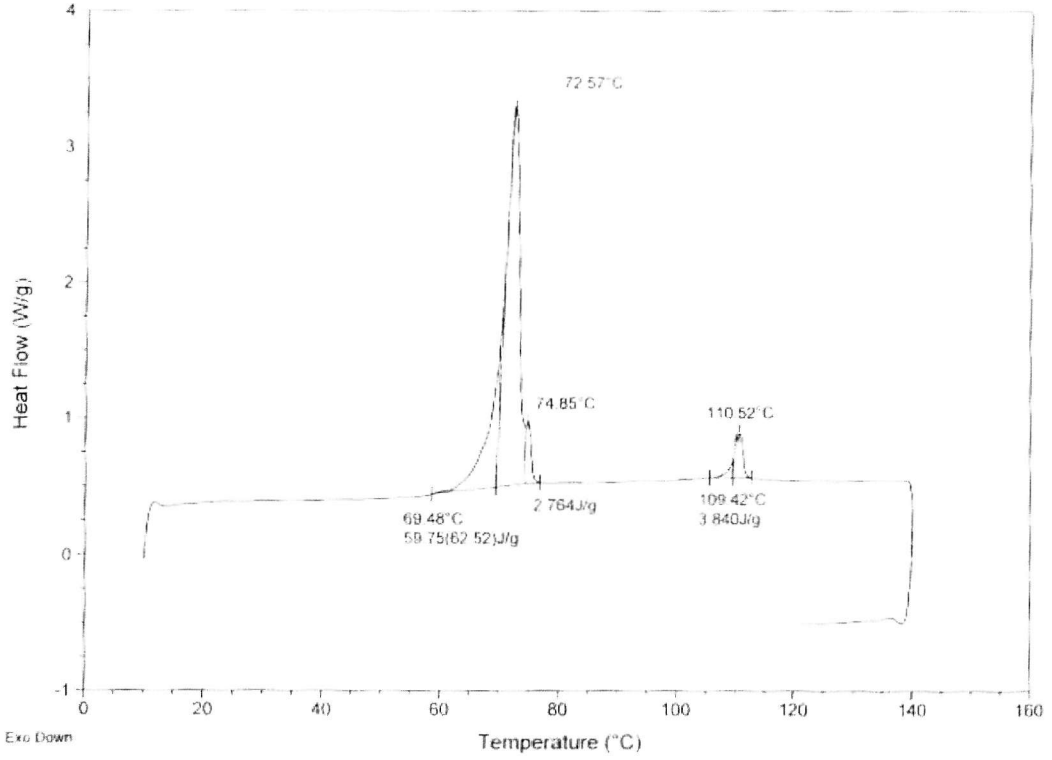

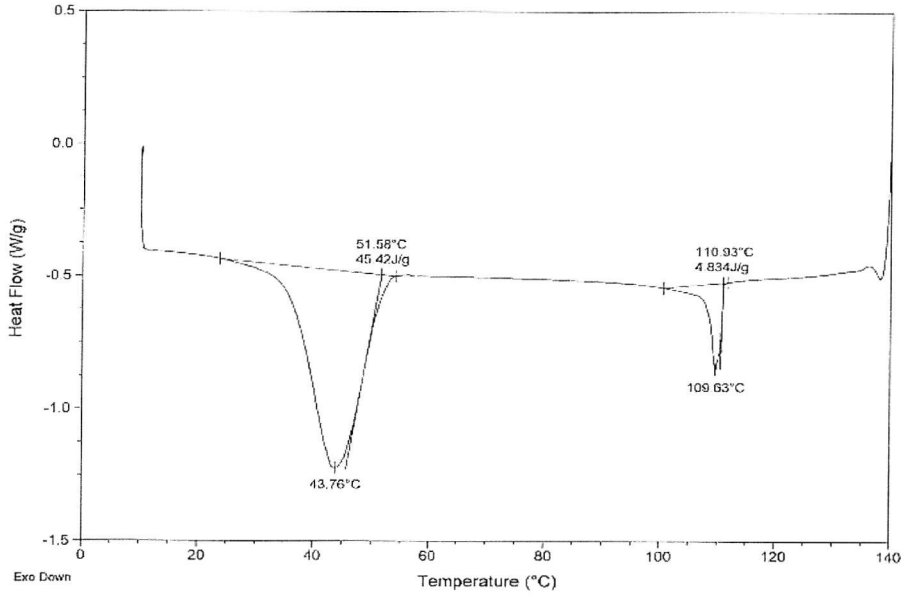

Figure 3.13 Typical DSC plots for CBO9OBF$_2$ heating (previous page) and cooling (this page) run. Endotherms are given as peaks, and exotherms as negative peaks and the areas under or above these regions are measured in Jg^{-1}.

For each material the entropy data is compared with those of the symmetric cyanobiphenyl dimers which are taken to be typical, behaving as theory would predict[19, 20] and thus make a good benchmark by which the non-symmetric behaviour can be compared.

Also of interest is the magnitude of the N-I transitional entropy. Theory predicts that the more biaxial the ordering of the molecules the smaller the transitional entropy will be. It would also be interesting to compare the results for probing the orientational ordering with the transitional entropy. The difference in orientational order between the nematic and isotropic is known in monomers to make the major contribution to $\Delta S_{NI}/R$. If the same is true in dimers then we may expect the results to correlate.

n	ΔH_{CrN}/ kJmol^{-1}	$\Delta S_{CrN}/R$	ΔH_{NI}/ kJmol^{-1}	$\Delta S_{NI}/R$
4	35.2	10.2	4.66	1.3
5	26.8	8.9	1.14	0.4
6	39.5	12.2	4.72	1.3
7	43.7	14.3	1.86	0.6
8	43.0	13.5	5.49	1.6
9	35.7	12.4	2.23	0.7
10	38.5	12.5	5.89	1.8
11	38.9	13.8	2.45	0.8

Table 3.4 Transitional entropy and enthalpy data for Cr-N and N- I transitions for $CBOnOBF_2$.

Generally, the results for the entropy change at the N-I transition showed that $CBOnOBF_2$ dimers series gave an odd-even alternation which was consistently lower than the corresponding symmetric cyanobiphenyl dimers (see Table 3.4). We also see moderate Cr-N transitional entropy which is comparable to values seen in the symmetric cyanobiphenyls.

Examining the data from the $CBOnOBF_2$ series (see Figure 3.14), the non-symmetric dimer follows the alternating odd-even pattern of the CBOnOCB series, however, the magnitude of the alternation is smaller.

The difference in $\Delta S_{NI}/R$ is relatively consistent across the series and greater than the 10% experimental error generally associated with entropy data.[28, 29]

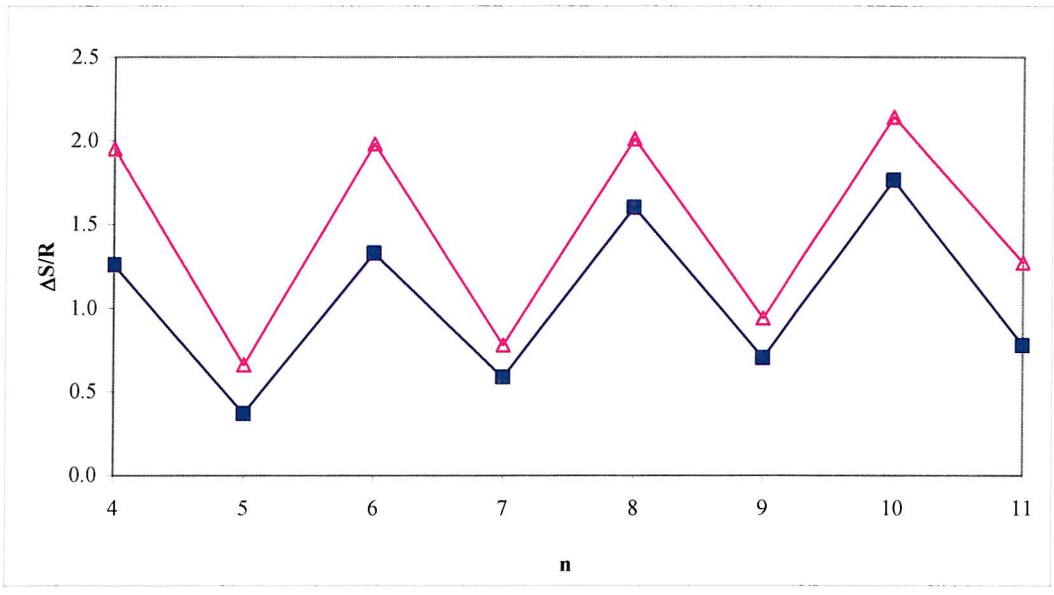

Figure 3.14 Transitional entropy for N-I transitions for the CBOnOCB series[19] and $CBOnOBF_2$, where Δ denotes $\Delta S_{NI}/R$ for CBOnOCB and ■ denotes $\Delta S_{NI}/R$ for $CBOnOBF_2$.

We know from the measurements on the orientational order of anthracene in the n = 9 dimer that there is a difference in the ordering between the two dimers at T_{NI}. However, based on the data from the ^2D NMR experiments, we might have expected the transitional entropy of $CBO9OBF_2$ to be closer to that of CBO9OCB. The percentage difference of $\Delta S_{NI}/R$ for $CBO9OBF_2$ compared to CBO9OCB is 25% compared to a difference of 15%

in S_{zz} at $T_s = 0$ for these two compounds. The Maier-Saupe theory for uniaxial rods says there should be no correlation between the ordering and T_{NI}. However in dimers it is possible that the higher T_{NI}, the greater the effect of straightening the flexible chain (and hence the molecule) which will raise $\Delta S_{NI}/R$. This is a conformational change rather than an orientational one. Therefore the difference between the orientational ordering and the transitional entropy reflect a difference in the conformational distribution to include more bent conformers for the compound with the lower T_{NI} (e.g. CBO9OBF$_2$).

3.5. Analyzing the physical data for CBOnOBFOCF$_3$

The first of the novel non-symmetric dimers to be considered is the CBOnOBFOCF$_3$ series. Simple estimations on the size of the dipole[30] show that the -OBFOCF$_3$ moiety is the most polar group both totally and the component resolved along the mesogenic long axis. From this and differences in molecular shape we might expect the T_{NI} for these materials to be the largest of the non-symmetric dimers considered in this Chapter and to be the most comparable to the CBOnOCB series.

3.5.1. Optical microscopy

The optical microscopy was performed as described in Section 3.4.1. The optical textures for this series were found to be very similar to that seen in the CBOnOBF$_2$ series. Generally each material was found to be nematogenic, most being enantiotropic. Each showed characteristic textures associated with nematic phases. The thread-like texture was visible for each material although tended to be too fine to show in clearly in the pictures (see Figure 3.15). As would be expected the best schlieren textures were seen just below the T_{NI} transition and we can see that the odd dimers generally show less detailed textures than the even dimers.

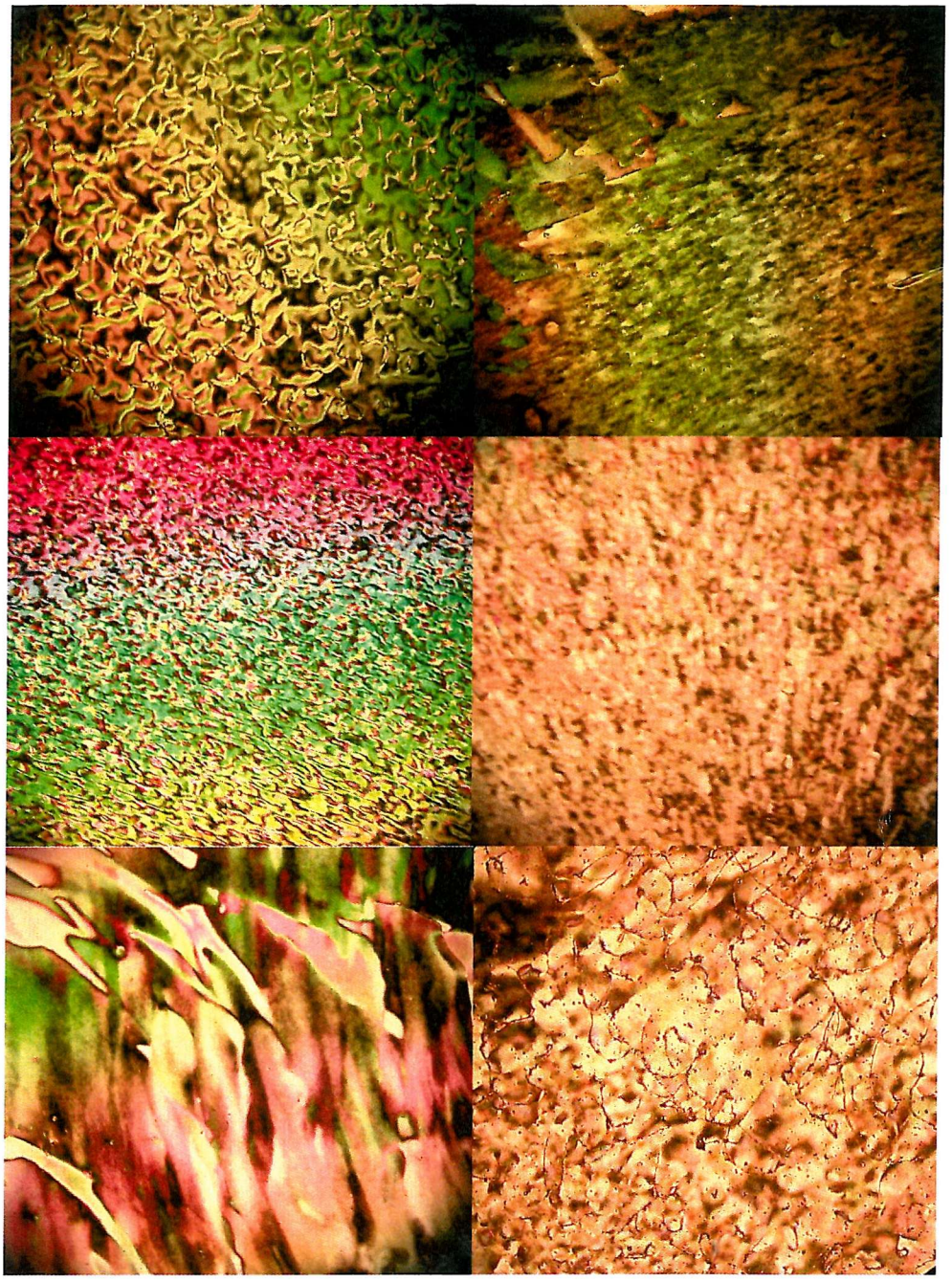

Figure 3.15 All optical texture pictures taken on cooling, showing nematic phases. CBO6OBFOCF$_3$ taken at 138 °C, 0.96T$_{NI}$ (top left); CBO7OBFOCF$_3$ taken at 100 °C, 0.99T$_{NI}$ (top right); CBO8OBFOCF$_3$ taken at 128 °C, 0.99T$_{NI}$ (middle left); CBO9OBFOCF$_3$ taken at 102 °C, 0.99T$_{NI}$ (middle right); CBO10OBFOCF$_3$ taken at 110 °C, 0.96T$_{NI}$ (bottom left); CBO11OBFOCF$_3$ taken at 91 °C, 0.97T$_{NI}$ (bottom right).

3.5.2. Phase behaviour

The transition temperatures are given in Table 3.5 where we can see that almost all the members of the series are enantiotropic with the exception of n = 5 and all are nematogenic.

n	Cr		N		I
4	•	135	•	174	•
5	•	94	•	(89)	•
6	•	129	•	153	•
7	•	81	•	104	•
8	•	111	•	133	•
9	•	83	•	104	•
10	•	100	•	128	•
11	•	88	•	104	•

Table 3.5 The transition temperatures in °C for $CBOnOBFOCF_3$ series. n = 12 was not synthesised.

For the purposes of comparison, this and subsequent series will be contrasted to the cyanobiphenyl symmetric dimers because it is the only symmetric analogue available. The other series which will be used for comparison is the $CBOnOBF_2$. It is the most similar non-symmetric dimer available in the literature.

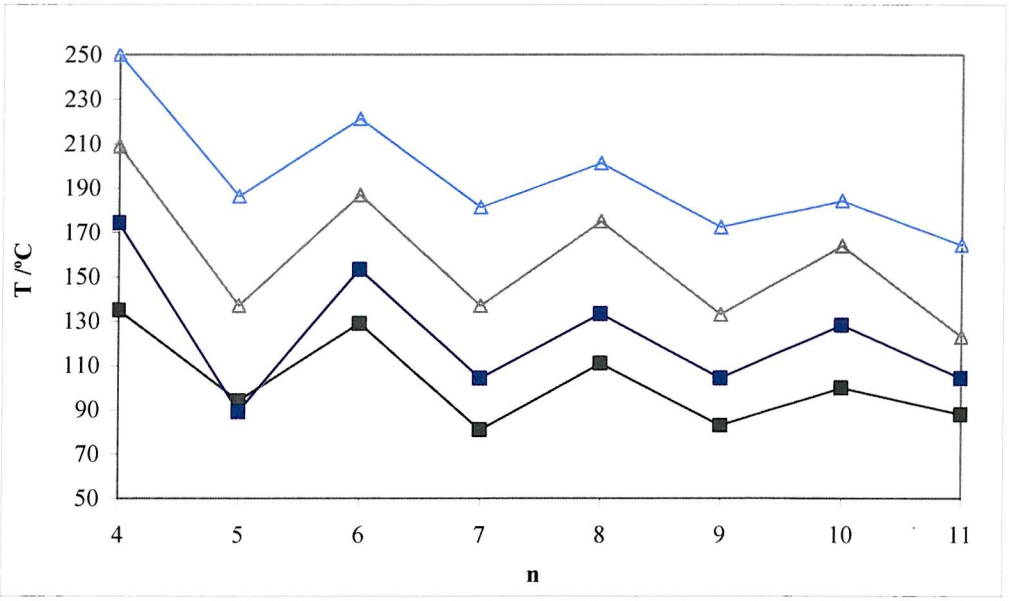

Figure 3.16 The Cr-N/Cr-I and N-I transition temperatures of $CBOnOBFOCF_3$ and CBOnOCB where △ denotes T_{CrN} for CBOnOCB; ▲ denotes T_{NI} for CBOnOCB; ■ denotes $T_{CrN/CrI}$ for $CBOnOBFOCF_3$ and ■ denotes T_{NI} for $CBOnOBFOCF_3$.

However the data used for comparison come from measurements made on the in-house compounds allowing comparisons to be made on the entropy data and the ordering taken from the NMR experiments.

Considering the CBOnOBFOCF$_3$ series, the entire series is nematogenic, giving mostly enantiotropic transitions. Regarding the N-I transitions, the temperature of transition is considerably lower than that of the symmetric cyanobiphenyl series and the nematic range has been reduced (see Figure 3.16). Generally the T_{NI} attenuate in a similar fashion to the symmetric cyanobiphenyls and indeed are the closest comparator series out of the three novel series which have been synthesised. This is not unexpected as the -OCF$_3$ group (similar to the -OCH$_3$ group), is likely to be more stabilising of the nematic phase than a comparative fluorine atom in the other series. Unlike the CBOnOCB series, the nematic range of the CBOnOBFOCF$_3$ compounds for both odd and even members remains very similar (after n = 5).

Similarly the melting points also show an odd-even effect as we might expect. The introduction of the non-symmetric group has had the unfortunate effect of depressing the T_{NI} more than the melting points resulting in the monotropic behaviour seen in n = 5. However, to lower the melting point further, eutectic mixtures could be made and clearly the n = 7, 9 or 11 would provide the lowest melting transition although an even dimer would give a larger nematic range. n = 9 and 11 are significant as, we shall see, they gave particularly high flexoelastic ratios and the presence of an even member from this series would lower this ratio significantly.

In comparison with the CBOnOBF$_2$ dimers, both series follow very similar odd-even patterns (see Figure 3.17). Perhaps most surprising is that the larger T_{NI} for the -OBF$_2$ series suggests that the group has a slightly greater mesogenic character than the -OBFOCF$_3$ moiety. This is unexpected as the -OCF$_3$ group should increase the mesogenicity of the material far more than the corresponding fluorine on the -OBF$_2$ moiety. One possible explanation for this could be that the position of the lateral fluorine atom on the different phenyl ring to the longitudinal group is somehow more stabilising than placing the lateral fluorine adjacent to it on the same ring, although there is no known literature precedent for this. Generally the trend and behaviour of the T_{NI} are very similar. The nematic range is larger for the CBOnOBF$_2$ series than the CBOnOBFOCF$_3$

series although, as mentioned previously, the lower melting transitions for n = 7, 8 and 10 would lend themselves to possible use in low melting mixtures.

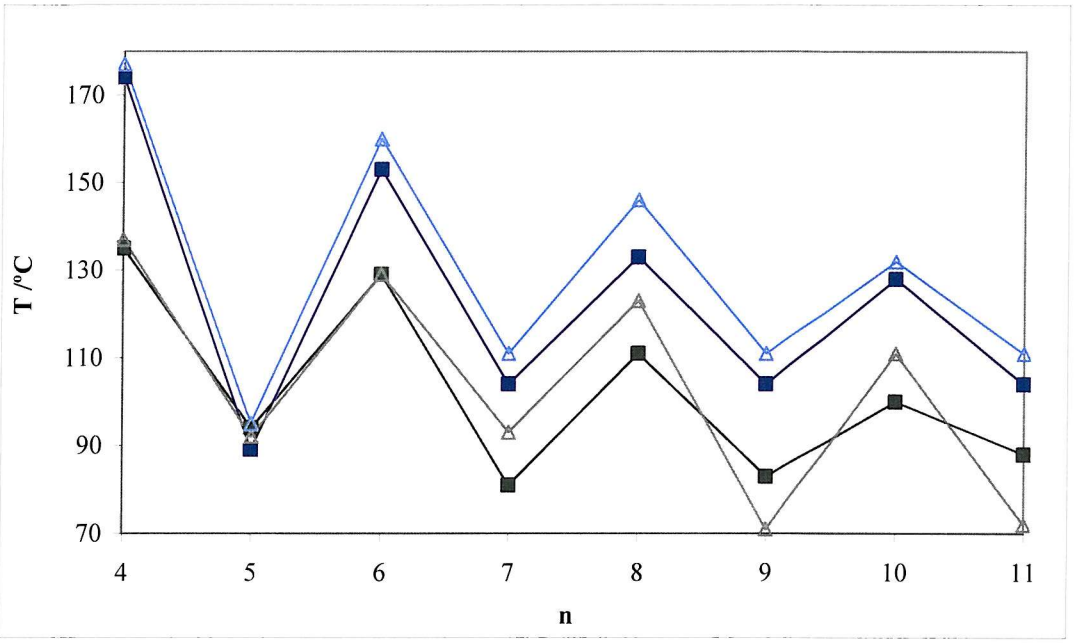

Figure 3.17 The Cr-N/Cr-I and N-I transition temperatures of $CBOnOBFOCF_3$ and $CBOnOBF_2$ where Λ denotes T_{CrN} for $CBOnOBF_2$; Δ denotes T_{NI} for $CBOnOBF_2$; ■ denotes $T_{CrN/CrI}$ for $CBOnOBFOCF_3$ and ■ denotes T_{NI} for $CBOnOBFOCF_3$.

In the case of the $CBOnOBF_2$ the symmetric analogues ($F_2BOnOBF_2$) have been synthesised and a full review of their phase behaviour can be found elsewhere.[8] With regard to the remaining mesogenic groups, only $F_3COFBOnOBFOCF_3$ (n = 7, 9) dimers were synthesised and the results are shown in Table 3.6.

$F_3COFBOnOBOCF_3$		T/ °C		
n	**Yield**	**Cr**		**I**
7	37%	•	109	•
9	91%	•	92	•

Table 3.6 T_{CrI} for the two symmetric fluorinated dimer series. $F_3COFBOnOBFOCF_3$ α, ω-bis-(3'-fluor-4'-oxytrifluoromethylbiphenyl-4-oxy)alkane.

The melting points of these symmetric dimers are significantly lower than the cyanobiphenyl analogues and yet no liquid crystalline phase is observed, even when the isotropic phase is supercooled by ~20 °C. It is perhaps reasonable to conclude that the mesogenicity of these fluorinated biphenyl groups is not good as the $-OBF_2$ group since

the N-I transition are still significantly below that of the melting points which are comparable to the symmetric $F_2BOnOBF_2$ anlogues. The nematogenic behaviour observed in the non-symmetric materials is largely, if not entirely, due to the presence of the cyanobiphenyl group. We might also expect T_{NI} for non-symmetric dimers to be the mean of the two symmetric allowing a transition for these materials to be predicted (as found for binary mixtures of monomers).[31]

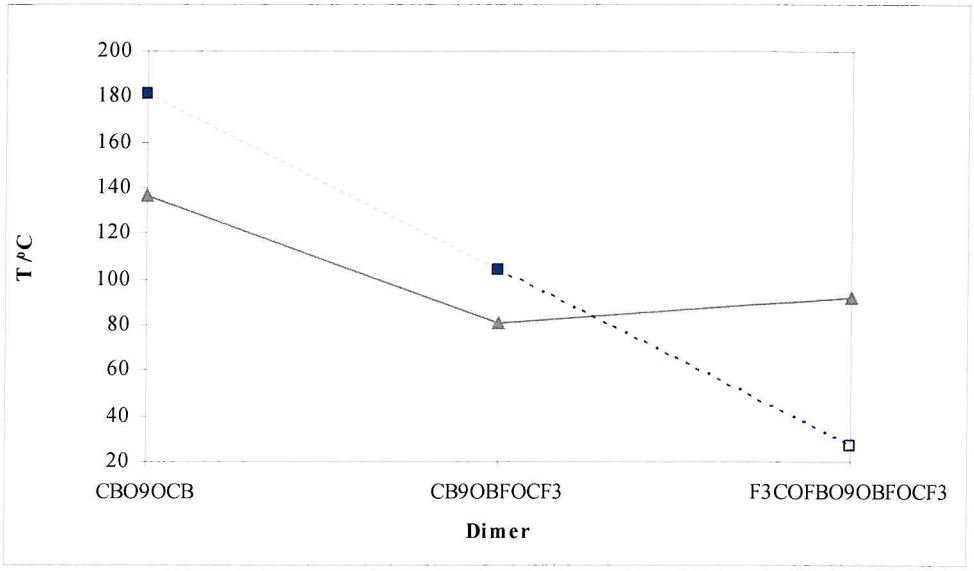

Figure 3.18 Estimating the N-I transition temperature of the symmetric $F_3COFBO9OBFOCF_3$ series by comparison to the CBOnOCB series and the non-symmetric analogue. Here, ▲ represents the Cr-N/Cr-I transition; ■ denotes the N-I transition and □ denotes the predicted T_{NI} transition.

It would have been ideal to be able to compare the non-symmetric fluorinated dimers with the transition temperatures for the symmetric fluorinated analogues. Since only a few examples were synthesised and did not show liquid-crystalline properties, no further materials were made. However using the non-symmetric dimers and the symmetric cyanobiphenyls, we can estimate the T_{NI} transition temperatures approximately by extrapolation. This gives a basis by which we can estimate the mesogenicity of the fluorinated biphenyl moiety (as shown in Figure 3.18), loosely defining mesogenicity as being related to the T_{NI} which in turn is related to the degree to which a group stabilises the liquid crystal (in this case nematic) phase. We know from examination of the symmetric $F_3COFBO9OBFOCF_3$ series that even on supercooling there was no nematic phase observed so it is no surprise that estimation of the T_{NI} shows it to be as low as

27 °C which is over 70 °C below the melting point of the symmetric dimer. Comparing this to the symmetric CBOnOCB we see that this is over 150 °C which is a difference in T_{NI} of approximately 20% taken on an absolute temperature scale.

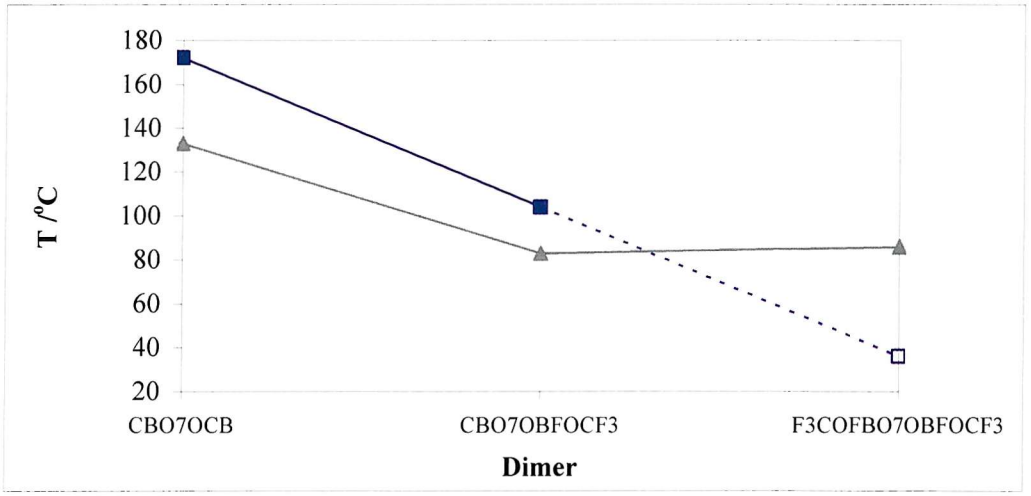

Figure 3.19 Estimating the N-I transition temperature of the symmetric $F_3COFBO7OBFOCF_3$ series by comparison to the CBO7OCB series and the non-symmetric analogue. Here, ▲ represents the Cr-N/Cr-I transition; Δ denotes the predicted Cr-N/Cr-I transition; ■ denotes the N-I transition and □ the predicted N-I transition.

This result is approximately the same for the n = 7 spacer shown in Figure 3.19. Here we see a slightly larger T_{NI} with a predicted transition at 36 °C which is consistent with the odd-even effect observed.

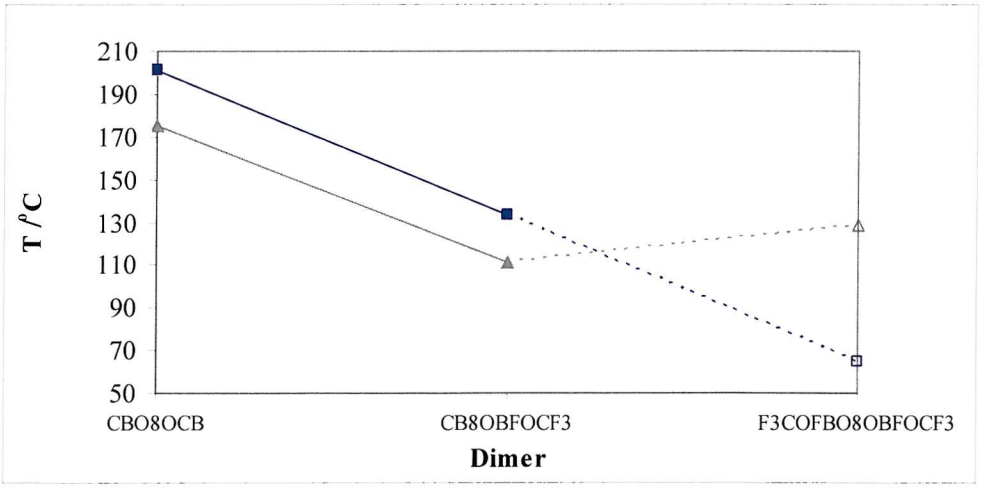

Figure 3.20 Estimating the transition temperatures of the symmetric $F_3COFBO8OBFOCF_3$ compound by comparison to CBO8OCB and the non-symmetric analogue. Cr-I transition temperatures estimated based on data for n = 7 and 9 compared to the respective CBOnOCB series. Here, ▲ represents the Cr-N/Cr-I transition; Δ denotes the predicted Cr-N/Cr-I transition; ■ denotes the N-I transition and □ the predicted N-I transition.

Although there cannot be too much read into results obtained from so little data, it may be possible to observe a nematic phase in the n = 5 since the melting points appear to be falling slightly and the T_{NI} is increasing.

Using the information of the two adjacent dimers, we can also make some estimate for the behaviour of the n = 8 symmetric dimer shown in Figure 3.20. It is impossible to verify these estimates without actual synthesis of the materials, however, given the nature of the data from which this has been extrapolated it is inevitable that from the data for n = 7 and 8 an odd-even effect should occur in both the predicted N-I transitions and the predicted and measured Cr-I transitions.

3.5.3. Orientational ordering of anthracene the nematic

Considering the ordering of the anthracene in the $CBO9BFOCF_3$ nematic phase and comparing it to both the CBO9OCB and $CBO9OBF_2$ mesogens, we see that around $T_s = 0$, S_{zz} for $CBO9OBFOCF_3$ is more similar to S_{zz} for $CBO9OBF_2$. For $T_s > 10$, S_{zz} for $CBO9OBFOCF_3$ is closer in value to that of CBO9OCB (See Figure 3.21).

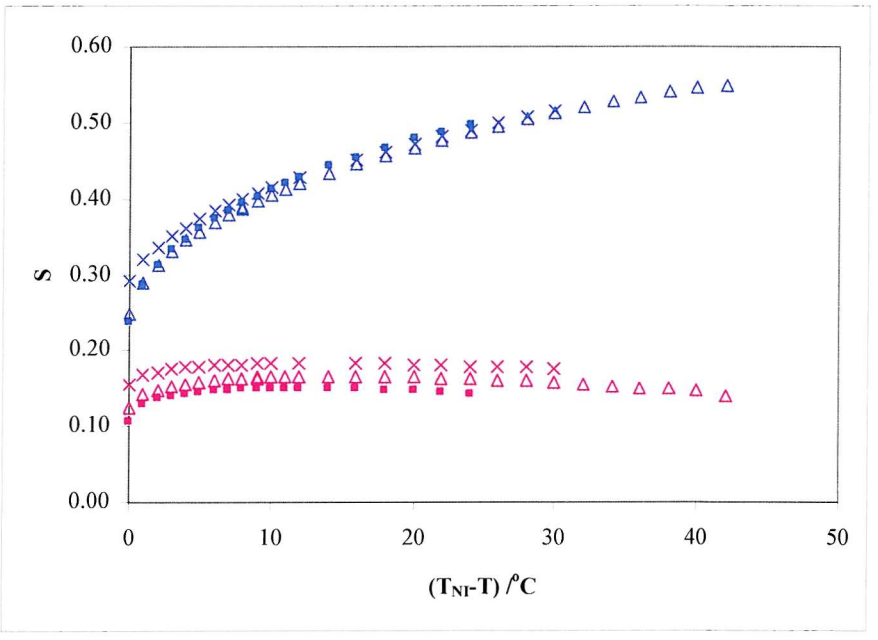

Figure 3.21 The order parameters of anthracene dissolved in CBOnOCB, $CBOnOBF_2$ and $CBOnOBFOCF_3$ as a function of shifted temperature. Here ■ denotes S_{zz} for $CBO9OBFOCF_3$; ■ denotes S_{xx}-S_{yy} for $CBO9OBFOCF_3$; × denotes S_{zz} for CBO9OCB; × denotes S_{xx}-S_{yy} for CBO9OCB; Δ denotes S_{zz} for $CBO9OBF_2$ and Δ denotes S_{xx}-S_{yy} for $CBO9OBF_2$.

The biaxial ordering of the probe in $CBO9OBFOCF_3$ is lower than both that of CBO9OCB and $CBO9OBF_2$. The difference in the molecular biaxiality between (S_{xx}-S_{yy})

for CBO9OCB and appears considerably larger but this is because of the scaling. If we use the biaxial ordering to estimate the biaxiality parameter, λ for CBO9OBFOCF$_3$ is 0.35 which compares to 0.37 for CBO9OBF$_2$ and 0.43 for CBOnOCB; showing the difference in molecular biaxiality for these materials is very small with CBOnOBFOCF$_3$ being lower than that of CBO9OBF$_2$.

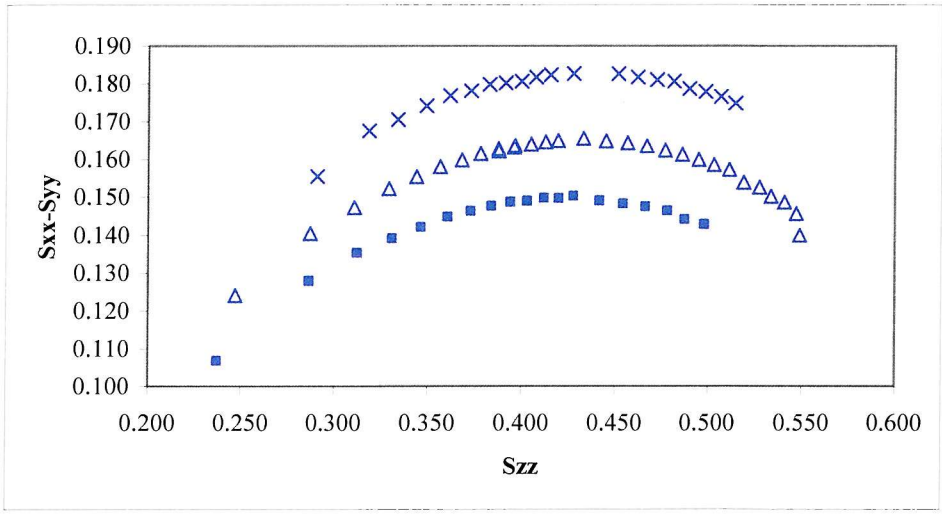

Figure 3.22 Plot of S_{zz} against S_{xx}-S_{yy} showing the difference in the biaxiality order parameter where ■ denotes CBO9OBFOCF$_3$; Δ denotes CBO9OBF$_2$ and × denotes CBOnOCB.

3.5.4. Entropy data

The results for the entropies of transition for the CBOnOBFOCF$_3$ series are given Table 3.7 and here we see that there is an odd-even effect in the N-I transitional entropy. The Cr-N / Cr-I transitional entropies are smaller than that seen for the CBOnOBF$_2$ and the symmetric cyanobiphenyl series.

n	$\Delta H_{CrN/CrI}$/ kJmol^{-1}	$\Delta S_{CrN}/R$	ΔH_{NI}/ kJmol^{-1}	$\Delta S_{NI}/R$
4	30.6	9.5	4.18	1.1
5	44.7	14.6	1.08	0.4
6	41.1	12.5	4.48	1.3
7	37.2	12.8	0.89	0.3
8	37.8	12.2	4.66	1.4
9	33.2	11.5	1.39	0.4
10	32.6	10.5	4.94	1.5
11	38.5	13.1	1.46	0.5

Table 3.7 Table of entropy and enthalpy data for the Cr-N/Cr-I and N-I transitions for CBOnOBFOCF$_3$.

Comparing the $CBOnOBFOCF_3$ series and the CBOnOCB series we see that the odd-even alternation in the $\Delta S_{NI}/R$ is about the same for both series, but the absolute values are smaller for the non-symmetric series (see Figure 3.23).

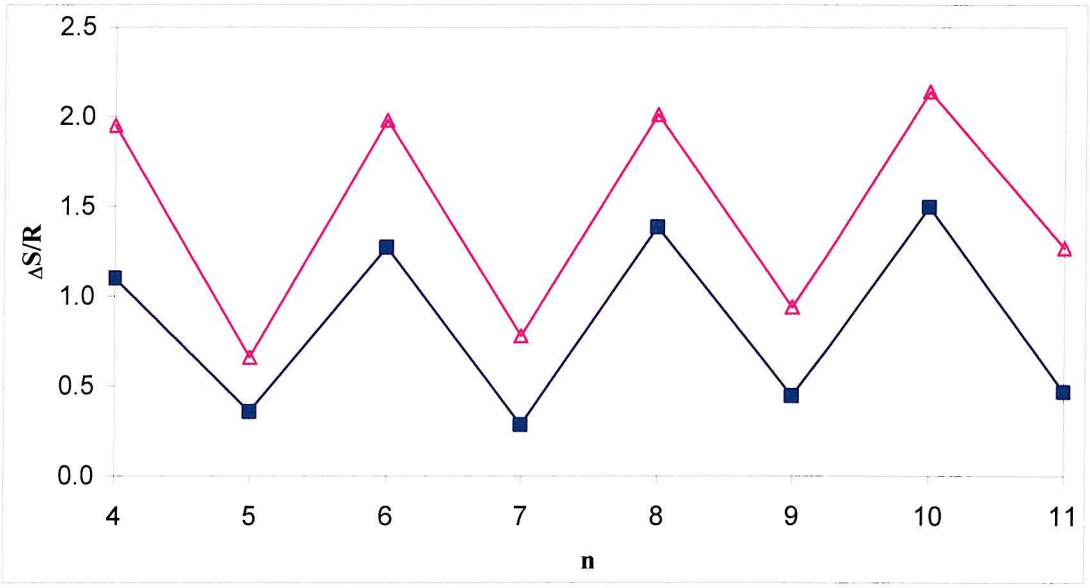

Figure 3.23 Entropy for N-I transitions for the CBOnOCB series[19] and $CBOnOBFOCF_3$, where Δ denotes $\Delta S_{NI}/R$ for CBOnOCB and ■ denotes $\Delta S_{NI}/R$ for $CBOnOBFOCF_3$.

Looking at the odd members of both series we see that the non-symmetric $CBOnOBFOCF_3$ $\Delta S_{NI}/R$ transitions are nearly half the size of the symmetric analogues. This is interesting because we know from the order parameter measurements in Section 3.5.3, that the ordering along the major axis for anthracene (S_{zz}) is largely the same for both series. We can compare $\Delta S_{NI}/R$ and S_{zz} for $CBO9OBFOCF_3$ and CBO9OCB taking the % difference of the non-symmetric dimers relative to CBO9OCB for each property. Thus for $\Delta S_{NI}/R$, $CBO9OBFOCF_3$ is 57% smaller than for CBO9OCB and S_{zz} is only 20% smaller at $T_s = 0$. This is very much larger than the difference we saw for $CBO9OBF_2$ and CBO9OCB yet T_{NI} for $CBO9OBFOCF_3$ and $CBO9OBF_2$ are not so dissimillar (see Figure 3.17). However if this integing result can be explained in terms of the difference in conformation then we would expect $CBOnOBFOCF_3$ to have many more bent conformers in the distribution compared to $CBOnOBF_2$ which would be beneficial in increasing the flexoelectric coefficient for these compounds.

Comparing these results with the entropy data for the $CBOnOBF_2$ we see that they are more similar, especially for smaller values of n. As noted previously, the transitional entropy for the $CBOnOBFOCF_3$ series does not increase very rapidly with n and so the difference between the series gets bigger the longer the spacer becomes.

As commented for the $CBOnOBF_2$ series, the precise nature of the differences between these series cannot be accounted for without modelling the system.

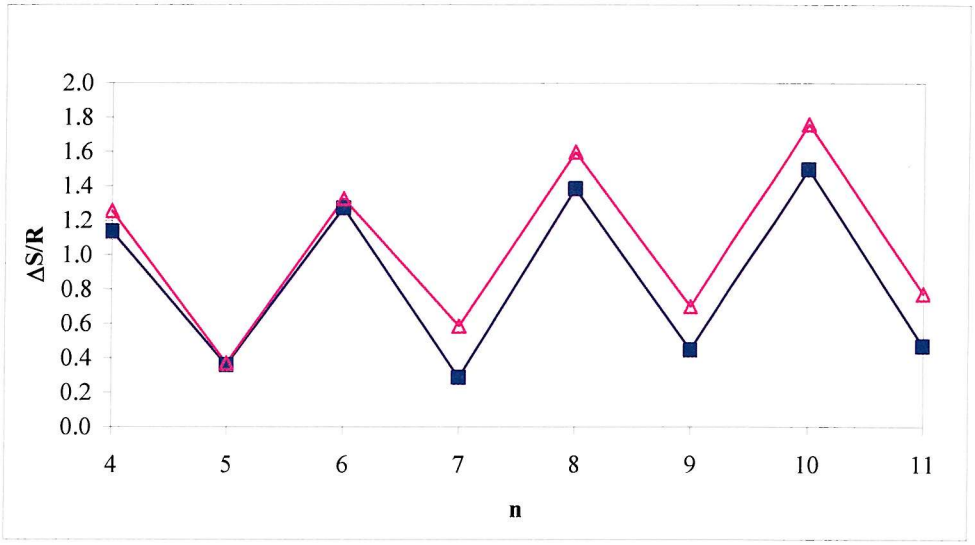

Figure 3.24 Entropy for N-I transitions for the $CBOnOBF_2$ series and $CBOnOBFOCF_3$, where Δ denotes $\Delta S_{NI}/R$ for CBOnOCB and ■ denotes $\Delta S_{NI}/R$ for $CBOnOBFOCF_3$.

3.6. Analyzing the physical data for $CBOnOBF_3$

The $CBOnOBF_3$ series is interesting because it is the only mesogenic group which has a symmetric spread of fluorines across the group. We may expect that this material should behave slightly differently compared to the two non-symmetric dimers considered previously.

3.6.1. Optical microscopy

The optical microscopy was conducted as described in Section 3.4.1. The samples in the series (see Figure 3.25) showed a variety of textures. Each of the materials is nematogenic and most show typical nematic phases with two and four brush schlieren textures and threads running through the texture. There is a dramatic contrast in the clarity of the texture. $CBO6OBF_3$ shows no apparent texture whereas $CBO7OBF_3$ shows

a highly detailed texture. For compounds with spacers n = 8 and 9 the thread-like nature is far more conspicuous whereas for n = 11 the threads are so fine the camera does not pick them up.

Figure 3.25 All optical texture pictures taken on cooling, showing nematic phases. CBO6OBF$_3$ taken at 114 °C, 0.97T_{NI} (top left); CBO7OBF$_3$ taken at 66 °C, 0.99T_{NI} (top right); CBO8OBF$_3$ taken at 112 °C, 0.98T_{NI} (middle left); CBO9OBF$_3$ taken at 86 °C, 0.99T_{NI} (middle right); CBO10OBF$_3$ taken at 104 °C, 0.98T_{NI} (bottom left); CBO11OBF$_3$ taken at 87 °C, 0.98T_{NI} (bottom right).

3.6.2. Phase behaviour

The transition temperatures for the $CBOnOBF_3$ series are given in Table 3.8. Almost all the members show enantiotropic phases (except n = 7) and all are nematogenic.

n	Cr		N		I
4	•	126	•	144	•
5	•	46	•	55	•
6	•	115	•	126	•
7	•	86	•	(73)	•
8	•	108	•	120	•
9	•	79	•	88	•
10	•	123	•	(108)	•
11	•	77	•	92	•

Table 3.8 The transition temperatures in °C for $CBOnOBF_3$. n = 12 was not synthesised.

Looking at the $CBOnOBF_3$ series it clearly exhibits an odd-even effect in both the T_{NI} and the T_{CrN} (see Figure 3.26). Comparing the symmetric and the non-symmetric series, the nematic stability has fallen quite considerably. The mesogenicity of the $-OCF_3$ group appears substantially less than that of the cyanobiphenyl. The alternation in T_{NI} attenuates in a similar fashion to the CBOnOCB series although the N-I transition for the odd members of the non-symmetric series increases with n contrary to the symmetric cyanobiphenyls. The values of T_{NI} across the series varies in a similar way to the alternating values of T_{CrN}. There is a very small nematic range for each dimer, two of which show monotropic phases (n = 7 and 10). The melting points for the $CBOnOBF_3$ series are small compared to the CBOnOCB series, but as has been the case for all of these materials, the fall in T_{NI} is greater than the reduction in the melting point leading to a less favourable nematic range.

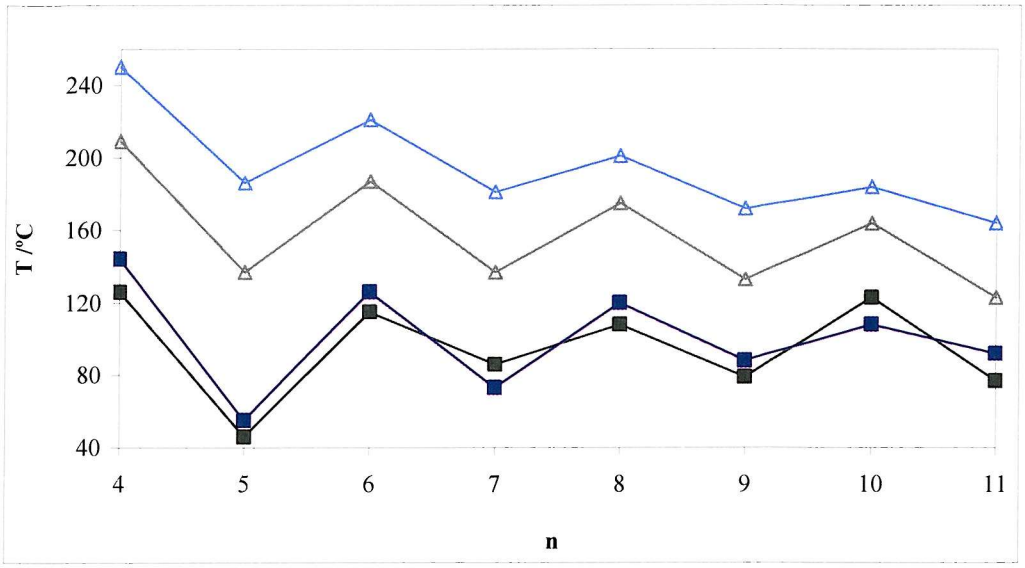

Figure 3.26 The Cr-N/ Cr-I and N-I transition temperatures of $CBOnOBF_3$ and CBOnOCB where Δ denotes T_{CrN} for CBOnOCB; Δ denotes T_{NI} for CBOnOCB; ■ denotes $T_{CrN/CrI}$ for $CBOnOBF_3$ and ■ denotes T_{NI} for $CBOnOBF_3$.

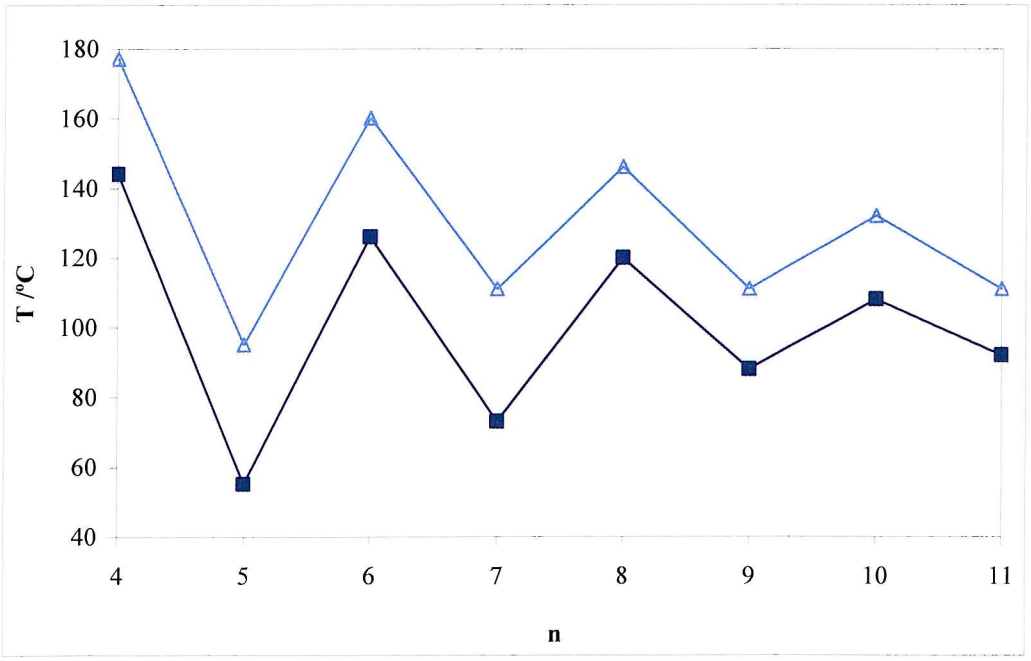

Figure 3.27 The N-I transition temperatures of $CBOnOBF_3$ and $CBOnOBF_2$ where Δ denotes T_{NI} for $CBOnOBF_2$ and ■ denotes T_{NI} for $CBOnOBF_3$.

Not surprisingly the properties of the $CBOnOBF_3$ non-symmetric series are very similar to those of the non-symmetric $CBOnOBF_2$ series (see Figure 3.27). Significantly the T_{NI}

are consistently lower than the $CBOnOBF_2$ series. Again, the reduced T_{NI} for the $CBOnOBF_3$ series is due to the extra lateral fluorine.

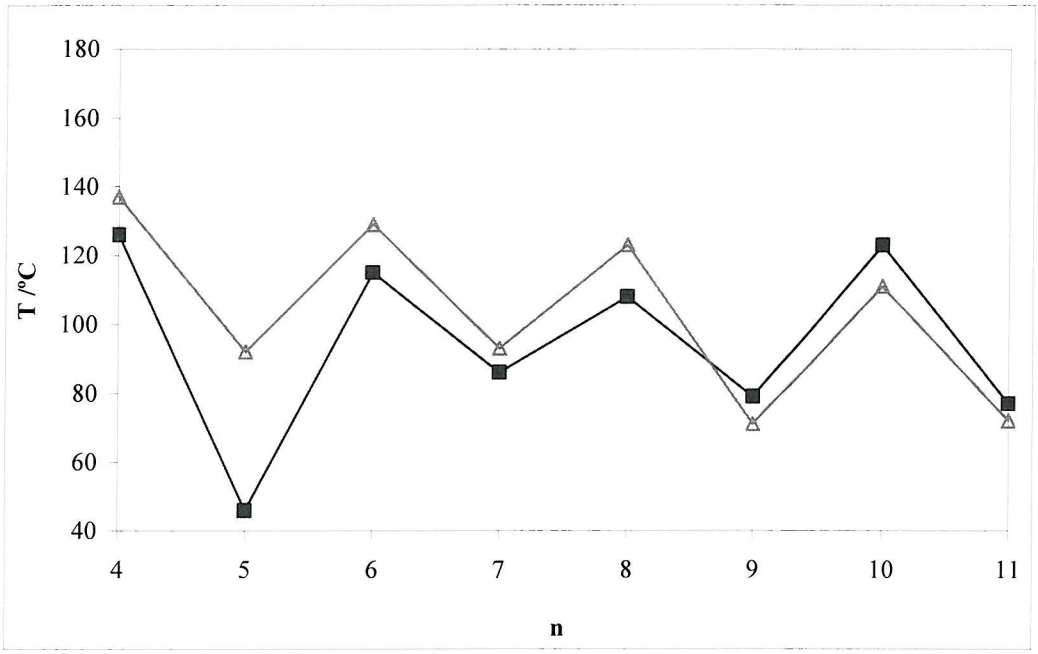

Figure 3.28 The Cr-N/Cr-I transition temperatures of $CBOnOBF_3$ and $CBOnOBF_2$ where △ denotes T_{CrN} for $CBOnOBF_2$; ■ denotes $T_{CrN/CrI}$ for $CBOnOBF_3$.

Considering the results in Figure 3.28 we see that although the odd-even effect in the melting point is erratic in the $CBOnOBF_3$ series, the average melting point across the series does not vary a great deal as the spacer length increases. In contrast, within the $CBOnOBF_2$ series the T_{CrN} for the $CBOnOBF_3$ series fall as the spacer length increases, so much so that it dips below the T_{CrN} transitions for analogous materials in the $CBOnOBF_3$ series.

3.6.3. Orientational ordering of anthracene in the nematic

The orientational ordering of anthracene in the nematic for $CBO9OBF_3$ is compared to that in the symmetric cyanobiphenyl and the non-symmetric $CBO9OBF_2$ dimer. The difference between the two non-symmetric dimers is, in terms of the chemical structure, very small. However, consideration of the T_{NI} shows there is quite a significant difference in the liquid crystal character between the two mesogens.

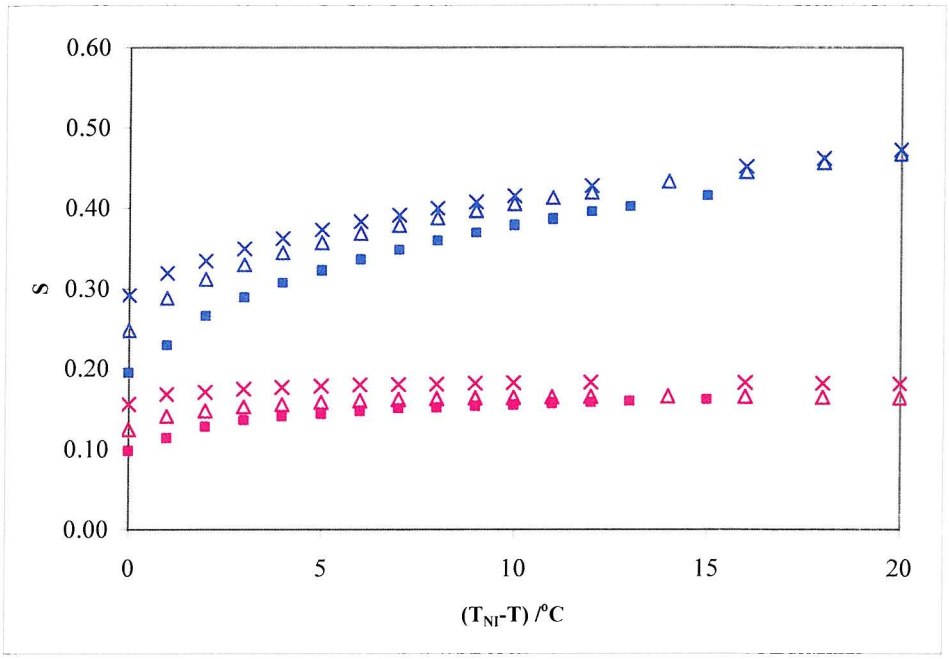

Figure 3.29 The order parameters of anthracene dissolved in CBOnOCB, $CBOnOBF_2$ and $CBOnOBF_3$ as a function of the shifted temperature. Here ■ denotes S_{zz} for $CBO9OBF_3$; ■ denotes S_{xx}-S_{yy} for $CBO9OBF_3$; × denotes S_{zz} for CBO9OCB; × denotes S_{xx}-S_{yy} for CBO9OCB; Δ denotes S_{zz} for $CBO9OBF_2$ and Δ denotes S_{xx}-S_{yy} for $CBO9OBF_2$.

Looking at the order parameters (see Figure 3.29) we see that the difference between the two non-symmetric materials is quite significant particularly for S_{zz} at $T_s = 0$. In both cases $CBO9OBF_3$ has a smaller value of S than CBO9OCB or $CBO9OBF_2$.

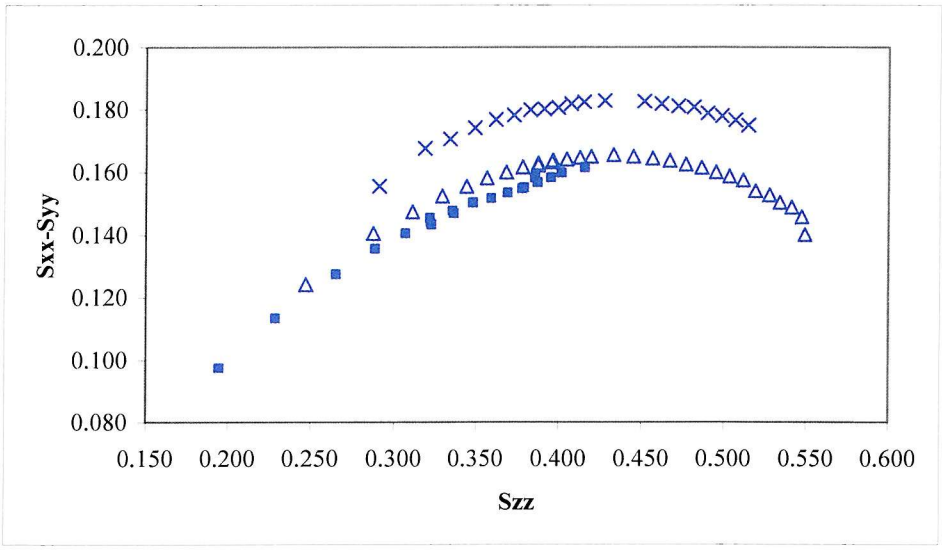

Figure 3.30 Plot of S_{zz} against S_{xx}-S_{yy} showing the difference biaxiality where ■ denotes $CBO9OBF_3$; Δ denotes $CBO9OBF_2$ and × denotes CBO9OCB.

Due to the smaller enantiotropic nematic range and smaller supercooling range the number of data points for $CBOnOBF_3$ is considerably smaller than that for the two comparator series. As a result it is impossible to be certain of whether the results are following the expected pattern shown for CBO9OCB and $CBO9OBF_2$. The indication is that the new dimer is following the pattern of the non-symmetric $CBO9OBF_2$ showing a slightly smaller biaxial ordering. Given the similarity in molecular structure this is not a surprising result. Determining λ for $CBO9OBF_3$ is less certain but should fall around λ = 0.38 which, as can be seen in Figure 3.30, is very close to that of $CBO9OBF_2$.

3.6.4. Entropy data

Given the similarity in the data for the ordering of anthracene in the nematic for $CBO9OBF_3$ compared to $CBO9OBF_2$ we might expect the transitional entropy for the two series to be similar. Looking at the data in Table 3.9 we see that, as expected, there is a clear odd-even effect in the transitional entropies which is apparent in both the melting and the N-I transitions. We should also note that the values are significantly smaller than those for the $CBOnOBF_2$ series. There is no value for n = 5 as the material crystallised on cooling before the nematic transition occurred.

n	$\Delta H_{CrN/CrI}$/ kJmol^{-1}	$\Delta S_{CrN/CrI}/R$	ΔH_{NI}/ kJmol^{-1}	$\Delta S_{NI}/R$
4	25.4	8.2	2.67	0.8
5	38.2	14.3	N/A	N/A
6	28.0	9.0	2.46	0.7
7	39.3	13.3	0.97	0.3
8	31.4	10.7	3.19	1.0
9	31.5	11.2	1.03	0.3
10	30.0	9.8	2.40	0.8
11	38.8	13.4	1.38	0.5

Table 3.9 The transitional entropy data for the $CBOnOBF_3$ series.

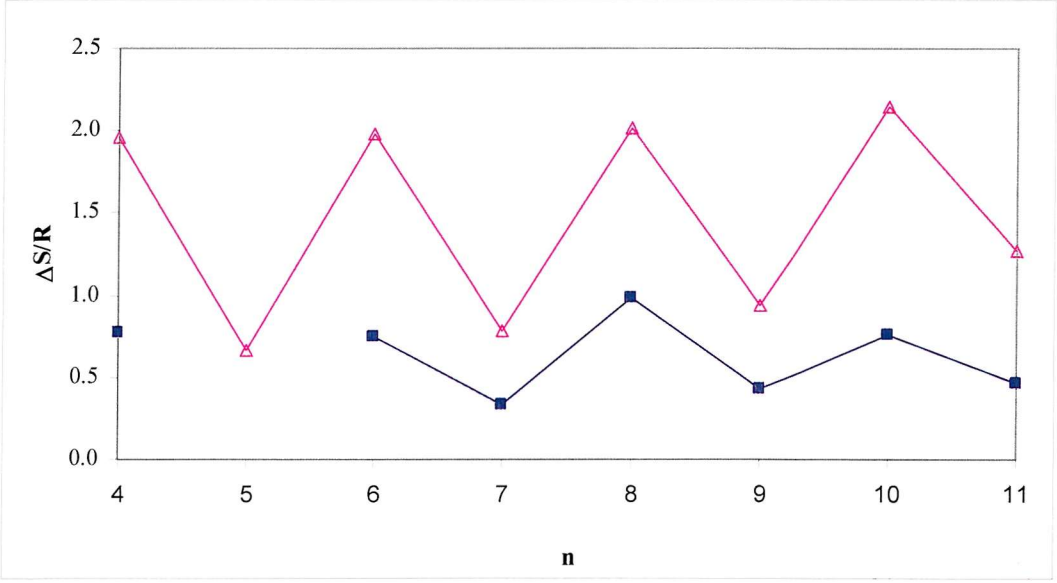

Figure 3.31 Entropy change for N-I transitions for the CBOnOCB series[19] and $CBOnOBF_3$, where △ denotes $\Delta S_{NI}/R$ for CBOnOCB and ■ denotes $\Delta S_{NI}/R$ for $CBOnOBF_3$.

The plot of the entropies of transition for $CBOnOBF_3$ are shown in Figure 3.31. Here we see $\Delta S_{NI}/R$ across this fluorinated series is substantially smaller than the results for the symmetric cyanobiphenyls.[19] The result deviates from the expected behaviour in a number of ways. First, the trend shows a slightly less than regular pattern, although the odd-even effect does appear to start to attenuate as n becomes larger. Secondly, the values for the odd dimers are rising slowly but the even dimers are falling after n = 8. Finally, and most significantly, the magnitiude of $\Delta S_{NI}/R$ is considerably smaller across the series. Interestingly, where n is small, the values for the even dimers is almost exactly the same as those seen for odd dimers in the CBOnOCB series.

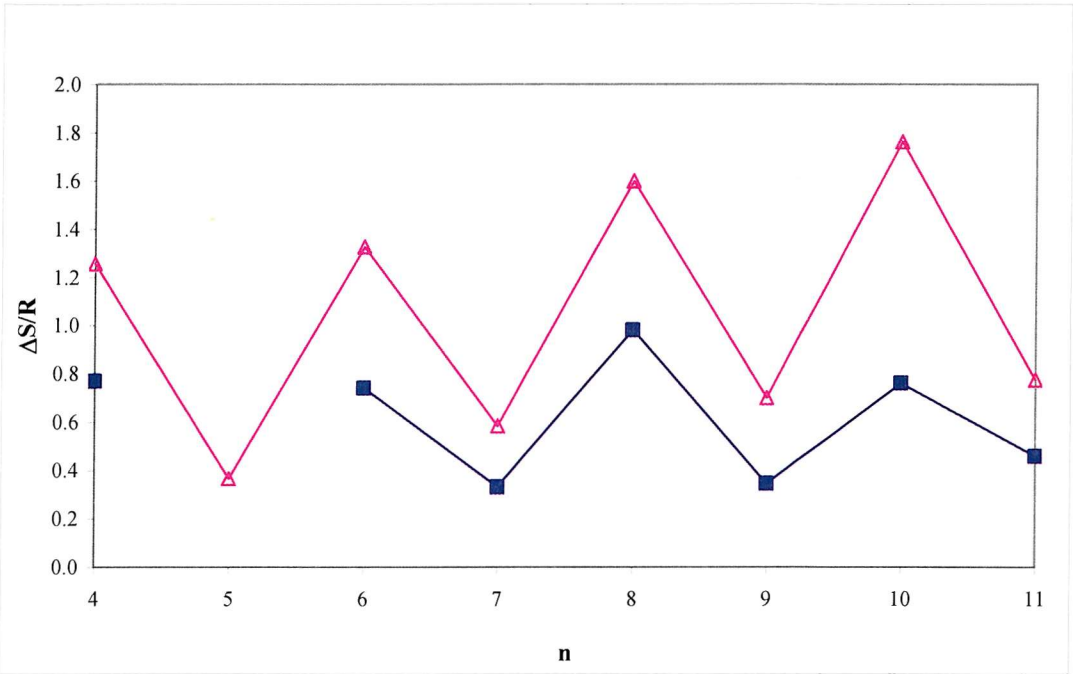

Figure 3.32 Entropy change for N-I transitions for the $CBOnOBF_2$ series and $CBOnOBF_3$, where △ denotes $\Delta S_{NI}/R$ for $CBOnOBF_2$ and ■ denotes $\Delta S_{NI}/R$ for $CBOnOBF_3$.

Comparing the $CBOnOBF_3$ series with the $CBOnOBF_2$ series we can see they are somewhat more similar. Generally speaking $\Delta S_{NI}/R$ for the $CBOnOBF_3$ series is just over half the value of the $CBOnOBF_2$ series. This is interesting as yet again this considerable difference does not show up in the results for the ordering of the anthracene in the nematic. As with $CBO9OBFOCF_3$ the difference between $\Delta S_{NI}/R$ and S_{zz} at $T_s = 0$ compared to CBO9OCB is substantial.

3.7. Analyzing the physical data for $CBOnOBF_4$

The structural difference between the $-OBF_3$ and $-OBF_4$ mesogenic group is small, yet the effect of the extra fluorine could be significant. However we will see that there is very little difference between the two series of dimers in terms of T_{NI} and entropy.

3.7.1. Optical microscopy

The optical microscopy was conducted as described earlier in Section 3.4.1. Generally there is a great deal of similarity in the optical textures of both the $CBOnOBF_3$ and $CBOnOBF_4$ series. The latter tended to form textures which had a more discernible schlieren texture. However, this is probably related more to the untreated glass surface

rather than the material itself. Each material showed the diagnostic thread-like texture and flashed when subjected to mechanical stress. As with all these non-symmetric series some of the threads in the textures were less conspicuous than others and as such are less apparent in the pictures. All of the schlieren textures that did form, showed a similar number of two and four brush defects. The less textured materials often only gave a schlieren texture for less than half a degree right at the transition and disappeared before the phase had properly established.

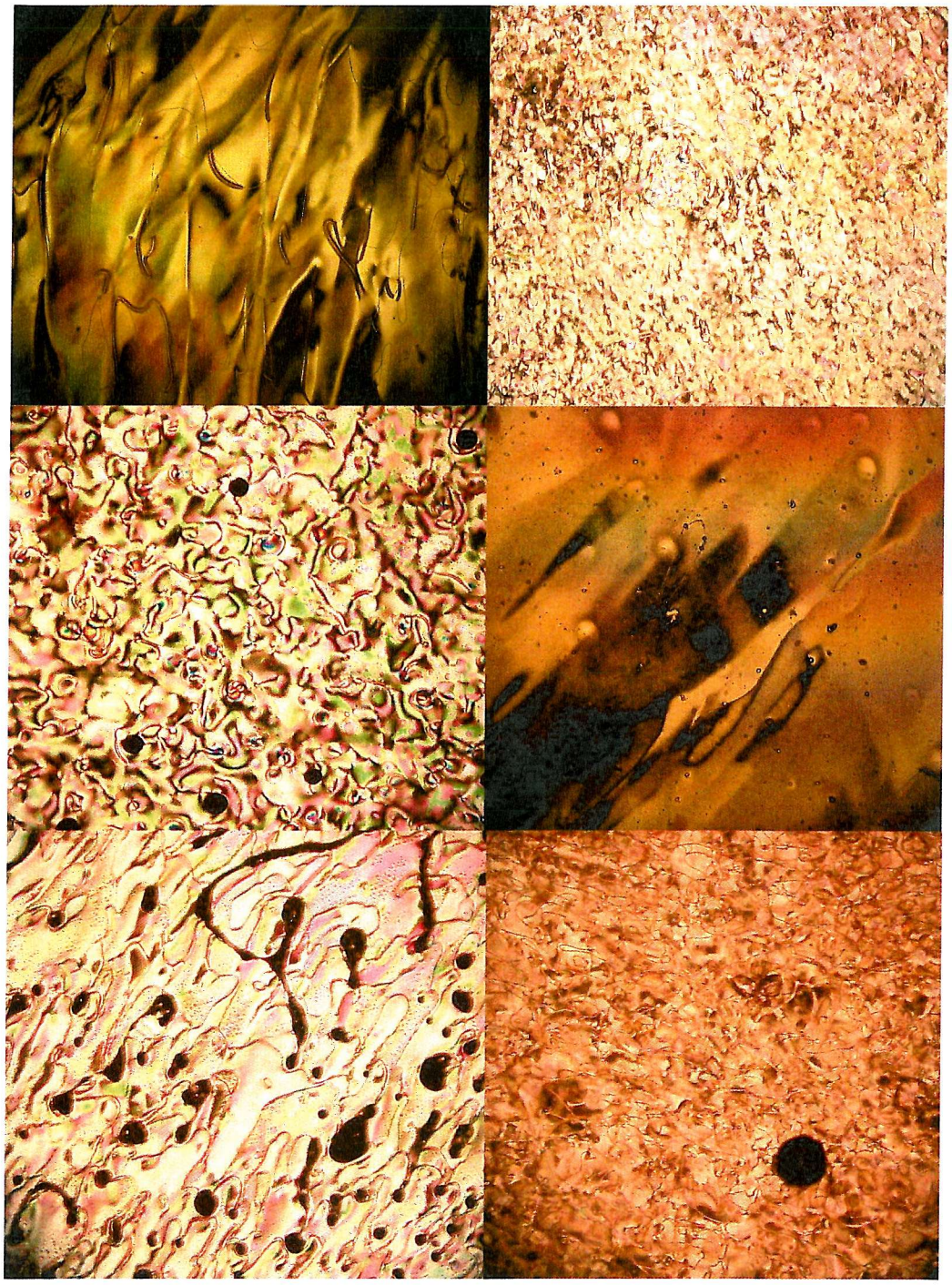

Figure 3.33 All optical texture pictures taken on cooling, for the nematic phases. CBO6OBF$_4$ taken at 111 °C, 0.98T_{NI} (top left); CBO7OBF$_4$ taken at 75 °C, 0.99T_{NI} (top right); CBO8OBF$_4$ taken at 100°C, 0.99T_{NI} (middle left); CBO9OBF$_4$ taken at 73 °C, 0.99T_{NI} (middle right); CBO10OBF$_4$ taken at 101 °C, 1.00T_{NI} (bottom left); CBO11OBF$_4$ taken at 75 °C, 0.99T_{NI} (bottom right).

3.7.2. Phase behaviour

The transition temperatures for the $CBOnOBF_3$ series are given in Table 3.10. Almost all the members show enantiotropic phases (except n = 5 and 7) and all are nematogenic.

n	Cr		N		I
4	•	113	•	127	•
5	•	92	•	(51)	•
6	•	96	•	120	•
7	•	92	•	(78)	•
8	•	95	•	104	•
9	•	63	•	78	•
10	•	93	•	102	•
11	•	62	•	80	•

Table 3.10 The transition temperatures for $CBOnOBF_4$ given in °C. n = 12 was not synthesised.

The similarity in the N-I transition temperatures between the $CBOnOBF_3$ and $CBOnOBF_4$ series means both dimer series compare very similarly with the CBOnOCB and $CBOnOBF_2$ series. Therefore in this section the $CBOnOBF_4$ series is only compared to $CBOnOBF_3$ series in Figure 3.34.

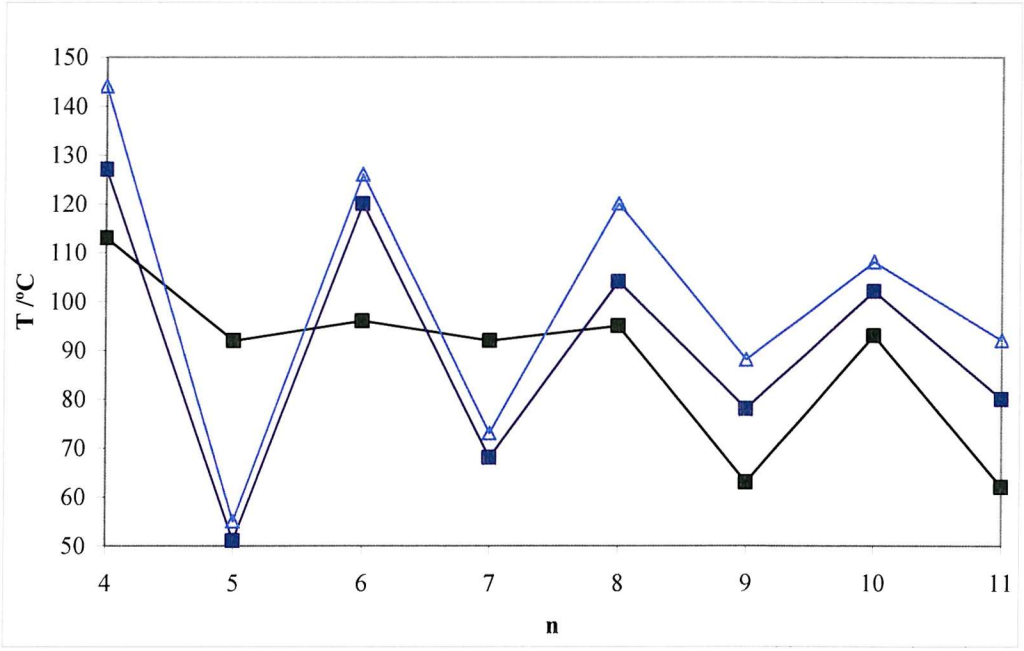

Figure 3.34 The Cr-N/Cr-I and N-I transition temperatures of $CBOnOBF_4$ and the N-I transition temperatures of $CBOnOBF_3$ where ■ denotes $T_{CrN/CrI}$ for $CBOnOBF_4$; ■ denotes T_{NI} for $CBOnOBF_4$ and Δ denotes T_{NI} for $CBOnOBF_3$.

The arguments given for the trends in the transition temperatures for the $CBOnOBF_3$ series should be valid in this series except to say that the extra lateral fluorine appears to be destabilising to the nematic phase further. This is apparent throughout the series where, by comparison to the $CBOnOBF_3$ series, the T_{NI} of $CBOnOBF_4$ is consistently lower.

In the case of the melting points, unlike the previous examples, the $CBOnOBF_4$ series do not show a pronounced odd-even effect until $n > 8$ which renders the nematic phases for the $n = 5$ and 7 dimers monotropic.

3.7.3. Orientational ordering of anthracene in the nematic

For the ordering of anthracene in the $CBO9OBF_4$ nematic we see a similar behaviour compared to that of $CBO9OBF_3$. The values for S_{zz} at shifted temperatures are compared to both CBO9OCB and $CBO9OBF_2$ (see Figure 3.35) and we see as for $CBO9OBF_3$, S_{zz} for $CBO9OBF_4$ is quite a bit lower than either $CBO9OBF_2$ or CBO9OCB. For the biaxial ordering we see that the $CBO9OBF_4$ dimer is close to that of both CBO9OCB and $CBO9OBF_2$ dimers.

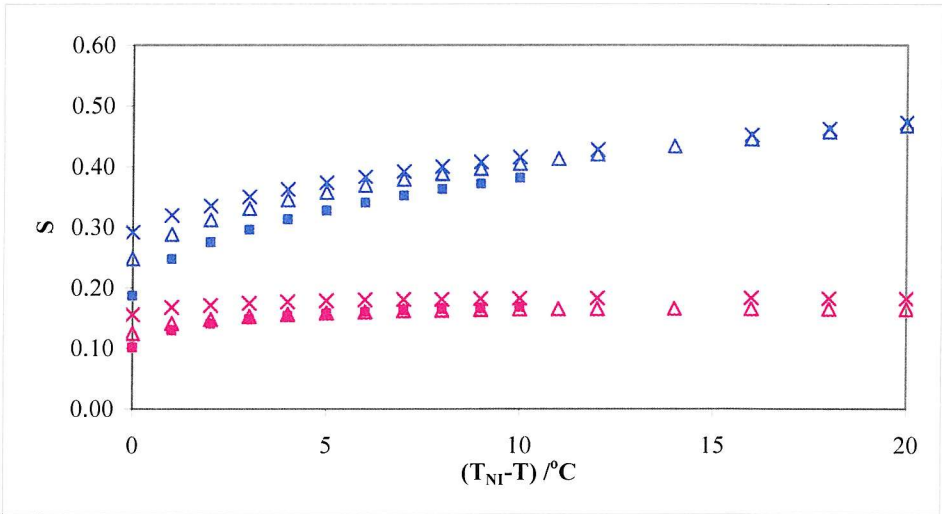

Figure 3.35 The order parameter for anthracene plotted as a function of shifted temperature. Here ■ denotes S_{zz} for $CBO9OBF_4$; ■ denotes S_{xx}-S_{yy} for $CBO9OBF_4$; × denotes S_{zz} for CBO9OCB; × denotes S_{xx}-S_{yy} for CBO9OCB; Δ denotes S_{zz} for $CBO9OBF_2$ and Δ denotes S_{xx}-S_{yy} for $CBO9OBF_2$.

As we saw with $CBO9OBF_3$ there is a much smaller nematic range and smaller supercooling range, hence we have data for a much smaller shifted temperature than for the CBO9OCB and $CBO9OBF_2$ dimers. This is apparent in Figure 3.36 where S_{zz} is

plotted S_{xx}-S_{yy}. There it is impossible to work out λ as S_{xx}-S_{yy} clearly does not reach its maximum value. Interestingly it does appear that λ will be greater for CBO9OBF$_4$ than for CBO9OBF$_2$ which is in contrast to the structurally similar CBO9OBF$_3$ which had a value of λ slightly less than that of CBO9OBF$_2$.

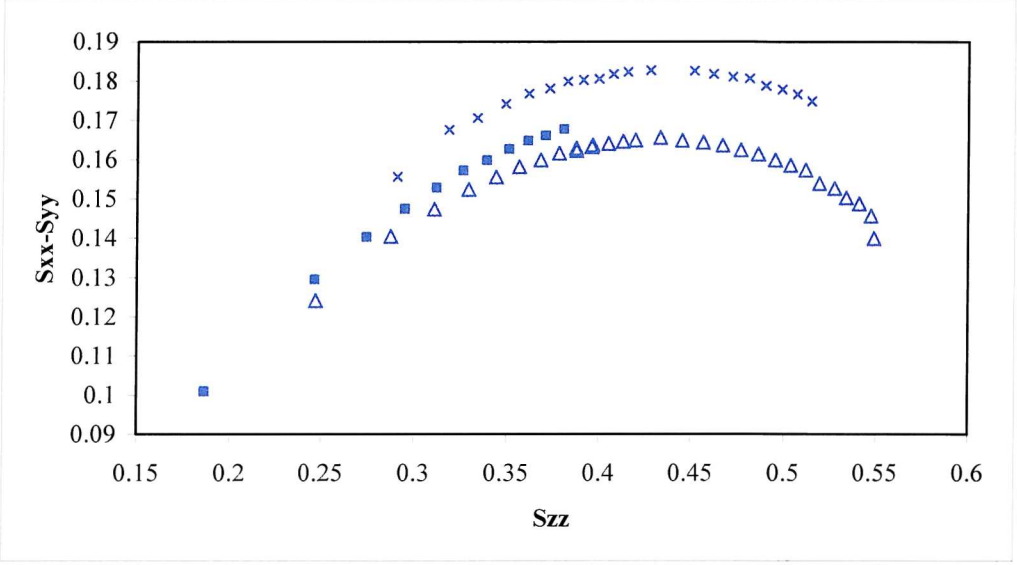

Figure 3.36 Plot of S_{zz} against S_{xx}-S_{yy} showing the difference biaxiality where ■ denotes CBO9OBF$_4$; Δ denotes CBO9OBF$_2$ and × denotes CBO9OCB.

It is interesting that the presence of the extra fluorine substituent should cause such a big difference compared to the CBO9OBF$_3$ dimer, especially as it appears to have had very little effect on the T_{NI}.

3.7.4. Entropy data

The transitional entropy data in Table 3.11 shows several features. The first is that there is an odd-even effect as we would expect for a dimer series. The second is that $\Delta S_{NI}/R$ is generally small compared the values for CBOnOCB and this is seen in Figure 3.37 and is similar to the behaviour for the CBOnOBF$_3$ series (see Figure 3.32).

n	$\Delta H_{CrN/CrI}$/ kJmol^{-1}	$\Delta S_{CrN}/R$	ΔH_{NI}/ kJmol^{-1}	$\Delta S_{NI}/R$
4	11.6	3.6	2.18	0.7
5	32.1	10.8	0.41	0.2
6	36.1	11.7	2.63	0.8
7	42.9	14.4	0.79	0.3
8	39.4	13.1	2.54	0.8
9	26.7	9.7	0.77	0.3
10	45.1	15.5	2.67	0.8
11	35.5	12.0	1.28	0.4

Table 3.11 The transitional entropy data for the $CBOnOBF_4$ series.

Comparison of $CBOnOBF_4$ with the CBOnOCB series shows that there is almost no absolute increase in $\Delta S_{NI}/R$ as n gets larger, the size of the alternation is not as large and the overall magnitude of the entropy of transition is much smaller. Most significantly, as with $CBOnOBF_3$, the size of the entropy of transition for $CBOnOBF_4$ is much smaller than for the symmetric cyanobiphenyls. As seen with the $CBOnOBF_3$, the even dimers exhibit a $\Delta S_{NI}/R$ approximately the same as the odd dimers in the CBOnOCB series where n is small.

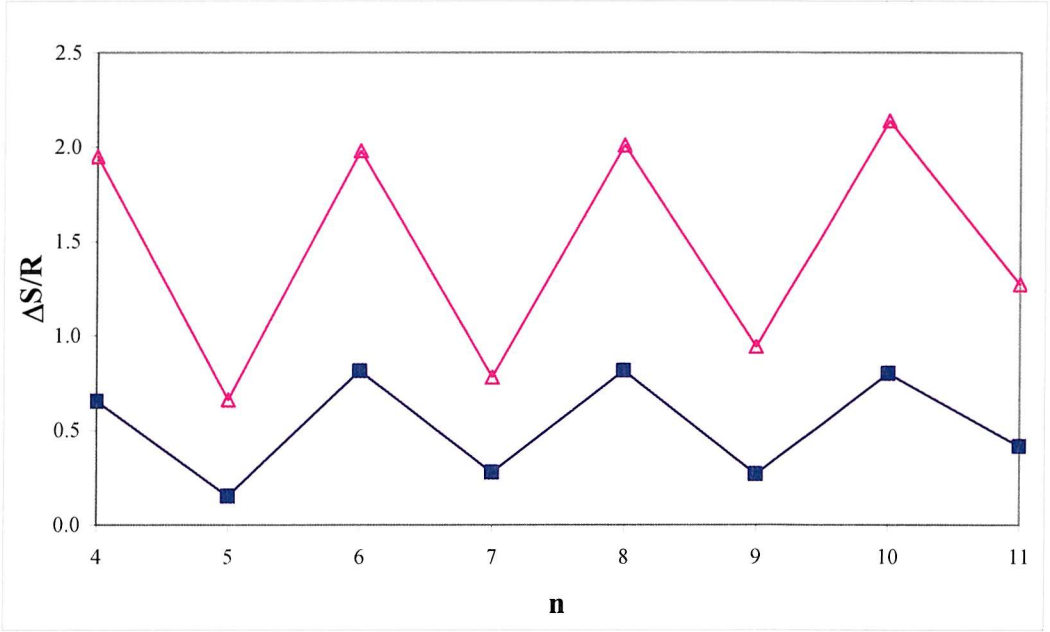

Figure 3.37 The entropy change for N-I transitions for the CBOnOCB series[19] and the $CBOnOBF_4$ series, where Δ denotes $\Delta S_{NI}/R$ for CBOnOCB and ■ denotes $\Delta S_{NI}/R$ for $CBOnOBF_4$.

Comparing $CBOnOBF_4$ with the $CBOnOBF_3$ series we see that as the chain length gets longer the transitional entropies become more similar between the series. Without the

data for n = 5 for the -OBF_3 series it is hard to compare the shorter spacer entropies, however where n > 8 the similarity between the two series is remarkable.

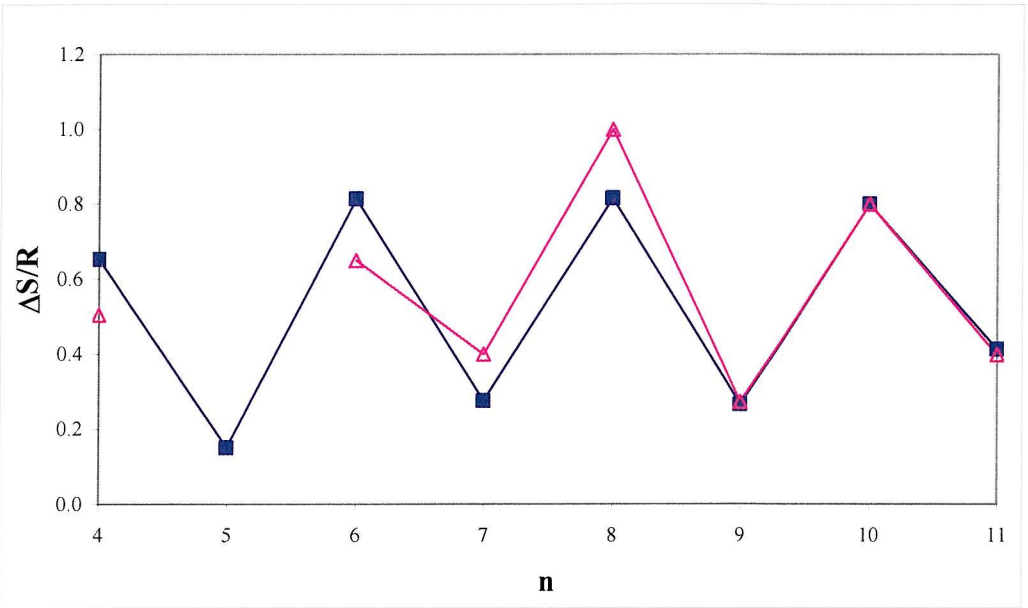

Figure 3.38 Entropy for N-I transitions for the $CBOnOBF_3$ series and $CBOnOBF_4$, where Δ denotes $\Delta S_{NI}/R$ for $CBOnOBF_3$ and ■ denotes $\Delta S_{NI}/R$ for $CBOnOBF_4$.

In a qualitative sense we may expect this as the chain length gets longer, proportionally it accounts for more of the molecule and dominates more the molecular interactions.[20] The mesogenic effect of the -OBF_3 and -OBF_4 is diluted and thus the effect on the ordering becomes less. The molecules become effectively more similarly ordered and thus the transitional entropy become similar. Interestingly this is not quite the case for T_{NI} for each series which do not converge as n becomes large.

3.8. Comparisons made across the four series

Although the data has been analysed, it is important to consider the properties of these four series by comparing all the members together.

3.8.1. Comparing the T_{NI} across each series

In terms of the phase behaviour of each of the materials, of key importance is the N-I transition. It gives a good indication of how mesogenic the compound is and is also important when considering the nematic range in mixtures. As reported, all the materials are nematic, most show enantiotropic phases but there are some monotropic examples.

There is, in all four cases, a strong odd-even variation in the nematic-isotropic transition. This is unsurprising given their basic shape anisotropy is very similar to the symmetric cyanobiphenyl dimers where the geometry of the odd and even homologues differ substantially thus they would also show this pronounced odd-even effect – a typical characteristic of liquid crystal dimers. To enable a meaningful comparison between the four series the T_{NI} of each series are plotted, in Figure 3.39.

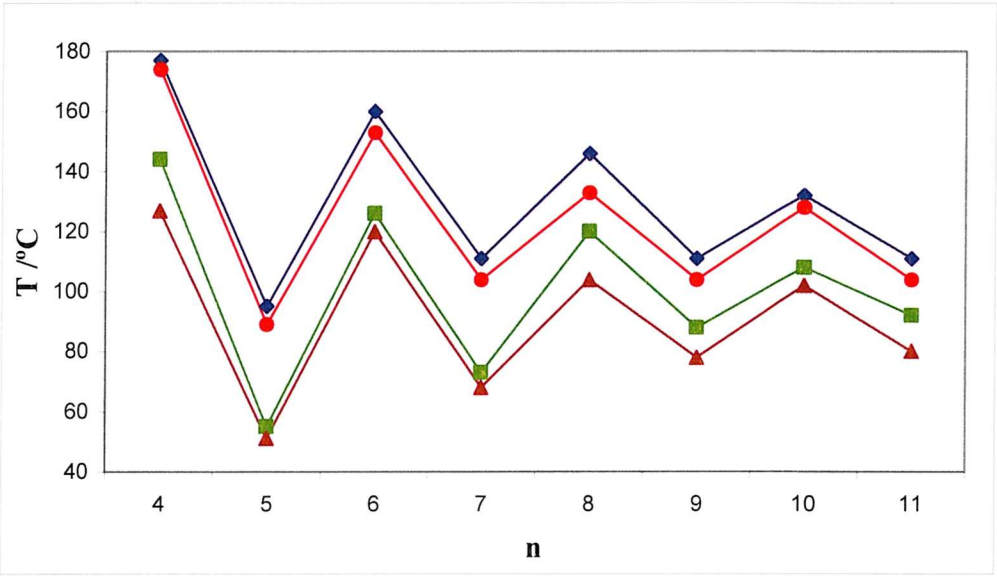

Figure 3.39 The N-I transition temperatures for the four series of non-symmetric fluorinated liquid crystal dimers where ♦ denotes T_{NI} for $CBOnOBF_2$; ■ T_{NI} for $CBOnOBF_3$; ● denotes T_{NI} for $CBOnOBFOCF_3$ and ▲ denotes T_{NI} for $CBOnOBF_4$.

It is perhaps striking that these dimers share a very similar overall trend. Comparison shows that, even for $CBOnOCFOCF_3$ which has quite a different mesogenic group in terms of both shape and polarity, the trend remains consistent and does not even cross the other trend lines despite being at most only 8 °C different to the T_{NI} of the $CBOnOBF_2$ series.

In each case the odd-even effect attenuates with increasing spacer length, a feature common to liquid crystal dimers as the effect of the mesogenic groups becomes diluted by the increasing spacer. There are differences between the series; the T_{NI} consistently falls across each series for a given value of n, but more interesting is comparing how the odd dimers behave between each group. Within a series it is clear that n = 5 shows a

significant drop in nematic stability in comparison with n = 4 and 6. However the extent to which this recovers for n = 7, 9 and 11 differs depending on the series. In the case of CBOnOBF$_4$ T_{NI} for the odd dimers increases and levels off at n = 9. In the case of CBOnOBF$_2$ the stability of n = 7 is proportionally much higher and the T_{NI} in the odd dimers fall from n = 7 to n = 11.

In terms of the mesogenicity, the -OBF$_2$ group appears to offer the greatest nematic stability, the largest nematic range and no monotropic behaviour. This is perhaps not so surprising given it has the least number of off-axis fluorines and can be estimated to have the largest molecular dipole resolved through the major axis.

Using the general rules established by Gray *et al.*[14], relating molecular shape and substituents to how liquid-crystalline the materials are, these non-symmetric materials fit reasonably well with established theory and predictions. Off-axis fluorines act to lower the mesogenicity (-OBF$_3$ and -OBF$_4$ < -OBFOCF$_3$ and -OBF$_2$) and all four materials have lower isotropic transition temperatures that the symmetric cyanobiphenyl. The only surprise is that it might have been expected that the -OBFOCF$_3$ group would have been better than -OBF$_2$ given that both groups have one off axis fluorine and that the -OCH$_3$ group is shown by Gray to generally be a significantly better mesogenic substituent than –F (assuming that -OCF$_3$ ≈ -OCH$_3$).

3.8.2. Comparing $T_{CrN/CrI}$ across each series

Although the trends in the melting points do not have a direct impact on the liquid crystal properties of the materials, they are significant in allowing us to see this behaviour. Key to a large nematic range (a favourable property for a material used in a display device) is a high nematic stability and a low melting point. Thus understanding and controlling the melting points is important not only for individual materials but also when forming eutectic mixtures.

Consideration of the melting points of all four series shows that there is an odd-even effect in the melting points of almost all the dimers (see Figure 3.40). This effect is less pronounced in the CBOnOBF$_4$ series where, for shorter spacer lengths, there is little variation in the melting point. This could be linked with the greater number of lateral

fluorine atoms and hence larger number of short contacts in the crystal phase both longitudinally and laterally.

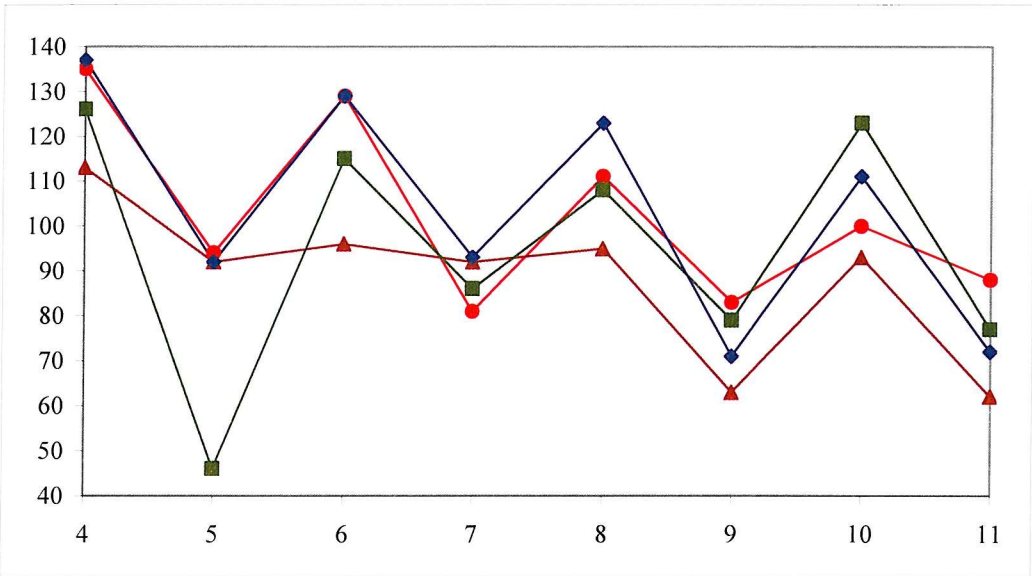

Figure 3.40 The Cr-N/Cr-I transition temperatures for the non-symmetric fluorinated liquid crystal dimers where ♦ denotes $T_{CrN/CrI}$ for $CBOnOBF_2$; ■ denotes $T_{CrN/CrI}$ for $CBOnOBF_3$; ● denotes $T_{CrN/CrI}$ for $CBOnOBFOCF_3$ and ▲ denotes $T_{CrN/CrI}$ for $CBOnOBF_4$.

Plotting the $T_{CrN/CrI}$ transitions for each series together shows a much wider variation between the series suggesting a substantially more complex system to describe. So much so that with the limited information available in terms of X-ray crystal data (1 structure in Appendix E) it would be impossible to offer any meaningful explanation as to why these materials behave as they do.

3.8.3. Comparing the mesogenicity of the different fluorinated biphenyl groups

We have already considered and made extrapolations on the T_{NI} data for the symmetric cyanobiphenyl and non-symmetric dimers to obtain theoretical N-I transitions for the symmetric fluorinated dimers. The general aim of this venture has been to establish why it would be unlikely that any of the other symmetric fluorinated dimers (other than the $F_2BOnOBF_2$ series) would show any mesogenic behaviour. However it is possible to use this information to better understand the mesogenicity of the different mesogenic end groups, ranking them accordingly.

If we take the percentage difference between the T_{NI} of CBOnOCB and each non-symmetric dimer for each of n = 7 – 9 and average, we see that, for example, the -$OBFOCF_3$ moiety has 32% smaller mesogenicity than the -OCB moiety. In this way we can generate a table of these moieties and rank them according to their percentage difference, relative to the OCB moiety (see Table 3.12) which we could use as a way to rank the groups' mesogenicity.

Moiety	% difference in mesogenicity compared to -OCB
OBF_2	26
$OBFOCF_3$	32
OBF_3	38
OBF_4	42

Table 3.12 Ranking the percentage difference in mesogenicity compared to OCB moiety, which is being used as a measure of relative mesogenicity.

Given what we know about the symmetric -$OBFOCF_3$ dimers it would be unlikely that any of the symmetric fluorinated dimers other than the -OBF_2 dimers already known would be of any practical use in mixtures as they would depress the T_{NI} by too great an amount to be observed.

3.8.4. Relating these observations to the flexoelectric properties

The mesogenicity of the mesogenic group is directly related to the thermal stability of the liquid crystal (in this case nematic) phase. By varying one mesogenic group in a series of dimers we have ranked the mesogenicity and related it to cyanobiphenyl mesogenic group. Measuring the size of $\Delta S_{NI}/R$ across the series happens to (on average) show a ranking of the mesogenic groups identical to the mesogenicity.

Theory predicts for monomers that there should be no relationship between the nematic stability and the N-I entropy of transition (which is related to the primarily the orientational but also the configurational ordering of the nematic). This has been shown to be true[17] for monomers, however as we have already seen this may not hold for dimeric systems. We have seen that the λ does not vary to any great extent with changing the mesogenic end group yet we have observed a significant difference between results

for transitional entropy and the orientational ordering. This may be explained in terms of a difference in the conformational distributional where the smaller values in the transitional entropy represent a system with more bent conformers. The more non-linear conformers there are present in the contribution, the lower the T_{NI} would become. Therefore there may be a tenuous link between the small entropy of transition and the lower T_{NI}, however, it should be noted that the decrease in $\Delta S_{NI}/R$ across the four series are considerably smaller than the difference in T_{NI}. If there are a greater number of bent conformers in the conformational distribution then we would expect this to have a positive impact on the size of the flexoelectric coefficients. It should also be noted however that the flexoelectric effect is related not only to the shape, but also couples to the dipole. The larger the dipole, the larger the expected coupling, so the number of bent conformers needs to be high, but also the dipole would have to be large (but not so large as to increase $\Delta\varepsilon$). The balance between a system which has a smaller net dipole and more bent conformers compared to one which has a larger dipole but less bent conformers has not been formally addressed in the literature and can only be properly answered by means of theoretical modelling. However, studying several structurally similar series may lead to some interesting qualitative insights on this issue.

The link between the entropy data and an increase in the number of V-shaped molecules in the conformational distribution is entirely speculatory; however it does suggest that dimers with a balance favourable shape (possibly denoted by the lower entropy) and a larger dipole in the mesogenic group should give larger flexoelectric coefficients.

3.9. Flexoelastic properties

Whilst we are interested in increasing the flexoelectric coefficients, for the purposes of the flexoelectro-optic effect and, more importantly, what is practically possible to measure with the equipment available, it is the flexoelastic ratio ($\bar{e}/\bar{K}$) which is of primary concern. This means that it is as important to minimise the elastic constant as it is to maximise the flexoelectric coefficient and for this reason we expect the best responses to be found from the odd dimers which are known to generally have smaller values of K[8] because of their lower orientational order and higher number of the bent conformers.

The flexoelastic ratios were measured using the apparatus set-up as described in Chapter 2. The materials were studied at a reduced temperature of 0.98 T_{NI}. This is to be consistent with results reported in Chapter 4 where this temperature was selected to be comparable with results in the literature. For the purposes of this Chapter there is no consistent reduced temperature for comparison as the only relevant materials for comparison are the dimers investigated by Coles *et al.*[2] which we studied at a reduced temperature too low to be reached on most of the new dimers presented here.

3.9.1. Pure systems

The flexoelastic ratios for these materials were all measured using the pure system forming a ULH by adding approximately 2 mol% of the chiral dopant R5011 supplied by Merck. The purpose of this study was to try and relate the molecular properties already considered to the flexoelastic ratio to further our understanding of how molecular structure affects the flexoelastic properties. Because of this, we have adopted the approach of studying materials in the pure system rather than using them to dope existing mixtures and extrapolating the result to the pure system. The effect of making mixtures on the flexoelastic ratio is not well understood and is sometimes assumed to simply be a weighted average of $\bar{e}/\bar{K}$ for the components. This idea is to a limited extent explored in Chapter 4, however, given the uncertainty of extrapolating what is measured in the mixture back to the pure material, it was deemed more useful to have information on the pure systems. This is particularly important as it is our aim to relate the flexoelastic properties of the pure system to the molecular structure.

One of the key problems of studying materials in the pure systems close to T_{NI} is the high temperatures which are encountered, these complicate the procedure considerably. The main problem proved to be keeping the sample stationary whilst making the measurements. This was achieved, eventually, using heat proof tape both to secure the cell and thermally insulate the solder joints. This setup generally allowed measurements to be made up to a known temperature of 230°C, however, heat loss from the sample probably created a significant thermal gradient at this temperature. The highest estimated practical temperature for this setup is 250°C, which corresponds to the threshold temperature of the adhesive holding the cell together. It is unlikely in the future that

measurements would need to be made on materials above this temperature so the methodology is thermally robust enough to be consistently used for high temperature nematics. (The importance of being able to measure materials to high temperatures is that most of the different methods of measuring $\bar{e}/\overline{K}$ are unsuitable or not designed to cope with temperatures above 100°C and so the number of practical approaches available to us was limited. This is significant since most of the materials studied here melt at temperatures over 100°C.)

3.9.2. Estimating the pitch

In the experiment, the change in the size of the tilt of the optic axis, φ, is measured as a function of increasing voltage. By plotting tan(φ) over a range of voltages (applied fields), we can determine the gradient of this change which taken from

$$\tan\varphi = \frac{\bar{e}E}{\overline{K}} \cdot \frac{P}{2\pi}, \tag{2}$$

can be rearranged to give

$$\frac{\tan\varphi}{E} = \frac{\bar{e}}{\overline{K}} \cdot \frac{P}{2\pi}, \tag{3}$$

where φ is the tilt in the optic axis from the original position (i.e. when E = 0), E is the applied field, $\overline{K}$ is the elastic constant (taken to be the average of K_1 and K_3) and $\bar{e}$ is the flexoelectric coefficient (where $\bar{e} = e_1 + e_3$).

To determine $\bar{e}/\overline{K}$ from tan(φ)/E we need to know the pitch and there were two methods for measuring the pitch; the first and more common is the Cano wedge method, [32] which involves filling a wedge cell with the chirally doped material and counting the lines created by the helical rotation in the cell. Having counted the lines for a measured distance in the cell and using the wedge angle (supplied with the cells as used at Merck) it is possible to determine the pitch. However, the practicalities of this method made making measurements on high temperature nematics prohibitively difficult. The second method uses selective reflection of light by the periodic structure of the chiral nematic. From analysis of the wavelength of the reflections the pitch (which is proportional to this wavelength) can be deduced. There were not sufficient facilities to allow these measurements to be made.

Having no direct way of measuring the pitch in the chiral nematic, the flexoelastic ratios were estimated by accounting for the unknown pitch in two different ways. The pitch is related to the quantity of the chiral dopant by the helical twisting power (HTP) by

$$P = \frac{100}{c(HTP)}, \tag{4}$$

where P is the pitch, c is the concentration (mol %), and the HTP is in nm^{-1} to give the pitch in nm (note the pitch is sometimes reported μm). From a wedge cell measurement made in Merck using very similar compounds in a low melting mixture and R5011 as the chiral dopant (used throughout this Thesis) we obtained an estimated HTP of 0.168 nm^{-1}. Using this value for the HTP and the known amount of chiral dopant used for each material, the pitch was calculated. There are several errors associated with this, the first being that it is expected that there will be different values of the helical twisting power (HTP) depending on the nature of the nematic (which will change from compound to compound) and in the case of dimers there will be different values for odd and even members. These differences arise from differences in K_2 for different mesogens and parities in dimers and from changing host-guest interactions resulting from using different hosts. The pitch is also known to change with temperature. The value of the HTP used was that measured for a novel room temperature dimer mixture made in-house by Merck. The exact constituents and proportions have not been released, however they do include odd dimers, most of which have been presented in this Chapter. This means that the estimate for the HTP is more accurate for odd dimers because K_2 will be larger than for the even dimers.

The potential for significant errors by estimating the pitch in this way is clearly quite large and less than ideal. However, the flexoelastic ratio is the most commonly quoted property for these types of materials in relation to a ULH cell and therefore this gives a reasonable means of comparison. From a pragmatic perspective, it could be argued that having the flexoelastic ratio and the pitch combined gives a good indication of the angular dependence on the field of a material which, for a device, is a very useful practical property. However, using this combination, makes comparisons between series less certain as it of course now also will be subject to inevitable changes in the pitch. In

spite of this $\bar{e}P/\overline{K}$ is reported here as well. $\bar{e}P/\overline{K}$ can be determined for published data where the pitch is often supplied with the flexoelastic ratio.

3.9.3. $CBOnOBF_2$

The measurements for $CBOnOBF_2$ are particularly important as these can be contrasted with the literature values. From this we can get an indication of how reliable the measurements are by how they compare with the literature. Another similar check is made in Chapter 4 by making measurements on neat E7 and comparing them with the literature values. For these values $\bar{e}/\overline{K}$ is quoted more confidently (since the HTP for E7 is known).

As described in Chapter 2, for each value of $\bar{e}/\overline{K}$ typically between 8 and 10 angular measurements are taken over a range of voltages (evenly spaced) and a plot of tan φ as a function of the field should give a linear relationship from which the gradient is taken.

Unwind Voltage /V	44.1	**Est. Pitch /nm**	323	**T_{NI} /°C**	111
Thickness of cell /μm	4.96	**Tan(φ)/E /Vμm^{-1}**	0.084	**T /°C**	103
Threshold Field /Vμm^{-1}	8.89	**(e/K) /CN^{-1}m^{-1}**	1.62	**T/T_{NI}**	0.98

Table 3.13 Table of data taken from the spreadsheet for $CBO11OBF_2$ showing a range of data important for determining $\bar{e}/\overline{K}$.

Tables 3.13 and 3.14 show typical data used on a spreadsheet to evaluate the flexoelastic ratio. The results in Table 3.14 are used to plot the graph in Figure 3.41. From the gradient measured from the graph the result for $\bar{e}/\overline{K}$ can be calculated by rearranging and substituting in data found in Table 3.13 into Equation 2. $\bar{e}P/\overline{K}$ can be obtained simply by not dividing by the pitch in the final calculation (see Equation 3).

Voltage	Electric field per micron	Max Angle /°	Min Angle /°	tilt angle /°	tan ϕ
4.3	0.87	368.4	358.3	5.0	0.088
8.6	1.74	371.9	353.8	9.0	0.159
12.9	2.61	376.6	349.9	13.4	0.237
17.2	3.48	380.5	347.8	16.4	0.293
21.6	4.34	384.5	343.9	20.3	0.370
25.9	5.21	388.9	341.7	23.6	0.437
30.2	6.08	391.2	337.2	27.0	0.510
34.5	6.95	389.2	330.7	29.3	0.560

Table 3.14 Table of data taken from the spreadsheet for $CBO11OBF_2$ used to construct the plot shown in Figure 3.41.

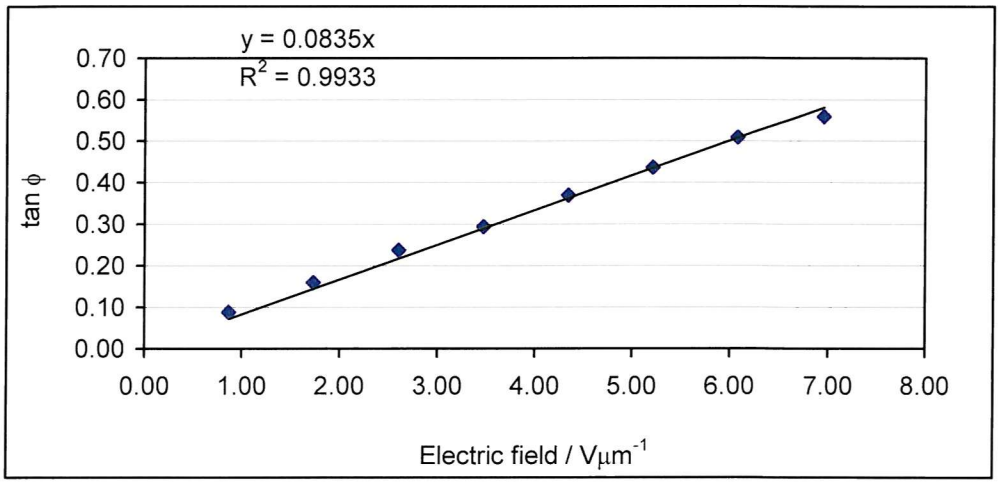

Figure 3.41 The field dependence of tan of the angle made by the optic axis for $CBO11OBF_2$.

A full set of these data sheets (the information in Tables 3.13 and 3.14 and Figure 3.41) can be found in Appendix C.

The $CBOnOBF_2$ series synthesised in-house were studied for comparison with the literature values and the results are found in Tables 3.15 and 3.16. Practical examination has shown that the flexoelastic ratio is largely independent of temperature;[4] the literature results for the flexoelastic ratio for $CBOnOBF_2$ are all taken at $0.84T_{NI}$, however, to be consistent with all the other measurements made in this Thesis, measurements on the in-house $CBOnOBF_2$ dimers were made at $0.98T_{NI}$. In the case of the literature values, it should be noted that the type of chiral dopant used (BDH1281) was different with a smaller HTP (~0.1 nm^{-1} for $CBO6OBF_2$ using 2% chiral dopant).[8]

n	(e/K) /$CN^{-1}m^{-1}$	P /μm	(eP/K) /$x10^{-7}CN^{-1}$
5	1.45	305	4.42
6	0.45	440	1.98
7	1.29	307	3.96
8	0.52	495	2.57
9	1.24	313	3.88
10	0.52	445	2.31
11	1.33	340	4.52
12	0.55	367	2.02

Table 3.15 Literature values of $\bar{e}/\bar{K}$ with the pitch[2] taken at $T^* = 0.84T_{NI}$ showing the flexoelastic ratio, the pitch and, for comparison, the scaled flexoelastic ratio $\bar{e}P/\bar{K}$.

n	(e/K) /$CN^{-1}m^{-1}$	E_{th} /$V\mu m^{-1}$	%R5011	eP/K /$x10^{-7}CN^{-1}$
7	1.44	40.0	2.0	4.31
8	0.59	30.0	1.4	2.65
9	1.37	36.0	2.1	4.02
10	1.06	30.0	2.6	2.51
11	1.62	44.1	1.9	5.25

Table 3.16 Flexoelastic data for $CBOnOBF_2$ measured in-house on in-house synthesised samples. Here n = 7 – 11 taken at $T^* = 0.98T_{NI}$; showing the flexoelastic ratio, threshold voltage, the percentage molar concentration of the chiral dopant and scaled flexoelectric ratio $\bar{e}P/\bar{K}$.

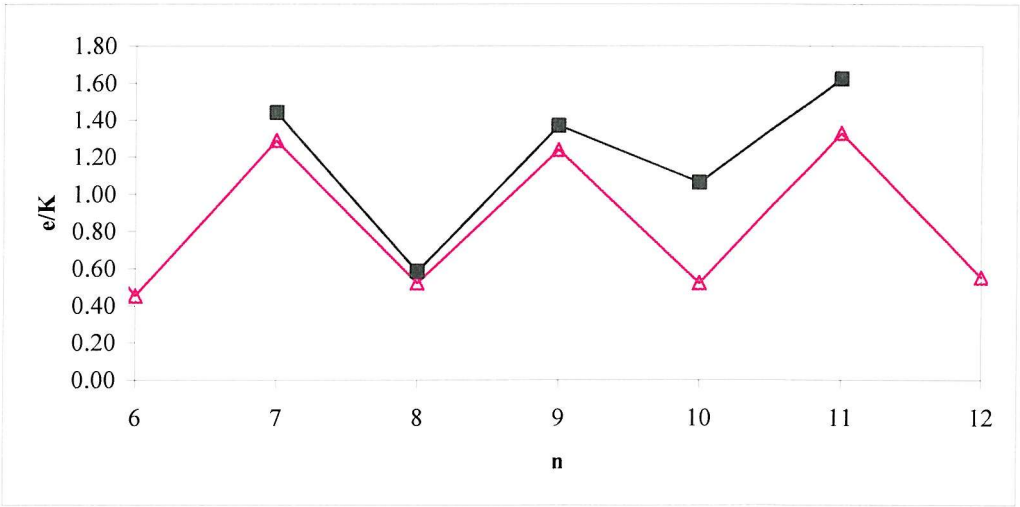

Figure 3.42 A comparison of the literature and in-house measured values for $\bar{e}/\bar{K}$ for the $CBOnOBF_2$ series taken at $T^* = 0.84T_{NI}$ and $0.98T_{NI}$ respectively. Here ■ denotes $\bar{e}/\bar{K}$ for the in-house measured series and Δ denotes $\bar{e}/\bar{K}$ derived from the literature values.

The plot of $\bar{e}/\bar{K}$ in Figure 3.42 shows that the values for this series are similar to those published[2] and that using the estimated HTP gives reasonable results albeit slightly

higher than those reported. This is surprising as the chiral dopant used in the literature measurements is known to have consistently a smaller HTP than R5011 and therefore for similar concentrations of chiral dopant (~2-5%[8]) we might expect the in-house measurements to be slightly smaller as the pitch would be smaller. However there is a distinct odd-even effect as expected with values of comparable magnitude. By plotting $\bar{e}P/\overline{K}$ for the literature and the in-house measured materials we see in Figure 3.43 that there is generally good agreement between the two sets of data. There is some deviation for n = 7 and 11 where the in-house measurements are somewhat larger.

Both series show the intuitively expected odd-even effect with reasonable agreement from n = 7 – 11. The in-house measured values were consistently slightly larger than those in the literature. From this we can have confidence in the measurements for the other series reported in this Thesis. Since the data set for the literature values is larger than that for the measured values (i.e. n = 5 – 12, (lit.) compared to the n = 7 – 11 (in-house) values) and because there is generally good agreement between them, this Thesis uses the literature values for general comparison.

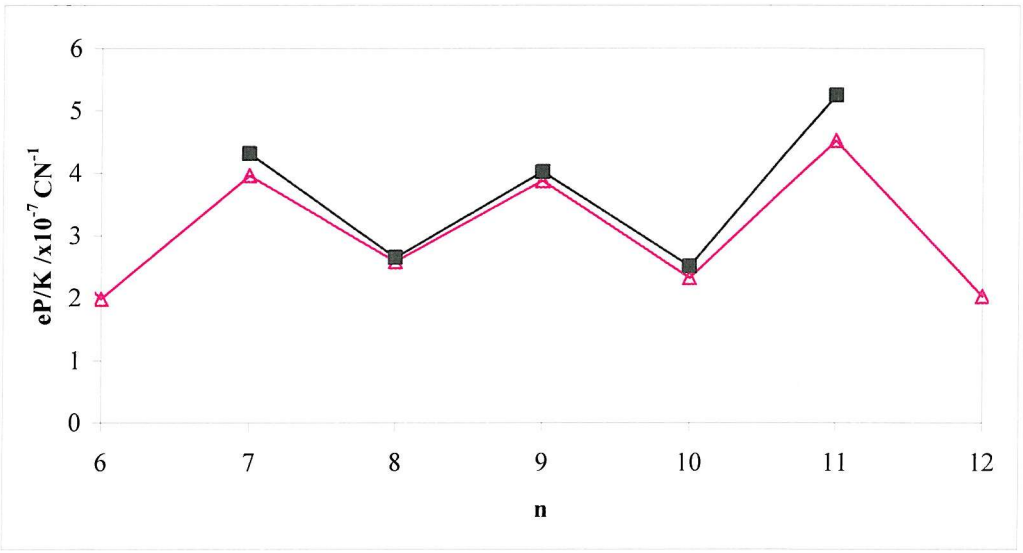

Figure 3.43 A comparison of the literature and in-house measured values for $\bar{e}P/\overline{K}$ for the CBOnOBF$_2$ series taken at $T^* = 0.84T_{NI}$ and $0.98T_{NI}$ respectively. Here ■ denotes $\bar{e}P/\overline{K}$ for the in-house measured series and Δ denotes $\bar{e}P/\overline{K}$ derived from the literature values.

Interestingly $\bar{e}P/\overline{K}$ gives a better fit to the literature data than $\bar{e}/\overline{K}$ using the estimated HTP.

3.9.4. $CBOnOBFOCF_3$

Analysis of the $CBOnOBFOCF_3$ series is particularly interesting as, out of all the non-symmetric dimers, it possesses the largest dipole along the long axis of the fluorinated mesogenic group with a slightly smaller transitional entropy than the $CBOnOBF_2$. Therefore, we may expect that with a larger dipole and possibly more bent conformers in the liquid crystal, that the flexoelectric coefficient may be larger. This leads to the expectation that $\bar{e}/\overline{K}$ should be particularly large for this series.

n	(e/K) /$CN^{-1}m^{-1}$	E_{th} /$V\mu m^{-1}$	%R5011	(eP/K) x10^{-7}/CN^{-1}
4	0.61	28	1.35	2.78
5	1.37	80	1.90	4.42
6	0.79	30	2.23	2.16
7	1.83	33	2.15	5.21
8	0.44	40	1.53	1.75
9	2.33	30	2.04	6.99
10	0.69	40	1.83	2.31
11	2.50	40	1.97	7.75

Table 3.17 Table of data for $CBOnOBFOCF_3$ where n = 4 – 11 taken at $T^* = 0.98T_{NI}$; showing the flexoelastic ratio, threshold field, the percentage molar concentration of the chiral dopant R5011 and scaled flexoelectric ratio $\bar{e}P/\overline{K}$.

As we can see from Table 3.17, the values for $\bar{e}/\overline{K}$ are extremely high, between 30 – 40% larger than those recorded for the $CBOnOBF_2$ series. A more reliable, comparison, however can be made by plotting the flexoelastic ratio for both series as a function of the spacer (see Figure 3.44).

Here we can see a typical odd-even effect in both the $CBOnOBF_2$ and $CBOnOBFOCF_3$ series. The most notable difference is how much larger the $\bar{e}/\overline{K}$ for $CBOnOBFOCF_3$ (n = 6, 7, 9 and 11) is compared to the $CBOnOBF_2$ series.

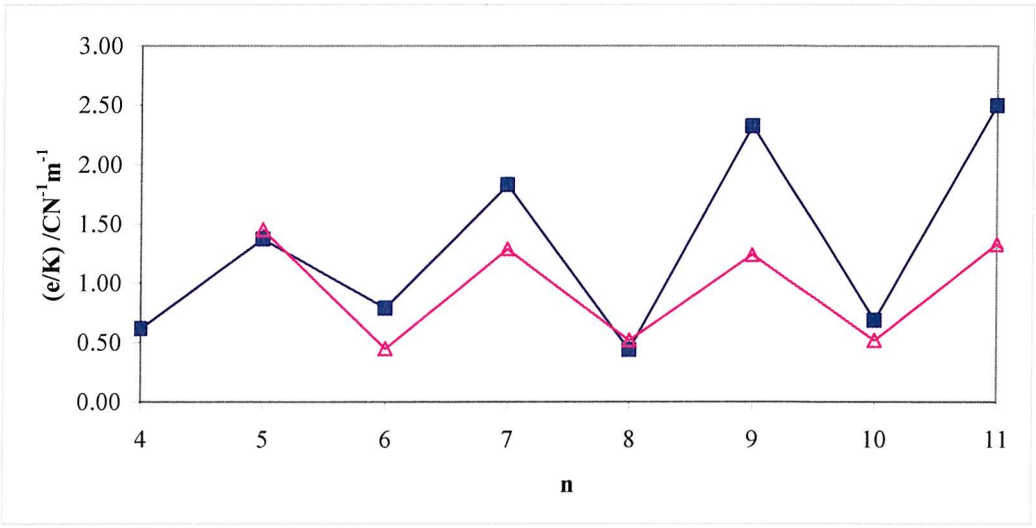

Figure 3.44 The flexoelastic ratio of $CBOnOBFOCF_3$ taken at $T^* = 0.98T_{NI}$ compared to the literature value for $CBOnOBF_2$ taken at $T^* = 0.84T_{NI}$ plotted as a function of spacer length. Here ■ denotes $\bar{e}/\overline{K}$ for $CBOnOBFOCF_3$ and Δ denotes the values for $CBOnOBF_2$.

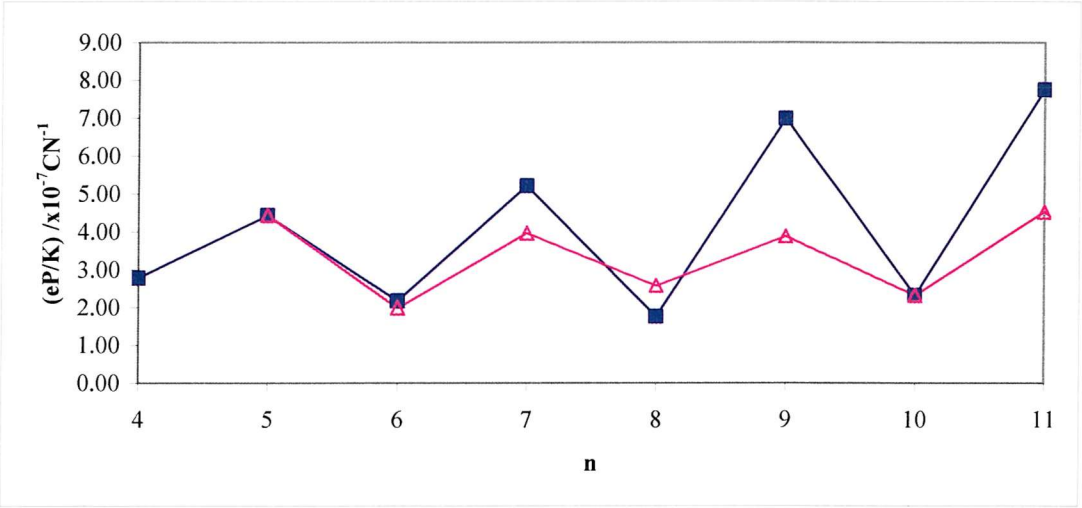

Figure 3.45 The scaled flexoelastic ratio of $CBOnOBFOCF_3$ taken at $T^* = 0.98T_{NI}$ compared to the literature value for $CBOnOBF_2$ taken at $T^* = 0.84T_{NI}$ plotted as a function of spacer length. Here ■ denotes the $\bar{e}P/\overline{K}$ for $CBOnOBFOCF_3$ and Δ denotes $\bar{e}P/\overline{K}$ for $CBOnOBF_2$.

By plotting $\bar{e}P/\overline{K}$ against spacer length (see Figure 3.45), we see that again the $CBOnOBFOCF_3$ dimers have generally larger for $\bar{e}P/\overline{K}$ (albeit by a smaller amount). From this comparison it would appear that the results for $CBOnOBFOCF_3$ (n = 9 and 11) are the largest flexoelastic ratios reported for a pure liquid crystal dimer. A qualitative

appreciation of the dipoles on the different mesogenic groups shows that the CBOnOBFOCF$_3$ dimers have a larger local dipole from the -OCF$_3$ group compared to the –F atom in the corresponding position in the CBOnOBF$_2$ series. Although the melting points are too high for these compounds to be used individually, the very large flexoelastic ratios in the odd non-symmetric dimers make them ideal additives to mixtures.

3.9.5. CBOnOBF$_3$

From the results for the CBOnOBFOCF$_3$ series we have seen that larger flexoelastic ratios were obtained in some cases than compared to the CBOnOBF$_2$ series. It was suggested that this could be attributed to the larger dipole contribution from the -OBFOCF$_3$ group. If this is true then we may also expect the -OBF$_3$ group to give large flexoelastic ratios (since the net dipole along the biphenyl for the -OBF$_3$ group is larger than for that of the -OBF$_2$ group). The data for the flexoelastic ratio and the scaled flexoelastic ratio are given in Table 3.18. Results for n = 4 and 5 were not obtained due either to monotropic behaviour or to poor alignment of the helix.

n	(e/K) /CN^{-1}m^{-1}	E_{th} /Vμm^{-1}	%R5011	(eP/K) /x10^{-7}CN^{-1}
6	0.72	5.94	1.48	2.96
7	1.30	7.92	1.61	4.94
8	1.62	3.96	2.48	4.00
9	1.66	5.94	1.76	5.77
10	0.76	7.92	1.66	2.79
11	1.58	7.92	2.26	4.27

Table 3.18 The flexoelastic data for CBOnOBF$_3$ where n = 6 – 11 taken at $T^* = 0.98T_{NI}$; showing the flexoelastic ratio, threshold field, the percentage molar concentration of the chiral dopant R5011 and scaled flexoelectric ratio $\bar{e}P/\bar{K}$.

Examination of the results shows that there is an unexpected result for n = 8 which is larger than that for n = 7 and comparable to that of n = 9. The measurement was repeated with a similar result obtained which is curious but can be rationalised by considering the influence of the threshold field. We can see that E_{th} is clearly lower for n = 8 compared to n = 7 and 9 suggesting that the pitch of the helix is significantly less for n = 8 which would give rise to larger $\bar{e}/\bar{K}$ results. We can compare the results for CBOnOBF$_3$ with those for the literature values for CBOnOBF$_2$ in Figure 3.46.

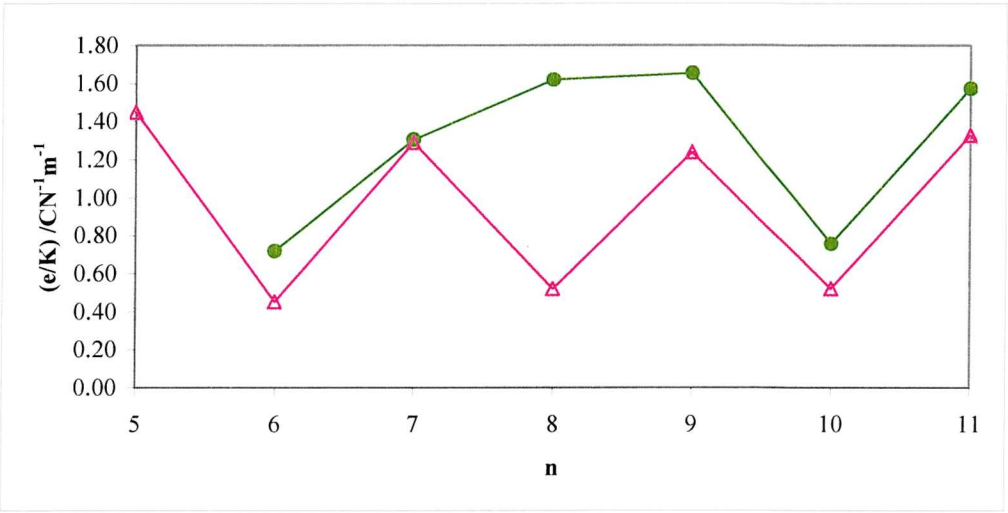

Figure 3.46 The flexoelastic ratio of $CBOnOBF_3$ taken at $T^* = 0.98T_{NI}$ compared to the literature value for $CBOnOBF_2$ taken at $T^* = 0.84T_{NI}$ plotted as a function of spacer length. Here • denotes $\bar{e}/\overline{K}$ for $CBOnOBF_3$ and Δ denotes $\bar{e}/\overline{K}$ for $CBOnOBF_2$.

Examining the data in Figure 3.46 we note two interesting features. The first is the apparent interruption in the odd-even effect by the abnormally high result for n = 8 which is likely to be due to K_2 being larger for this dimer resulting in the pitch being large. The other is that a number of the results are larger than that of the $CBOnOBF_2$ series.

Using the scaled flexoelastic ratio in Figure 3.47 we can see that the n = 8 result fits the trend of the rest of the series which is a continuous odd-even alternation. Significantly we note that for all the members of the series (except n = 11) $\bar{e}P/\overline{K}$ is larger than for the $CBOnOBF_3$ than the $CBOnOBF_2$ series. These materials have slightly lower melting points than the $CBOnOBFOCF_3$ series which is likely to improve their solubility. It should be noted that the even dimers (n = 6 and 8 in particular) have a larger $\bar{e}P/\overline{K}$ compared to both the corresponding $CBOnOBF_2$ and $CBOnOBOCF_3$ series. As additives to a mixture, these compounds would provide components with higher T_{NI} but also with an $\bar{e}P/\overline{K}$ comparable to the odd members of the $CBOnOBF_2$ series (e.g. taking $CBO8OBF_3$, T_{NI} = 120 °C and $\bar{e}P/\overline{K} = 4.0 \times 10^{-7}$ CN^{-1} compared with $CBO9OBF_2$, T_{NI} = 111 °C, $\bar{e}P/\overline{K} = 3.8 \times 10^{-7}$ CN^{-1} [lit] and $\bar{e}P/\overline{K} = 4.0 \times 10^{-7}$ CN^{-1} [measured]).

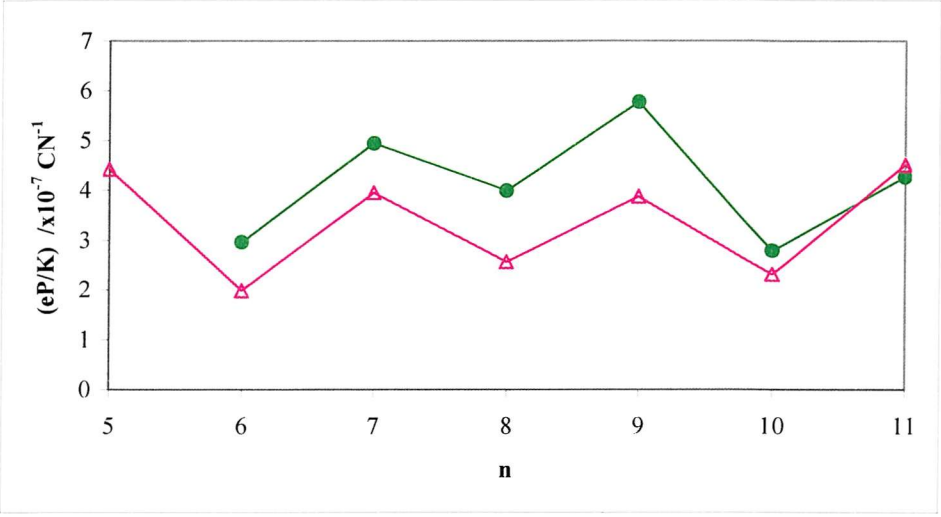

Figure 3.47 The scaled flexoelastic ratio of $CBOnOBF_3$ taken at $T^* = 0.98T_{NI}$ compared to the literature value for $CBOnOBF_2$ taken at $T^* = 0.84T_{NI}$ plotted as a function of spacer length. Here • denotes $\bar{e}P/\bar{K}$ for $CBOnOBF_3$ and Δ denotes $\bar{e}P/\bar{K}$ for $CBOnOBF_2$.

We may wish to briefly consider why n = 8 is large for $\bar{e}/\bar{K}$ and smaller for $\bar{e}P/\bar{K}$. Taking the relationship between the pitch and K_2 we see in Equation 5 that

$$P = \frac{1}{E_{th}}\sqrt{\frac{K_2}{\varepsilon_0 \Delta\varepsilon}}, \tag{5}$$

where K_2 is the twist elastic constant and $\Delta\varepsilon$ is the dielectric anisotropy. If we re-write the pitch in terms of the HTP and concentration of chiral dopant, c, we see that

$$\left(\frac{E_{th}}{c(HTP)}\right)^2 = \frac{K_2}{\varepsilon_0 \Delta\varepsilon}, \tag{6}$$

from which we quickly see that the HTP has an inverse squared relationship with K_2. This means that a moderate increase in K_2 would create a larger and significant decrease in the HTP. This means that for n = 8, should K_2 be large, the HTP for R5011 for $CBO8OBF_3$ will be much smaller than 0.163 nm^{-1}. However, the plot of $\bar{e}P/\bar{K}$ does not include the estimate of the HTP and thus the result for the scaled flexoelastic ratio for $CBO8OBF_3$ behaves as expected giving an odd-even alternation.

3.9.6. $CBOnOBF_4$

The encouraging results from the previous series lead us to consider the $CBOnOBF_4$ series. The $-OBF_4$ mesogenic group could be structurally considered like a combination

of the -OBF_2 and -OBF_3 and we have already noted with regard to the nematic stability the similarity in behaviour between the $CBOnOBF_3$ and $CBOnOBF_4$ series.

n	(e/K) /$CN^{-1}m^{-1}$	E_{th} /$V\mu m^{-1}$	mol% R5011	(eP/K) /$x10^{-7}$ CN^{-1}
4	0.93	8.08	2.12	2.70
5	Not measured	Not measured	Not measured	Not measured
6	1.26	16.10	2.05	3.76
7	2.36	10.08	2.62	5.52
8	1.28	16.16	2.44	3.21
9	1.51	20.16	1.88	4.91
10	0.89	16.10	2.12	2.56
11	1.75	8.51	3.11	3.44

Table 3.19 The flexoelastic data for $CBOnOBF_4$ where n = 4 – 11 taken at $T^* = 0.98T_{NI}$; showing the flexoelastic ratio, threshold field, the percentage molar concentration of the chiral dopant R5011 and scaled flexoelectric ratio $\bar{e}P/\bar{K}$.

Considering the data in Table 3.19 we can that again the ratios for the even dimers are larger than for the corresponding examples seen in the $CBOnOBFOCF_3$ and $CBOnOBF_2$ series. As expected from the other physical data analysed, the $CBOnOBF_3$ and $CBOnOBF_4$ series behave in a very similar fashion. Looking at both $\bar{e}/\bar{K}$ in Figure 3.48 we see that the generally all the values for $CBOnOBF_4$ are larger than that of $CBOnOBF_2$.

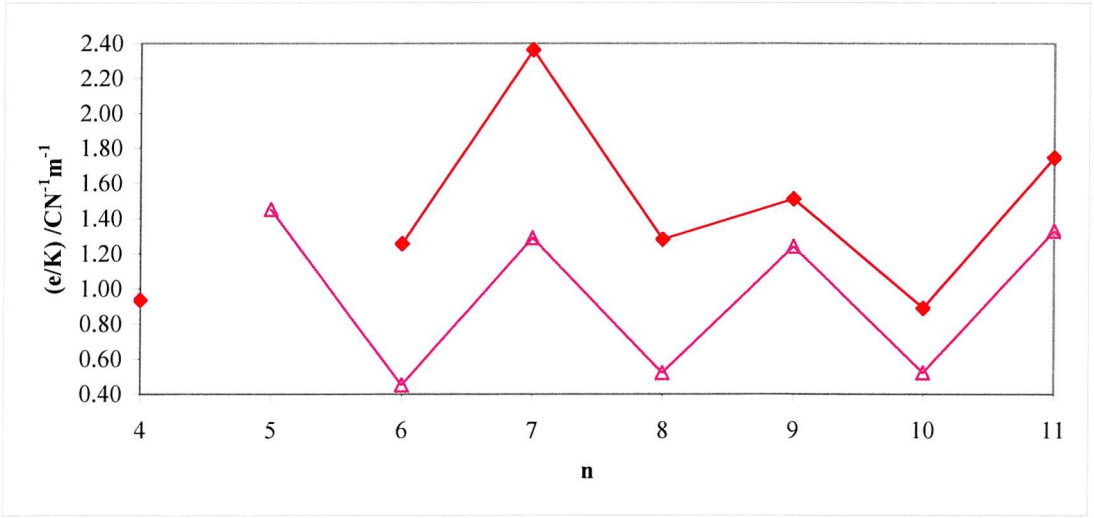

Figure 3.48 The flexoelastic ratio for $CBOnOBF_4$ taken at $T^* = 0.98T_{NI}$ compared to the literature value for $CBOnOBF_2$ taken at $T^* = 0.84T_{NI}$ plotted as a function of spacer length. Here ♦ denotes the $\bar{e}/\bar{K}$ for $CBOnOBF_4$ and Δ denotes that for $CBOnOBF_2$.

This seems reasonable since we know intuitively there is a larger net dipole along the -OBF_4 group than across -OBF_2. However given the result for CBO8OBF_3 we should also examine the scaled flexoelastic ratio in Figure 3.49.

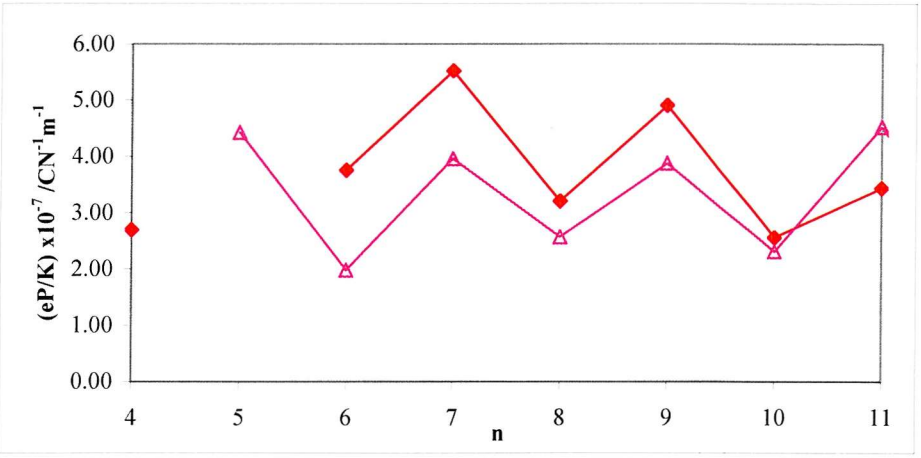

Figure 3.49 The scaled flexoelastic ratio for CBOnOBF_4 taken at $T^* = 0.98T_{NI}$ compared to the literature value for CBOnOBF_2 taken at $T^* = 0.84T_{NI}$ plotted as a function of spacer length. Here ♦ denotes the $\bar{e}P/\bar{K}$ for CBOnOBF_4 and Δ denotes that for CBOnOBF_2.

Here we see that the CBOnOBF_4 series generally has larger $\bar{e}P/\bar{K}$ values then the CBOnOBF_2 series. $\bar{e}P/\bar{K}$ for CBOnOBF_4 decreases with increasing n. With the exception of n = 11, the CBOnOBF_4 series has a larger $\bar{e}P/\bar{K}$ than the CBOnOBF_2 dimers across the series which is encouraging since the CBOnOBF_4 series tend to have significantly lower melting meaning the solubility is likely to be better than the other non-symmetric dimer series. Once again as we saw for the CBOnOBF_3 series, the even dimers (in particular n = 6 and 8 of this series) are of comparable value to the $\bar{e}/\bar{K}$ for n = 7 and 9 which is of value to increase the nematic stability in a mixture.

Comparing the variation in $\bar{e}P/\bar{K}$ for the CBOnOBFOCF_3 and CBOnOBF_4 series we can see that in the case of the odd parity dimers the CBOnOBFOCF_3 series are the largest, as expected, with considerably higher values of $\bar{e}P/\bar{K}$ for n = 9 and 11 but a comparable value for n = 7.

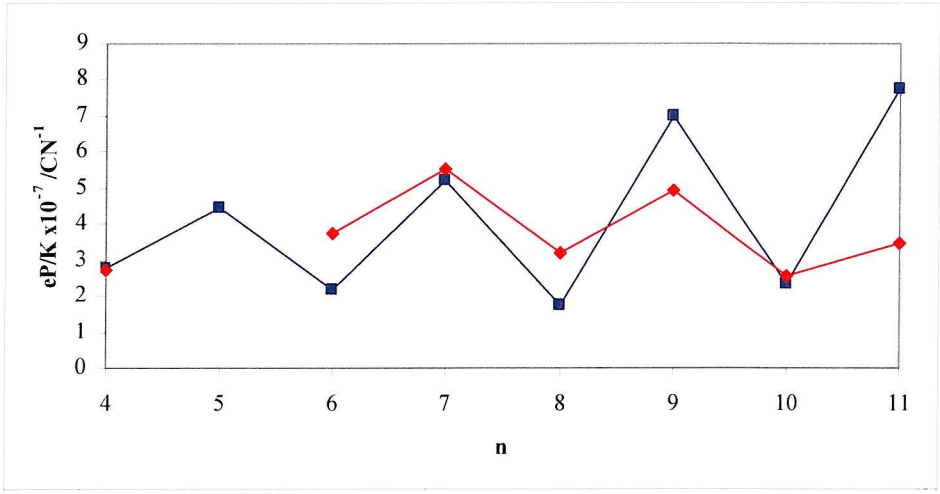

Figure 3.50 The scaled flexoelastic ratio of $CBOnOBF_4$ taken at $T^* = 0.98T_{NI}$ compared to the literature value for $CBOnOBFOCF_3$ taken at $T^* = 0.98T_{NI}$ plotted as a function of spacer length. Here ♦ denotes the $\bar{e}P/\overline{K}$ for $CBOnOBF_4$ and ■ denotes $\bar{e}P/\overline{K}$ for $CBOnOBFOCF_3$.

Significantly just as with the $CBOnOBF_3$ series, the value of $\bar{e}P/\overline{K}$ for the even dimers (particularly n = 6 and 8) is larger than the $CBOnOBFOCF_3$ series. As we noted for the $CBOnOBF_2$ series this is significant as it is these materials which have higher N-I transitions and will therefore tend to increase the nematic stability in a mixture.

We have seen that the $CBOnOBF_4$ series has by comparison behaved similarly to the $CBOnOBF_3$ dimers so it would be prudent to look at how these two series compare. This is done in Figure 3.50 and we can see that the series do behave in a very similar manner. Generally we can note in Figure 3.51 that the $CBOnOBF_3$ series has a larger $\bar{e}P/\overline{K}$ than for the $CBOnOBF_4$ series (particularly for n = 9 and 11) which is perhaps unexpected as the local dipole across the biphenyl is smaller for the $-OBF_3$ moiety than for the $-OBF_4$ moiety. Significantly $CBO6OBF_4$ has a larger $\bar{e}P/\overline{K}$ making it the largest even parity flexoelastic dimer out of the four series with a reasonably low T_{NI} of 120 °C.

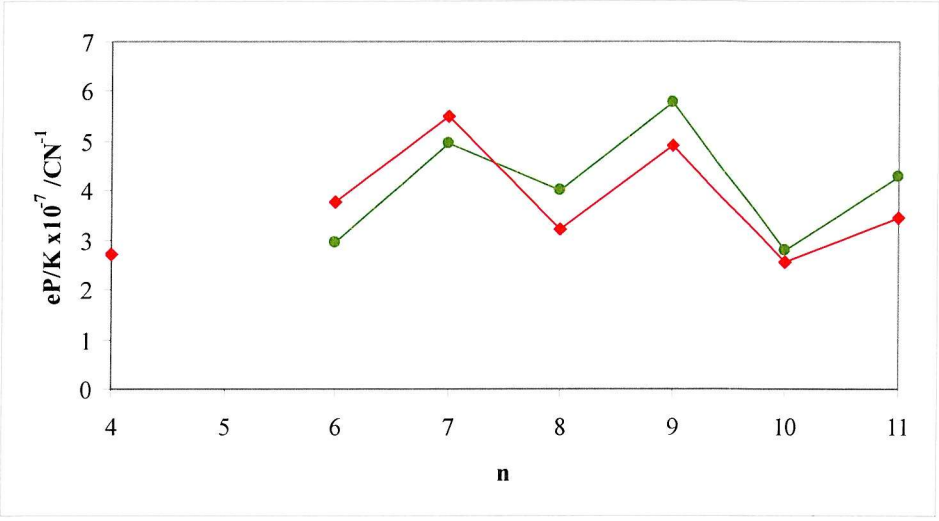

Figure 3.51 The scaled flexoelastic ratio of $CBOnOBF_3$ taken at $T^* = 0.98T_{NI}$ compared to the literature value for $CBOnOBF_2$ taken at $T^* = 0.84T_{NI}$ plotted as a function of spacer length. Here ♦ denotes the $\overline{e}P / \overline{K}$ for $CBOnOBF_4$ and ● denotes those for $CBOnOBF_3$.

3.10. Conclusions

The three novel dimer series which are presented in this Chapter show a wide variety of behaviour whilst maintaining similarities across the series, most notably an odd-even trend in the transition temperatures, transitional entropies and flexoelastic properties. All of the materials are relatively low melting although none form room temperature nematics. As such it is necessary to appreciate the properties of these compounds in the context of using them as potential components in mixtures which is necessary to lower the melting point.

There are many properties which need to be optimised when making or adding to a mixture for use in a flexoelectric device. Three of the most important properties are the nematic range, the solubility of the components and the flexoelastic ratio. One way of increasing the nematic range is by increasing the nematic stability, that is T_{NI}, which can by done by choosing components which themselves have a large T_{NI} with respect to the host. Solubility of the additives in the host is important and this can be approximately correlated to using components with low melting points. Finally, the flexoelastic ratio needs to be as large as possible which is thought to be achieved by using materials which themselves have large flexoelastic ratios.

The compounds discussed in this Chapter include candidates which could contribute to each of these different properties. The $CBOnOBF_2$ series as published by Coles *et al.* clearly have been successful as they have been demonstrated to be have good nematic stability, large flexoelastic ratios and can be mixed to produce low melting solids through the use of eutectic mixtures which can be used in working devices.[33]

However, we have shown in this Chapter three new series which indicate that there are materials possessing properties which, in come cases, are an improvement on those seen in the $CBOnOBF_2$ series. The first half of the Chapter compares, in detail, the transition temperatures of the four series and we see that the $CBOnOBF_4$ series include very much lower melting materials whereas the $CBOnOBFOCF_3$ series include materials with high N-I transition temperatures and reasonable nematic ranges. Using a range of different compounds from this library of materials we could, therefore, construct a room temperature mixture with a large nematic range and this has been achieved.[13] With this in mind it is therefore of considerable interest to find compounds which could be used as additives to increase the flexoelastic properties of these materials. The best way of doing this might be to overlay $\bar{e}P/\overline{K}$ for each series over each other (see Figure 3.52) and finding which compounds have the highest $\bar{e}P/\overline{K}$ for a given spacer length.

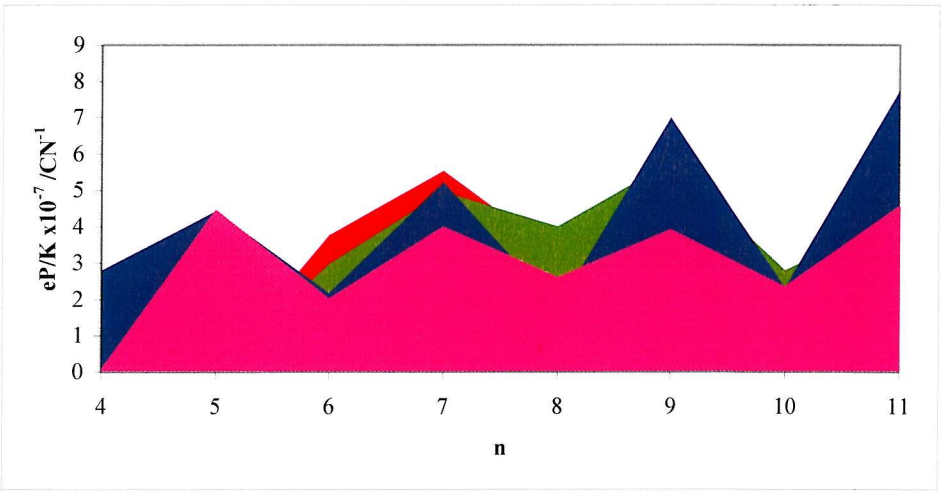

Figure 3.52 Overlay of $\bar{e}P/\overline{K}$ for each of the four liquid crystal dimer series considered in this Chapter. Here ■ denotes $\bar{e}P/\overline{K}$ for $CBOnOBF_2$; ■ denotes $\bar{e}P/\overline{K}$ for $CBOnOBFOCF_3$; ■ denotes $\bar{e}P/\overline{K}$ for $CBOnOBF_3$; ■ denotes $\bar{e}P/\overline{K}$ for $CBOnOBF_4$.

Interestingly we see that there are materials in each of the three novel series which have a similar or considerably larger value of $\bar{e}P/\overline{K}$. Significantly, there are potentially useful even parity dimers (e.g. CBO6OBF$_4$ and CBO8OBF$_3$) which are useful as they would increase the nematic range by increasing T_{NI} for the mixture without reducing the flexoelastic properties of the mixture. Clearly of greatest interest are the odd members of the CBOnOBFOCF$_3$ series particularly n = 9 and 11 as these give the largest values of $\bar{e}P/\overline{K}$ and also have reasonably high N – I transitions.

Overall, these series offer a wide variety of properties which are likely to be best accessed by using them as components of a liquid crystal mixture. This wide range of compounds and their properties paves the way for a well targeted investigation into a number of possible mixtures which would optimise the assets of various potential components from this small library of materials presented here.

3.11. References

1. G. E. Durand, Personal Communication, 10th ILLC, to G. R. Luckhurst, 1984.
2. S. M. Morris, M. J. Clarke, A. E. Blatch, H. J. Coles, *Phys. Rev. E*, **2007**, 75, 041701.
3. J. H. Wild, K. Bartle, N. T. Kirkman, S. Kelly, M. O'Neill, T. Stirner, T. P. Tuffin, *Chem. Mater.*, **2005**, 17, 6354.
4. H. J. Coles, B. Musgrave, M. J. Coles, J. Willmott,, *J. Chem. Mater.*, **2001**, 11, 2709.
5. B. Musgrave, P. Lehmann, H. J. Coles, *Liq. Cryst.*, **1999**, 26, 1235.
6. M. J. Clarke, A. E. Blatch, H. J. Coles, *Mol. Cryst. Liq. Cryst.*, **2005**, 434, 367.
7. Conference meeting, Flexoelectricity in Liquid Crystals. Oxford University: 2006.
8. M. J. Clarke. Ph.D. Thesis. University of Southampton, 2004.
9. J. S. Patel, R. B. Meyer, *Phys. Rev. Lett.*, **1987**, 58, 1538.
10. J. Harden, B. Mbanga, N. Eber, K. Fodor-Csorba, S. Sprunt, J. T. Gleeson, A. Jakli, *Phys. Rev. Lett.*, **2006**, 97, 157802.
11. L. M. Blinkov, L. A. Beresnev, S. A. Davydyan, S. G. Kononov, S. V. Yablonski, *Ferroelectrics (UK)*, **1988**, 84, 365.

12. P. R. Mahesware Murthy, V. A. Ragunathan, N. V. Madhusudana, *Liq. Cryst.*, **1993**, 14, 483.
13. Data available on the Merck internal Database.
14. G.W. Gray, *The Molecular Physics of Liquid Crystals*. Academic Press. Ed. G. W. Gray, G. R. Luckhurst 1979.
15. J. V. Crivello, M. Deptolla, H. Ringsdorf, *Liq. Cryst.*, **1988**, 3, 235.
16. C. J. R. Council, J. W. Emsley, N. J. Heaton, G. R. Luckhurst,, *Mol. Phys.*, **1985**, 54, 847.
17. G. R. Luckhurst, *Mol. Phys.*, **1994**, 82, 1063.
18. S. Marcelja, *J. Chem. Phys.*, **1974**, 60, 3599.
19. J. W. Emsley, G. R. Luckhurst, G. N. Shilstone, I. Sage, *Mol. Cryst. Liq. Cryst.*, **1984**, 102, 223.
20. G. S. Attard, R. W. Date, C. T. Imrie, G. R. Luckhurst, S. J. Roskilly, J. M.; Seddon, L. Taylor, *Liq. Cryst.*, **1994**, 16, 529.
21. W. Maier, A. Saupe, *Z. Naturforsch. A*, **1958**, 13, 564.
22. W. Maier, A. S., *Z. Naturforsch. A*, **1959**, 14, 882.
23. W. Maier, A. S., *Z. Naturforsch. A*, **1960**, 15, 287.
24. G. R. Luckhurst, C. Zannoni, P. L. Nordio, U. Segre, *Mol. Phys.*, **1975**, 30, 1345.
25. A. E. Blatch, M. J. Coles, B. Musgrave, H. J. Coles, *Mol. Cryst. Liq. Cryst.*, **2003**, 401, 47.
26. P. J. Barnes. Ph.D. Thesis. University of Southampton, 1994.
27. J. W. Emsley, G. R. Luckhurst, G. N. Shilstone, R. Hashim, *Liq. Cryst.*, **1986**, 1, 437.
28. E. M. Barrall II, J. F. Johnson, *Thermal Properties of Liquid Crystals*. Ed. G.W. Gray, P. A. Windsor 1974; p 254.
29. C. T. Imrie. Ph.D. Thesis. University of Southampton, 1988.
30. Molecular Mechanics minimisation from which the net dipole is calculated.
31. R. L. Humphries, P. G. James, G. R. Luckhurst, *Symp. Faraday. Soc*, **1971**, 5, 107.
32. G. Heppke, F. Oestreicher,, *Mol. Cryst. Liq. Cryst.*, **1978**, 41, 245.
33. H. J. Coles, 20th ILCC, Ljubliana, 2004.

Chapter 4

Non-symmetric conventional dimers using a phenyl cyclohexyl moiety

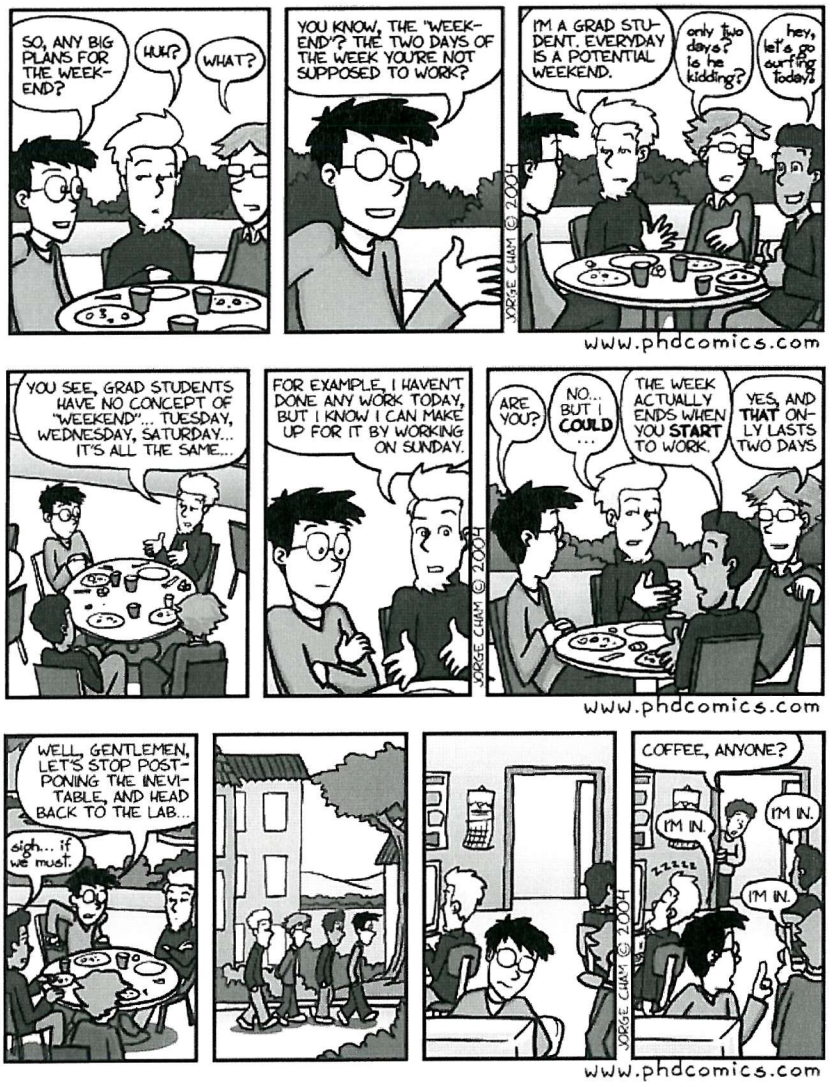

"Piled Higher and Deeper" by Jorge Cham
www.phdcomics.com

Used with permission

4. Non-symmetric conventional dimers using a phenyl cyclohexyl moiety

4.1. Background

One of the advantages of researching in a field for an extended period of time, even as short as three years, is a chance to see interest and opinion in the field change and shift as different questions compete for prominence in the minds of the scientific community who seek to answer them. In terms of the flexoelectric effect, one of the key questions in the years preceeding and immediately after the turn of the millenium was 'how?'. More specifically, how best to exploit flexoelectric coupling to gain the best use in devices through, amongst other avenues, molecular design. As time has progressed and ideas have had time to be assimilated properly by the community, the key questions now being asked are, 'why?' and 'which?'. More specifically, why do the difluorobiphenyl dimers investigated by Coles *et al.*[1] or the V-shaped esters reported by Harden *et al.*[2] produce such a large effect and which contribution to the flexoelectric effect is more dominant, the quadrupolar contribution, or the shape/dipolar contribution.[3] Clearly the aim of these questions is to gain a better understanding of flexoelectricity to be able to design materials which exhibit a larger flexoelectric effect. So the old questions have not gone away, they are just being approached from a different angle – as is the way when scientists are confounded.

This section seeks to comment briefly on which effect is more significant using both modelling and practical examples to address the question. This leads to a short but significant investigation into a potentially interesting set of non-symmetric dimers based on moieties which, according to literature reports, appear to be exceptions to the current understanding.

4.1.1. The practical evidence

Following from Durand,[4] it is currently accepted that liquid crystal dimers are one of the best design motifs for making materials which have large flexoelastic ratios.[5] The work of Coles *et al* has demonstrated that the choice of mesogenic groups used in the dimers is also crucial for developing low melting, fast switching materials with large flexoelectric coefficients.[5-7] The consensus of opinion in the community is that the shape and the

dipolar contribution from the charge distribution are largely responsible for this.[3] As we have commented previously, both odd and even dimers occupy a variety of different conformers. Although the shape and quantity of the conformers depends on the orientational order, many of them are non-linear and a significant proportion are assumed to adopt shapes which are symmetrically similar to the director deformation associated with either e_1 (splay) or e_3 (bend). In the case of the even dimers the number of non-linear conformers has been estimated to be about half of the total number of conformers and in the case of the odd dimers the figure is closer to 90%. We know that if the shape/dipolar contribution is dominant it would be expected that the non-linear conformers would be most likely to contribute to large flexoelectric coefficients. If we take the Prost and Marcerou[8] quadrupolar model, then, as already discussed in Chapter 2, for the quadrupole moment to be large the charge and charge separation must also be large. In the case of dimers this should mean having charges at the extremities of each mesogenic group and the molecule as linear as possible although, as we shall see later, it turns out that understanding how the molecular architecture impacts on the quadrupole and how that feeds into the flexeoelectric coefficient is not so intuitive as the shape/dipole mechanism. To make matters worse, the ordering in the system is also crucial to the flexoelectric coeffients. This can be most simply understood by examining the flexoelastic ratio $\bar{e}/\overline{K}$ (see Equations 1 and 2) which is invarient with the temperature[5] and hence the order parameter and appreciating that we know $\overline{K}$ does vary as the order changes so therefore $\bar{e}$ must show similar properties. How the order affects each individual flexoelectric coefficient is non-trivial and not well understood. Studies made by Clarke,[9] on the symmetric dimer and non-symmetric diflurobiphenyl/cyanobiphenyl dimer series show that there is an odd-even effect in the flexoelastic constants.[1, 9] When these values are multiplied by the average elastic constant $\overline{K}$ to give $\bar{e}$ where,

$$\bar{e} = (e_1 + e_3)/2 \tag{1}$$

and

$$\overline{K} = (K_1 + K_3)/2 \tag{2}$$

these also show an odd-even effect where the odd dimers have a larger value of $\bar{e}$ than the even dimers (see Figure 4.1[9]).

This would suggest that the more dominant mechanism is the shape and dipole. In fact if the percentage difference between values of $\bar{e}$ in odd and even dimers is obtained and the mean is taken across the series we see that on average the difference is exactly 40% which closely relates to the approximate difference in the probability of linear and bent conformers in odd and even dimers.

Although more qualitative than quantitative this evidence appears quite compelling. However, it was noted by Goodby,[10] that there are very few studied examples from which we can draw these conclusions and there really is not enough evidence to be certain.

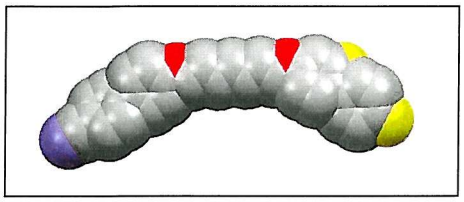

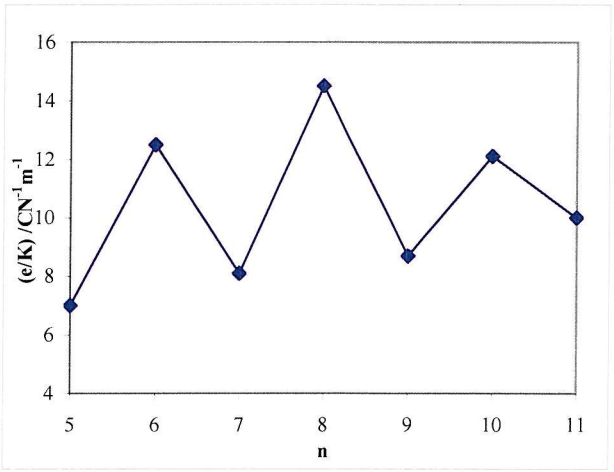

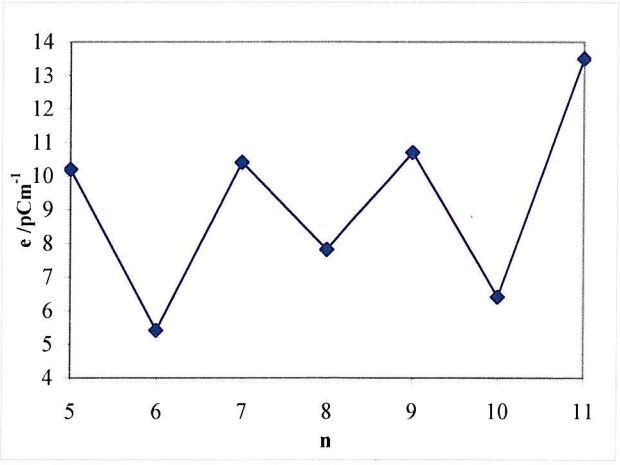

Figure 4.1 (top left) space filling model of $CBOnOBF_2$. (top right) flexoelastic constants ($\bar{e}/\bar{K}$) for $CBOnOBF_2$ plotted against the number of carbons in the spacer. (bottom right) average of the flexoelectric coefficients (e) for $CBOnOBF_2$ plotted against the number of carbon atoms in the spacer.

This assertation is probably true and with the pool of studied materials not likely to increase very rapidly in the near future it would be prudent to search for another, more theoretical, way of probing the dipolar and quadrupolar effect in the dimers.

4.1.2. The theoretical evidence

In her papers,[11, 12] Ferrarini outlines a model based on a combination of molecular field theory and elastic continuum theory to calculate the flexoelectric coefficients for a given molecular structure. The model was originally designed for rigid molecules and Ferrarini gives examples for real materials which have known flexoelectric coefficients and demonstrates that the predictions of the model are in good agreement with experimental data.[11] The key difference in Ferrarini's work was that she calculated the flexoelectric coefficients for splay and bend separately *including* contributions from both the quadrupole and the dipole. This provides a unique tool by which to probe how changing the molecular structure affects the size of the different contributions to the flexoelectric properties of the molecule.

Trying to extend this model to calculate flexoelectric coefficients for dimeric materials is more complicated compared to calculating the coefficients for the comparitively inflexible molecules Ferrarini describes in her paper.[11] Therefore, as a preliminary investigation to this work, it was suggested by Luckhurst[13] that a simple 'toy' model could be constructed to better understand how this effect altered with changing the angle θ between the mesogenic arms as shown in Figure 4.2.

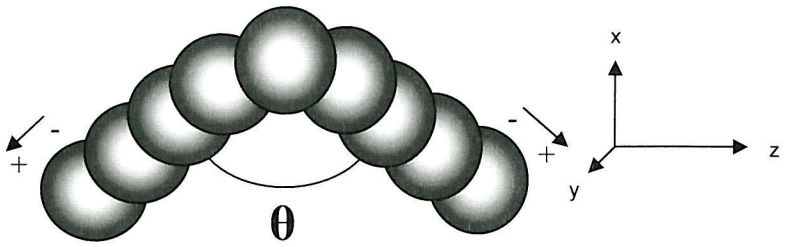

Figure 4.2 Sketch of the toy model consisting of 9 atoms with a dipole at each end of magnitude corresponding to that of a cyanobiphenyl group. The internal angle θ is varied through from 90° to 180°.

This idea had two aims. The first was to explore where the optimum angle to gain the largest flexoelectric coefficient would be in a simple system. The second was to try and explore different bent conformations in the model to see which conformers contributed most to the flexoelectric effect and where the contribution was coming from (either dipolar as expected or quadrupolar). The principle was to generate the same dipole as found on a cyanobiphenyl dimer by placing charges equivalent to a cyano group

separated by the C-N bond length, then to change the angle at centre of the V. The change in conformation is directly related to the internal angle, θ, and so the size of the flexoelectric coefficient could be plotted directly against this angle.

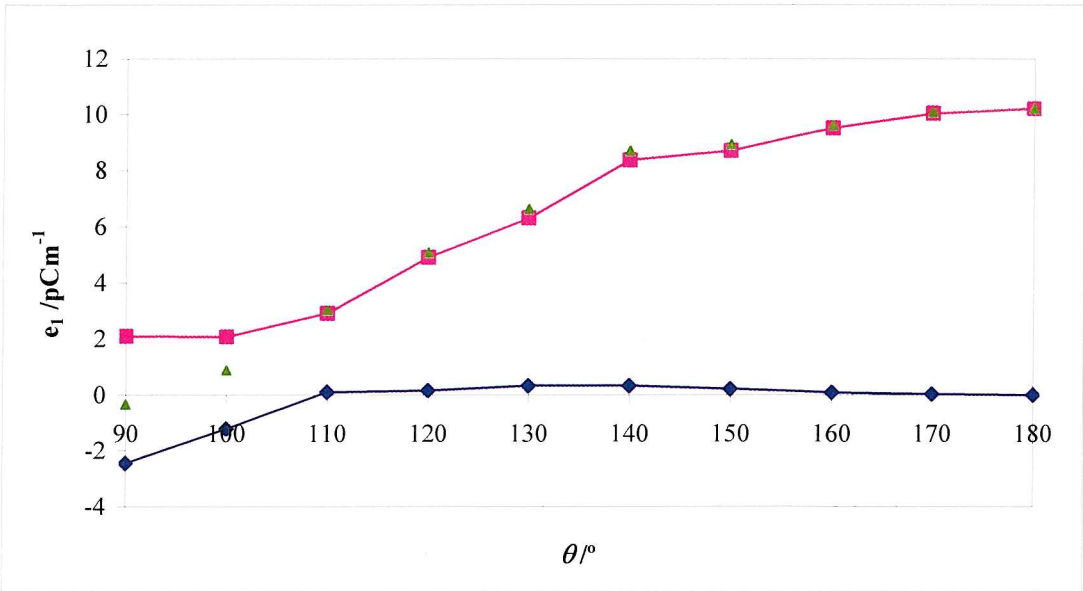

Figure 4.3 Quadrupolar (e_1^q) and dipolar (e_1^d) contributions to the splay flexoelectric coefficient.[14] ■ e_1 quadrupole, ◆ e_1 dipole, ▲ e_1 total (results calculated by Ferrarini).

The first and most important point to note is that the magnitude of the flexoelectric coefficients calculated are the of order of those observed in physical measurements.[1, 15] This is encouraging as it shows that even this simplistic model is giving results of a realistic magnitude. If we were to consider wedge shaped molecules being more likely to respond to a splay in the director and boomerang shaped molecules being more likely to respond to a bend in the director, we could regard the toy model as moving from a linear structure where $\theta = 0°$ and the atoms are effectively overlapping to a wedge shaped structure where the $\theta < 90°$ and some atoms are partially overlapping, through to a more banana shaped structure where $\theta > 90°$ and there is no overlap to where the structure is linear where $\theta = 180°$. To avoid situations where atoms could overlap, only the range $90° \leq \theta \leq 180°$ is considered. Given the shape of the model is more banana shaped, we might expect the splay contribution from the dipole to be minimal and, where $\theta > 110°$, this is the case (see Figure 4.3). Where $\theta < 110°$ the dipolar contribution becomes larger and more negative as the molecule becomes more wedge shaped. The sign of the flexoelectric

coefficient is only important in comparison with the other contributions but, in the case of this model, has no absolute significance. The quadrupolar contribution grows as the molecule becomes more linear which, although counter intuitive to how we understand the flexoelectric effect, is consistent with how we understand the maximisation of the quadrupole moment and will also increase the order. The surprise is how much larger the magnitude of the quadrupolar contribution is. By comparison with the dipolar contribution it dominates for most of the angular range considered. This has two serious implications, the first being that the current understanding of the flexoelectric effect considers chiefly the shape and dipole contribution yet this would appear not to be the dominant contribution. Secondly, it reaches a maximum when the molecule is linear which is counter intuitive to the original symmetry argument presented in Meyer's first paper[16] but predicted in the paper by Prost and Marcerou.[8] The conclusion reached on examining the splay flexoelectric effect is that for large angles the dipolar contribution is very small but positive and larger and negative at smaller angles where the molecular shape more closely resembles a wedge shape. The quadrupolar contribution is comparatively much larger and reaches its largest value for this range of θ when the molecule is linear. As θ gets closer to 90° the dipolar contribution dominates but it is much smaller than in the case where the quadrupole dominates. Also the change in sign of e_1^d below 110° means that the quadrupolar and dipolar contributions are competitive.

Examining the bend flexoelectric coefficient, we might expect there to be a much larger contribution from the shape/dipole and perhaps some kind of optimum angle. The results given in Figure 4.4 show that the dipolar contribution is larger compared to the respective splay flexoelectric coefficient, an intuitive result as the shape of the molecule will respond to a bend in the director much more easily. More unexpected is that there is no apparent maximum contribution corresponding to an optimum angle. The contribution is almost constant from $90° \leq \theta \leq 140°$ with the result steadily reducing to 0 where $\theta >$ 140°. This could be due to the orientational order being in competition with the effect of the molecular shape; the ordering gets larger as the molecule becomes more linear yet the molecular shape deviating away from the optimum angle. For angles less than 120° the dipolar contribution dominates but as the molecule becomes more linear the magnitude of

the quadrupole moment up to 2.5 times larger reaching the greatest value for this range of $\theta = 180°$ as for the splay.

Examination of the quadrupolar contributions for both coefficients shows it is true that when

$$e_1^q = -e_3^q, \tag{3}$$

the sum of these two components for $\bar{e}$ in Equation 1 would cancel.

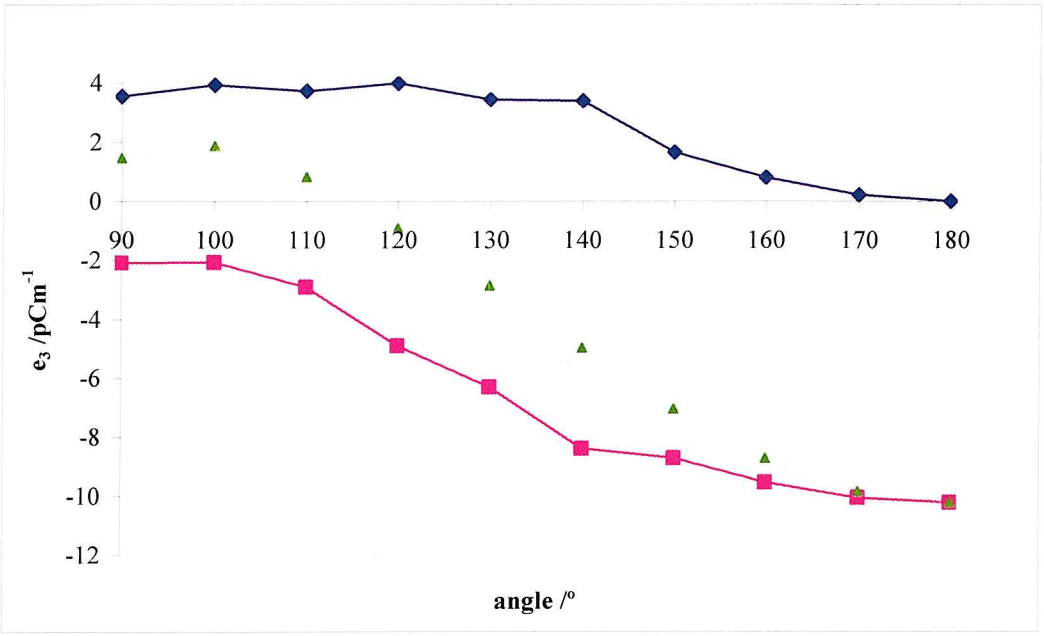

Figure 4.4 Quadrupolar (e_3^q) and dipolar (e_3^d) contribution to the bend flexoelectric coefficient.[14] ■ e_3 quadrupole, ◆ e_3 dipole, ▲ e_3 total (results calculated by Ferrarini).

Thus we conclude that again the quadrupolar contribution is very much larger than the dipolar contribution and opposite in sign. We can also note that the reason why we do not observe these large contributions in real materials is that the sum of both splay and bend quadrupolar contributions to $\bar{e}$ should, according to theory,[11] be negligible. We should also note that when comparing the dipolar contributions they too are often opposite in sign depending on the value of θ. They are, however, not equal and so give different contributions to $\bar{e}$ at different angles consistent with the molecule being more wedge or banana shaped (see Figure 4.5).

Historical attempts to determine the flexoelectric properties of materials has been to measure the combination of e_1 and e_3 as described in Equation 1. This would hide any

quadrupolar contribution as e_1^q and e_3^q would cancel. For display devices based on the ULH cell the quadrupolar effect would also be irrelevant since the response depends on this combination. This does not mean the quadrupolar contibution is unimportant, but it does mean that the consideration of $\bar{e}$ is necessary to predict the effects where the mean is what is measured or observed.

Thus taking the sum of the splay and bend flexoelectric coefficients will give the value of $\bar{e}$ (as defined in Eqution 1) resulting in the cancellation of the quadrupolar contribution and average of the dipolar contributions.

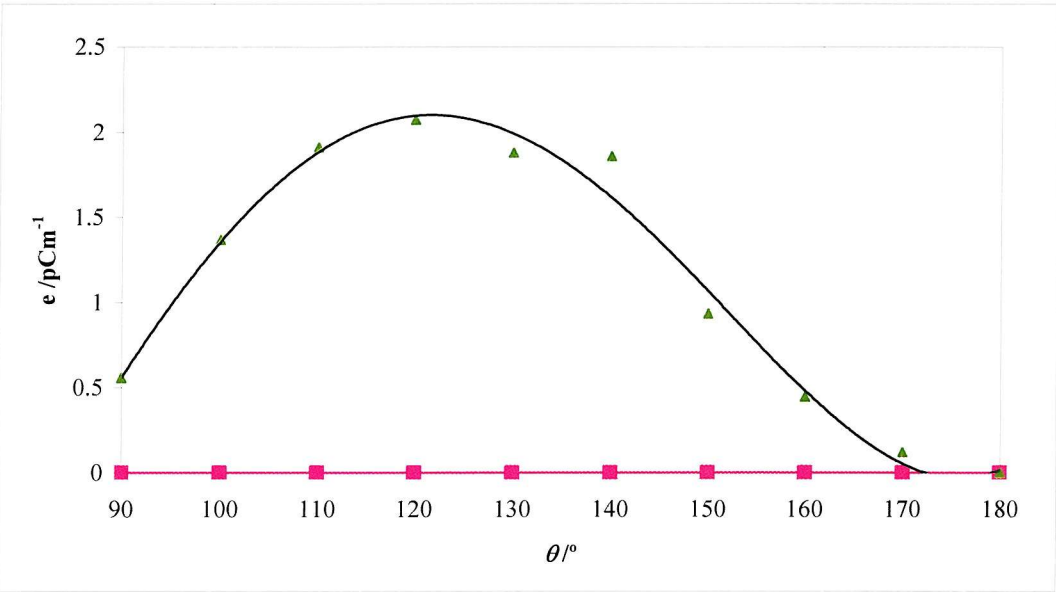

Figure 4.5 Quadrupolar and dipolar contribution to the difference of the splay and bend flexoelectric coefficients. ($\bar{e}$ =(e_1+e_3)/2) Line of best fit is a fifth power polynomial. ■ $\bar{e}$ quadrupole, ◆ $\bar{e}$ dipole, ▲ $\bar{e}$ total (results calculated by Ferrarini).

Looking at the difference of the two contributions, they show a clear rise in the dipolar flexoelectric contribution up to a maximum of approximately 2 pCm^{-1} which occurs as $\theta \approx 120°$. The value at 140° appears anomalous. The quadrupolar contribution is zero across the whole range leaving only a dipolar contribution.

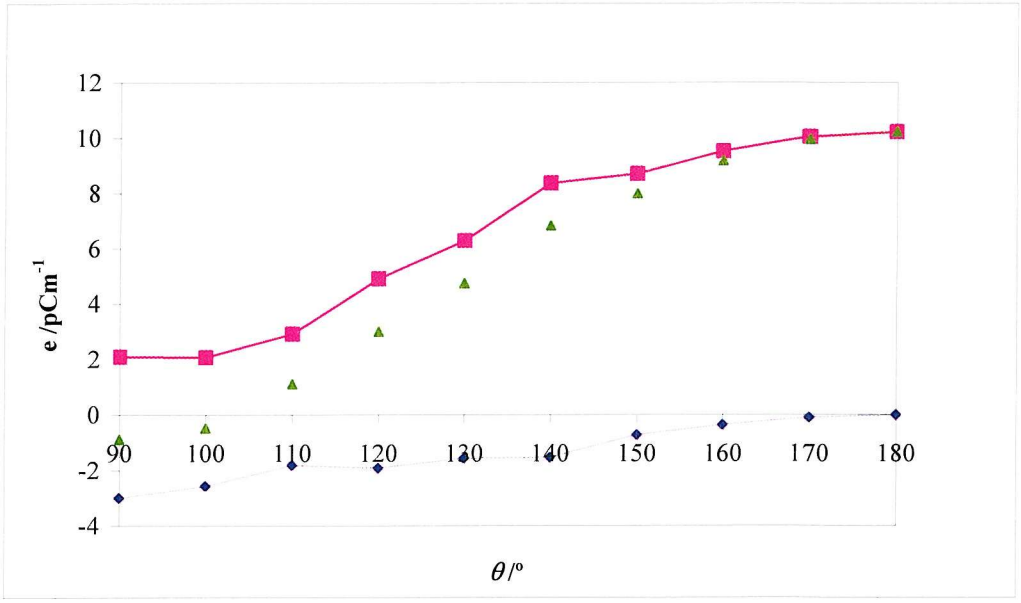

Figure 4.6 Quadrupolar and dipolar contributions for the sum of the splay and bend flexoelectric coefficients. ($\bar{e}$ =(e_1-e_3)/2). ■ $\bar{e}$ quadrupole, ◆ $\bar{e}$ dipole, ▲ $\bar{e}$ total.

The difference of the two flexoelectric coefficients gives a linear decrease in the magnitude of the dipolar flexoelectric effect which, by necessity, becomes zero when the molecule is linear. Conversely the quadrupolar minimum is roughly the same as the dipolar maximum and increases as the material becomes more linear and the size of the components of the quadrupolar tensor becomes larger (from the increase in charge separation). The result is that the quadrupole dominates at angles above 103° and becomes almost 4 times larger than the maxiumum value for the dipole contribution. Also the contributions are opposite in sign. Thus the quadrupolar effect would be in competition with the dipolar contribution.

In general the results show a significant contribution from the quadrupole and, by comparison, only a small contribution from the dipole. The angle for obtaining the maximum contribution from the dipole might be expected, intuitively, to be the tetrahedral angle of 109.47° however, this is clearly not the case and large flexoelectric coefficients appear to be obtained from a range of angles. As previously commented and addressed in Chapter 2, the optimum angle for a given material to give the largest dipolar flexoelectric contribution will be affected by the molecular shape, the charge distribution and ordering in the bulk. Because there is no simple relationship between the

combination of these factors and the flexoelectric effect, it is not trivial to predict what the maximum angle of θ should be for any given material.

Although major conclusions cannot be drawn from such a simple model it does raise the question as to why these large contributions are not observed? The answer lies primarily in how they are observed. If measured individually, we would expect there to be a dominant quadrupolar contribution. However, for ULH display devices, a combination of the two coefficients is used. This combination results in the quadrupolar contributions cancelling as seen in Figure 4.5.

Devices which rely on only splay or bend would expect to see a large contribution coming from the quadrupole which, depending on the molecular optimisation, should dwarf the dipolar contribution. Investigation on measuring the individual coefficients is currently being undertaken by Parry-Jones *et al.*[17] and if the result confirms the calculations then there will be a scientific and engineering gauntlet set down to develop a device which would exploit just one deformation.

Having examined the toy model clearly the next step is to look at real molecules which give large angle flexoelastic switching. Since the lowest melting materials that give the best responses appear to be dimers (predicted by Durand[4]), as reported by Coles[5] (discussed in Chapter 3), it was prudent to develop this work further to be able to model dimers. The first consideration was to look at simple symmetric examples and compare odd and even analogues and perhaps compare them both to their corresponding monomers. This has moved into its first stages with calculations being made on several conformers of two symmetric cyanobiphenyl dimers (one odd and one even).[12]

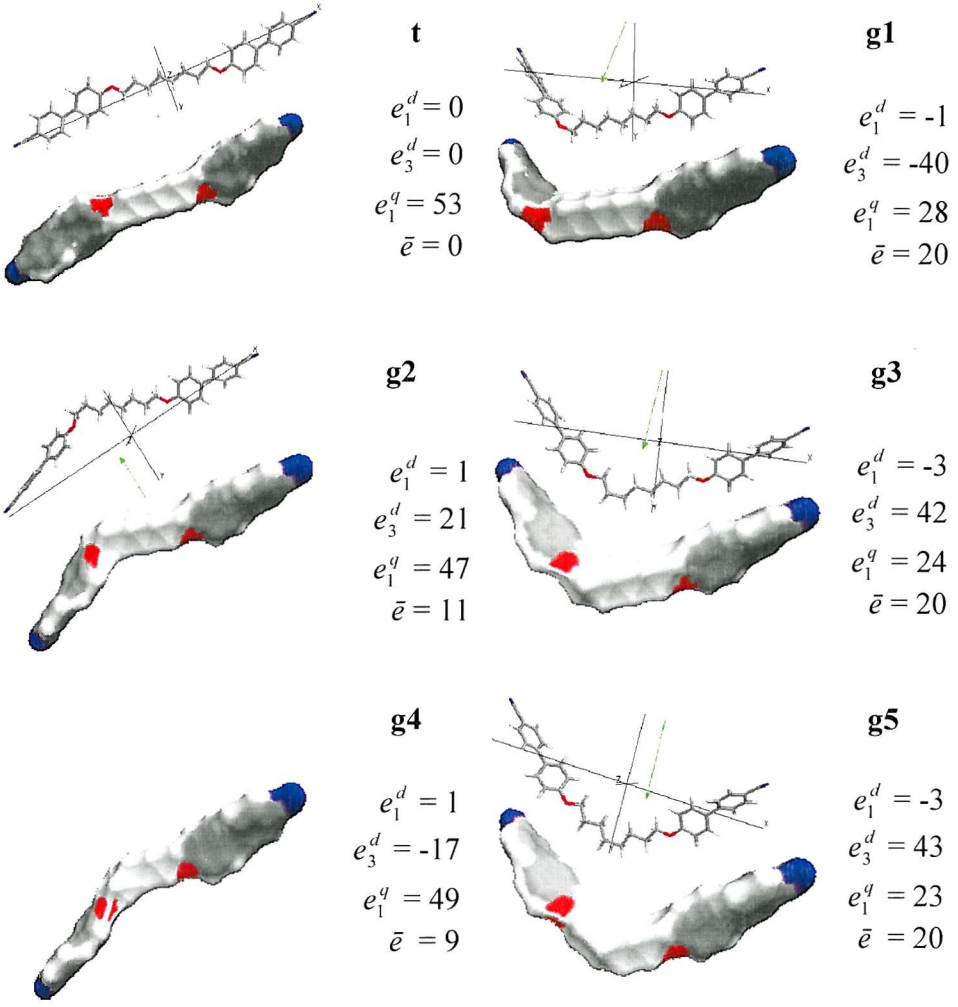

Figure 4.7 Calculations for even dimers in the all-trans conformer (**t**) and for conformers where a single gauche link has been introduced in the spacer (**g 1-5**). The flexoelectric coefficients are reported in units of pCm^{-1} ($\bar{e} = (e_1 + e_3)/2$) and the relationship $e_1^q = -e_3^q$ holds. The magnitude and direction of the electric dipole moment is shown in green. It should be noted that the dipole sign convention is defined in the direction of positive charge.

As well as the specifics of the molecular shape, there is also an added complication compared to the toy model and that is the charge contribution coming from the large number of atomic components, particularly the oxygen atoms.

The results in Figure 4.7 show a wide spread of different values for ē depending on the shape conformation of the dimer. As would be expected for the all-trans even dimer; where the mesogenic units are co-linear this gives a dipolar contribution of zero but a very much larger quadrupolar contribution (which cancels). For increasingly bent

conformers the dipolar contribution becomes much larger so much so that in some cases it rivals and exceeds the quadrupolar contribution.

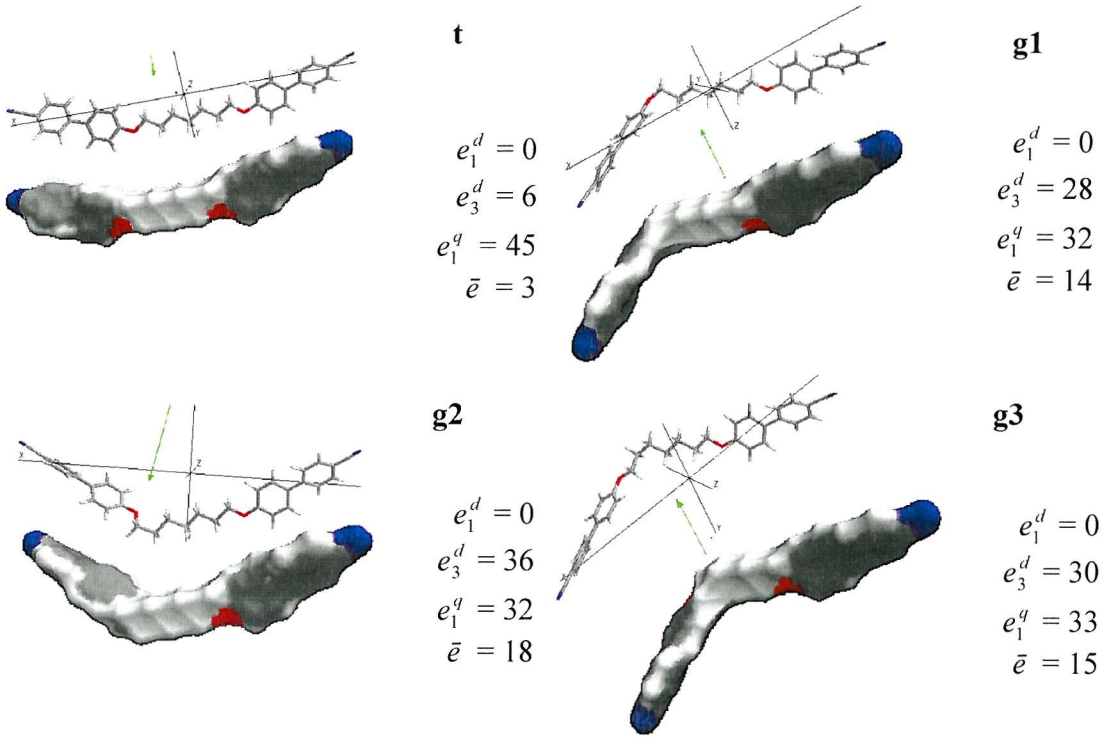

Figure 4.8 Calculations for odd dimers in the all-trans (**t**) and for conformers where a single gauche link has been introduced to a different position in the spacer (**g 1-4**). The flexoelectric coefficients are reported in units of pCm^{-1} ($\bar{e} = (e_1 + e_3)/2$) and the relationship $e_1^q = -e_3^q$ holds. The magnitude and direction of the electric dipole moment is shown in green. It should be noted that the dipole sign convention is defined in the direction of positive charge.

As the molecular conformations in the liquid crystal change so should the contribution to the flexoelectric coefficient. Thus each conformer would need to be statistically weighted according to the likelihood of it existing in the bulk. Most notably the all-trans conformer (which is that most commonly drawn) will contribute little to the overall effect.

With regards to the effect of temperature there is an interesting contradiction between what is understood by the flexoelectric properties of a material and what is observed. Flexoelectricity is largely understood to be a microscopic phenomina and measurements made on materials have shown them to be largely temperature independent.[5] In the light

of these theoretical results it is clear that conformational change from an increase or decrease in temperature would lead to a change in the flexoelastic ratio if the flexoelectric effect was purely microscopic. Since this is not true we may tentatively conclude that the effect is, at least in part, macroscopic. Much work needs to be done in this area before any firm assertations are made however this does emphasise the importance of making measurements on pure systems as well as doped systems if we are to understand the nature of the flexoelectric effect with regard to molecular design.

In the case of the odd dimer shown in Figure 4.8, the values for $e_{3(d)}$ are generally comparable to the quadrupolar contribution. This is in some contrast to the toy model and is likely to be an effect of the ordering. However, it is encouraging that this is the case as it would be expected that when a conformational average is performed it is likely that the odd dimers will show a larger flexoelectric contribution than the even dimer which is consistent with that observed.[1]

These first steps in modelling the flexoelectric effect in symmetric liquid crystal dimers show a promising start which could pave the way to be able to enhance significantly our understanding regarding the design of materials with large flexoelectric coefficients.

4.1.3. The exceptions

There are a limited number of liquid crystal dimers which have been studied in the context of flexoelectricity and of those many of the measurements are of the flexoelastic ratio, $\bar{e}/\overline{K}$, rather than the average coefficient $\bar{e}$. However, given that the elastic constants for dimers themselves give an odd-even effect,[9] where $\overline{K}$ is larger for the even dimers compared to the odd dimers; it is possible for any trend in the flexoelectric coefficients to be masked by the alternation in the elastic constants. This is why in Figure 4.1 (bottom) it was important that the odd-even effect is shown for $\bar{e}$ vs spacer length.

With so few examples in the literature it would be unexpected to find materials which clearly showed flexoelectric coupling irrespective of the shape unless there was another mechanism, such as the quadrupoler flexoelectric coupling, which could operate on a D_{2h} molecular symmetry rather than C_{2v}.

4.1.3.1. Linear monomeric materials with large flexoelectric coefficients

In the case of monomeric molecules we would expect any linear molecules to have at best very small flexoelectric coefficients. Taking each coefficient separately, the quadrupole is likely to be small since the charge separation would be short (e.g. in 5CB).[18] Taking the coefficients combined (ē as defined in Equation 1) the quadrupolar effect would be minimal since both quadrupolar contributions, which have been found to be equal and opposite in sign, would cancel.[12] This is consistent with comments made by Prost and Marcerou concluding their work on quadrupolar contributions to flexoelectricity where they predicted that the effect of the quadrupole would be secondary to the dipole if the dipole was large.[8]

There are, however, examples which question the simplicity of the view presented thus far. Steve Kelly *et al*, published a range of materials in a study of how molecular structure influences the size of the flexoelectric effect in host systems.[19]

Compound	Reported bend angle		Bend from crystal structure	Dipole μ	ē/K in E7
	Rad	Deg	Deg	D	$CN^{-1}m^{-1}$
Pure Host	-	-	-	-	0.9
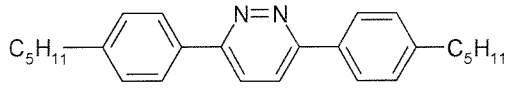	0.2	11.5	8.3[a]	2.94	1.7
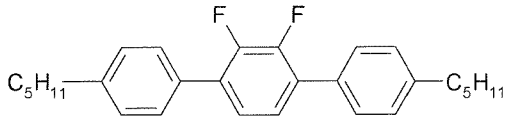	0.33	18.9	N/A	2.60	2.2
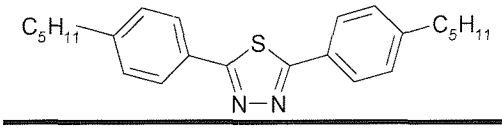	0.23	13.2	44.8[b]	3.46	1.3

Table 4.1 Three linear (as defined in the text) compounds reported by Kelly. All three showing comparable flexoelastic constants. Table adapted from published version.[19] [a]taken from an analogous crystal structure,[20] [b]taken from an analogous crystal structure.[21]

The materials presented were dissolved in the host and reported as 10% by wt in E7 however saturation was, in some cases, found to be higher than this. All the values were compared to the pure host.

It is clear from that reported by Kelly that all these materials have some bend in the molecular structure and so by an intuitive definition, none of these materials are linear. However simple studies of X-ray structures show that even small polyphenyl systems can be flexible enough to allow small bends in the structure.[20, 21] Some of the materials presented have a structure which have little or no significant bend in the molecular shape yet still exhibit significant flexoelastic constants (see Table 4.1).

Each of the three-ring systems which Kelly presents show a slight bend in the molecular shape. The effect on the flexoelastic ratio compared to the host is large in all cases (between a 1.4 and 2.4 fold increase) with only slight variation in $\Theta\mu$ (see Equation 4) (no greater than a 50% increase).

Kelly uses the Helfrich model[22] to attempt to make sense of the results which he obtained. The Helfrich model, being based on the shape/dipole mechanism previously derived by Meyer, from symmetry arguements, does not adequately explain the magnitude of the results reported by Kelly.[19] Indeed there is a factor of 70 – 125 difference between that predicted by the Helfrich model and that observed experimentally by Kelly. The Helfrich model also does not account for the trend he observes comparing the change in flexoelastic ratio measured with those estimated (shown in Table 4.1). As described in Chapter 2, the Helfrich model relates the molecular length (a), breadth (b), internal angle (Θ) and transverse dipole (μ) to the flexoelectric coefficient for the bend deformation, e_3, (Equation 4[22]).

$$e_3 \propto \Theta\left(\frac{b}{a}\right)^{2/3}\mu \qquad (4)$$

Equation 4 is best understood if defined pictorially (See Figure 4.9). It is important to note that the internal angle is made by the intersection of the lines made tangentrially to each end of the molecule.

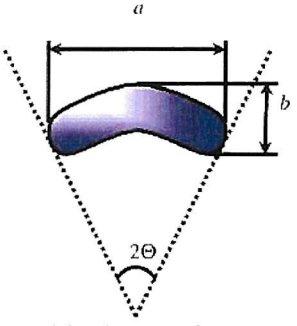

Figure 4.9 Diagram of the parameters used in the equation proposed by Helfrich in his model to relate molecular dimensions and dipole to the flexoelectric coefficient.[19, 22]

Kelly defines the internal angle Θ using the small angle approximation thus

$$\Theta \approx 2(b-w)/a, \tag{5}$$

where w is taken as the diameter of an aromatic ring. Kelly comments that the most linear materials which also had molecular dimensions which were long and thin, gave the largest flexoelastic constants and goes on to point out that '...these results disagree with expectations from dipolar theory.'[19]

Kelly also presents results for the same materials dissolved in ZLI-4792. The difference between this host and E7 is that the consituents of E7 have large dipole moments and tend to associate together in pairs. These supramolecular dimers can be regarded as having two dipoles with a large separation between them and hence would be expected to have a much larger quadrupole moment compared to ZLI-4792. Since the same materials in these very different hosts are, in most cases, similar, Kelly concludes that the quadrupolar contribution in these hosts is small. However, without having measured the quadrupole moment of E7 (a non-trival task), without knowing the extent of the macroscopic effect of flexoelectricity and without measuring the separate contibutions of the splay and bend flexoelectric coefficients it is perhaps too soon to make such estimations. More so, given the failure of molecular shape and dipole interactions to satisfactorily explain these results, the quadrupolar contribution would have appeared to be a potential answer to the unexplainable results.

4.1.3.2. Even dimers with odd effects

These observations on rigid cigar shaped materials in themselves suggest that there is more to comprehending the quadrupolar and dipolar components of the flexoelectric coefficients than is currently understood. Kelly also published results for a small number of homologues from a series of liquid crystal dimers which also show surprising results (see Table 4.2).

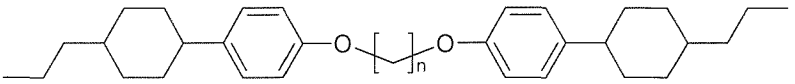

n	Cr		N		I	μ	e/K in E7
		°C		°C		D	$CN^{-1}m^{-1}$
7	•	84	•	(77)	•	2.57	1.7
10	•	106	•	120	•	1.89	3.0
11	•	92	•	97	•	2.16	0.6
12	•	108	•	113	•	2.5	3.4

Table 4.2 Transitions temperatures for symmetric phenylcyclohexyl dimer with corresponding dipole moments and flexoelastic constants. Table adapted from published version.[19] Temperatures of transition are given for the rest of the series in Table 4.6.[23]

The magnitude of the flexoelastic constants show no correlation to the size of the dipole but the most surprising trend is that of the odd-even effect in the $\bar{e}/\overline{K}$ which is the opposite of that expected. Not only is the reported trend contrary to that observed in other materials,[1, 9] the magnitude of the difference is significantly larger. It should also be noted that the flexoelastic ratio, because it incorporates the elastic constant, will have a smaller disparity than the flexoelectric coefficients because the elastic constants for even dimers should be larger than that for odd dimers.

There are several possible answers to these observations. The first is that the dominant mechanism is not that of the shape and dipole. However, if the quadrupolar mechanism is responsible for these results, then cancellation of the quadrupolar contributions seen in theoretical calculations are not being observed here. A prospect which would be as curious and exciting as it would be unexplainable.

The second possibility is that the flexoelectric effect is not simply related to a molecular property but related to the bulk material which, when dissolved into a host, amplifies the flexoelectric coupling of the host. There is very little evidence to support this hypothesis however and no mechanism has been proposed which properly deals with the flexoelectric properties of host-guest systems.

These possible explanations tend to generate more questions than answers. In the absence of more theoretical modelling data the only remaining approach is to make some similar materials and look to see how the flexoelectric effect alters accordingly. This may offer insight to the results suggesting that the even dimers of this series have larger flexoelectric coefficients than the odd. By investigating more of these types of materials

we shall seek to better understand this reversed odd-even effect. By examining the dimer series published by Kelly in a pure system rather than in a host we shall attempt to ascertain whether this effect is a result of the material and the host or if it is observable in the pure state. By examining non-symmetric analogues of these materials we can investigate whether, using a cyanobiphenyl group, we increase or decrease the flexoelectric effect in these materials.

4.2. Synthesis of some novel non-symmetric dimers.

To understand further and extend these findings by Kelly *et al*,[19] three sets of related liquid crystal dimers were synthesised. All the end groups used in synthesising the final product liquid crystals described in this section were provided by Merck. The first series were the symmetric PCH3 dimers which were the same as those published by Kelly *et al.* The other series were non-symmetric dimers with a cyanobiphenyl group and either a PCH3 or PCH7 group on the other side. Lack of time and availablilty of 4-hydroxyphenyl-4'-pentylcyclohexane meant that no symmetric or non-symmetric dimers using that moiety were made in spite of the example published by Kelly having the more favourable flexoelastic ratio. Limited supplies of PCH7 only allowed the non-symmetric series of the PCH7 series to be synthesised. The desired effect of the longer terminal chain would be to lower the melting point and increase the flexoelectric coefficient whilst the cyanobiphenyl group would increase the nematic stability. However, the long terminal chain is also likely to stabilize a smectic phase as seen in the symmetric and non-symmetric Schiff-base dimers and this is what is observed.[24, 25] It is of interest to see whether the cyanobiphenyl moiety supported the large flexoelectric coefficients or whether it acted to reduce them as this may provide some qualitative indication as to what extent the quadrupolar mechanism contributes to the total flexoelectric effect observed.

4.2.1. Details of the synthesis

Synthesis of the non-symmetric liquid crystal dimer series was achieved through reaction of a 4'-cyanobiphenyl-4-oxy-α-alkyl-ω-bromide with 4-hydroxyphenylcyclohexyl-4'-heptane (Scheme 4.1) or 4-hydroxyphenylcyclohexyl-4'-propane (Scheme 4.2)

respectively. Synthesis of the alkylating agent is described in full in Chapter 3 with experimental details in Chapter 7. Both series were synthesised smoothly in reasonable

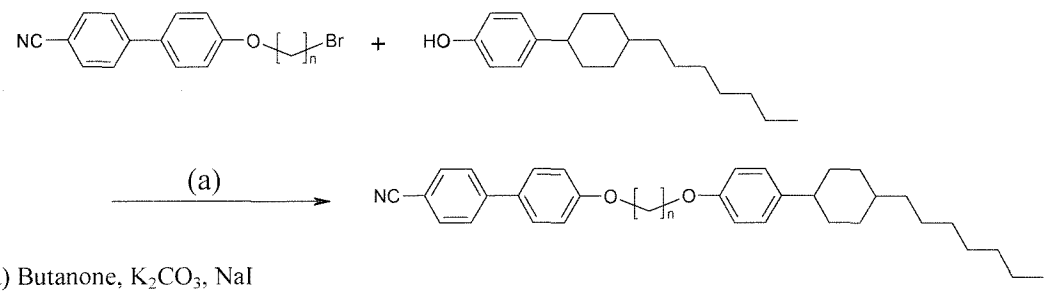

(a) Butanone, K_2CO_3, NaI
n = 4 – 12

Scheme 4.1 Synthesis of α-cyanobiphenyloxy-ω-(oxy-4-phenylcyclohexyl-4'-heptane)alkane non-symmetric liquid crystal dimer (CBOnOPCH7).

yield (shown in Table 4.5) and purification by recrystallisation from acetonitrile gave products (CBOnOPCH7 and CBOnOPCH3) sufficiently pure by NMR and TLC to not warrant further purification. Full experimental details are given in Chapter 7.

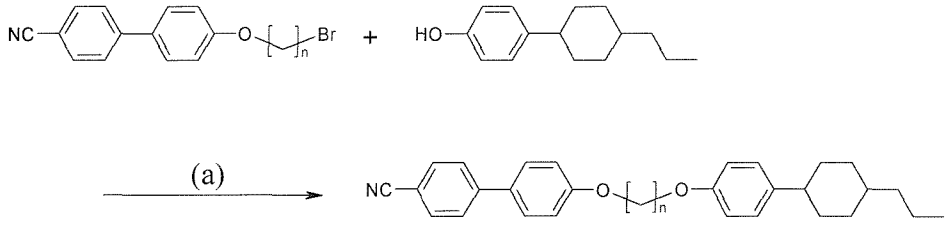

(a) Butanone, K_2CO_3, NaI
n = 4 – 12

Scheme 4.2 Synthesis of α-cyanobiphenyloxy-ω- (oxy-4-phenylcyclohexyl-4'-propane)alkane dimer (CBOnOPCH3)

The symmetric dimer series was synthesised under similar conditions. Two equivalents of 4-hydroxyphenylcyclohexyl-4'-propane were used with one equivalent of dibromoalkane (Scheme 4.3). Again purification was obtained through crystallisation with acetonitrile. Increased solubility of the product in the cold acetonitrile and decreased solubility in the boiling solvent meant purifiction was less trivial. However the final product gave sufficiently good NMR and TLC, showing no impurities that column chromatography was avoided.

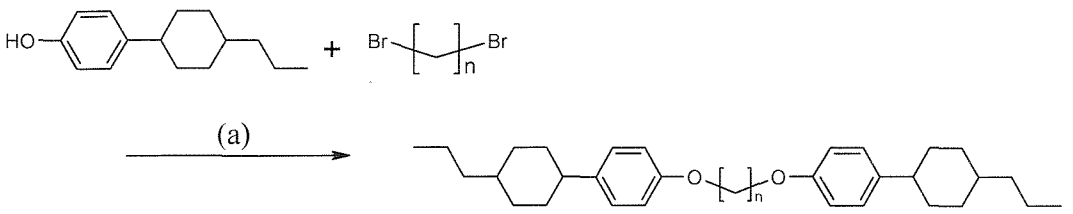

(a) Butanone, K_2CO_3, NaI
n = 4 – 12

Scheme 4.3 Synthesis of α,ω-bis(oxy-4-phenylcyclohexyl-4'-propane)alkane dimers (3CHPOnOPCH3).

Chain length n	Yield 3CHPOnOPCH3	Yield CBOnOPCH3	Yield CBOnOPCH7
4	Not Synthesised	Not Synthesised	65%
5	Not Synthesised	Not Synthesised	67%
6	71%	60%	81%
7	45%	60%	51%
8	71%	31%	76%
9	41%	35%	85%
10	34%	43%	72%
11	27%	85%	91%
12	57%	13%	82%

Table 4.3 Yields of pure product obtained for CBnOPCH7 series.

Looking at the CBOnOPCH7 higher yields were obtained where the reaction was left stirring for longer and was performed on a larger scale. This is true for n = 9 which was conducted at more than twice the scale of the other reactions whereas n = 8 and 6 were left stirring for six days rather than three. Generally 3-4 days gave the best yield for the shortest length of time. Crystallisation achieved better separation for the even dimers in comparison with the odd dimers (this is probably due to lower melting points and hence increased solubility in the crystallising solvent). Contaminated product left in the supernatant liquid could not be removed by successive recrystallisations and therefore was often left unpurified. In these cases isolated purified yields reported are lower than the actual yield of material produced in the reaction.

With the non-symmetric and symmetric PCH3 compounds a similar method of purification was adopted. This worked more effeicently for the non-symmetric compounds rather than the symmetric where a lack of available time in the laboritory did

not permit the employment of column chromatography which would have given better yields. Therefore with speed and purity being more important than quantity, pure materials were obtained at the expense of a better yield.

4.2.2. Analysing the molecular characterization

Chemical purity and confirmation of the identification of the new materials was monitored by a range of techniques; NMR, IR, Mass Spectroscopy and combustion analysis. Proton and carbon NMRs had peaks consistent with the product being formed with no evidence of impurities to within a certainty of 95%. Similarly EI mass spectroscopy showed no evidence of any alkyl bromide alkylating agent. Combustion analysis was performed on one of the members of the series and was consistent, within experimental error, of that predicted for the compound analysed.

NMR, as well as being useful for detection of any possibly impurities, was also useful in identifying which of two possible diastereomers (arising from the cyclohexyl ring) were present in the product. The 1,4-substituted cyclohexane ring can be locked in one of two positions giving rise to a difference in the groups located on carbon atoms A and B on the OPCH7 moiety. This gives rise to two different diastereoisomers (Figure 4.10).

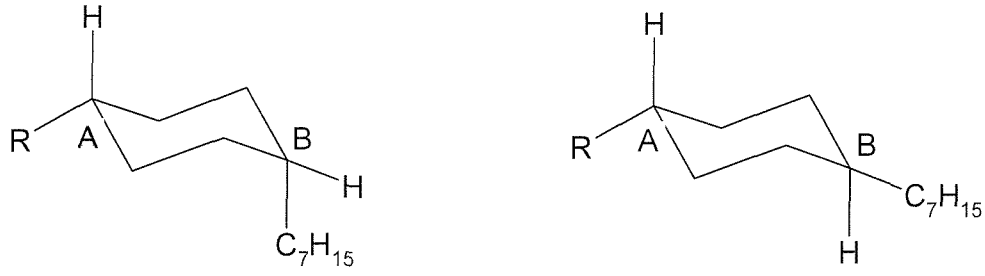

Figure 4.10 Two diastereoisomers caused by the cyclohexane rings being sterically locked

The different diastereoisomers would radically alter the shape of the end group which would have a significant impact on the liquid-crystalline properties. By ^{1}H NMR it could be seen by looking at the peak for H_a and considering the integrations of the other peaks relative to it that there is only one diastereomer present.

However although it has been established there is only one diastereoisomer, we have not determined which one. To do this, long and short range C-H correlation NMRs were run

on the HO-PCH7 starting material (since subsequent reactions would not alter the stereochemistry the starting material can be used for simplicity and convenience).

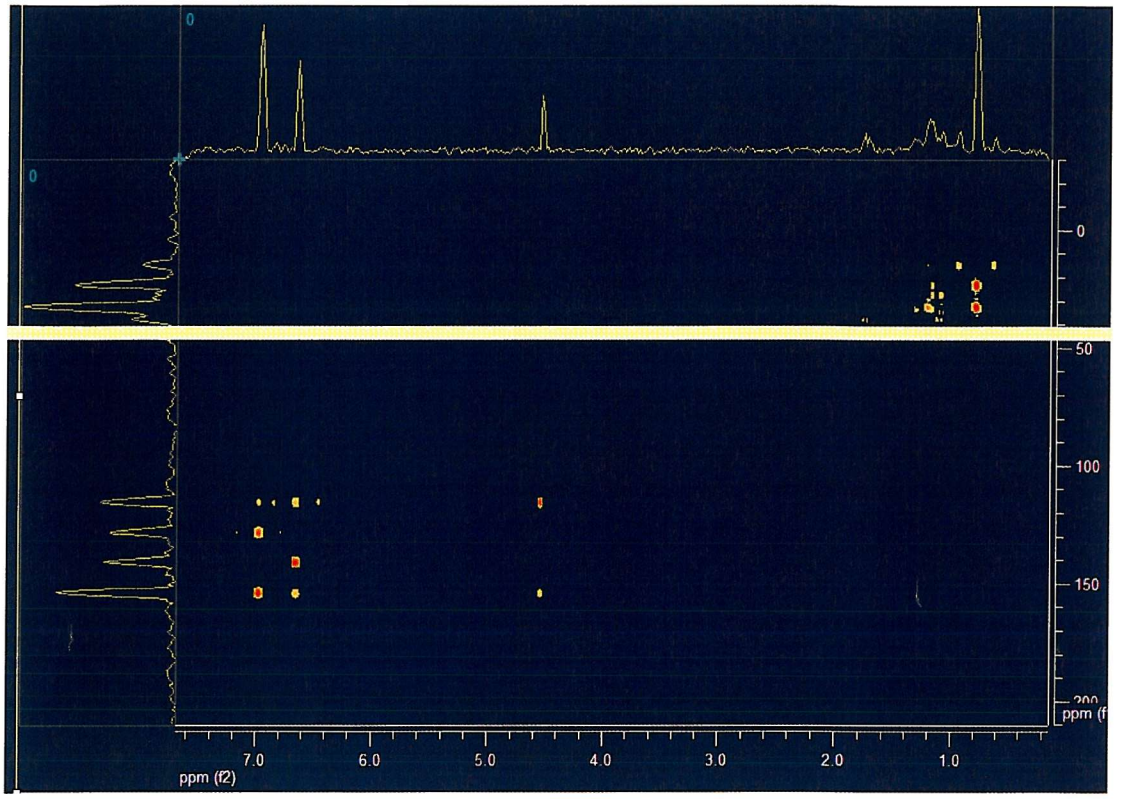

Figure 4.11 2D NMR plot showing ^{13}C DEPT 45 (vertical) and ^{1}H (horizontal) spectra of HOPCH7. Highlighted are the peaks which correspond to a chemical shift of ~45 ppm. Full analysis of this plot is given in the Chapter 7. Data reprocessed using Mestrec NMR analysis software.

Taking a general overview of the 2D NMR in Figure 4.11, the aromatic proton-carbon coupling occurs in the bottom left corner (down field) and the aliphatic interactions are in the top right corner (up field) as expected. It is predicted by simple molecular modelling[26] and shown in crystal structures[27, 28] that in these types of phenyl/cyclohexyl systems, the cyclohexyl group is orientated with axial protons parrallel to the plane of the aromatic ring. We can be certain therefore, that the carbon at $\delta = 45$ ppm is the carbon at A.

This is confirmed in the NMR by the presence of strong coupling between the carbon signal at 45 ppm (cyclohexyl carbons) and the aromatic protons ($\delta = 6.95$ ppm). The highlighted region in Figure 4.12 corresponds to protons which couple with carbons of chemical shift $\delta = 45$ ppm. Making the realistic assumption that the conformation of the cyclohexyl ring is chair and not boat shaped[29] and knowing the orientation of the

cyclohexyl ring and the position of the carbons closest to the aromatic ring enables the assignment of the diasteric pair by considering which other protons interact with these cyclohexyl carbons. Looking at the highlighted region we can see that the protons at 1.76 ppm also shows coupling to this carbon.

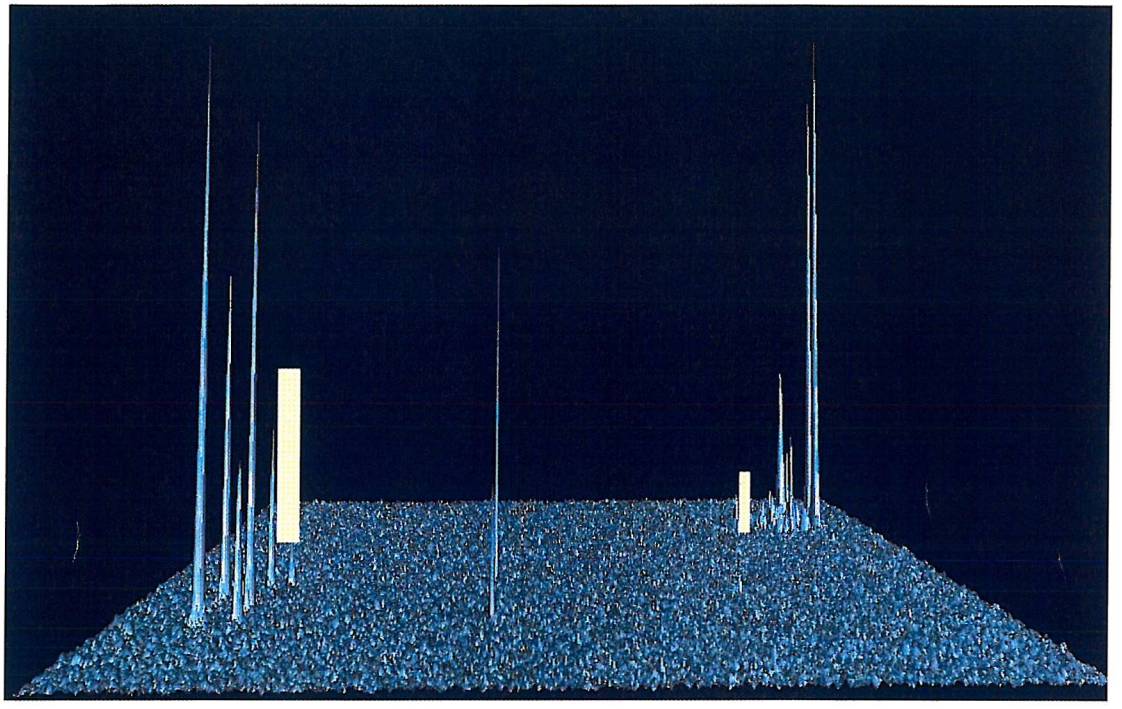

Figure 4.12 3D projection of the 2D plot shown in Figure 4.9. Peaks in yellow are proton interactions with cyclohexyl carbons with a chemical shift of 45 ppm.

The proton which is interacting with these carbons comes from the proton located at position B (See Figure 4.8) on the cyclohexyl ring. This can be determined by examining the splitting pattern in the proton NMR. By considering the two possible diasteriomers we can see that there is only one which has the proton at B close enough to have sufficient through-space interaction with the carbons at, and close to, A. Consideration of the relative intensities between the two peaks highlighted in Figure 4.12 corroborates this conclusion as the through-space distance between this proton at B and the associated carbons around A is much larger then would be the case for protons on the aliphatic chain. If the material had been the other diastereomer there would be no interaction between this single proton and the cyclohexyl carbons at A and there would be much greater interaction between the protons on the axial aliphatic chain and the carbons at A.

4.3. Analyzing the physical data for CBOnOPCH7

As described in the previous chapter, there are many properties of new materials which can be measured and are of importance in understanding how these materials behave. Other than the flexoelastic ratios which are reported in a later section, the key properties of concern are the phase behaviour examined by regarding the optical textures and the entropies of transition which gives some idea as to how ordered the materials are compared to the isotropic.

4.3.1. Optical microscopy

The procedure for making up samples was identical to that described in the similar section in Chapter 3. Where identification was more difficult to determine, for example where the materials were supercooled a long way below the melting point and prone to freezing before the phase had changed, droplets of material were examined and the assignment made. In some cases the textures which formed were not characteristic (e.g. the nematic n = 7 in Figure 4.13) in these cases there is normally enough evidence to confidently identify the phase either by looking for fine thread-like patterns in the material which are not well picked up by the camera. In the case of identifying the smectic phase and the transition point often cooling gave a much clearer and more readily identifiable pattern.

Figure 4.13 All optical textures are taken on cooling showing a smectic A (top left) and nematic (top right) from CBO5OPCH7 taken at 103 °C, $0.94T_{NI}$ and 121 °C, $0.99T_{NI}$ respectively; a smectic A (middle left) and nematic (middle right) from CBO6OPCH7 taken at 128 °C, $0.90T_{NI}$ and 151 °C, $0.95T_{NI}$ respectively; a smectic A (bottom left) and nematic (bottom right) from CBO7OPCH7 taken at 94 °C, $0.91T_{NI}$ and 121 °C, $0.98T_{NI}$ respectively.

Figure 4.14 All optical textures are taken on cooling showing a smectic A (top left) and nematic (top right) from CBO8OPCH7 taken at 116 °C, $0.89T_{NI}$ and 128 °C, $0.92T_{NI}$ respectively; a smectic A (middle left) and nematic (middle right) from CBO9OPCH7 taken at 75 °C, $0.87T_{NI}$ and 123 °C, $0.99T_{NI}$ respectively; nematics for CBO10OPCH7 (bottom left) and CBO11OPCH7 (bottom right) at 144 °C, $0.92T_{NI}$ and 133 °C, $1.02T_{NI}$ respectively.

The textures obtained using a polarising microscope demonstrate the presence of smectic A and nematic phases which are shown for CBOnOPCH7 where n = 5-11 in Figures 4.13 and 4.14. Smectic phases were observed for all of the smaller spacer lengths becoming increasingly less stable until they were completely obscured when the number of methylene groups was greater than 10. This is more fully covered in the following section on the phase behaviour. Typically the smectics gave fan shaped focal conics which were identified most unambiguously when viewed on cooling. All the smectics showed paramorphotic behaviour which can be seen most clearly in CBO8OPCH7 picture in Figure 4.14. Nematic phases were observed for all the materials and typically showed two and four brush defects which were most easily seen on cooling from the isotropic.

4.3.2. Phase behaviour

The temperature transitions for the different phases are reported in Table 4.4; almost all the materials gave enantiotropic phases showing both nematic and smectic behaviour in almost every case.

n	Cr		SmA		N		I
4	•	127	•	185	•	197	•
5	•	128	•	(111)	•	(127)	•
6	•	113	•	151	•	172	•
7	•	114	•	(104)	•	130	•
8	•	105	•	123	•	162	•
9	•	104	•	(81)	•	126	•
10	•	124	•	(92)	•	146	•
11	•	105	•		•	127	•
12	•	121	•		•	141	•

Table 4.4 Phase transitions for the CBOnOPH7 series in °C.

Unfortunately, the symmetric 7CHPOnOPCH7 materials are not known so the most structurally relevant symmetric series with which to compare these dimers is the symmetric cyanobiphenyl series and also the non-symmetric Schiff-base dimer reported by Date *et al.*[24] with a similar length terminal chain on the Schiff-base. In subsequent sections this series is also contrasted with the CBOnOPCH3 series and the symmetric 3PCHOnOPCH3 series (as reported by Kelly *et al.*[19]).

4.3.2.1. Comparing CBOnOPCH7 with CBOnOCB

The T_{NI} in CBOnOPCH7 showed a pronounced odd-even effect which slowly attenuates at a rate similar to that found for the symmetric cyanobiphenyls (see Figure 4.15). The effect of the PCH7 group has been to reduce the nematic stability with respect to the cyanobiphenyl by approximately 40-50 °C along the series.

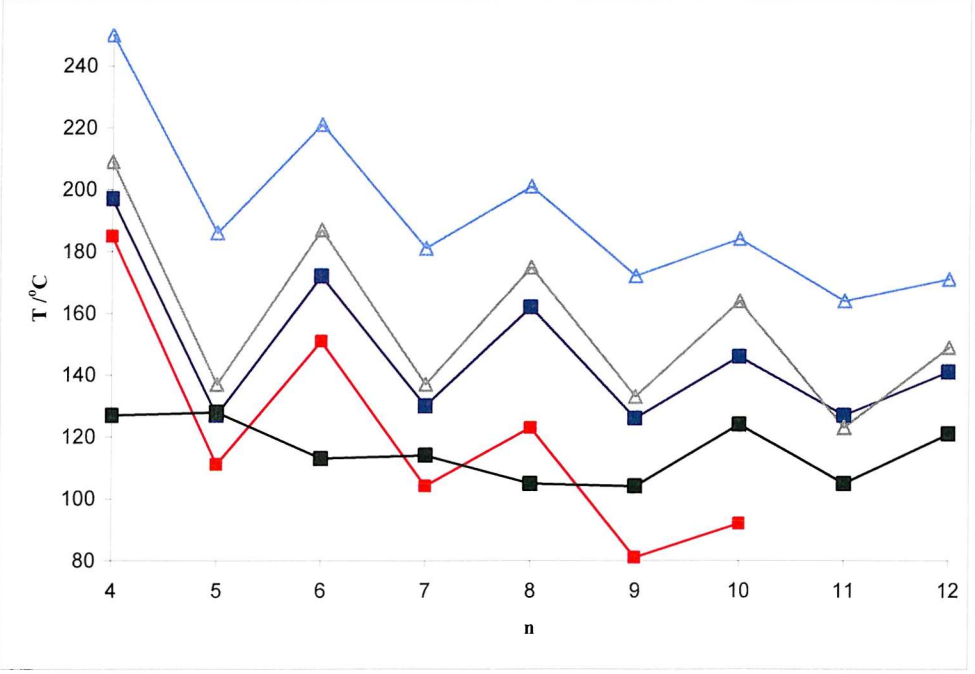

Figure 4.15 Transition temperatures for the CBOnOPCH7 series plotted against spacer length and compared with the CBOnOCB series. Here, ■ denotes $T_{CrI/CrN/CrSmA}$ for CBOnOPCH7; ■ denotes T_{SmAN} for CBOnOPCH7; ■ denotes T_{NI} for CBOnOPCH7; Δ denotes T_{CrN} for CBOnOCB and Δ denotes T_{NI} for CBOnOCB.

The transitions for the odd dimers show very little change in temperature with spacer length but those for the even dimers fall steadily as n increases. One of the advantages of the long chain terminal group is the effect of lowering the melting point. The Cr-N (and Cr-SmA) transition temperatures fall steadily with very little alternation until n = 10. Here the melting points display remarkably different behaviour showing an odd-even effect which, as found for the cyanobiphenyls, follows the T_{NI} transitions. In all cases the melting transitions are lower than those for the symmetric cyanobiphenyls resulting in a large liquid crystal range of 60 °C for the even dimers when n is small. As n becomes larger the trends follows the same pattern as the symmetric cyanobiphenyls, except that the melting points appear to start to converge.

The trend in the T_{NI} is very similar to that seen in the non-symmetric dimers described in Chapter 3. The even dimers have lower T_{NI} transitions as n increases, the odd dimers have constant or slightly increasing transition temperatures. The argument to explain each trend is much the same as with the fluorinated dimers. The terminal chain adds a little to the molecular length and as such stabilises the nematic slightly (although clearly not as much as the CN group). As the spacer length increases the mesogenic interactions become more diluted by the aliphatic core destabilising the nematic phase slightly which results in a drop in the transition temperatures as n increases. This drop in T_{NI} is countered in the odd members, where the nematic destabilising bent conformations are allowed to straighten slightly due to small concerted rotations in the spacer chain. The longer this chain length the more rotations are energetically permissible and the more linear odd conformers are found in the distribution. Since, for the odd dimers, there is little or no change in nematic stability as n increases, it could be speculated that the decline in stability of the T_{NI} transitions in the odd members of the CBOnOPCH7 series is almost completely compensated for by the small concerted rotations in the spacer chain.

The smectic A phase is enantiotropic for only short, even spacer lengths (n = 4 and 6). We can think of the smectic phase in monomers (e.g. the nCB series) as being stabilised by inhomogenicity of the rod and chain components. If we treated the rod and the chain as separate entities we can imagine the rods becoming less soluble in a longer chain solvent. In monomers, where the rod and terminal chain are connected and the chain gets longer so the driving force for the rods to associate only with rods and the chains only with themselves increases. The way this is best achieved is to form a lamellar structure as seen in the smectic phases.

However, the trend observed in the nCB series is the opposite to that seen in the CBOnOPCH3 dimer series. If we treat the flexible spacer as part of the rod then we are left with a situation similar to the monomer (so long as the interaction between the mesogenic groups is weak), however this time the length of the anistropic component of the molecule is getting longer and the chain is remaining the same size. Thus the effect of the terminal chain on the dimer decreases as the spacer length (and effectively the rod) increases. As the effect of the terminal chain lessens, the smectic character also lessens.

Another way of considering the trend would be to regard increasing the spacer chain as increasing the aliphatic component of the dimer. This increases the 'micibility' of the rod and the terminal chain decreasing the likelihood of separation via a lamellar structure.

It would have been valuable to have had the X-ray data to identify the type of SmA phase which forms. From the layer spacings it would have been trivial to determine whether the phase was a simple lamellar structure or intercalated.

Regarding the melting points, the change in the trend at n = 10 also appears to be related to the size of the spacer compared with the length of the terminal chain. In the absence of any X-ray crystal data it can only be speculated that the molecular packing in the crystal where the spacer was of comparable size or shorter than the terminal group was significantly different to the packing where the spacer is longer. However, there is no obvious difference in the crystal phase as evidenced by the optical texture.

4.3.2.2. Comparing CBOnOPCH7 with the non-symmetric Schiff-base CBOnO.6

Comparison between the phase behaviour of the CBOnOPCH7 series and the CBOnO.6 Schiff-base series[30] shows that the nematic transitions are behaving in a similar way in both series (see Figure 4.16).

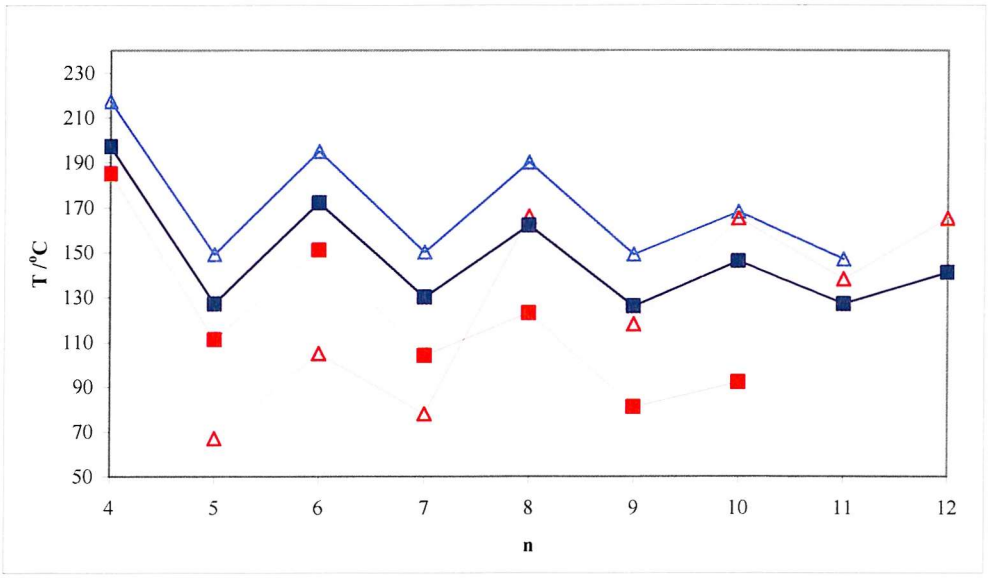

Figure 4.16 The transition temperatures for non-symmetric Schiff-base dimer (CBOnO.6) against the CBOnOPCH7 series (The smectic C and melting transitions have been omitted to simply the graph). Here, ■ denotes T_{SmAN} for CBOnOPCH7; ■ denotes T_{NI} for CBOnOPCH7; Δ denotes T_{SmAN} for CBOnO.6 and Δ denotes T_{NI} for CBOnO.6.

The T_{NI} alternate in an odd-even fashion by the same amount with the T_{NI} of the CBOnOPCH7 series being aproximately 20 °C lower than those of the CBOnO.6 series. In contrast the smectic phase stabilisation in the two series is very different. Whilst both show an odd-even effect in the SmA-N transitions, the SmA phase of the Schiff-base dimers increase in stablilty with increasing spacer length until the nematic is no longer observed where n > 11; whereas for the CBOnOPCH7 series, the SmA transitions are destabilised as the core increases in length till the phase is unobservable for n > 10 (the materials can be supercooled by about 20 °C) (see Figure 4.17). The primary difference lies in the stability in the SmA phase for the Schiff-base dimers being driven by the interactions between the mesogenic groups supported by the length of the spacer.[30]

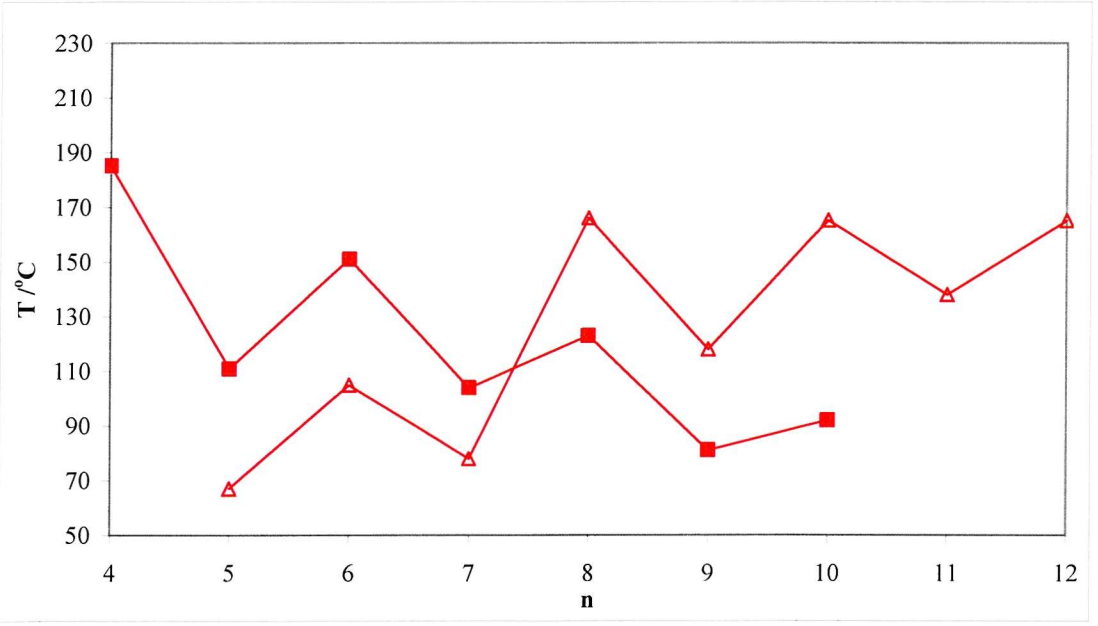

Figure 4.17 The transition temperatures of the smectic A phase for the non-symmetric Schiff-base dimer (CBOnO.6) and the CBOnOPCH7 series. Here, ■ denotes T_{SmAN} for CBOnOPCH7; and Δ denotes $T_{SmAN/SmAI}$ for CBOnO.6.

The favourable interaction between the Schiff-base and the cyanobiphenyl is not mimicked in the CBOnOPCH7 series. This is not surprising as the type of strong electrostatic interactions resulting from the polar nitrogen in the Schiff-base are not present in the comparitively non-polar -OPCH7 group. As has already been described, for

the CBOnOPCH7 series, the smectic phase is stabilised by the anisotropic rod being small compared to the length of the terminal chain and effect of the terminal chain on the phase is reduced by the spacer length, and therefore rod, increasing. Where the interactions between the mesogenic groups is large, as in the Schiff-base dimers, the driving force for the phase formation are these mesogenic interactions which are supported by longer terminal and spacer chain lengths. Hence for Schiff-base dimers (especially the non-symmetric cyanobiphenyl/Schiff-base) dimers, smectic phase becomes increasingly stabilised with increasing spacer length.[30]

4.3.3. Entropies of transition

The data for the entropies of transition for this series are interesting not only in their own right, but also in how they are found to compare quite closely with the symmetric CBOnOCB series and the non-symmetric Schiff-base series.

n	Cr-SmA, Cr-N†,Cr-I‡	N-I
4	10.8	1.51
5	14.0‡	0.46
6	11.2	1.58
7	11.2	0.51
8	12.9	2.00
9	15.1†	0.73
10	16.3†	1.66
11	11.1†	0.86
12	12.8†	2.21

Table 4.5 The transitional entropy data for the CBOnOPCH7 series. Data for the SmA-N is not given as it was too small to within ±0.05 Jg^{-1} on the DSC plot to measure reliably.

From the optical microscopy we know that there is a smectic transition although any transition in the DSC plot is either unobservable or so small as to be within experimental error. From Table 4.5 we can clearly see that there is an odd-even alternation in the $\Delta S_{NI}/R$ as the spacer length increases. From Figure 4.18 we can see that the effect of the terminal chain on the alternation appears to be negligible as the T_{NI} for the even and odd members respectivly increases as the spacer length increases.

The pattern of alternation is very similar to that found for the CBOnOCB series. Generally the CBOnOPCH7 has a smaller $\Delta S_{NI}/R$ compared to that of the symmetric cyanobiphenyl. This is not surprising given the higher mesogenicity of the CBO group compared to the OPCH7 moiety (given by simple comparison of the T_{NI}) which is likely

to lead to a more ordered system at the T_{NI} transition. Interestingly there is an unexpected increase in $\Delta S_{NI}/R$ at n = 8 compared to the n = 6 and 10. We might speculate that this may be due to slightly better orientational packing of the molcules in the liquid crystal where the terminal chain and the spacer are approximately the same length. However if this were the case it would be hard to see why for n = 7 this would not also be the case. It should also be noted that applying a 10% error to the data (which is generally taken to be the case for transitional entropy measurements[31, 32]) the lower bound for n = 8 is approximately the same as the higher bound for n = 6 and 10. This slightly high result for n = 8 is therefore just within the bounds of experimental error.

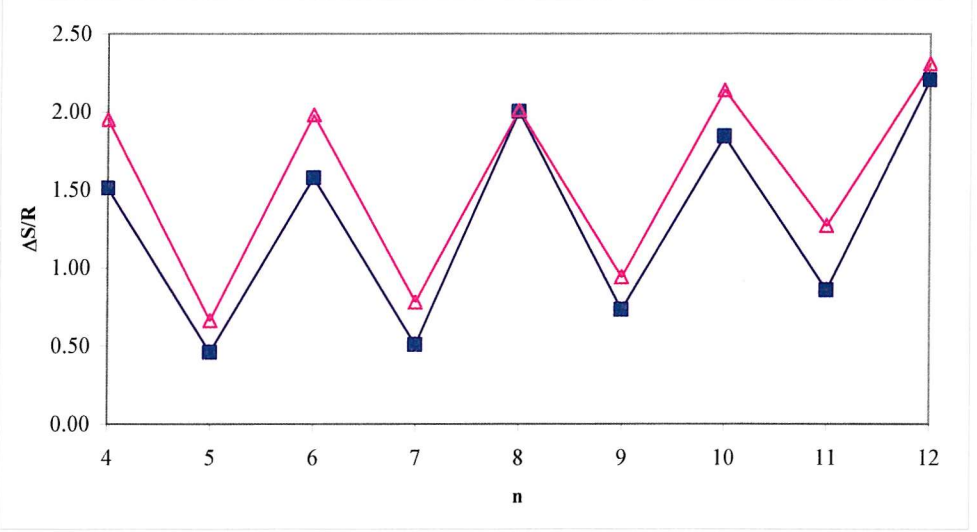

Figure 4.18 Entropy change for the N-I transition for CBOnOPCH7 compared with those for the symmetric CBOnOCB series.[33] Here, Δ denotes $\Delta S_{NI}/R$ for CBOnOCB and ■ denotes $\Delta S_{NI}/R$ for CBOnOPCH7.

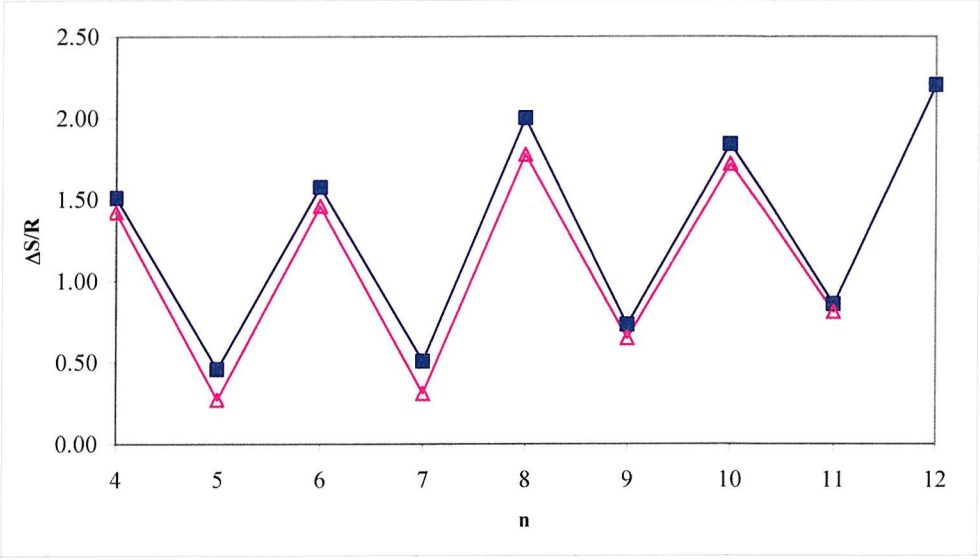

Figure 4.19 Entropy change for the N-I transition for CBOnOPCH7 compared with the non-symmetric cyanobiphenyl/Schiff-base dimers where the terminal chain on the Schiff-base is 6 carbon atoms long and is the best literature available mimic for the CBOnOPCH7 series (n = 12 not given in the literature).[30] Here, Δ is $\Delta S_{NI}/R$ for CBOnO.6 and ■ $\Delta S_{NI}/R$ for CBOnOPCH7

If this unusual increase in transitional entropy for n = 8 is as a result of the terminal chain then we might expect be able to find similar behaviour in materials with a similar terminal chain, i.e. the non-symmetric Schiff-bases.

It can be seen from Figure 4.19 that there is a simialar behaviour but contrary to expectation, the increase in $\Delta S_{NI}/R$ for the Schiff-base dimer is also at n = 8. Given that the terminal chain is 6 carbons long for this example we would expect the increase in transitional entropy to be around n = 6 if the increase is related to better packing. Given that the molecular length of the -O.6 moiety is approximately the same molecular length as the -OPCH7 group (see Figure 4.20) it is possible that at a specific spacer length the mesogenic group is offset with relation to neighbouring molecules resulting in the spacer being better ordered. There is some evidence for this in the Schiff-base dimer CBOnO.10 where the value for n = 10 is slightly higher than would be expected looking at the trend in even members of that series.[30]

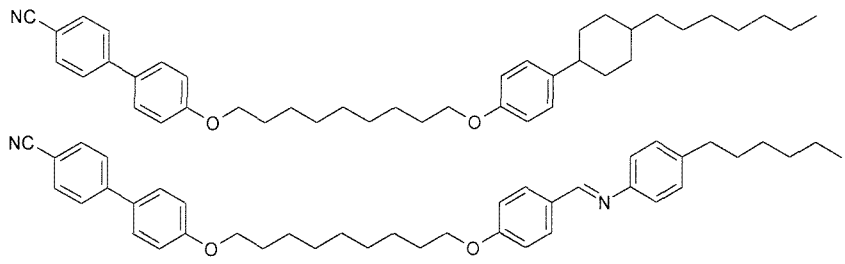

Figure 4.20 Comparing the chemical structure of a Schiff-base/cyanobiphenyl dimer with the phenyl-cyclohexyl/cyanobiphenyl dimer

4.4. Analyzing the physical data for the CBOnOPCH3 series

One of the key factors for investigating the CBOnOPCH7 series was the availability of the HOPCH7 moiety from Merck and the similarity in structure between this material and symmetric dimers by Kelly *et al.*[19] which showed interesting and unusual flexoelectric response in liquid crystal hosts. The subsequent availability of the HOPCH3 moiety some time later permitted the synthesis of the symmetric and non-symmetric -OPCH3 series and so a closer study of the properties of these liquid crystal dimers.

4.4.1. Optical microscopy

The optical microscopy was conducted under similar conditions as those described in 4.3.1 and the transition temperatures are given later. The materials were purely nematogenic, no smectic behaviour was observed, even after supercooling, as expected for shorter terminal chains.

Most of the samples in this series showed a clear schlieren texture (see Figure 4.21) consisting of two and four brush defects, a characteristic feature of nematic phases. Each phase exhibited thread-like textures which persisted throughout the phase and the sample flashed when subjected to mechanical pressure on the top of the cover slip. The materials all supercooled by between 10 °C and 20 °C with the longer chain odd dimers generally supercooling by a larger amount (e.g. n = 7, 9 and 11).

Figure 4.21 All optical texture pictures taken on cooling showing nematic phases. CBO6OCH3 130 °C, $0.95T_{NI}$ (top left); CBO7OCH3 taken at 133 °C, $1.15T_{NI}$ (top right); CBO8OCH3 taken at 127 °C, $0.99T_{NI}$ (middle left); CBO9OCH3 taken at 138 °C, $1.10T_{NI}$ (middle right); CBO10OCH3 taken at 166 °C, $1.09T_{NI}$ (bottom left); CBO11OCH3 taken at 135 °C, $1.09T_{NI}$ (bottom right).

4.4.2. Phase behaviour

The results of the phase behaviour obtained from optical microscopy are shown in Table 4.7. All the members of the series show enantiotropic nematic phases.

n	Cr		N		I
6	•	143	•	187	•
7	•	119	•	139	•
8	•	136	•	170	•
9	•	111	•	134	•
10	•	113	•	162	•
11	•	108	•	135	•
12	•	100	•	145	•

Table 4.6 Transition temperatures for CBOnOPCH3 in °C

As in Section 4.3 this series is compared with the symmetric cyanobiphenyl series (CBOnOCB) and the Schiff-base non-symmetric dimers CBOnO.2 (the data for n = 7 – 12 for the CBOnO.3 series is not available).

4.4.2.1. Comparing the CBOnOPCH3 dimers with the CBOnOCB series

The transitional properties of the CBOnOPCH3 series are shown in Figure 4.22, the T_{NI}s which exhibits a familiar alternation, show a larger variance in temperature with change in parity than those for the CBOnOCB series but attenuates more rapidly as n increases. The N - I transition temperatures for the non-symmetric dimers are consistently lower for the CBOnOPCH3 series which is expected as the -OPCH3 group is known in monomers to be less mesogenic than the -OCB group.[34] The entire series is nematogenic indeed even when supercooled by approximately 40 °C there was no optical evidence (and no evidence by DSC) of a transition to a smectic phase. The influence of the terminal chain here is much less apparent, presumably due to it being considerably smaller in relation to the size of the molecule and in comparison with the terminal chain in the CBOnOPCH7 dimers. Curiously, comparing the melting points for the non-symmetric -OPCH3 and -OPCH7 dimers we see something of the opposite behaviour in melting points. In the CBOnOPCH3 series there is an odd-even effect in the melting points which disappears as n > 9. It is unclear as to why this should occur at this chain length, however the dilution effect of both aliphatic chains may overcome any effect the rigid aromatic units may have on the packing, altering the unit cell resulting in a change in the trend across the group.

Naturally an X-ray crystallography study would give more evidence to this speculation. Unfortunately time and a disappointing lack of suitable crystals halted any further investigation.

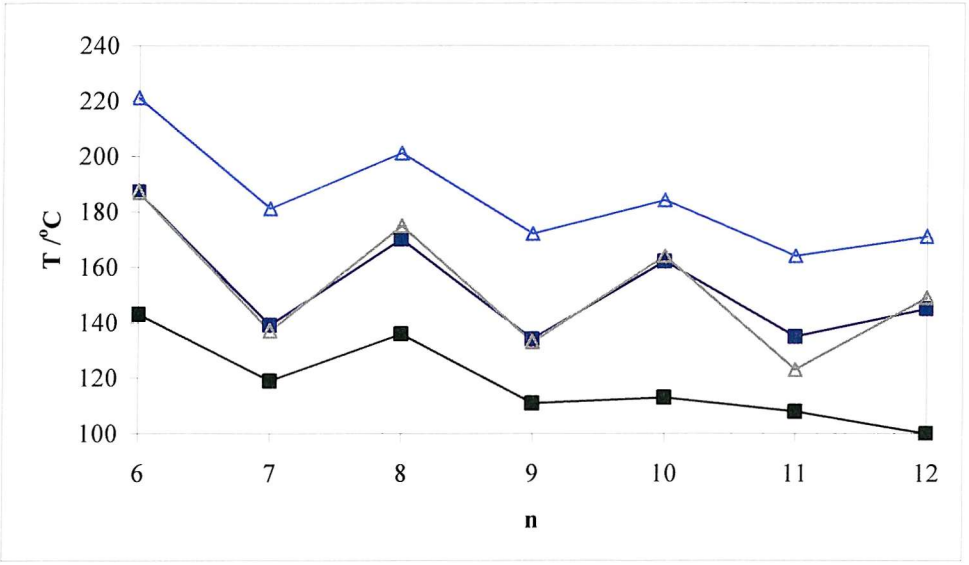

Figure 4.22 Transition temperatures for the CBOnOPCH3 series are plotted as a function of spacer length and compared with the CBOnOCB series. Here, ■ is T_{CrN} for CBOnOPCH3; ■ is T_{NI} for CBOnOPCH3; Δ is T_{CrN} for CBOnOCB and Δ is T_{NI} for CBOnOCB.

It should be noted, however, that the melting points of the non-symmetric group of dimers although moderate are consistently and significantly lower than those of the symmetric cyanobiphenyl series increasing the likelihood of their being soluble in mixtures.

4.4.2.2. Comparing CBOnOPCH3 with non-symmetric Schiff-base CBOnO.2

In the absence of a complete set of data for CBOnO.3 (n = 4 – 12, only n = 3-6 available[35]) this we shall compare this series to CBOnO.2[30] which is shown in Figure 4.23. Looking at the T_{NI} in both series we see an odd-even effect which again is more pronounced in the CBOnOPCH3 series. The CBOnO.2 series shows a smaller degree of alternation between odd and even dimers in the T_{NI} compared to the CBOnOPCH3 series and all the mesophases in the non-symmetric Schiff-base dimers are more stable across the series. This could be related to the interactions between unlike mesogenic groups in the CBOnO.2 series being stronger than in the CBOnOPCH3 group due to the electron

rich Schiff-base and the comparatively electron poor cyanobiphenyl group. In the case of the CBOnOPCH3 neither mesogenic group is as electron rich as the Schiff-base and therefore these lamellar stabilising interactions are not observed.

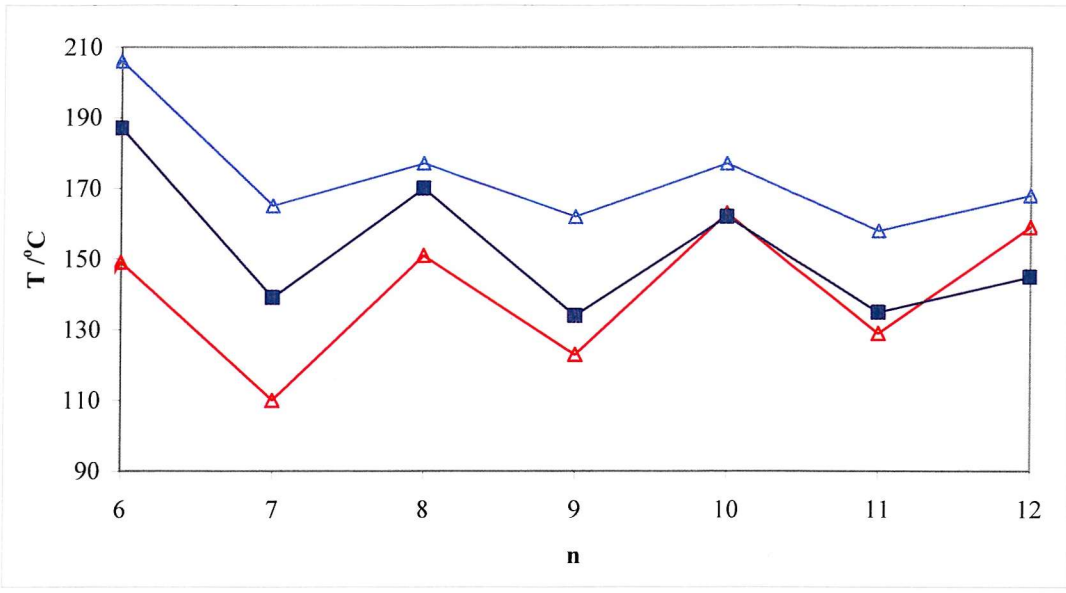

Figure 4.23 The liquid crystal transitions plotted as a function of spacer length for non-symmetric Schiff-base dimer (CBOnO.2) against the CBOnOPCH3 series. Here, ■ denotes T_{CrI} for CBOnOPCH3; Δ denotes T_{NI} for CBOnO.2; Δ denotes T_{SmAN} for CBOnO.2.

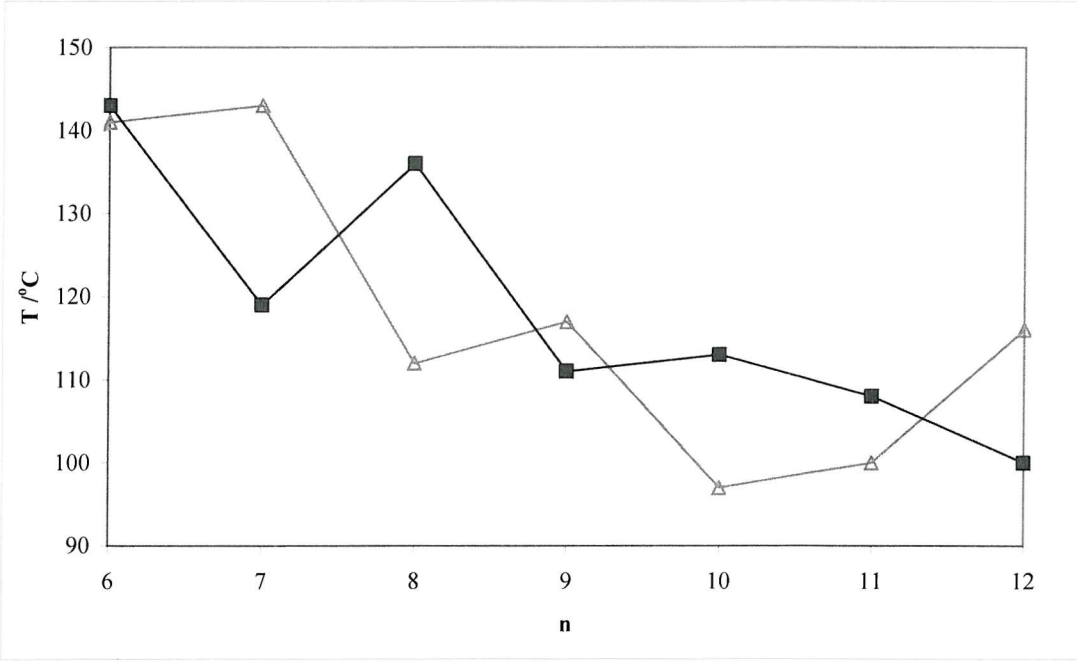

Figure 4.24 The melting transitions plotted as a function of spacer length for non-symmetric Schiff- base dimer (CBOnO.2) against the CBOnOPCH7 series Here, ■ denotes T_{CrI} for CBOnOPCH3 and Δ denotes $T_{CrSmA/CrN}$ for CBOnO.2.

There are two interesting differences between the two series, CBOnOPCH3 and CBOnO.2. The first is the smectic behaviour seen, becoming more stable as n increases for the Schiff-base dimer. Indeed higher order phases (e.g. SmC) are observed when n > 8 but for simplicity these are not shown in Figure 4.23. This is likely to be due to the nature of the Schiff-base/cyanobiphenyl interactions. The fact that no smectic behaviour is observed in CBOnOPCH3 even when n is larger again reinforces the idea that smectic behaviour seen in the -OPCH7 moiety is mostly due to the long terminal chain in comparison to shorter rods.

Finally, looking at the melting points in Figure 4.24, we see that there is a reverse odd-even effect in the melting points for the Schiff-base series. However, this effect also disappears when the spacer is sufficiently long (i.e. after n ≈ 10). Again further comment is limited by the lack of crystallographic evidence and X-ray scattering in the liquid crystal phases.

4.4.3. Entropies of transition

The entropies of transition for CBOnOPCH3 are given in Table 4.7. As expected the dimeric materials show an odd-even effect in the N-I transitional entropies and it is interesting to note how these values compare with the CBOnOPCH7 series (see Table 4.5).

	$\Delta S_{CrN}/R$	$\Delta S_{NI}/R$
6	6.9	1.8
7	13.0	0.5
8	8.7	2.0
9	12.8	0.7
10	11.4	2.1
11	14.4	1.0
12	14.4	2.3

Table 4.7 The transitional entropy data for the CBOnOPCH3.

The CBOnOPCH3 non-symmetric dimers appear to have a larger $\Delta S_{NI}/R$ compared to the analogues with the longer terminal chain (see Figure 4.25) and are very similar to the transitions for the symmetric CBOnOCB series (see Figure 4.24) .

The comparing the symmetric CBOnOCB and non-symmetric CBOnOPCH3 series, the alternation in the odd-even effect is very similar although slightly larger in the case of the CBOnOPCH3. The even members of both series have almost identical transitional

entropies (certainly to within experimental error) and the odd members are slightly different, the symmetric series more ordered in the nematic. The degree of ordering between these two series appears to be very similar and this could be due to the terminal group being short and therefore not much larger than the CN group. Indeed from the crystal structure, the molecular length of the cyanobiphenyl is comparable to the propyl-cyclohexylphenyl (~16Å for OCB compared to ~19Å for OPCH3).[36, 37]

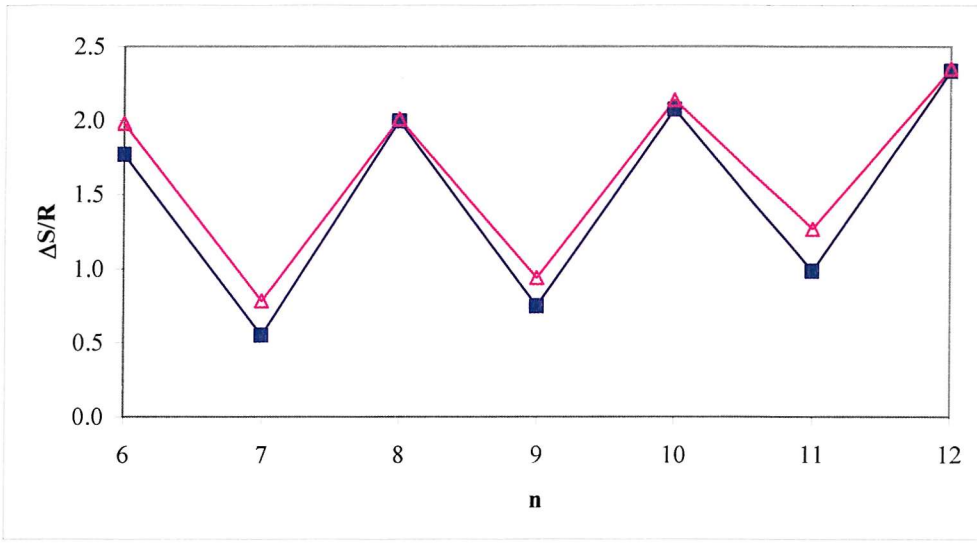

Figure 4.25 Entropy change for the N-I transition for CBOnOPCH3 compared with those for the symmetric CBOnOCB series.[33] Here, Δ is $\Delta S_{NI}/R$ for CBOnOCB and ■ $\Delta S_{NI}/R$ for CBOnOPCH3.

The difference in transitional entropy between the two series for the odd dimers is slightly smaller in CBOnOPCH3. The entropy change increases with spacer length but the difference between CBOnOCB and CBOnOPCH3 dimers remains consistent (within an estimated experimental error of 10%[31]) indicating that the comparative difference in ordering in the odd members is not dramatically altered with increasing spacer length.

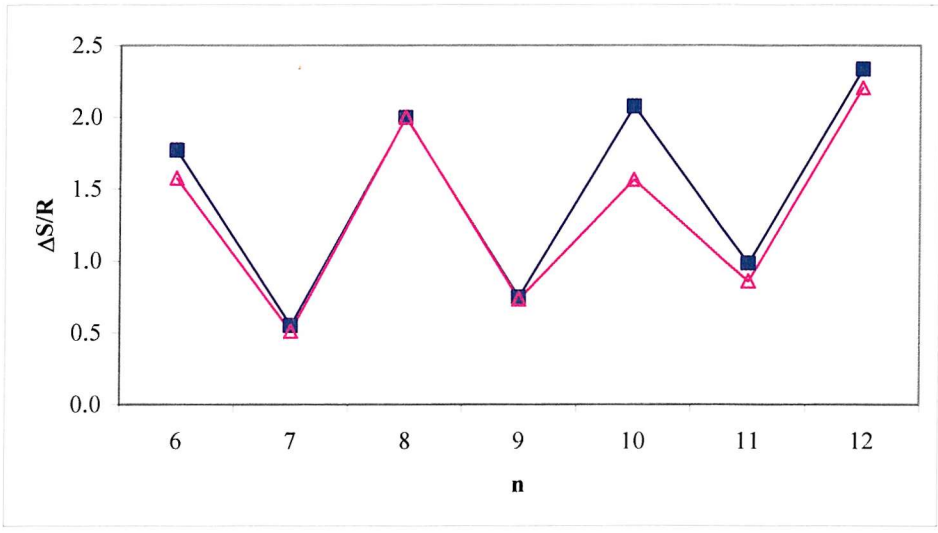

Figure 4.26 Entropy change for the N-I transition for CBOnOPCH3 compared with those for the CBOnOPCH7 series. Here, Δ denotes $\Delta S_{NI}/R$ for CBOnPCH7 and ■ $\Delta S_{NI}/R$ for CBOnOPCH3

Making a comparison with the CBOnOPCH7 series is complicated by the unusual behaviour seen for $n \geq 10$. For the shorter chain homologues we see the transitional entropies are almost identical with agreement for both odd and even dimers. It is unclear why there should be a break down in this similarity between series purely because of the terminal chain length being longer in the -OPCH7 case. However, the similarity in $\Delta S_{NI}/R$ for shorter spacer lengths suggests this deviation is related more to the terminal chain than to the phenyl-cyclohexyl moiety.

No entropy data for the Schiff-base non-symmetric dimers with a small enough terminal chain were available to make a relevant comparison.

4.5. Analyzing the physical data for 3CHPOnOPCH3

Synthesis of the symmetric dimers 3CHPOnOPCH3 allowed a more complete look at the phase behaviour and the transitional entropy as well as allowing a study of the pure systems for their flexoelectric responses. It also allows for a brief examination of whether the T_{NI} of the non-symmetric dimers are the arithmetic mean of the symmetric analogues as has been found for short chain Schiff-base dimers and is predicted in theory.[38]

4.5.1. Optical microscopy

The samples were set up and optical microscopy conducted as described in Section 4.3.1 and the images are given in Figure 4.26. The compounds all showed nematic textures and although some (e.g. n = 6, 8 and to a lesser extent, 10) showed classic two and four brush schlieren textures, many were somewhat less obviously nematic in character. Short chain mesogenic groups are known to display smectic behaviour (e.g. CBOnO.3[35]) although it is more commonly seen in long terminal chain groups (e.g. CBOnO.10[30]). Knowing this, some care was taken in ensuring the observed phases were definitely nematics. For n = 9 and 11 these optical textures, although devoid of schlieren textures in the image, briefly showed a texture at T_{NI} whilst the phase was still forming and the texture disappeared when the phase was properly established (over the course of 1-2 °C). The most curious texture, in terms of appearance, was that of n = 7. Clearly the optical texture is not characteristic but careful study of the texture under the microscope (and just visible in the image) reveals the diagnostic thread-like pattern. The sample also flashes when subject to mechanical pressure.

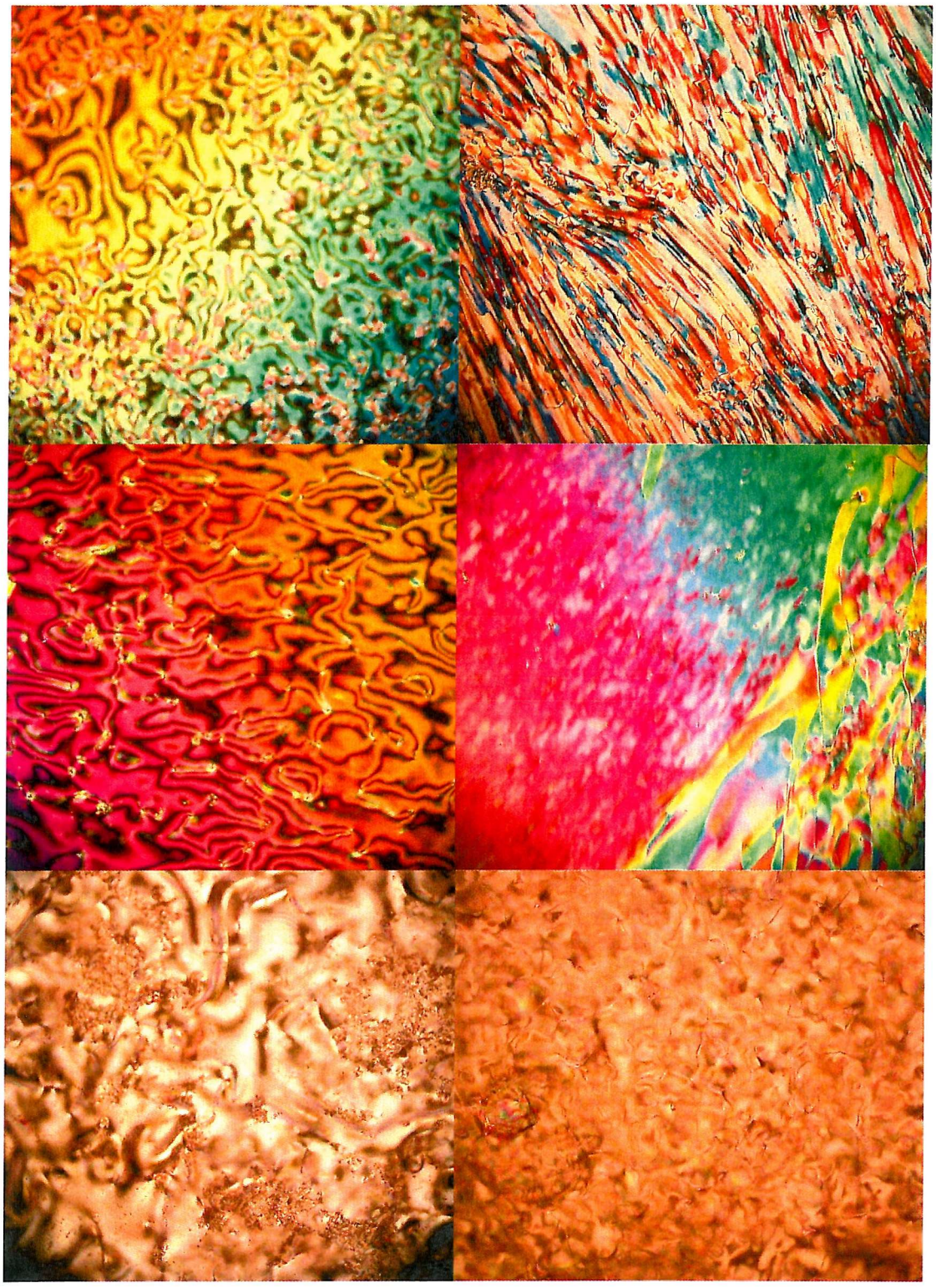

Figure 4.27 All optical texture pictures taken on cooling showing nematic phases. 3CHPO6OCH3 taken at 145 °C, $0.99T_{NI}$ (top left); 3CHPO7OCH3 taken at 78 °C, $0.99T_{NI}$ (top right); 3CHPO8OCH3 taken at 129 °C, $0.99T_{NI}$ (middle left); 3CHPO9OCH3 taken at 94 °C, $0.98T_{NI}$ (middle right); 3CHPO10OCH3 taken at 126 °C $0.99T_{NI}$ (bottom left); 3CHPO11OCH3 taken at 101 °C, $1.00T_{NI}$ (bottom right).

4.5.2. Phase behaviour

The phase behaviour of this series is interesting not only because of the anticipated lower melting points but also because it will improve our understanding of the -OPCH3 group as a mesogenic moiety and the types of phase it supports. The temperatures of transition are given in Table 4.8 as well as the literature values for the same series.[23] We can see there is some variation between the literature data and the measured values, however most of the differences are systematic (~4 °C). Taking this into account, most of the results are within a degree of each other. There are two notable exceptions to this, T_{NI} for n = 8 has no 4 °C discrepancy and T_{NI} for n = 10 is still 5 °C out after taking the systematic difference into account.

Literature values

n	Cr		N		I
6	•	128	•	146	•
7	•	84	•	(77)	•
8	•	105	•	132	•
9	•	88	•	96	•
10	•	106	•	120	•
11	•	92	•	97	•
12	•	108	•	113	•

Measured values

n	Cr		N		I
6	•	136	•	150	•
7	•	88	•	(81)	•
8	•	109	•	132	•
9	•	91	•	101	•
10	•	111	•	129	•
11	•	95	•	102	•
12	•	111	•	117	•

Table 4.8 The transition temperatures for the 3CHPOnOPCH3 series showing the T_{NI} as reported in the literature[23] (left) and the T_{NI} measured on the materials synthesised in-house.

We can see that all members of the series listed in Table 4.8 are nematogenic and almost all are enantiotropic (with the exception of n = 7). The melting points have dropped slightly, as expected, compared to either the symmetric cyanobiphenyl dimers or the non-symmetric CBOnOPCH3 dimers. In addition there is no apparent smectic character despite supercooling the materials by, in some cases (n = 9 and 11), over 40 °C.

4.5.2.1. Comparing 3CHPOnOPCH3 with CBOnOCH3

The series of dimers most closely related to these materials is the CBOnOPCH3 series reported in the previous section and the comparison with this series is shown in Figure 4.28. Looking at the T_{NI} we see that, as expected, both series show an odd-even effect in the T_{NI} and the CBOnOPCH3 has a more stable nematic phase, mostly due to the cyanobiphenyl. As mentioned previously the melting points in the symmetric series are

lower than those of the CBOnOPCH3 series, however, the larger drop in T_{NI} has resulted in the nematic range being reduced for the symmetric dimers.

It is interesting to note for the melting points that whereas the odd-even effect disappears for longer spacer lengths, it persists in the symmetric dimers. This results in a gradual reduction in the nematic range across the series compared to the non-symmetric CBOnOCPCH3 dimers where the nematic range tends to increase with increasing n.

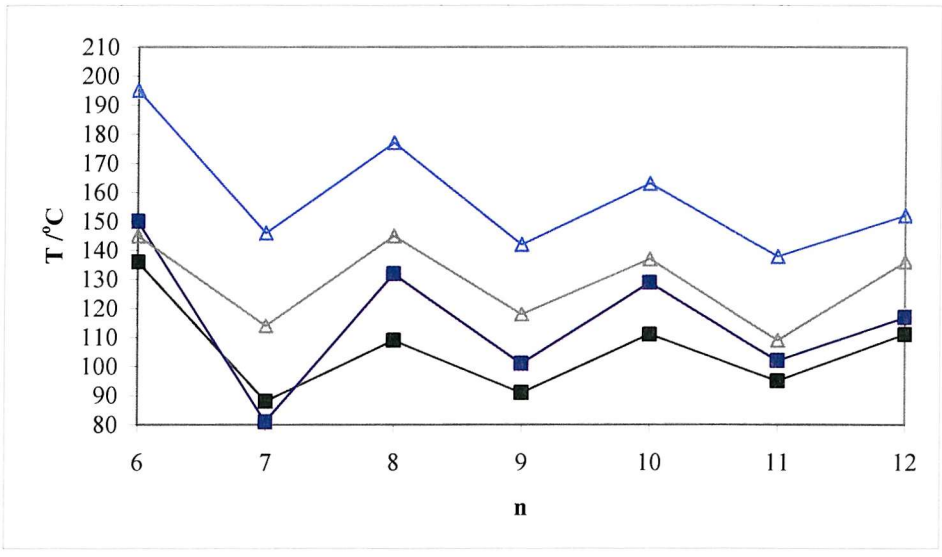

Figure 4.28 The transition temperatures for the 3CHPnOPCH3 series plotted against spacer length and compared with the CBOnOPCH3 series. Here, ■ is T_{CrN} for 3CHPOnOPCH3; ■ is T_{NI} for 3CHPOnOPCH3; \ is T_{CrN} for CBOnOPCH3 and Δ is T_{NI} for CBOnOPCH3.

Comparing the T_{NI}s of the non-symmetric dimers with the average of those for the two series of symmetric dimers (see Table 4.9 and 4.10) we can see, from Figure 2.29, that for the even dimers there is a good fit for n = 6 and 8 but less so for n = 10.

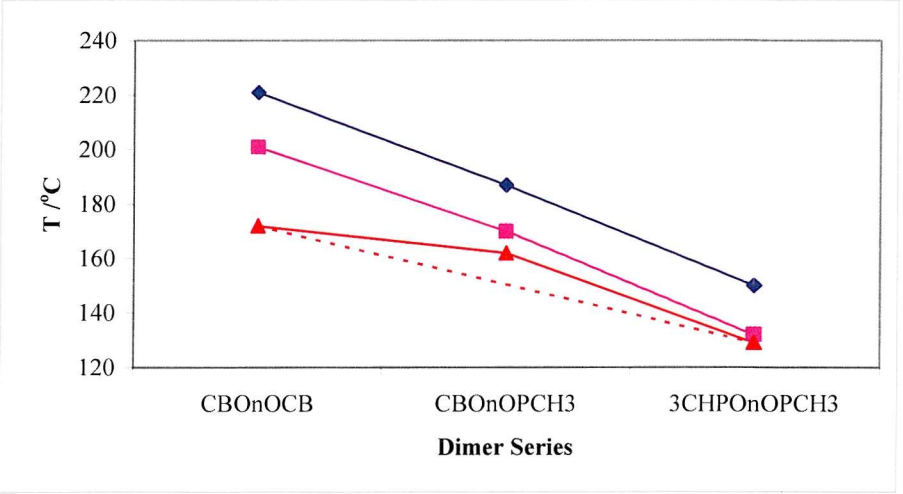

Figure 4.29 T_{NI} for the even members of the three series; CBOnOCB, CBOnOPCH3 and 3CHPOnOPCH3. Here ♦ is n = 6; ■ is n = 8 and ▲ = 10.

Theory suggests that for short terminal chains, agreement between the arithmetic mean of T_{NI} of the two symmetric dimers should be good[30] and this is the case. Even for n = 10 there is only a 12 °C discrepancy which if taken on an absolute temperature scale is less than 3%. What is interesting is that this deviation occurs when n gets larger which is contrary to what is predicted. However without modelling this specific system further speculation is limited other than to look at the odd dimers and to see if similar behaviour is observed.

n	CBOnOCB	CBOnOPCH3	3CHPOnOPCH3
6	221	187	150
8	201	170	132
10	172	162	129

Table 4.9 Table of T_{NI} for even dimers for the two symmetric and one non-symmetric liquid crystal dimers containing the mesogenic groups OCB and OPCH3.

n	CBOnOCB	CBOnOPCH3	3CHPOnOPCH3
7	181	139	81
9	172	134	101
11	164	135	102

Table 4.10 Table of T_{NI} for odd dimers for the two symmetric and one non-symmetric liquid crystal dimers containing the mesogenic groups OCB and OPCH3.

We note in fact the opposite behaviour for the odd members in Figure 4.30. Here, for n = 9 and 11 there is almost no deviation from the mean. For n = 7 there is an 8 °C deviation from linearity which corresponds to a discrepancy of under 2% thus generally in good agreement with theory.

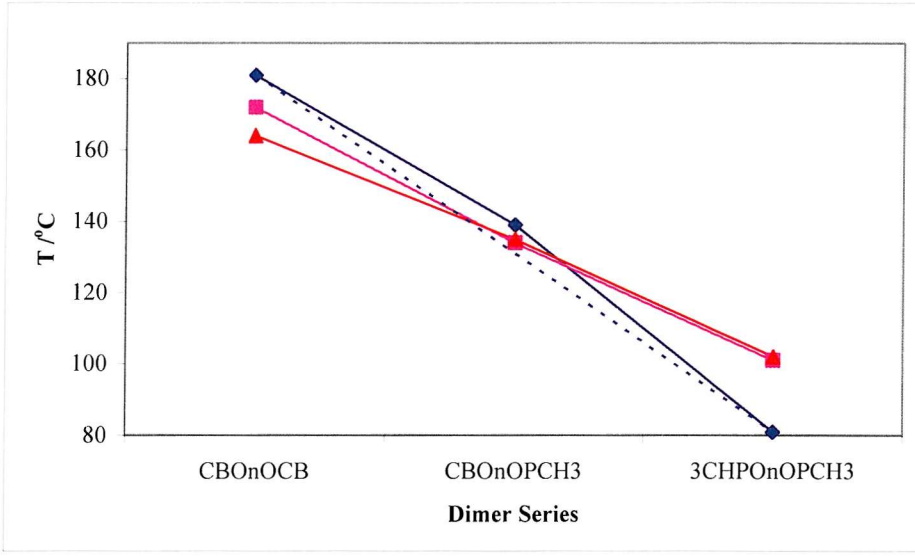

Figure 4.30 T_{NI} for the odd members of the three series CBOnOCB, CBOnOPCH3 and 3CHPOnOPCH3. Here ♦ is n = 7; ■ is n = 9 and ▲ = 11.

It should be noted, however, that if we were to use the symmetric CBOnOCB and the non-symmetric dimer T_{NI} to estimate the N – I transitions for the symmetric PCH3 dimers, with n = 7 and 10 they would be ~20 °C higher than is actually the case.

Finally just to note that if the same plots are made for the Schiff-base dimers (specifically using the mesogenic group with the 2 carbon terminal chain) then we would see a far greater disparity between the non-symmetric dimers and the two symmetric analogues. This presumably is due to the interactions between the different mesogenic groups in the non-symmetric dimers.

4.5.2.2. Comparing 3CHPOnOPCH3 with CBOnOPCH7

Comparisons between the CBOnOPCH3 and 3CHPOnOPCH3 dimers show that the nematic phase is less stable for the symmetric dimer; similarly increasing the terminal chain also destabilises the nematic (comparing the CBOnOPCH7 with the CBOnOPCH3 series).

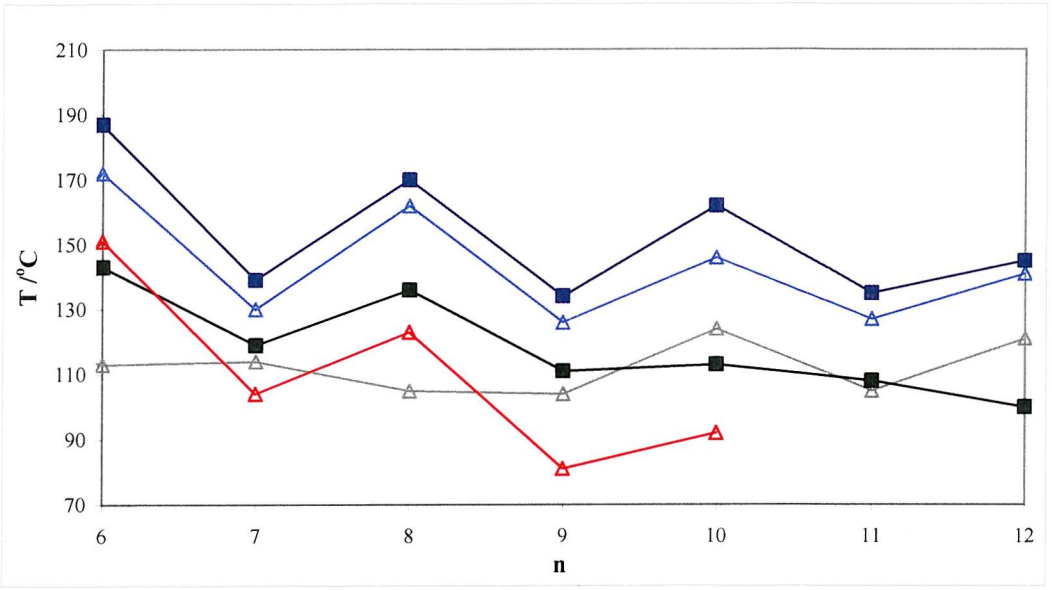

Figure 4.31 The nematic and smectic A transition temperatures as a function of the spacer length for the CBOnOPCH7 dimers against the 3CHPOnOPCH3 series. Here, ■ denotes $T_{CrI/CrN}$ for 3CHPOnOPCH3; ■ denotes T_{NI} for 3CHPOnOPCH3; △ denotes $T_{CrI/CrN/CrSmA}$ for CBOnOPCH7; Δ denotes T_{SmAN} for CBOnOPCH7 and Δ denotes T_{NI} for CBOnOPCH7.

By comparing the symmetric 3CHPOnOPCH3 dimers with the non-symmetric CBOnOPCH7 dimers we see the extent to which increasing the terminal chain affects the mesophasic behaviour compared to changing the cyanobiphenyl to a -OPCH3 group. Comparison with the CBOnOPCH7 series shows the nematic range to be much smaller for the symmetric dimers (see Figure 4.31) which is an unsurprising result given the stabilizing nature of the cyanobiphenyl group and the anisotropic effect of the seven carbon long terminal chain compared to the shorter three carbon long terminal chain on the -OPCH3 group.

Generally the presence of the longer alkyl terminal chain serves to depress the melting point whilst still allowing a reasonably high T_{NI} transition. Although the large nematic range is undoubtedly due to the presence of the cyanobiphenyl, a symmetric 7CHPOnOPCH7 dimer series may be expected to give a range of low melting nematics which, like the symmetric 3CHPOnOPCH3 series, are likely to be relatively low melting (compared to the non-symmetric CBOnOPCH7). With the increased terminal chain length there is the likelihood that the smectic phase would be stabilised further possibly resulting in purely smectogenic behaviour for smaller spacer lengths (this is to some

extent supported by data reported by Kelly for 5CHPO10OPCH5.[19] For examining flexoelectric behaviour the phase must be in the nematic and therefore, for studying this particular property, smectogens are of little practical use.

4.5.2.3. Comparing 3CHPOnOPCH3 with the symmetric Schiff-base 3.OnO.3

Having noted the similarities between the non-symmetric CBOnOPCH3 series and the non-symmetric CBOnO.2 dimers, we can now compare the analogous symmetric dimers. In the previous Section, the closest series for comparison was the CBOnO.2 as the CBOnO.3 data was unavailable. For this Section the data for the analogous Schiff-base 3.OnO.3 is available.[39]

In Figure 4.32 we see much of the same contrasts as in the CBOnOPCH3. In fact what is remarkable is the near identical phase behaviour of the seemingly unrelated series CBOnOPCH3 and 3.OnO.3. The T_{NI}s for both of the symmetric series show an odd-even effect throughout the series with the Schiff-base supporting a more stabilised nematic throughout. The 3.OnO.3 series also consistently has a larger nematic range than the 3CHPOnOPCH3 series despite it also having higher melting points (which also exhibit an odd-even effect).

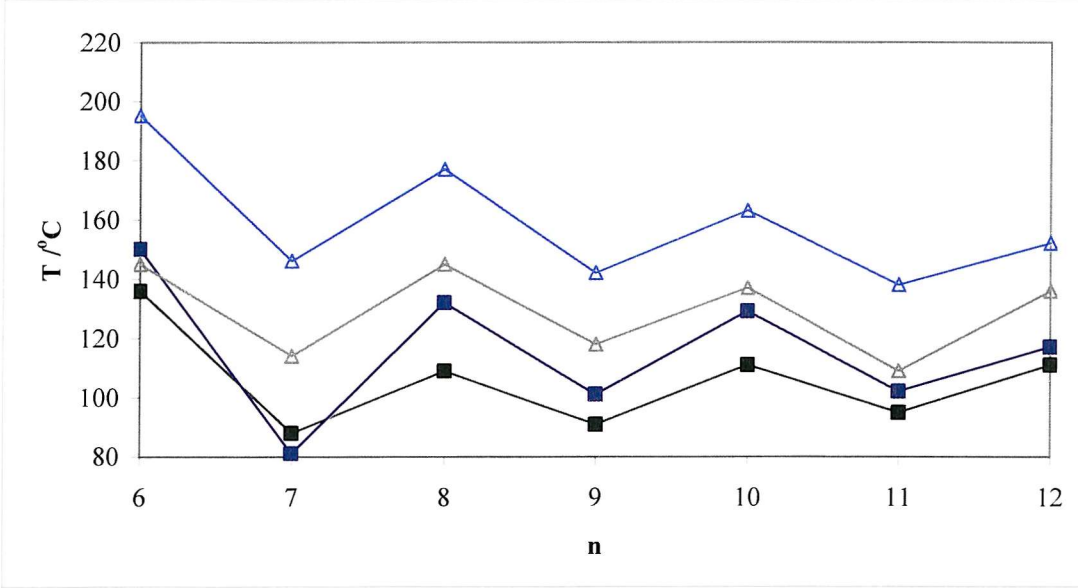

Figure 4.32 The transition temperatures for the 3CHPOnOPCH3 compared with the 3.OnO.3 series plotted as a function of spacer length. Here, ■ denotes T_{CrN} for 3CHPOnOPCH3; ■ denotes T_{NI} for 3CHPOnOPCH3; Δ denotes T_{CrN} for 3.OnO.3 and Δ denotes T_{NI} for 3.OnO.3.

What is interesting to note is that there is no smectic behaviour observed in either series. Although the Schiff-base mesogen does in many dimers support a rich morphology of smectic phases, where the terminal chain is small we see primarily nematic phases and it is reasonable to assume a similar situation exists with the -OPCH3 dimers. Generally, long terminal chains lead to more stable and higher order smectic phases and this appears to be the case for both the non-symmetric and symmetric examples in the -OPCHm series (Kelly *et al.* also publishes data for 5CHPO10OPCH5 which shows a smectic phase[19]).

4.5.3. Entropies of transition

The transitional entropies are given in Table 4.11 and show a behaviour remarkably similar to that seen for the CBOnOPCH3 series.

n	$\Delta S_{CrN}/R$	$\Delta S_{NI}/R$
6	10.0	1.64
7	9.9	0.48
8	12.2	1.94
9	12.1	0.67
10	11.2	2.02
11	14.0	1.00
12	11.7	2.33

Table 4.11 The transitional entropy data for 3CHPOnOPCH3.

Here we see an odd-even effect typical of liquid crystal dimers. It compares closely with both the 3.OnO.3 series and very closely with the CBOnOPCH3 dimers. As can be seen in Figure 4.32 there is almost no difference in $\Delta S_{NI}/R$ for the symmetric CBOnOCB and the non-symmetric 3CHPOnOPCH3 dimers. Given the similarity between the CBOnOCB and CBOnOPCH3 series this should not be so surprising. Clearly the effect of the -OPCH3 mesogenic group on the ordering of the dimers is very similar to that of the cyanobiphenyl.

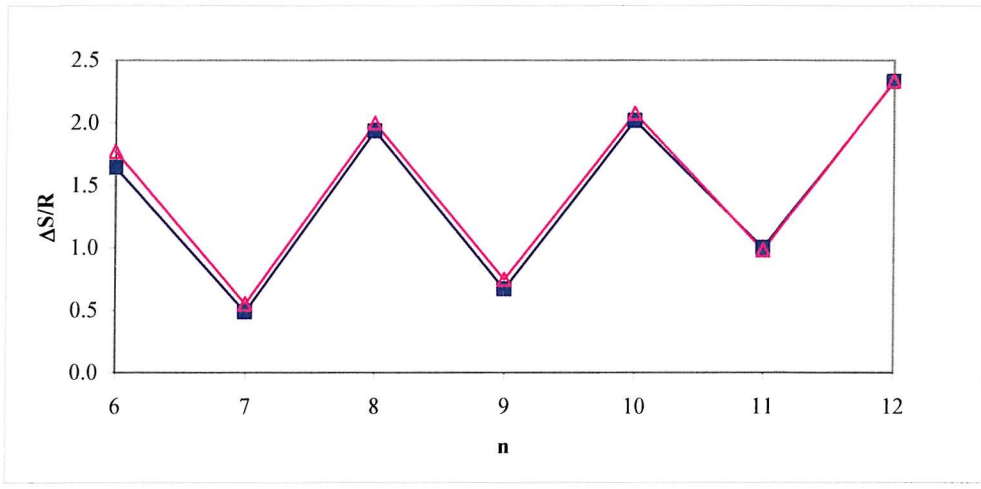

Figure 4.33 Entropy change for the N-I transition for 3CHPOnOPCH3 compared with those for the symmetric CBOnOPCH3 series as a function of spacer length. Here, Δ denotes $\Delta S_{NI}/R$ for CBOnOPCH3 and ■ denotes $\Delta S_{NI}/R$ for 3CHPOnOPCH3.

Without making measurements on the orientational order parameter we cannot quantify the similarity between the CBOnOPCH3 and 3CHPOnOPCH3 series but it does mean that any differences between the materials in terms of the flexoelastic ratio is unlikely to be due to differences in the order of the materials.

Comparing the symmetric CBOnOPCH3 series with the symmetric Schiff-base (see Figure 4.34) we see that there is again a similarity however it is not as close as with the CBOnOPCH3 series. This is to be expected given the difference in shape and electronic structure of the mesogenic groups. However we see that as the spacer chain gets longer the transitional N-I entropies of the materials become more similar. This may simply be due to the dilution effect of the mesogenic groups by the increase in the chain length. Thus the difference in ordering between the liquid crystal and the isotropic liquid becomes more dependent on the spacer (which is common between the two series) and less on the mesogenic groups.

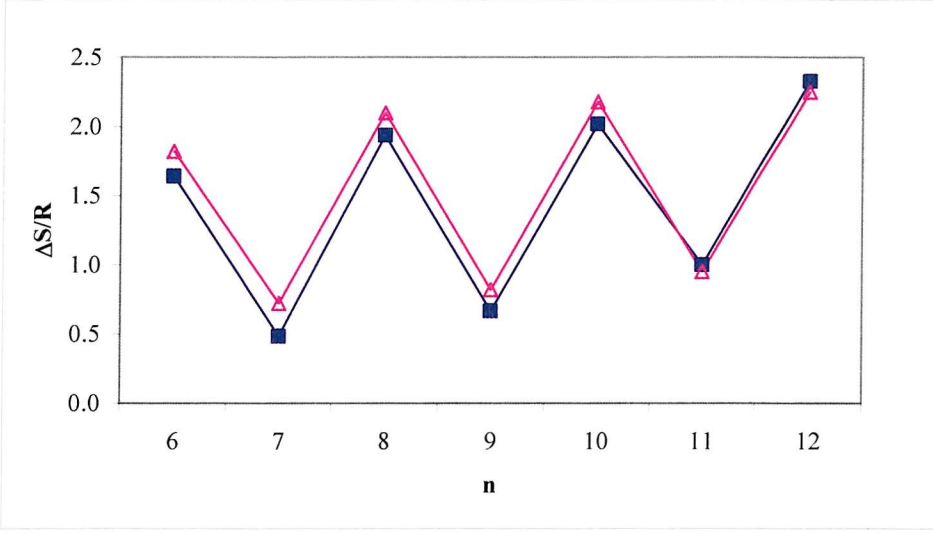

Figure 4.34 Entropy change for the N-I transition for 3CHPOnOPCH3 compared with those for the symmetric 3.OnO.3 series.[39] Here, Δ denotes $\Delta S_{NI}/R$ for 3.OnO.3 and ■ denotes $\Delta S_{NI}/R$ for 3CHPOnOPCH3.

4.6. Flexoelastic properties

The surprising results published by Kelly *et al.* with an odd-even effect in $\bar{e}/\bar{K}$ which shows the even dimers dissolved in E7 as having a larger flexoelastic ratio than the odd can now be better understood by placing them in a wider context. The order in which the following results are presented may seem counter intuitive; however, the results from the symmetric series changed the course of the study leading us back to examine mixtures using materials from the CBOnOPCH3 series. In all cases the materials were studied using the experimental setup and procedure described in Chapter 2. Thus using the Meyer convention (again described in Chapter. 2) the results presented are for the flexoelastic ratio $\bar{e}/\bar{K}$ and the scaled flexoelastic ratio $\bar{e}P/\bar{K}$ where $\bar{e} = e_1 + e_3$ and $\bar{K} = K_1 + K_3$.

As with measurements made with materials in Chapter 3, measurements on the pitch of the system were critically compromised by the high melting points and relatively small nematic range of the pure dimer systems. As described in Chapter 3, for the purposes of comparison the data were handled in two ways, each with their own shortcomings. To extract $\bar{e}/\bar{K}$ from the results the pitch was estimated based on the concentration of the chiral dopant and the HTP (helical twisting power) of the chiral dopant R5011 (supplied by Merck) in a low melting dimer mixture (developed by Merck) which was found to be

163 $mol^{-1}\mu m^{-1}$. As explained in Chapter 3 the HTP is known to change significantly with spacer parity but also with different mesogenic groups. The compounds studied in this Chapter, have significantly different mesogenic end groups compared to these in used in the mixture which increases the potential error in using this estimation. The other method of comparison involves incorporating the pitch with the flexoelastic ratio to give $\bar{e}P/\overline{K}$. This eliminates errors from estimating the pitch poorly but by incorporating the pitch into the measurement we are really getting a measure of angular dependence of the optic axis on the flexoelastic ratio for a specific pitch rather than a general measure.

4.6.1. Investigating the symmetric CBOnOPCH3 series

Previous studies of the flexoelastic ratio across a series of dimers show an odd-even effect across the series.[1, 9]

n	E_{th} /Vμm^{-1}	R5011 /mol%	(e/K) /$CN^{-1}m^{-1}$	eP/K /x$10^{-7}CN^{-1}$
6	6.21	1.98	0.55	1.69
7	6.53	2.07	0.83	2.44
8	7.16	2.28	0.65	1.74
9	9.15	2.63	0.83	1.93
10	4.10	1.96	0.85	2.66
11	6.64	2.07	0.83	2.46
12	7.96	3.00	0.71	1.45

Table 4.12 Data for CBOnOPCH3 where n = 6 – 12 taken at $T^* = 0.98$; showing the flexoelastic ratio, threshold voltage, the percentage molar concentration of the chiral dopant R5011 and scaled flexoelectric ratio $\bar{e}P/\overline{K}$.

The pattern of the alternation is not necessarily expected to be consistent; however, as the contribution from the elastic constant is known to be larger for even dimers than for odd members[9] and the reverse understood to be true for the flexoelectric coefficients.[1, 9]

We can see from Table 4.12 that the magnitude of $\bar{e}/\overline{K}$ is not as large as that seen for many of the fluorinated non-symmetric liquid crystal dimers. More interesting is the interruption in the odd-even effect at n = 10. This is more obviously seen in Figure 4.35 where there is a clear odd-even effect throughout the series with the exception of n = 10. In terms of understanding whether this is as a result of the elastic constants or the flexoelectric ratio it is impossible to be certain. Clearly the effect of $\overline{K}$ for the even dimers preceding and after this result has not been to increase $\bar{e}/\overline{K}$ by any great amount

so there is no clear reason to assume it should do so in this one isolated case. Again there is no real evidence to suggest why $\bar{e}$ should be so much larger for n = 10 when n = 6, 8 and 12 increase quite smoothly.

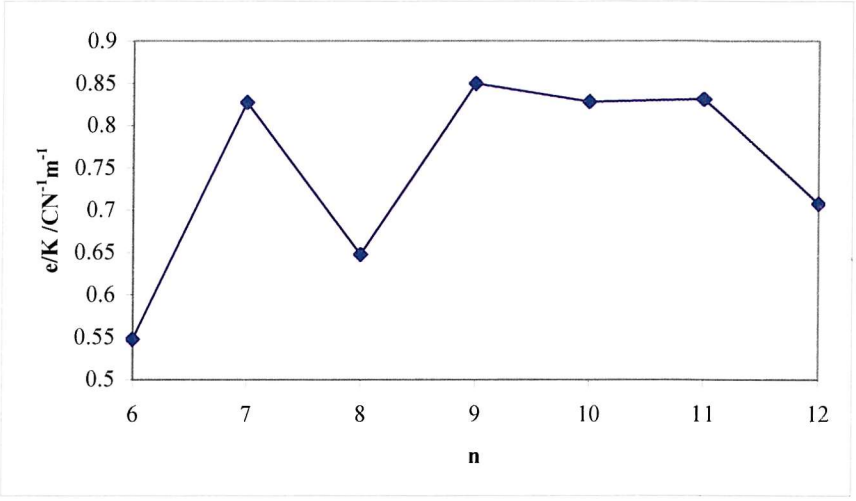

Figure 4.35 The flexoelastic ratio plotted as a function of spacer length taken at $T^* = 0.98$. Here ■ denotes $\bar{e}/\overline{K}$ for CBOnOPCH3.

One possible answer could lie in the very different value for E_{th} measured for this material (E_{th} = 4.10 Vμm^{-1} for n = 10 compared to E_{th} = 6.21 Vm^{-1}, 7.16 Vm^{-1} and 7.96 Vm^{-1} for n = 6, 8 and 12 respectively). This could suggest a significant difference in K_2 for this material which would mean a much larger error in using a constant value of 163 μm^{-1} for the HTP of the chiral dopant. For example a value of 120 μm^{-1} would give a value closer to 0.7 CN^{-1}m^{-1}.

n	(e/K) /CN^{-1}m^{-1}	P /nm	eP/K /x10^{-7}CN^{-1}
5	1.45	305	4.423
6	0.45	440	1.980
7	1.29	307	3.960
8	0.52	495	2.574
9	1.24	313	3.881
10	0.52	445	2.314
11	1.33	340	4.522
12	0.55	367	2.019

Table 4.13 Published data for $CBOnOBF_2$ where n = 5 – 12 taken at $T^* = 0.84$; showing the flexoelastic ratio, the pitch and the scaled flexoelastic ratio $\bar{e}P/\overline{K}$.[1]

As mentioned previously, another way of examining the data is to incorporate the pitch into $\bar{e}/\overline{K}$ and seeing how $\bar{e}P/\overline{K}$ varies with spacer length. This quantity is contrasted with that calculated from the published data for the $CBOnOBF_2$ series (see Table. 4.13).[1] Plotting $\bar{e}P/\overline{K}$ against the spacer length, n, (see Figure 4.36) we see that for the CBOnOPCH3 series there is now a distinct, continuous odd-even effect. The published values of the $CBOnOBF_2$ series show a much larger odd-even alternation where both the odd and the even dimers have generally larger values of $\bar{e}P/\overline{K}$ than the CBOnOPCH3 series. The $\bar{e}P/\overline{K}$ for the odd members of the CBOnOPCH3 series are about the same magnitude as the even members of the $CBOnOBF_2$ series.

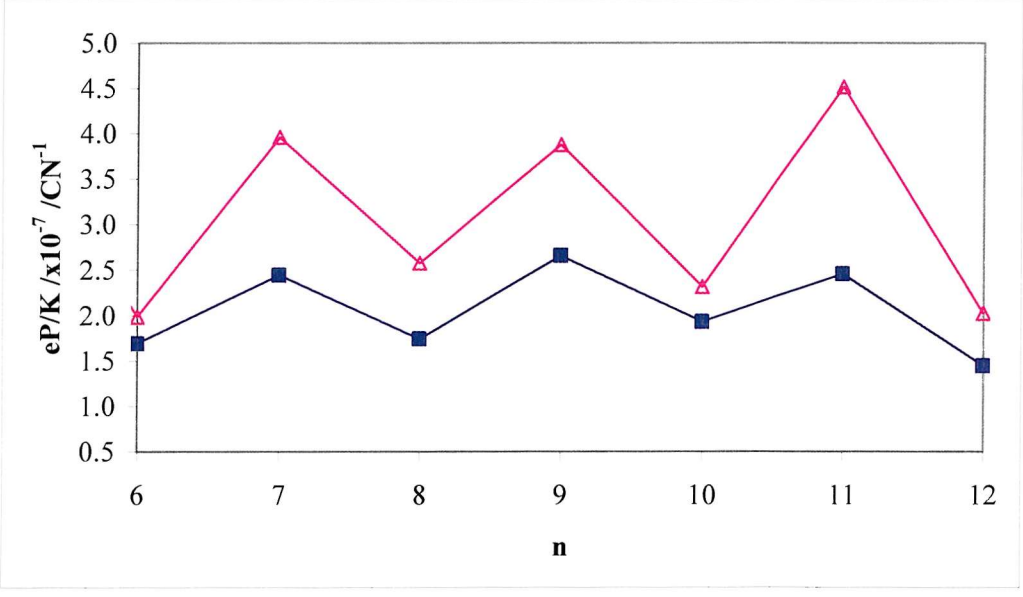

Figure 4.36 The scaled flexoelastic ratio of CBOnOPCH3 taken at $T^* = 0.98T_{NI}$ compared to the literature value for $CBOnOBF_2$ taken at $T^* = 0.84$ plotted as a function of temperature. Here ■ denotes the $\bar{e}P/\overline{K}$ for CBOnOPCH3 and Δ denotes $\bar{e}P/\overline{K}$ for $CBOnOBF_2$.

Generally the odd dimers consistently show a slightly higher value of $\bar{e}P/\overline{K}$ although this is with the exception of n = 10. With the inclusion of the pitch in the elastic constant it suggests that the unusually high value for n = 10 is related to using an estimated value of the HTP of R5011. We can also use the threshold unwinding field as a guide to the pitch of the helix and we see that the $E_{th} \sim 4$ $V\mu m^{-1}$ for n = 10 compared to ~ 9 $V\mu m^{-1}$ for the other materials.

The conclusion is that the series generally follows the trend expected in $\bar{e}/\overline{K}$ for a typical dimer series. The magnitude of the values for $\bar{e}/\overline{K}$ are smaller than those of the $CBOnOBF_2$ series but this is not surprising as the number of polar atoms and groups in the -OPCH3 moiety is much less than that of the $-OBF_2$ group would tend to increase $\bar{e}$.

4.6.2. Investigating the symmetric 3CHPOnOPCH3 series

The flexoelastic ratios published by Kelly *et al.*, which gave such large values of $\bar{e}/\overline{K}$, but more curiously gave a reverse odd-even effect for the dimers when dissolved in E7, were an obvious target for examination. The mystery surrounding what was causing this result and to what extent it was related to the materials or to the host was a key motivating force to make the materials reported in this Chapter. In this section we look at pure symmetric systems and try to find some answers to the questions posed by these unusual results.

4.6.2.1. Pure system

Clearly we have seen that, with one exception, the CBOnOPCH3 series gives typical odd-even behaviour in $\bar{e}/\overline{K}$ when plotted against the spacer length (i.e. the odd is greater than the even). However, the effect of the cyanobiphenyl group on the system is clearly profound (seen in the difference in T_{NI}) so making the symmetric dimer series enables us to evaluate of the flexoelectric behaviour of these materials in the pure system.

However there were problems encountered in the procedure for making the flexoelastic measurements which proved prohibitive to obtaining reliable data. These problems relate to the nature of the material and the method used to create the ULH texture (described fully in Chapter 2). The procedure depends on being able to align the helix axis parallel to the plane of the cell. Uniform alignment is then achieved by unwinding the helix and then applying mechanical action to the cell causing the nematic to move. The field strength is reduced and the director arranges itself into a helix which is in a uniform direction. There are two key properties which the nematic must possess for this procedure to work. The first is that the dielectric anisotropy is large enough to interact with the field. A first glance at the molecular structure in Figure 4.37 may beg the belief that this is not the case although it can be shown to a reasonable approximation that the size of the

dipole in these molecules should be sufficient to give a reasonable $\Delta\tilde{\varepsilon}$. The second requirement is that $\Delta\tilde{\varepsilon}$ must be positive. This is crucial for this methodology as the helix would align perpendicular to the plane of the cell resulting in a dark state corresponding to the helix axis being perpendicular to the plane of the cell. Qualitative analysis looking purely at the idealised structure of any of the 3CHPOnOPCH3 materials would suggest that these materials would be likely to have a negative dielectric anisotropy.

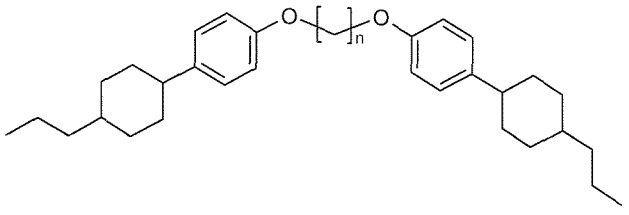

Figure 4.37 General structural formula for 3CHPOnOPCH3. Note: the bent shape is only true when n is odd.

The effect of applying a potential of approximately 7.5 V to a sample of CBO9OPCH3 compared with the symmetric analogue is profound (see Figure 4.38).

In the case of the non-symmetric dimer, the helix axis starts aligned in any direction but in the case shown in Figure 4.38a it is predominantly with the helix axis perpendicular to the plane of the cell. The dark regions of the cell are the liquid crystal, when the field is applied (see Figure 4.38b) the helix axis moves to the plane of the cell but is not in a uniform direction. With the helix axis now in the plane of the cell light can pass though the cell as shown.

In the case of the 3CHPO9OPCH3 the helix axis is again in all directions but again predominantly perpendicular to the cell (note the difference in colour of the dark state for Figure 4.38a and 4.38c and d is a result of the camera rather than something intrinsic to the cell). When the field is applied the cell still remains dark. In fact if the field is increased the region becomes darker as more of the helix is aligned with its axis perpendicular to the plane of the cell. Again mechanically manipulating the cell has the same effect.

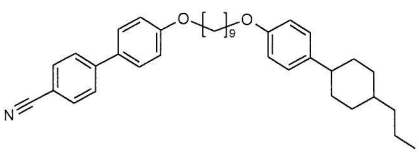

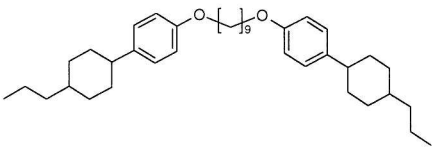

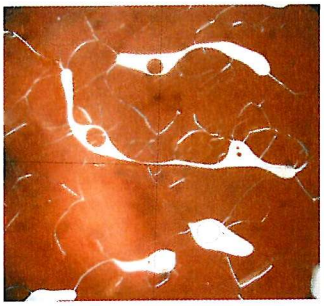

E = 0

c)

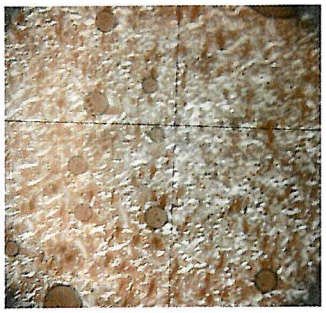

E ≠ 0

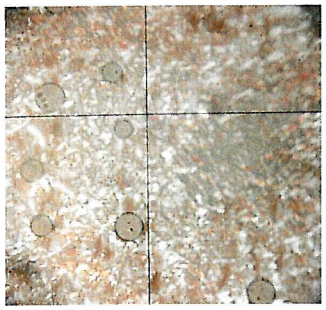

cells were filled and measurements made as described previously. The results are given in Table 4.14.

n	(e/K) /$CN^{-1}m^{-1}$	P /nm	e /pCm^{-1}
6	0.37	523	5.35
7	0.25	597	3.58
8	0.33	500	4.79
9	0.12	559	1.76
10	0.23	590	3.42
11	0.33	498	4.77
12	0.45	536	6.55

Table 4.14 The flexoelastic ratio of 3CHPOnOPCH3 as a 20% (by wt) solution in E7 at $T^* = 0.98$.

The key advantages of using E7 as a host is that values for the HTP (which was taken to be 100 $\mu m^{-1}mol^{-1}$) and for $\overline{K}$ of E7 can be used to estimate the pitch and the flexoelectric coefficient more accurately. The flexoelectric coefficients were determined by multiplying by the elastic constant using $\overline{K} = 14.6$ pN (value taken from the Merck database of information for the properties of E7). Before analysing these materials we should note that the methodology employed by Kelly and that which was available to measure the flexoelastic ratios of these materials is quite different. Kelly *et al.* used an in-plane electric field on a HAN cell without the addition of a chiral dopant. However as commented in Chapter 2, since both Kelly and ourselves are using the same convention (that is $\mathbf{B} = \mathbf{n} \times \nabla \times \mathbf{n}$) both methods should give $\bar{e} = e_1 + e_3$.[40] It is of some concern that we are getting results which are very different in magnitude.

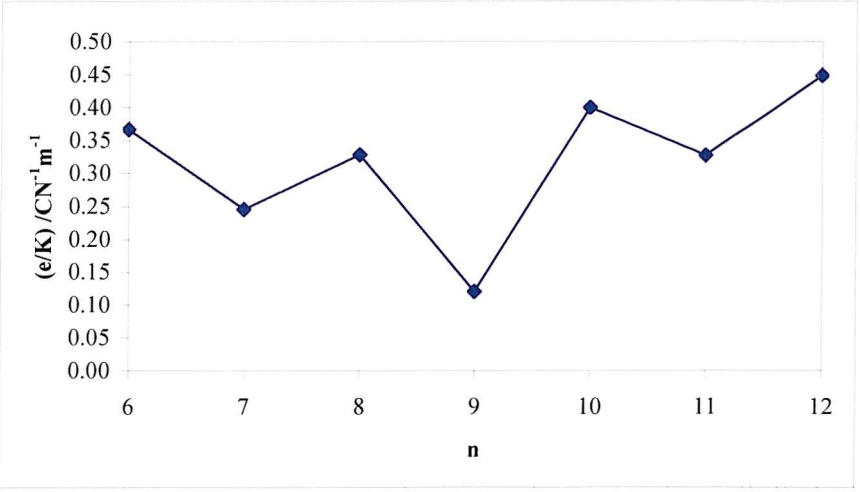

Figure 4.39 The flexoelastic ratios of 3CHPOnOPCH3 in E7 compared to $\bar{e}/\bar{K}$ in undoped E7 taken at T^* = 0.98. Here ■ denotes $\bar{e}/\bar{K}$ for 3CHPOnOPCH3 and - - - denotes the value for E7 not doped with a dimer.[41]

Although the size of $\bar{e}/\bar{K}$ is different, we see in Figure 4.39 that there is indeed a reverse odd-even effect in E7. The values of $\bar{e}/\bar{K}$ are quite small, in most instances smaller than that of E7 which is in stark contrast to the huge increase in $\bar{e}/\bar{K}$ reported by Kelly. Although Kelly does not report any organic characterisation data we can assume that such a difference in results is unlikely to occur due a small impurity and more likely as a result of the method used to measure the property. Without using both methods on the same materials there is no way of being certain why there is such a discrepancy. Several samples were re-measured and verified the results given.

Kelly clearly reports the method and correctly states that, given the convention he is using, this should give the sum of the flexoelectric coefficients. However if we consider how $\bar{e}$ varies depending on whether the sum or the difference is taken, we note a counter-intuitive result. Using the data calculated by Ferrarini for the CBOnOCB dimers (see Table 4.15 and 4.16) we can show the difference between adding e_3 and subtracting e_3 from e_1. These results are only useful as a guide as they do not include conformational weighting and of course they are calculated for dimers with very different mesogenic group.

	Dipolar		Quadrupolar		Sum	Difference
	e_1	e_3	e_1	e_3	$e_1 + e_3$	$e_1 - e_3$
t	0	0	53	-53	0	106
g1	-1	40	28	-28	39	15
g2	1	21	47	-47	22	74
g3	-3	42	24	-24	39	3
g4	1	17	49	-49	18	82
g5	-3	43	23	-23	40	0
				Mean	26	47

Table 4.15 The sum and difference of e_1 and e_3 using the results calculated by Ferrarini (see Figure 4.8) for CBO8OCB with the spacer in the all trans form (t) and with a gauche link in different places along the chain (g1-5).

	Dipolar		Quadrupolar		Sum	Difference
	e_1	e_3	e_1	e_3	$e_1 + e_3$	$e_1 - e_3$
t	0	6	45	-45	6	84
g1	0	28	32	-32	28	36
g2	0	36	32	-32	36	28
g3	0	30	33	-33	30	36
g4	0	33	33	-33	33	33
				Mean	27	43

Table 4.16 The sum and difference of e_1 and e_3 using the results calculated by Ferrarini (see Figure 4.9) for CBO7OCB with the spacer in the all trans form (t) and with a gauche link in different places along the chain (g1-4).

Taking the unweighted mean for the sum and the difference of e_1 and e_3 for each of the conformers calculated, we see that e_1 - e_3 gives consistently larger values of $\bar{e}$. This is largely due to the dominance of the quadrupole contribution which is not seen for $e_1 + e_3$ where the two contributions cancel. Therefore, should Kelly have in fact measured $e_1 - e_3$, for compounds such as the 3CHPOnOPCH3 series where clearly the dipolar contribution will be quite small, we might expect his results to be substantially larger.

A possible explanation for the peculiar odd-even effect could lie in the ordering of the host. When subject to either splay, bend or a combination of both director deformations, the more ordered the material, the greater the director deformation. Using this logic, if the even dimers were to order the host more than the odd, we may anticipate a reverse odd-even effect such as that seen.

4.6.2.3. Studying binary mixtures of 3CHPO11OPCH3 and CBO11OPCH3

To determine an approximate value for $\bar{e}/\overline{K}$ for the symmetric dimers, one member of the series was investigated by creating a binary mixture with the equivalent non-symmetric dimers. Ideally this would be done for the entire series, but the lack of available materials made this more extended study impossible within the time available. The aim of this study was not only to try and determine an absolute value for $\bar{e}/\overline{K}$ but also to examine systematically the effects of changing the concentration of one dimer mixed with another on the flexoelastic ratio. The compounds used were 3CHPO11OPCH3 and CBO11OPCH3 and the results are given in Table 4.17.

% mol composition of 3CHPO11OPCH3	(e/K) /$CN^{-1}m^{-1}$	T_{N*I} /°C
0	0.83	135
20	1.09	131
40	0.65	126
60	0.23	120

Table 4.17 Results for $\bar{e}/\overline{K}$ and the N-I transition temperature measured for the symmetric 3CHPO11OPCH3 and the non-symmetric CBO11OPCH3 for mixtures of varying composition. Measurements taken at $T^* = 0.98$.

Consideration of the N-I transition temperatures shows that there is a linear relationship between the T_{NI} as composition changes in the mixture. This can best be seen in Figure 4.40.

A linear decrease in T_{NI} with changing composition is the expected result[38] which is encouraging in that it suggests that there are no unusual interactions between the two dimers. Had there been an unexpected behaviour the result would have complicated interpreting the results for $\bar{e}/\overline{K}$.

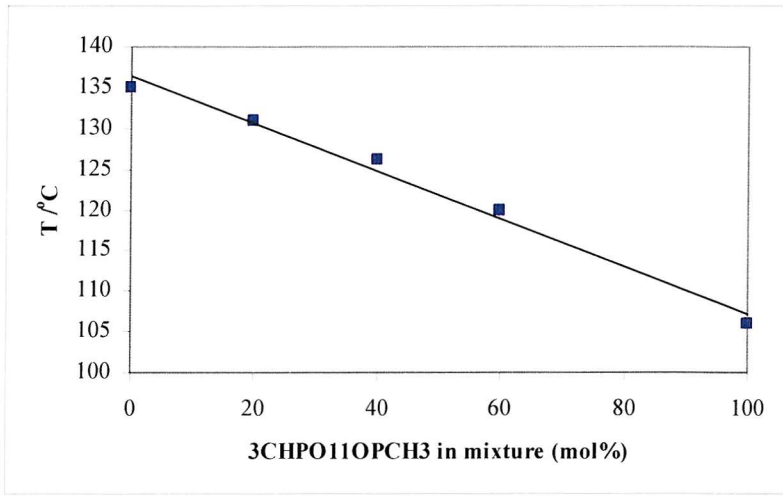

Figure 4.40 The change in N-I transition temperature with changing concentration of the 3CHO11OPCH3 dimer in CBO11OPCH3. Results taken from microscope observations.

Plotting $\bar{e}/\overline{K}$ for the mixture against concentration of 3CHPO11OPCH3 (see Figure 4.41) we can see several interesting features. The first and most important is that the relationship is not linear and that $\bar{e}/\overline{K}$ actually increases slightly with the addition of low concentrations of the symmetric dimer.

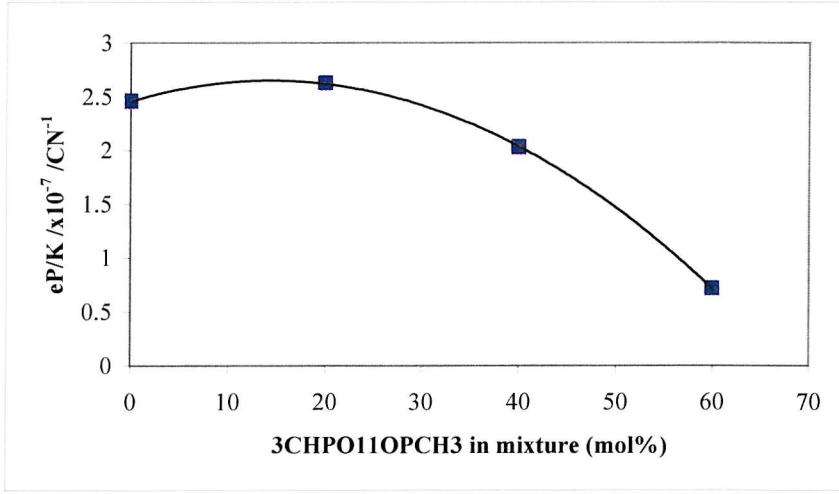

Figure 4.41 The scaled flexoelastic ratio for a binary mixture of 3CHPO11OPCH3 and CBO11OPCH3.

With changing the composition there would be a change in the flexoelectric coefficients and the elastic constant and both properties are affected by any change in the orientational order in the nematic. These properties all contribute to the size of $\bar{e}/\overline{K}$ so it

is likely that the relationship would be complex (i.e. not linear). This is an important result as no pure materials with large flexoelastic ratios exist that are room temperature melting and as such we are reliant on mixtures to achieve practical materials which could be used in devices. Therefore if the relationship between two very similar materials in a binary mixture is not simple, then there is a need to study how varying the composition of mixtures generally affects the flexoelastic ratio through either a practical or theoretical means.

The other interesting feature to note is that as the composition contains more of the symmetric dimer, $\bar{e}/\overline{K}$ becomes more negative. Trying to make sense of what this means physically is more complicated. The change from positive $\bar{e}/\overline{K}$ to negative will approximately correspond to the change from a positive to a negative dielectric anisotropy with $\bar{e}/\overline{K} = 0$ corresponding to $\Delta\tilde{\varepsilon}$ being almost zero. This is the same observation made by Rudquist *et al.* when they used a liquid crystal with a temperature sensitive $\Delta\tilde{\varepsilon}$ to improve their flexoelectric measurements[42]. They noted a change in phase which they attributed to a change in sign of $\bar{e}$ which correlated to the change in sign of the dielectric anisotropy of the sample. This relationship between the flexoelectric effect and the dielectric anisotropy is a product of the experimental setup rather than an general relationship.

Using the original diagrams denoting the bend and splay deformation and the direction of the field, a negative value of either e_1 or e_3 would correspond to a reversing in the direction. of the director deformation.

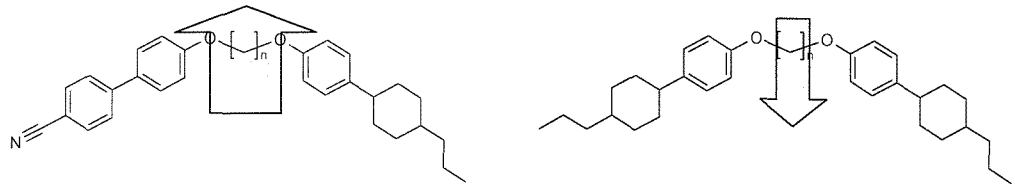

Figure 4.42 The structures of the dimers 3CHPO11OPCH3 and CBO11OPCH3. Here the net dipole across the molecule is described in a qualitative fashion by the size and direction of the green arrow going from negative to positive.

Considering the all-trans form of the non-symmetric and symmetric dimers (see Figure 4.42) we can see that by estimating the net dipole across the molecule we can deduce that

the direction of the polarisation is opposite in sign for the two molecules and larger for the non-symmetric dimer. This result is reflected in $\bar{e}/\overline{K}$, assuming that e_1 is small and e_3 is positive for the CBOnOPCH3 (and others examples) and negative for 3CHPOnOPCH3.

4.6.3. Investigating the non-symmetric CBOnOPCH7 series

Considering the non-symmetric CBOnOPCH7 we are faced with structural differences in the molecule compared to that of the CBOnOPCH3. The extra length of the terminal chain can contribute to the bent shape of the molecule (which should have a positive impact of the flexoelectric effect) however the dilution of the dipole from the increase in molecular volume should reduce the size of the effect.

n	% R5011	E_{th} /Vμm^{-1}	(e/K) /CN^{-1}m^{-1}	eP/K /x10^{-7}CN^{-1}
4	2.16	2.62	0.67	1.88
5	1.65	3.22	0.51	1.88
6	2.23	5.63	0.76	2.09
7	1.90	5.04	0.67	2.15
8	1.91	5.23	0.44	2.18
9	1.93	6.04	0.55	2.97
10	1.95	5.23	0.71	2.24
11	2.01	5.69	0.81	2.48
12	4.50	8.65	1.00	1.36

Table 4.18 Table of data for CBOnOPCH7 where n = 6 – 12 taken at $T^* = 0.98$; showing the flexoelastic ratio, threshold voltage, the percentage molar concentration of the chiral dopant and scaled flexoelectric ratio $\bar{e}P/\overline{K}$.

In Table 4.18 we see there is considerable variation in threshold voltage, however when the quantity of chiral dopant is also taken into consideration this variation is not quite so large. For n = 6 – 11 the variation threshold field remains constant with chiral dopant. The large threshold fields do not however correlate with the larger flexoelastic coefficients. For example n = 9 has an E_{th} of 6.04 Vμm^{-1} but only an $\bar{e}/\overline{K}$ of 0.55, smaller than that for n = 11 which has a smaller threshold voltage.

We can clearly see that the results of $\bar{e}/\overline{K}$ for the CBOnOPCH7 series (see Table 4.18) are generally smaller than for the CBOnOPCH3 series (see Table 4.12). More interesting is that there is no odd-even effect for the early members of this series. This is most clearly seen graphically in Figure 4.43 where $\bar{e}P/\overline{K}$ for the CBOnOPCH7 series is

plotted against $\bar{e}P/\overline{K}$ for the CBOnOPCH3 series. Contrasting this data we see that there are some interesting differences in the CBOnOPCH7 series. We can see that where there is no odd-even alternation (n = 4 – 8), the even members give quite large $\bar{e}P/\overline{K}$ values, larger than the comparative CBOnOPCH3 series. After n = 8 an odd-even alternation emerges and this appears to follow the alternation in the CBOnOPCH3 series fairly well becoming closer in value for n = 11 and 12.

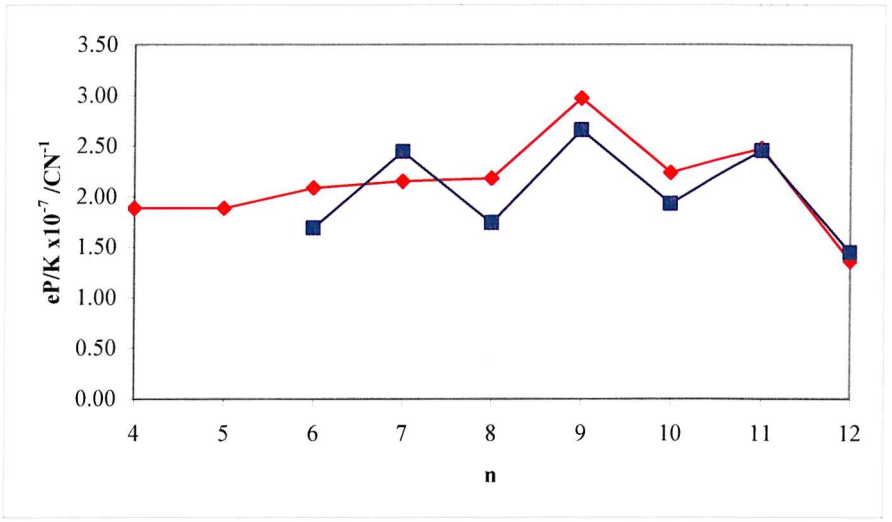

Figure 4.43 The scaled flexoelastic ratio as a function of spacer length for CBOnOPCH7 and CBOnOPCH3 measured at $T^* = 0.98$. Here ♦ denotes $\bar{e}/\overline{K}$ for CBOnOPCH7; ■ denotes $\bar{e}P/\overline{K}$ for CBOnOPCH3.

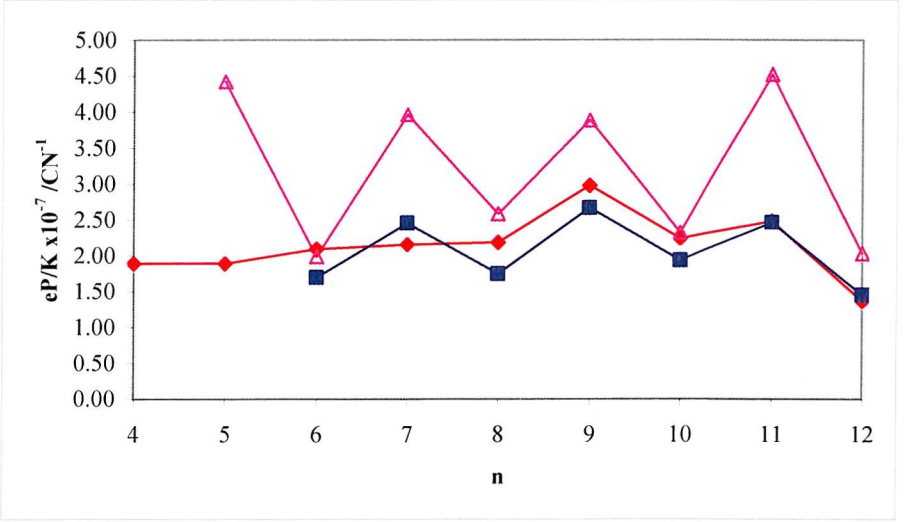

Figure 4.44 Plot of the scaled flexoelastic ratio for CBOnOPCH7 measured for $T^* = 0.98\ T_{NI}$ compared to CBOnOPCH3 and the literature value for $CBOnOBF_2$ taken at $T^* = 0.84\ T_{NI}$. Here ♦ denotes the $\bar{e}P/\overline{K}$ for CBOnOPCH7, ■ denotes $\bar{e}P/\overline{K}$ for CBOnOPCH3 and Δ denotes $\bar{e}P/\overline{K}$ for $CBOnOBF_2$.

Contrasting these results with those of $CBOnOBF_2$ in Figure 4.44 we see that, as expected, the non-symmetric fluorinated group does give a larger scaled flexoelastic ratio. However, considering how much less polar the CBOnOPCH7 group is it is surprising to note that the results for n = 6 and n = 10 the results are almost identical.

4.7. Conclusions

By publishing a series of materials which showed a peculiar behaviour in $\bar{e}/\bar{K}$, Kelly *et al.* unwittingly spawned an investigation into several series of seemingly unlikely candidates for flexoelectric liquid crystal dimers. Investigation of these materials clearly shows that they do not give as large values for $\bar{e}/\bar{K}$ as seen in some of the symmetric and non-symmetric fluorinated dimers. However, by investigating their curious behaviour this has moved the community to consider the significance of the quadrupolar contribution to the flexoelectric effect and the synthesis has produced two novel series where a relatively non-polar mesogenic group is studied and a consideration as to the nature of the flexoelectric effect in simple binary and multi-component mixtures (e.g. E7).

Observations made about the flexoelastic measurements are to some extent hampered by the difficulties in measuring and estimating the pitch in the pure systems. The approximations made in E7 are reasonable as it is a host/guest system (where the HTP of R5011 in the host, E7, has been measured previously[43]) however the estimated value of 163 μm^{-1} taken from the Merck dimer mixture is almost certainly least accurate here where the non-symmetric moieties are PCHm rather than fluorinated biphenyls (some of which are used in the mixture itself). As was the case for the pure dimer systems described in Chapter 3, the high melting points and short nematic range made reliable standard measurements using wedge cells practically impossible.

The CBOnOPCH7 series showed an interesting smectic A phase which became less stable as the spacer length increased. This is believed to be influenced by the relationship between the terminal chain and the remaining anisotropic part of the dimer (treating the spacer as part of the rod) in the absence of strong interactions between the mesogenic groups as seen in the Schiff-base non-symmetric dimers. An interesting investigation would be to determine the spacing in the smectic phase by X-ray scattering. This would further explain the structure of the phase (i.e. whether it is intercalated as in the non-

symmetric Schiff-base dimers) and hence tell us more about the molecular interactions in the phase.

The curious change in the $\Delta S_{NI}/R$ for CBOnOPCH7 (n = 10) is not, however, understood and perhaps could be unravelled by examining the ordering in the nematic to see if there is any significant change for n = 8 – 12. There are, however, marked similarities between this series and the shorter chain non-symmetric CBOnOPCH3 series.

One of the main aims of this chapter was to investigate this unusual flexoelectric properties of the symmetric 3CHPOnOPCH3 dimers. The focus of this study was originally to investigate the behaviour of the pure systems but this was not possible due to limitations in the procedure used to measure the flexoelastic ratio. The primary reason for this is the suspected negative $\Delta\tilde{\varepsilon}$ for the material. Measurements on high temperature negative $\Delta\tilde{\varepsilon}$ materials are said to have been made[44] however the procedure is not available in the literature and the time and quantity of the dimers did not allow further investigation into this technique. Further study of these dimers and other dimers with similar dielectric anisotropies would require a quick and robust technique for measuring the $\bar{e}/\overline{K}$. In the mean time it may be possible to obtain an extrapolated result for $\bar{e}/\overline{K}$ for these systems by studying binary mixtures of symmetric and non-symmetric systems and fitting a polynomial line to the change in the scaled flexoelastic ratio with composition.

The result we do have for 3CHPOnOPCH3 also shows an interesting change in sign in $\bar{e}/\overline{K}$ compared to the non-symmetric dimers. A qualitative analysis of the molecular structure in the all-trans form leads us to the conclusion that this is due to the change in direction of the net dipole across the molecule. Thus the sign of $\Delta\tilde{\varepsilon}$ simply reflects the orientation of the dipole.

It would, of course, be interesting to design and investigate a system where $\Delta\tilde{\varepsilon}$ is positive but the net dipole across the molecule resulted in a negative $\bar{e}/\overline{K}$. This may be possible by employing the use of poly ethylene glycol chain spacers.

The non-symmetric CBOnOPCH3 series was synthesised to compare the general properties of the symmetric dimers with that of non-symmetric analogues which included a cyanobiphenyl group. The aim was to increase the T_{NI} as well as the flexoelastic constants by the introduction of a more mesogenic group. This was achieved and

comparing CBO11OPCH3 and 3CHPO11OPCH3 the magnitude of $\bar{e}/\overline{K}$ is certainly larger (although if there is a reverse odd-even effect in the pure symmetric system we may see a larger value for n = 10 or 12).

4.8. References

1. S. M. Morris, M. J. Clarke, A. E. Blatch, H. J. Coles, *Phys. Rev. E*, **2007**, 75, 041701.
2. J. Harden, B. Mbanga, N. Eber, K. Fodor-Csorba, S. Sprunt, J. T. Gleeson, A. Jakli, *Phys. Rev. Lett.*, **2006**, 97, 157802.
3. Conference meeting, Flexoelectricity in Liquid Crystals. Oxford University: 2006.
4. G. E. Durand, Personal Communication, 10th ILLC, to G. R. Luckhurst, 1984.
5. H. J. Coles, B. Musgrave, M. J. Coles, J. Willmott,, *J. Chem. Mater.*, **2001**, 11, 2709.
6. B. Musgrave, P. Lehmann, H. J. Coles, *Liq. Cryst.*, **1999**, 26, 1235.
7. M. J. Clarke, A. E. Blatch, H. J. Coles, *Mol. Cryst. Liq. Cryst.*, **2005**, 434, 367.
8. J. Prost, J. P. Marcerou, *J. Phys. (Paris)*, **1977**, 38, 315.
9. M. J. Clarke. Ph.D. Thesis. University of Southampton, 2004.
10. J. Goodby, Personal Communication, Flexoelectricity in liquid crystals, to D. Jackson, 2005.
11. A. Ferrarini, *Phys. Rev. E*, **2000**, 64, 021710.
12. A. Ferrarini, G. R. Luckhurst, C. Greco, *J. Mater. Chem.*, **2007**, 17, 1039.
13. G. R. Luckhurst, Personal Communication, to A. Ferrarini, 2003.
14. A. Ferrarini, Personal Communication, to Luckhurst, G. R., 2003.
15. A. G. Petrov, *Physical properties of Liquid Crystals: Nematics*. INSPEC: Ed. D. A. Dunmer, A. Fukuda, G. R. Luckhurst 2001.
16. R. B. Meyer, *Phys. Rev. Lett.*, **1969**, 22, 918-921.
17. R. A. Ewings, C. Kischka, L. A. Parry-Jones, S. J. Elston, *Phys. Rev. E*, **2006**, 73, 011713
18. T. Hanemann, W. Haase, I. Svoboda, H. Fuess, *Liq. Cryst.*, **1995**, 19, 699.
19. J. H. Wild, K. Bartle, N. T. Kirkman, S. Kelly, M. O'Neill, T. Stirner, T. P. Tuffin, *Chem. Mater.*, **2005**, 17, 6354.

20. Y. Chen, Y, Lam, Soo-Ying Lee, *Chem. Lett.*, **2001**, (274).
21. Z. V. Zvonkova, A. N. Khvatkina, *Kristallografiya (Russian)(Crystallogr. Rep.)*, **1965**, 10, (734).
22. W. Helfrich, *Z. Naturforsch.*, **1971**, 26a, 833.
23. N. L. Campbell, W. L. Duffy, G. I. Thomas, J. H. Wild, S. M. Kelly, K. Bartle, M. O'Neill, V. Minter, R. P. Tuffin, *J. Mater. Chem.*, **2002**, 12, 2706.
24. R. W. Date, C. T. Imrie, G. R. Luckhurst, J. M. Seddon, *Liq. Cryst.*, **1992**, 12, 203.
25. G. S. Attard, R. W. Date, C. T. Imrie, G.R. Luckhurst, S.J. Roskilly, J.M.; Seddon, L. T., *Liq. Cryst.*, **1994**, 16, 529.
26. Molecular Mechanics minimisation of a phenyl-cyclohexyl system, Using Chem3d from ChemOffice 4.0.
27. H. Tukada, K. Mochizuki,, *Org. Lett.*, **2001**, 3, 3305.
28. J. K. Foitzik, H. Paulus, W. Haase, *Mol. Cryst. Liq. Cryst. (Lett.)*, **1985**, 1, 1.
29. M. C. Grossel, *Alicyclic Chemistry*. Ed. Primer, A. O. C. 1997.
30. G. S. Attard, R. W. Date, C. T. Imrie, G. R. Luckhurst, S. J. Roskilly, J. M.; Seddon, L. Taylor, *Liq. Cryst.*, **1994**, 16, 529.
31. E. M. Barrall II, J. F. Johnson, *Thermal Properties of Liquid Crystals*. Ed. G.W. Gray, P. A. Windsor 1974; p 254.
32. C. T. Imrie. Ph.D. Thesis. University of Southampton, 1988.
33. J. W. Emsley, G. R. Luckhurst, G. N. Shilstone, I. Sage, *Mol. Cryst. Liq. Cryst.*, **1984**, 102, 223.
34. R. A. Orwoll. V. J. Sullivan, G. C. C., *Mol. Cryst. Liq. Cryst.*, **1987**, 149, 121.
35. C. T. Imrie. Ph.D. Thesis. University of Southampton, 1988.
36. C. I. V. Shastry, A. M. Babu, M. A. Sridhar, S. B. Bellad, A. Indira, J. S. Prasad, *Curr. Sci.*, **1992**, 62, 302.
37. K. Hori, M. Iimuro, A. Nakao, H. Toriumi, *J. Mol. Struct.*, **2004**, 699, 23.
38. R. L. Humphries, P. G. James, G. R. Luckhurst, *Symp. Faraday. Soc*, **1971**, 5, 107.
39. R. W. Date. Ph.D. Thesis. University of Southampton, 1991.
40. P. Rudquist, S.T. Lagerwall, *Liq. Cryst.*, **1997**, 23, (4), 503-510.

41. Measured in-house, Merck.

42. P. Rudquist, M. Buivydas, L. Komitov, S.T. Langerwall, *J. Appl. Phys.*, **1994**, 76, 7778.

43. Taken from the Merck Database, Measured in Merck, Chilworth.

44. H. J. Coles, Personal Communication, Merck CASE conference, to D. Jackson, 2007.

Chapter 5

Examining cyanobiphenyl dimers with a kink in the spacer

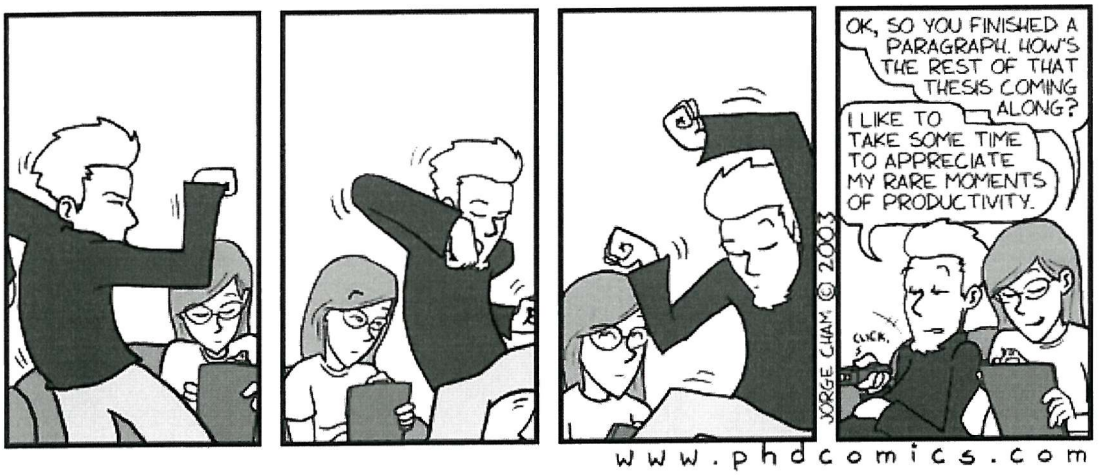

"Piled Higher and Deeper" by Jorge Cham
www.phdcomics.com

Used with permission